Technische Universität München

III. Medizinische Klinik (Hämatologie und Onkologie)

Klinikum rechts der Isar

The role of the ubiquitin-proteasome system in the pathology and treatment of B-cell lymphoma

Ursula Baumann (M.Sc)

Vollständiger Abdruck der von der Fakultät für Medizin der Technischen Universität München zur Erlangung des akademischen Grades eines

Doktors der Naturwissenschaften (Dr. rer. nat.)

genehmigten Dissertation.

Vorsitzende/r: Prof. Dr. Jürgen Ruland

Prüfer der Dissertation:

1: Prof. Dr. Florian Bassermann

2: Prof. Dr. Bernhard Küster

3: Prof. Dr. Claus Belka

Die Dissertation wurde am 23.08.2016 bei der Fakultät für Medizin der Technischen Universität München eingereicht und durch die Fakultät für Medizin am 17.05.2017 angenommen.

Für meine ehemalige Biologielehrerin Fr. Halbauer

Danke für die Faszination für die Biologie

1 Abstract

Apoptosis is an essential requirement for the faithful differentiation and development of B-lymphocytes, whereas evasion of apoptosis has been appreciated as a central pathomechansim in B-cell lymphomagenesis.

The HCLS1-associated protein X-1 (HAX1) is a key regulator of programmed cell death and migration, and has been implicated in different aspects of hematopoiesis. Particularly, HAX1 functions in B-cell development and survival, while inactivating HAX1 mutations have been identified as causal aberrations in severe congenital neutropenia (SCN), a human autosomal recessive trait, thus indicating a further role in myeloid progenitor cell survival. In line with its pro-survival function, high expression levels of HAX1 have been detected in different malignancies, especially in B-cell lineage derived lymphomas. So far, a functional characterization of the regulation of HAX1 abundance has been absent, and the role of HAX1 in the etiology of B-cell lymphomas and other cancers has remained unclear.

The present study identifies a novel apoptotic pathway, which involves the ubiquitin-proteasomal degradation of HAX1 by the previously orphan SCF^{FBXO25} E3 ubiquitin ligase (SKP1/Cullin1/F-box complex defined by the F-box protein FBXO25). The degradation process is initiated by the pro-apoptotic kinase protein kinase C delta (PRKCD), which sequentially phosphorylates FBXO25 within the nucleus, and HAX1 within an FBXO25-specific phospho-degron motif at site of mitochondria. The phosphorylation events prime the translocation of FBXO25 to mitochondrial HAX1, thereby mediating its SCF^{FBXO25}-dependent ubiquitylation and degradation. In addition, PRKCD exerts its pro-apoptotic function only in the presence of FBXO25 and HAX1, indicating an essential role of FBXO25 and HAX1 for PRKCD-mediated apoptosis. Moreover, shRNA-mediated silencing of *FBXO25* increases survival of HAX1 wildtype cells, while no effect could be observed in *Hax1* knock-out cells. Significantly, analyses in mantle cell lymphoma (MCL) patient samples reveal a substantial enrichment of monoallelic *FBXO25* deletions and tumor specific stabilizing HAX1 mutations. FBXO25 re-expression in *FBXO25* deleted MCL cell lines promotes cell death, whereupon expression of the HAX1 phospho-degron mutant protects cells from apoptosis. In addition, both the spontaneous Eμ-myc lymphoma mouse model and an isogenic MCL xenograft transplantation model demonstrate accelerated lymhoma development upon FBXO25 knock-down. Independent of its pro-survival function, HAX1 is presented as an essential regulator of C-X-C chemokine receptor 4 (CXCR4) cell surface expression and downstream activity, underlining an important role of the PRKCD-FBXO25-HAX1 axis in the regulation of CXCR4-dependent migration.

In summary, the present study identifies a PRKCD-dependent pro-apoptotic mechanism controlling HAX1 stability, and proposes that FBXO25 functions as a haploinsufficient tumor suppressor, and HAX1 as a proto-oncogene with potential therapeutic implications in B-cell lymphoma.

2 Abbreviations

3` UTR	3` untranslated region
Aa	Amino acid
ABC [transporter]	ATP-binding cassette [transporter]
aCGH	Comparative genomic hybridization array
ACK	Ammonium-Chloride-Potassium [with reference to red blood cell lysis buffer]
ACTB	Beta actin gene
AID	Activation-induced cytidine deaminase
AKT	V-Akt murine thymoma viral oncogene homolog 1
AMD3100	AMD3100 octahydrochloride hydrate/Plerixafor
AMP	Adenosine monophosphate
ANOVA	Analysis of variance
AP	Affinity purification
APAF-1	Apoptotic protease activity factor 1
Approx.	Approximately
ARF	ADP-ribosylation factor 1
ARPP_P0	Acidic ribosomal phosphoprotein P0
ASCT	Autologous stem cell transplantation
ATM	Ataxia telangiectasia mutated
ATP	Adenosine triphosphate
BAC	Bacterial artificial chromosome
BAX	BCL2-associated X protein
BBMM	Basal bone marrow medium
BCL2	B-cell lymphoma 2 gene
BCR	B-cell antigen receptor
BER	Base excision repair

BES	N,N-Bis(2-hydroxyethyl)-2-aminoethanesulfonic acid, N,N-Bis(2-hydroxyethyl)taurine
BLASTP	Protein basic local alignment search tool
B-NHL	B-cell non-Hodgkin lymphoma
BRCA1	Breast cancer 1
BS	Bovine serum
BSA	Bovine serum albumin
BSEP	Bile salt export protein
BTK	Bruton tyrosine kinase
C	Cytosine [main base of DNA and RNA]
cABL	Abelson murine leukemia viral oncogene homolog 1
Casp. 3	Caspase 3
CCND1	Cyclin-D1 gene
CD5+	Cluster of differentiation 5 positive [surface marker]
CD20+	Cluster of differentiation 20 positive [surface marker]
CDC25	Cell division cycle 25 phosphatase
CDK	Cyclin-dependent kinase
cDNA	Complementary desoxyribonucleic acid
cFOS	Homolog of the retroviral oncogene v-fos
CGH	Comparative genomic hybridization
CHOP	Cyclophosphamide, doxorubicin, vincristine and prednisone [chemotherapeutic combination]
CHX	Cycloheximide
Cl. casp. 3	Cleaved caspase 3
CLL	Chronic lymphoid leukemia
c-Myc	Homolog of the retroviral v-myc oncogene
CNV	Copy number variation

Cp	Crossing point
CRBN	Cereblon
CRLs	Cullin-RING ubiquitin ligases
CRM1	Chromosomal maintenance 1/exportin 1
CSR	Class switch recombination
C-terminal	Carboxyl-terminal
Ctrl	Control
CUL1	Cullin 1
CVAD	Cyclophosphamide, vincristine, doxorubicin and dexamethasone [chemotherapeutic combination]
CXCR4	C-X-C chemokine receptor type 4
Cyclohex.	Cycloheximide
Cyt.	Cytoplasmic
D	Diversity [antigen receptor region]
DAPI	4`, 6-Diamidin-2-phenylindol
DLBCL	Diffuse large B-cell lymphoma
DMEM	Dulbecco`s modified eagle medium [cell culture medium formulation]
DNA	Desoxyribonucleic acid
DNA-PK	DNA-dependent protein kinase
dNTP	Deoxynucleotide
DTT	Dithiothreitol
DUB	Deubiquitylating enzyme
E	Day of embryonic development
E1	Ubiquitin-activating enzyme
E2	Ubiquitin-carrier enzyme
E2F	E2F transcription factor
E3	Ubiquitin ligase

ECL	Enhanced chemiluminescence
EDTA	Ethylene diamine tetraacetic acid
E.g.	*Exempli gratia*
EGR1	Early growth response protein 1
ELK1	ETS domain-containing transcription factor 1
Endog.	Endogenous
ER	Endoplasmatic reticulum
Etop.	Etoposide
EV	Empty vector
Exog.	Exogenous
Exp.	Exposure
FACS	Fluorescence activated cell sorting
FAND	FBXO25-associated novel subnuclear structure
FBS	Fetal bovine serum
FBXO1	F-box protein 1
FBXO25	F-box protein 25
FDA	US Food and Drug Administration
FDG	Fluorodesoxyglucose
FFPE	Formalin-fixed paraffin-embedded
FISH	Fluorescence *in situ* hybridization
FITC	Fluorescein isothiocyanate
FL	Follicular lymphoma
FL1/FL3	Fluorescein 1/3 [measurement channel of FACS]
fs	Frameshift [with reference to DNA sequence]
fw	Forward [sequence orientation]
Gα13	Heterotrimeric G protein G13
GAPDH	Glyceraldehyde 3-phosphate dehydrogenase

GFP	Green fluorescent protein
GrB	Granzyme B
GST	Glutathione S-transferase
h	hours [with reference to a treatment period of cells]
h	Human [with reference to cDNA, DNA or protein sequence]
HA	Hemagglutinin [used as tag on proteins of interest]
HAX1	HCLS1-associated protein X-1
HBSS	Hanks` balanced salt solution
HCLS1	Hematopoietic cell specific Lyn substrate 1
H&E	Hematoxylin/Eosin
HECT	Homologous to E6-AP C-terminus
HEPES	4-(2-hydroxyethyl)-1-piperazineethanesulfonic acid
HRP	Horseradish peroxidase
H-score	Histo-score
HSPC	Hematopoietic stem cell progenitor cell
HtrA2	High temperature regulating A2 protein/Omi
IAP	Inhibitor of apoptosis protein
IF	Immunofluorescence
IG	Immunoglobulin gene
IgG	Immunoglobulin G
IGH	Immunoglobulin heavy gene
IGL	Immunoglobulin light gene
IHC	Immunohistochemistry
IL	Interleukin
IP	Immunoprecipitation
IPTG	Isopropyl-β-D-thiogalactopyranosid
IRES	Internal ribosomal entry site

J	Joining [antigen receptor region]
kb	Kilobase
L	Length
Lambda-phos.	Lambda phosphatase
LB	Lysogeny broth
LE	Long exposure
m	Murine [with reference to cDNA, DNA or protein sequence]
M	Molar
Mb	Mega base pairs
MCL	Mantle cell lymphoma
MCS	Multiple cloning site
MDM2	Mouse double minute 2 homolog E3 ligase
MEF	Mouse embryonic fibroblast
MG132	*N*-Benzyloxycarbonyl-L-leucyl-L-leucyl-L-leucinal
Min	Minute(s)
mM	Millimolar
MS	Mass spectrometry
mTOR	Mammalian target of rapamycin
mTORC1	Mammalian target of rapamycin complex 1
MW	Molecular weight
n	number
NEAA	Non-essential amino acids
NES	Nuclear export signal
NF-κB	Nuclear factor kappa-light-chain-enhancer of activated B-cells
NHEJ	Non-homologous end-joining
NHL	Non-Hodgkin lymphoma

NKX2-5	Homebox protein NKX-2.5
NLS	Nuclear localization signal
NOD-SCID	Nonobese diabetic severe combined iummunodeficient
NOXA	Phorbol-12-myristate-13-acetate-induced protein 1
NP	Pubmed reference number
N-terminal	Amino-terminal
Nuc.	Nuclear
P-bodies	Processing bodies
Pac.	Paclitaxel
PARL	Presenilin-associated, rhomboid-like
PARP	Poly(ADP-ribose)-Polymerase 1
PBS	Phosphate buffered saline
PCR	Polymerase chain reaction
PEST	Prolin (P), glutamic acid (E), serine (S), and threonine (T) rich peptide sequence
PET	Positron emission tomography
p.i.	post infection
PI	Propidium iodide
PI3K	Phosphoinositide 3-kinase
PKC	Protein kinase C
PLK1	Polo-like kinase 1
PLN	Phospholamban
POLB	DNA polymerase beta
PPi	Pyrophosphate
PRKCD	Protein kinase C delta
PRKCE	Protein kinase C epsilon
PRKCG	Protein kinase C gamma
PRKCH	Protein kinase C eta

PTEN	Phosphatase and tensin homolog
PTM	Post translational modification
PVDF	Polyvinylidene fluoride
qPCR	Quantitative polymerase chain reaction
rad	Radiation absorbed dose
RAG1/2	Recombination activating gene 1/2
RB1	Retinoblastoma protein 1
RBX1	RING-box protein 1
RFP	Red fluorescent protein
RING	Really interesting new gene
RNA	Ribonucleic acid
RPMI	Roswell Park Memorial Institute [cell culture medium formulation]
RRE	Rev response element
RT	Room temperature
rv	Reverse [sequence orientation]
SCF-complex	SKP1-CUL1-F-box-complex
SCN	Severe congenital neutropenia
SD	Standard deviation
SDF-1	Stromal cell-derived factor 1
SDS	Sodium dodecyl sulfate
SDS-PAGE	Sodium dodecyl sulfate-polyacrylamide gel electrophoresis
SE	Short exposure
SEM	Standard error of the mean
SERCA	Sarcoendoplasmic reticulum Ca^{2+} transport ATPase
SF	Strep-FLAG [protein tag]
SHM	Somatic hypermutation

siRNA	Small interfering RNA
SKP1	S-phase kinase-associated protein 1
SKP2	S-phase kinase-associated protein 2
shRNA	Short hairpin ribonucleic acid
SOC	Super optimal broth
SV40	Simian vacuolating virus 40
t	Translocation
TAP	Tandem affinity purification
TBE	Tris-borate-EDTA
TBX5	T-box transcription factor 5
TCP	Two pore channel
TMA	Tissue microarray
TNF	Tumor necrosis factor
TNFR1	Tumor necrosis factor receptor 1
TP53	Tumor protein p53
TR	Texas red
TRAIL	Tumor necrosis factor-related apoptosis-inducing ligand
U	Uracil [main base of RNA]
Ub	Ubiquitin
Ub(n)	Polyubiquitin [variable chain length]
UbcH5(A/B/C)	Ubiquitin-conjugating enzyme(s)
UBE1	Ubiquitin-activating enzyme E1
UBE2D3	Ubiquitin-conjugating enzyme E2 D3
UPS	Ubiquitin-proteasome system
UV	Ultraviolet [long wave radiation]
V	Variable [antigen receptor region]
VPR	Human immunodeficiency virus type 1 viral protein R

v/v	Volume/volume
W	Width
WB	Western blot
WCE	Whole cell extract
WHIM	Warts, hypogammaglobulinemia, immunodefficiency and myelokathexis
WT	Wildtype
w/v	Mass/volume
XIAP	X-linked inhibitor of apoptosis protein

3 Introduction

3.1 B-cell non-Hodgkin lymphoma

B-cell non-Hodgkin lymphoma (B-NHL) represents a heterogeneous group of hematopoietic malignancies derived from the B-cell compartment. According to the accumulation of genomic aberrations during different phases of B-cell development, B-NHL can be divided into different subtypes with different clinical behavior and variable susceptibility towards molecular targeting therapies (Harris, Jaffe et al. 1994);(Nogai, Dorken et al. 2011). The most common B-NHL subtypes are diffuse large B-cell lymphoma (DLBCL), follicular lymphoma (FL), mantle cell lymphoma (MCL) and Burkitt lymphoma (Figure 1) (Nogai, Dorken et al. 2011).

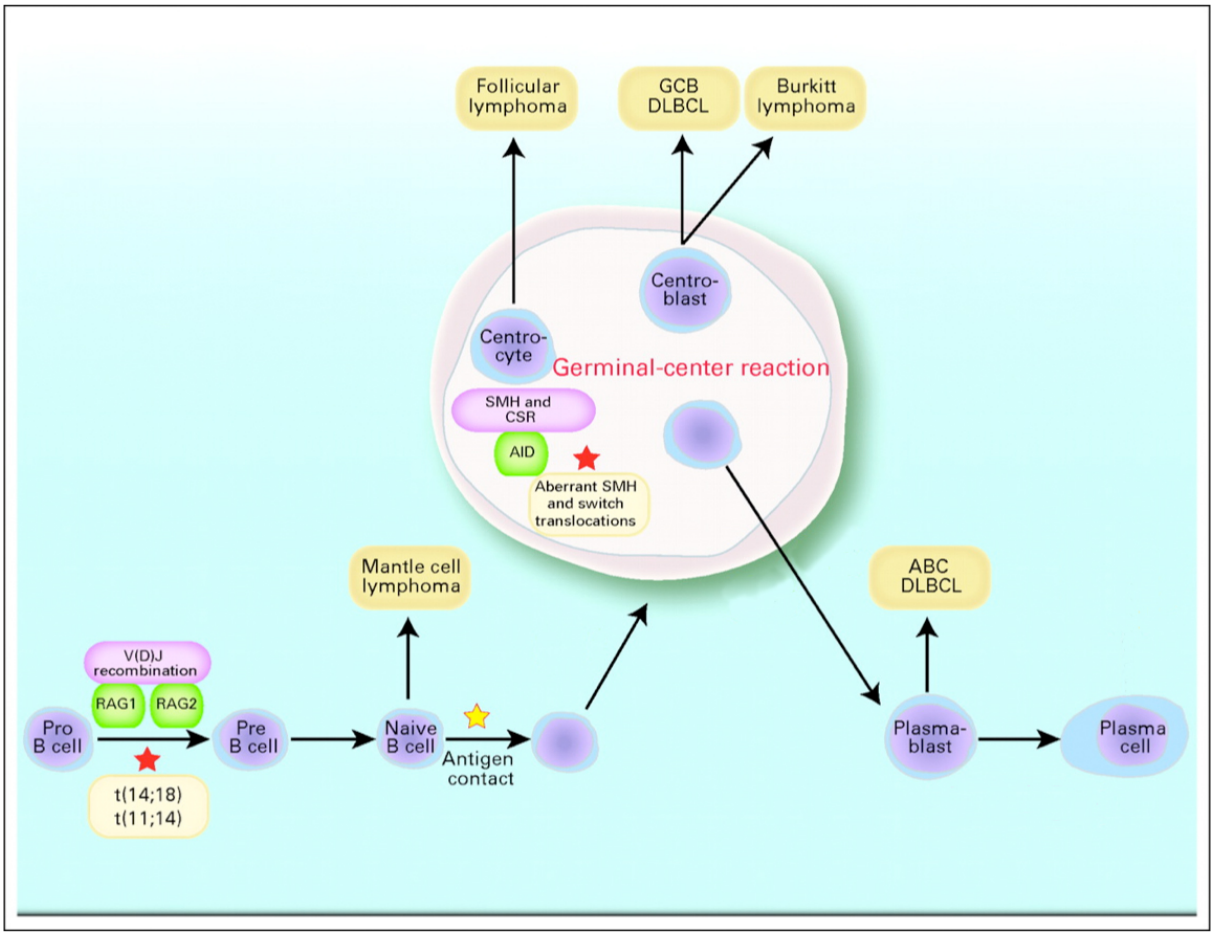

Figure 1. B-NHLs originate from different phases of B-lymphocyte development, where specific recombination events can give rise to malignant B-cell clones. RAG1/2 mediated V(D)J recombinations within the bone marrow potentially cause translocation events (e.g. t(14;18)) that represent critical steps in initial lymphomagenesis and give rise to MCL. After antigen contact, B-lymphocytes migrate to lymph nodes. During the local germinal center reaction SHM and CSR cause additional genomic instability. Figure modified from Nogia et al., 2011 (Nogai, Dorken et al. 2011).

In the physiological setting of diversification of the B-cell receptor (BCR), the genomic information for immunoglobulin heavy (IGH) and light (IGL) chains has to undergo recombination and somatic hypermutation (Blombery, Wall et al. 2015). This denotes that the antigen binding regions of the BCR are assembled during the differentiation from pro B-cell to naive B-cell in the bone marrow. Therein, the RAG complex, composed of recombination activating gene 1 (RAG1) and recombination activating gene 2 (RAG2), induces DNA double strand breaks between the variable (V), diversity (D) and joining (J) regions of the *IGH* locus as well as between the V and J regions of the *IGL* gene locus (Tonegawa 1983);(Eastman, Leu et al. 1996). Broken DNA strands are subsequently repaired by non-homologous end-joining (NHEJ) (Ma, Pannicke et al. 2002), thus leading to a unique re-combined V(D)J sequence fused to the constant regions of the immunoglobulin gene. The successful BCR gene rearrangement leads to survival of B-lymphocytes and their translocation to secondary lymphoid tissues. In the case of contact with specific antigens, B-cells translocate to germinal centers and undergo additional genetic modifications to present BCRs with increased affinity towards the corresponding antigen (Blombery, Wall et al. 2015). During the process of somatic hypermutation (SHM) the activation-induced cytidine deaminase (AID) deaminates cytosine (C) residues within single-stranded DNA to uracil (U) (Sohail, Klapacz et al. 2003). The resulting G:U base mismatch within the corresponding DNA sequence is subsequently repaired by base excision repair (BER), thus inducing mutations within transcribed regions of IG chain DNA (Di Noia and Neuberger 2002). Moreover, AID also regulates class switch recombination (CSR), thus allowing the generation of different immunoglobulin isotypes (e.g. IgG, IgM or IgA) with variable effector functions (Blombery, Wall et al. 2015).

Albeit V(D)J recombination, SHM and CSR are tightly controlled processes, they harbor an increased risk of a potential uncontrolled genomic instability within the B-lymphocyte compartment. Therefore, initial steps in the malignant transformation of B-cell clones often occur during V(D)J recombinations. The most frequent aberrant translocations are t(14;18) and t(11;14) (Nogai, Dorken et al. 2011). The translocation t(14;18)(q32;q21), observed in approximately 90 percent of FL and some cases of DLBCL (Cleary, Smith et al. 1986);(Iqbal, Sanger et al. 2004), involves the *IGH* and *BCL2* loci, resulting in a constitutive active *BCL2* promotor that is controlled by the *IGH* gene regulatory elements (Duan, Xiang et al. 2008);(Xiang, Noonan et al. 2011). The emerging unphysiological high expression of the anti-apoptotic protein BCL2 prevents B-cell apoptosis by blocking the release of cytochrome C from mitochondria (Yang, Liu et al. 1997). The t(11;14)(q13;q32) translocation constitutes the hallmark of MCL (Avet-Loiseau, Garand et al. 1998). In a similar manner to *BCL2*, the *CCND1* gene is put under the control of the *IGH* regulators, leading to overexpression of cyclin-D1 and misregulation of cell cycle control (Blombery, Wall et al. 2015).

In summary, B-NHL represents a heterogeneous group of hematopoietic malignancies derived from the B-lymphocyte compartment. Errors in different processes of B-cell development (V(D)J recombinations, SHM and CSR) give rise to a variety of disease-associated translocations and tumor promoting mutations.

3.2 Mantle cell lymphoma

Mantle cell lymphomas (MCLs) represent an aggressive subtype of B-NHL that accounts for around six percent of all diagnosed non-Hodgkin lymphomas (NHLs) in adults (Skarbnik and Goy 2015). The vast majority of all MCL tumors arise from naive pre-germinal center B-cells, what means that the variable immunoglobulin regions are largely unaffected by mutations (Nogai, Dorken et al. 2011). Diagnosis of MCL often occurs after incidence of general lymphadenopathy (75%) (Cheah, Seymour et al. 2016) - the abnormal size or number of lymph nodes (King, Ramachandra et al. 2014) - whereat most cases show already extranodal disease at sites of peripheral blood, bone marrow, spleen, liver and gastrointestinal tract (Fisher 1996);(Argatoff, Connors et al. 1997). The median age at point of diagnosis is 60 to 70 years, and the majority of affected individuals is male (75 - 80%) (Skarbnik and Goy 2015). After a lymph node biopsy the presence of MCL can be determined by immunohistochemistry (IHC). This immunoprofiling distinguishes MCL from other lymphoma entities and shows a high abundance of CD5+/CD20+/cyclin-D1+ cells (Barekman, Aguilera et al. 2001). Additionally performed FISH-analyses on biopsy material can uncover the characteristic chromosomal t(11;14) translocation, underlining the cyclin-D1 overexpression diagnosed by IHC (Fisher 1996). Due to morphologic and cytogenetic differences, MCLs can be subdivided into the four categories "mantle-zone", "nodular", "diffuse" and "blastoid", in which the blastoid variant resembles the most proliferative and aggressive form (Fisher 1996).

Although increasing amounts of novel therapeutic agents are available, MCL represents an entity with a poor overall survival of 51 to 60 months (Hoster, Dreyling et al. 2008). The additional presence of mutations or deletions of TP53 as well as high KI67 proliferation indexes within this tumor entity lead to an even worse survival prognosis of only 29 months (Greiner, Moynihan et al. 1996);(Bernard, Gressin et al. 2001);(Rubio-Moscardo, Climent et al. 2005);(Hoster, Dreyling et al. 2008);(Skarbnik and Goy 2015).

3.2.1 Molecular characteristics of mantle cell lymphoma

The lymphomagenesis of MCL is characterized by three main pathogenetic features: the deregulation of cell cycle control, the disruption of DNA damage response and the inhibition of apoptosis (Jares, Colomer et al. 2012);(Jares, Colomer et al. 2007);(Jares and Campo 2008).

As previously mentioned, the primary oncogenic translocation t(11;14) juxtaposes the *CCND1* gene under the control of *IGH* regulatory elements. This translocation event induces a constitutive high expression of cyclin-D1, which is normally not expressed at high levels in B-cells (Jares, Colomer et al. 2012);(Jares, Colomer et al. 2007). Cyclin-D1 forms a complex with cyclin-dependent kinases 4 and 6 (CDK4/6) which then phosphorylate retinoblastoma protein 1 (RB1). The phosphorylation of RB1 blocks its inhibitory effect on the E2F transcription factor, thus inducing the transcription of S-phase promoting genes (Jares, Colomer et al. 2012);(Jares, Colomer et al. 2007). Additionally, the *CDK4* gene itself has been described to be amplified or overexpressed in MCL tumor samples (Hernandez, Bea et al. 2005), while the *RB1* gene has been found to be deleted in the more aggressive cases of MCL (Pinyol, Bea et al. 2007). Both of the described genetic aberrations deregulate cell cycle control by promoting G1-S transition. Moreover, deletions affecting $p16^{INK4a}$, the main inhibitor of CDK4/CDK6/cyclin-D1 interaction, promote cellular proliferation particularly of aggressive forms of MCL (Pinyol, Hernandez et al. 1997).

Especially the aggressive blastoid variant of MCL shows high levels of chromosomal aberrations and tetraploid chromosome clones, underlining the loss on an intact DNA damage response as the second pathogenic main feature of MCL (Ott, Kalla et al. 1997). Mutations and deletion of ataxia telangiectasia mutated (*ATM*), a gene involved in the initiation of cell cycle arrest after DNA double strand breaks (Lee and Paull 2007), are found in MCL cases characterized by high genomic instability (Camacho, Hernandez et al. 2002). Also, the direct ATM effector CHK2 kinase that phosphorylates and activates TP53, CDC25 phosphatase and BRCA1 to initiate DNA repair and apoptosis after DNA damage, was found to be deregulated in MCL (Jares, Colomer et al. 2007);(Stolz, Ertych et al. 2011). TP53 itself is inactivated by mutation in around 15% of MCL cases (Greiner, Moynihan et al. 1996). This described inactivation of TP53 leads to a block of anti-proliferative processes after DNA damage and correlates with poor overall survival (Halldorsdottir, Lundin et al. 2011);(Greiner, Moynihan et al. 1996);(Zilfou and Lowe 2009). Alternatively, TP53 is inactivated by the upregulation of MDM2 (Solenthaler, Matutes et al. 2002), which mediates ubiquitylation and degradation of TP53 (Freedman, Wu et al. 1999), as well as by deletion of ARF, an inhibitor of TP53 protein-turnover (Hernandez, Bea et al. 2005);(Sherr and Weber 2000).

The activation of cellular survival mechanisms represents the third main feature of MCL. Aberrations within the PI3K/AKT/mammalian target of rapamycin (PI3K/AKT/mTOR) pathway (Dal

Col, Zancai et al. 2008), including loss of the PI3K regulator PTEN (Franke, Hornik et al. 2003), promote cell survival and resistance against chemotherapy induced apoptosis (Rao, Jiang et al. 2012). Besides deregulation of this major pathway, the overexpression of BCL-family members, like BCLX, renders MCL cells more resistant against apoptotic stimulation (Rummel, de Vos et al. 2004). Tackling MCL therefore means targeting a big variety of deregulated pathways in genetically very unstable tumor cells. More recent studies focus on novel therapeutic target structures including the transcription factor SOX11 (Ferrando 2013), Bruton tyrosine kinase (BTK), a regulator of B-cell receptor signaling (Cinar, Hamedani et al. 2013) and C-X-C chemokine receptor type 4 (CXCR4), a mediator of the interaction with stromal microenvironment and migration (Kurtova, Tamayo et al. 2009). Despite the known efficiency of these treatments, the underlying molecular mechanisms of these new target structures still need to be uncovered.

In summary, MCL represents an aggressive tumor variant with divers deregulations of cell cycle control, DNA damage response and apoptosis that give rise to the application of novel molecular therapeutic targeting approaches.

3.2.2 Current treatment

Mantle cell lymphoma (MCL) resembles a tumor entity with high biological heterogeneity, variable clinical outcome and overall poor survival, therefore the determination of standard therapies represents a major challenge for treatment (Jares, Colomer et al. 2012);(Smith 2011).

Under consideration of disease stage and patient fitness, a high-dose chemotherapy followed by autologous stem cell transplantation (ASCT) represents the current standard of first line therapy (Dreyling and Ferrero 2016). High-dose chemotherapy is administered by hyper-CVAD (hyperfractionated cyclophosphamide, vincristine, doxorubicin, dexamethasone alternating with methotrexate and cytarabine) (Dreyling and Ferrero 2016);(Vallumsetla, Paludo et al. 2015), CHOP (cyclophosphamide, doxorubicin, vincristine and prednisone (Dreyling and Ferrero 2016) or bendamustine (Becker, Tschechne et al. 2015). The implementation of rituximab with chemotherapeutic agents has been shown to be associated with superior outcomes compared to chemotherapy alone (Schulz, Bohlius et al. 2007);(Vallumsetla, Paludo et al. 2015). An application of the anti-CD20 antibody rituximab with the described chemotherapeutic combinations (R-hyper-CVAD, R-CHOP and BR) induces apoptosis of CD20-positive mature B-cells by activating cell intrinsic apoptotic signaling pathways as well as by promoting the lysis of rituximab bound B-cells by affector cells of the immune system (Solimando, Ribatti et al. 2016);(Weiner 2010). Due to the actual standards of care, chemotherapy is often followed by an ASCT (Gopal, Rajendran et al.

2002);(Dreyling and Ferrero 2016). During ASCT, stored hematopoietic stem cells from blood are retransplated into the corresponding patient, thus allowing for regeneration of the hematopoietic system (Stadtmauer, O'Neill et al. 2000). Although standard therapies are improved, frequent observed relapses and treatment resistances account for the implication of novel molecular approaches in the therapy of MCL (Dreyling 2011).

The recent description of cell survival promoting pathways, deregulated in MCL gave rise to the use of four new agents for patients with MCL: lenalidomide, temsirolimus, ibrutinib and bortezomib (Figure 2) (Cheah, Seymour et al. 2016).

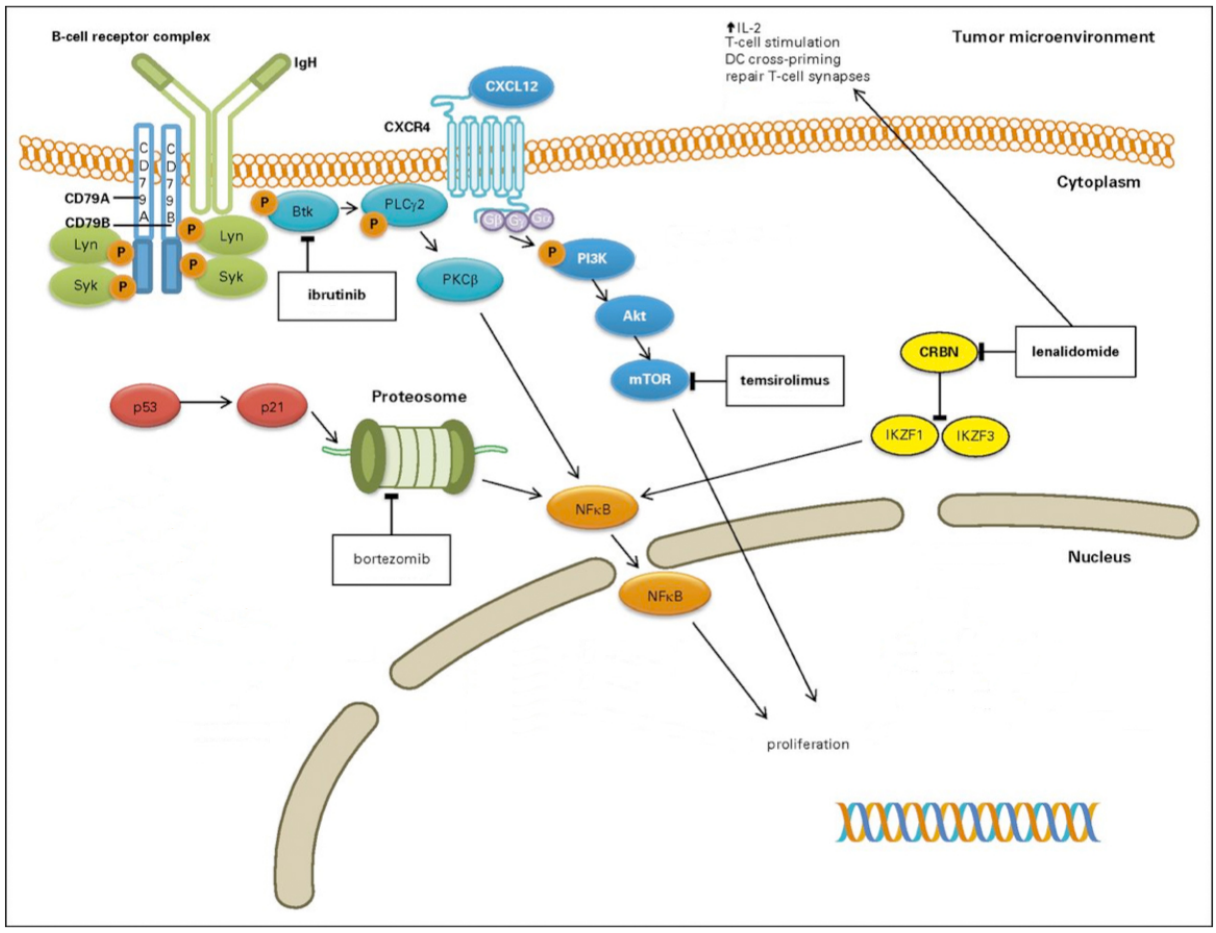

Figure 2. Central cellular pathways for proliferation and apoptosis of MCL cells are targeted by the four new therapeutic agents: lenalidomide, temsirolimus, ibrutinib and bortezomib. The immunomodulatory drug lenalidomide targets cereblon (CRBN) and blocks CRBN-mediated angiogenesis and tumor-stroma interaction, whereupon temsirolimus allosterically inhibits mTORC1 thus inducing cell cycle arrest by disruption of PI3K/AKT/mTOR signaling. The Bruton tyrosine (BTK) inhibitor ibrutinib blocks B-cell antigen receptor (BCR) signal transduction and shows anti-proliferative and pro-apoptotic effects, whereat bortezomib induces cell cycle arrest and ER stress mediated apoptosis of MCL cells by inhibiting the 26S-proteasome. Figure modified from Cheah et al., 2016 (Cheah, Seymour et al. 2016).

Lenalidomide is an immunomodulatory drug targeting the E3 cullin-4-RING ligase Cereblon (CRBN) (Lopez-Girona, Mendy et al. 2012). Systemic inhibition of this protein induces tumor cytotoxity, inhibition of angiogenesis and disruption of the tumor-stroma interaction (Qian, Zhang et

al. 2011);(Desai, Newberry et al. 2014). Moreover, lenalidomide functions as an immunomodulator by activating anti-tumor T-cells effective against the lymphoma cells (Desai, Newberry et al. 2014).

The second new drug recently approved for the treatment of MCL is temsirolimus, a rapamycin analogon which induces the allosteric inhibition of mTORC1 (Jares, Colomer et al. 2012). Inhibition of mTORC1 subsequently leads to the disruption of the PI3K/AKT/mTOR signaling pathway and results in a p21 dependent cell cycle arrest in G0/G1 with subsequent autophagy of the affected lymphoma cells (Smith 2012);(Galimberti and Petrini 2010).

Recently, ibrutinib a covalent inhibitor of Bruton tyrosine kinase (BTK) has been approved as therapeutic agent for patients with relapsed MCL (Vose 2015). Application of ibrutinib inhibits B-cell antigen receptor (BCR) signaling downstream of BTK and shows anti-proliferative and pro-apoptotic effects, thereby inhibiting MCL growth and progression (Ponader, Chen et al. 2012);(Kim and Dhillon 2015).

The fourth new therapeutic agent is represented by bortezomib, a reversible small molecule proteasome inhibitor that has been approved by the US Food and Drug Administration (FDA) for treatment of patients with relapsed/refractory MCL (Mujtaba and Dou 2011). By application of this drug, the ubiquitin-proteasome system (UPS) is inhibited, preventing the degradation of ubiquitylated $p27^{Kip1}$, a cyclin-dependent kinase inhibitor (Montagnoli, Fiore et al. 1999). Elevated $p27^{Kip1}$ levels lead to disruption of cyclin-D1/CDK4 interaction and block cell cycle progression (Ray, James et al. 2009);(Paoluzzi and O'Connor 2006);(Vallumsetla, Paludo et al. 2015). Moreover, bortezomib suppresses the transcription of NF-κB target genes, thus leading to a downregulation of cell growth and proliferation promoting genes (Palombella, Rando et al. 1994);(Juvekar, Manna et al. 2011). In addition to the previously described effects, bortezomib also leads to upregulation of NOXA, a downstream effector of endoplasmatic reticulum (ER) stress, triggered by the accumulation of polyubiquitylated proteins (Perez-Galan, Mora-Jensen et al. 2011);(Jares, Colomer et al. 2012). Accumulation of the BH-3 only protein NOXA subsequently results in TP53-induced apoptosis (Oda, Ohki et al. 2000).

In summary, MCL tumors are initially treated by a combination of high-dose chemotherapy followed by autologous stem cell transplantation. In case of relapse, the novel molecular agents: lenalidomide, temsirolimus, ibrutinib and bortezomib are used to induce apoptosis of targeted MCL cells. Albeit MCL can be treated by a broad range of combinations of chemotherapy with molecular targeting drugs, high rates of relapsed/refractory tumors can be observed, giving rise to scientific effort to evaluate novel biomarkers and therapeutic target structures.

3.3 The ubiquitin-proteasome system

The ubiquitin-proteasome system (UPS) mediates the selective and programmed proteasomal degradation of approximately 80% of all cellular proteins (Skaar, Pagan et al. 2014), thus regulating variable biological processes including proliferation, differentiation, transcription, DNA damage response and apoptosis (Hershko and Ciechanover 1998);(Muratani and Tansey 2003);(Buckley, Aranda-Orgilles et al. 2012);(Clague and Urbe 2010). Because ubiquitin-mediated protein degradation is an irreversible mechanism, the UPS represents the main regulatory hub in the regulation of mono-directional processes like cell cycle progression (by degradation of cell cycle regulators) and apoptosis (by degradation of anti-apoptotic proteins) (Skaar, Pagan et al. 2014);(Neutzner, Li et al. 2012). The processing of corresponding substrates requires covalent linkage to ubiquitin, a process that is controlled by a three step enzymatic cascade comprising an E1 (ubiquitin-activating) enzyme, an E2 (ubiquitin-conjugating) enzyme and an E3 ubiquitin ligase (Hershko and Ciechanover 1998). The outcome of the marked substrate (e.g. 26S-proteasomal degradation or involvement in signal transduction) is dependent on the number and topology of the attached ubiquitin molecules (Pickart and Fushman 2004);(Komander and Rape 2012). Although, ubiquitin-mediated proteolysis is irreversible, ubiquitylation itself is a post translational modification (PTM) which is reversible by deubiquitylating enzymes (DUBs) that remove ubiquitin from specific substrates and lead to a release of these substrates from UPS-mediated processing (Hershko and Ciechanover 1998);(Amerik and Hochstrasser 2004).

In summary, the UPS represents a tightly controlled system for the regulation of activity and abundance of a wide range of proteins among them tumor suppressors and oncogenes. Deregulation of the system can lead to destabilization of tumor suppressors or stabilization of oncogenes thus promoting tumorigenesis such as lymphoma development (Suh, Tanaka et al. 2013);(Liu and Mallampalli 2016).

3.3.1 The E1-E2-E3 enzyme cascade

All UPS processing steps include the covalent attachment of the 76 amino acid polypeptide ubiquitin to specific substrates. This ubiquitylation reaction occurs through a three step enzymatic-cascade. Within the initial step, the C-terminal glycine residue of ubiquitin gets activated in an ATP-dependent manner by an E1 (ubiquitin-activating) enzyme. The initial formation of an ubiquitin-adenylate intermediate (under release of pyrophosphate) is therein followed by the transfer of the ubiquitin-molecule to a thiol-group within the catalytic center of E1 (under release of AMP), thereby

forming an energy-rich thioester bond. Subsequently, the ubiquitin-molecule is transferred to an active-site cysteine residue of the E2 (ubiquitin-carrier) enzyme, a reaction referred to as thioesterification. In the terminal step, which is catalyzed by an E3 ligase, ubiquitin is transferred to either an epsilon-amino group of an internal lysine or an alpha-amino group of the N-terminal residue of a specific substrate (Figure 3). (Hershko and Ciechanover 1998);(Pickart and Eddins 2004);(Neutzner and Neutzner 2012);(Ciechanover 2005)

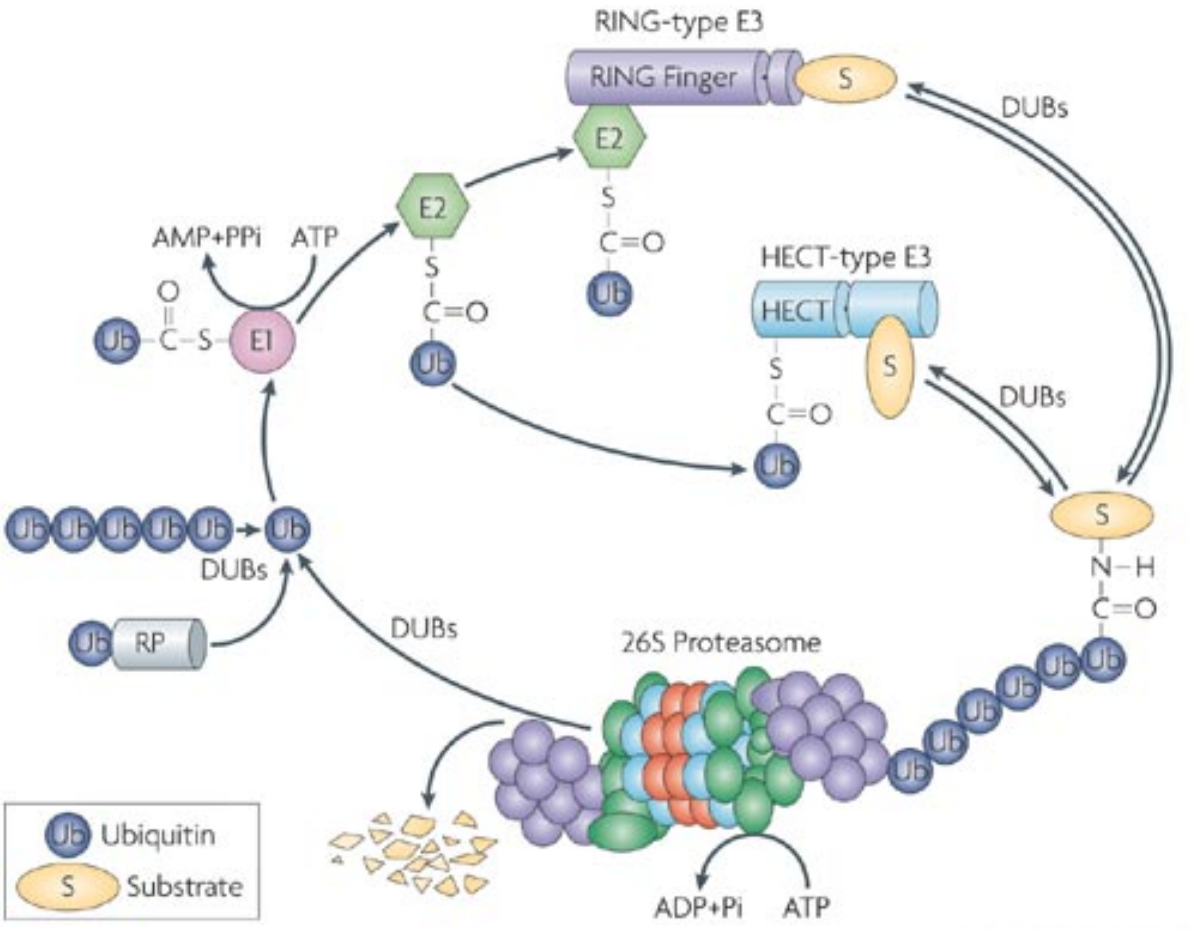

Figure 3. The ubiquitylation circle. The ubiquitylation reaction occurs in a three-step enzymatic cascade. Ubiquitin gets activated by an E1 (ubiquitin-activating) enzyme in an ATP-dependent manner and is transferred to an active-site cysteine residue of an E2 (ubiquitin-carrier) enzyme. The subsequent transfer of ubiquitin to lysine residues of a specific substrate is mediated by HECT- or RING-type E3 ligases. Ubiquitylated substrates can be recognized and degraded by the 26S-proteasome in an ATP-dependent manner. Although protein degradation is irreversible, ubiquitin chains themselves can be removed by deubiquitylating enzymes (DUBs) regenerating free ubiquitin. Figure modified from Murata et al., 2009 (Murata, Yashiroda et al. 2009).

The number and topology of attached ubiquitin molecules subsequently decide the biological faith of the marked substrate (Pickart and Fushman 2004). Extensions of the ubiquitin chain via lysine K11 and K48 of ubiquitin commit the corresponding substrate for degradation to the proteasome, whereupon polyubiquitylation on other residues (K6, K27, K29, K33, K63 and the

C-terminal methionine) as well as monoubiquitylation lead to non-proteolytic outcomes e.g. protein trafficking or signal transduction (Skaar and Pagano 2009);(Heo, Eki et al. 2016). All ubiquitylation reactions catalyzed by E3 ligases are functionally opposed by de-ubiquitylation enzymes (DUBs), which are able to remove all kinds of ubiquitin-modifications from specific substrates thus preventing their proteolysis or modifying involvement in signal transduction (Nijman, Luna-Vargas et al. 2005);(Skaar, Pagan et al. 2014).

UPS substrates marked by K11 or K48 polyubiquitylation for 26S-proteasomal degradation, are recognized by the 19S-cap subunit of the proteasome and unfolded in an ATP-dependent manner. Subsequent translocation of the recognized substrate to the proteolytic chamber of the 20S-core subunit leads to the degradation of targeted proteins (Schmidt, Hanna et al. 2005);(Suh, Tanaka et al. 2013).

So far, in humans there have been identified two E1 (ubiquitin-activating) enzymes, approximately 30 E2 (ubiquitin-carrier) enzymes and around 600 different E3 ligases (Li, Bengtson et al. 2008);(Skaar, Pagan et al. 2013). E3 ligases thereby contribute substrate specificity to the whole UPS, a fact that is underlined by the high number and structural variability of these ubiquitin ligases.

3.3.2 E3 ubiquitin ligases and the SCF-complex

Active E3 ubiquitin ligases catalyze the transfer of ubiquitin from E2 to a specific target, thus resembling the substrate recruiting components of the UPS. Dependent on structural domain homologies, ligase molecules can be separated into two major groups, the HECT (homologous to E6-AP C-terminus) E3 family and the RING (really interesting new gene) E3 family (Metzger, Hristova et al. 2012). HECT domain ligases possess an internal active-site cysteine residue and are therefore capable of forming a covalent intermediate with the activated ubiquitin before transferring it to a substrate, while RING ligases represent scaffold factors that catalyze the direct transfer of ubiquitin from E2 to a target protein (Figure 4) (Ciechanover 2006);(Neutzner and Neutzner 2012).

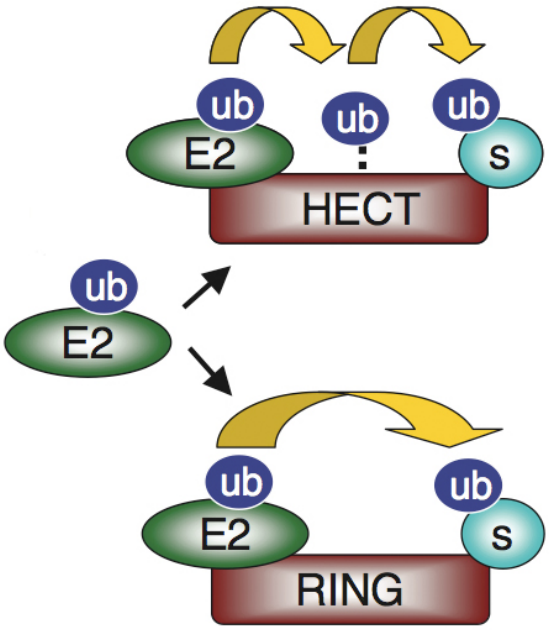

Figure 4. HECT and RING family of E3 ubiquitin ligases. RING-type E3s bind the E2 enzyme and a specific substrate, mediating the direct transfer of ubiquitin from E2 to the targeted protein. In contrast, HECT-type E3s first form a thio-ester with the activated ubiquitin before transferring it to the specific substrate. Figure modified from Nethe et al., 2010 (Nethe and Hordijk 2010).

Cullin-RING ubiquitin ligases (CRLs) constitute the largest and best described family of E3s (Heo, Eki et al. 2016). Eight so called Cullin proteins form the scaffold for approximately 200 different CRLs, of which the CUL1-dependent CRL1/SCF complexes represent the best characterized CRL complex (Lydeard, Schulman et al. 2013). SCF ligases are SKP1-CUL1-F-box (SCF) protein complexes, in which CUL1 represents the central scaffold protein. The C-terminus of CUL1 binds to the RING protein RBX1/ROC1, thus recruiting the E2 enzyme. In contrast, the N-terminus of CUL1 associates with SKP1 and bridges to a variable substrate recruiting F-box protein (Figure 5) (Cardozo and Pagano 2004);(Petroski and Deshaies 2005).

The exchange of the substrate recruiting SCF-subunit in this complex allows the ubiquitylation of a wide range of specific target proteins.

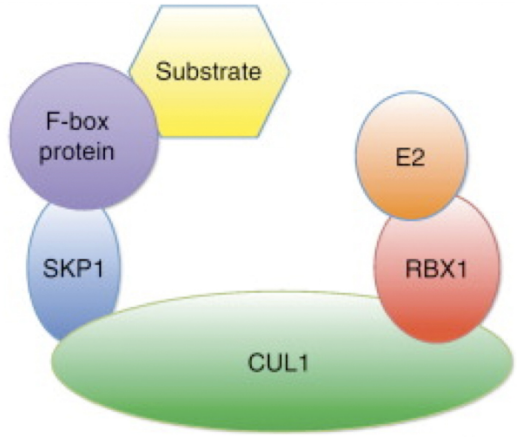

Figure 5. The SCF complex. SCF (SKP1/CUL1/F-box) complexes are assembled using the scaffold molecule CUL1. The C-terminus of CUL1 binds to RBX1 and recruits the E2 ubiquitin-carrier protein. The N-terminus of CUL1 associates with SKP1 and bridges to a variable substrate recruiting F-box protein. Figure adopted from Silverman et al., 2012 (Silverman, Skaar et al. 2012).

3.3.3 F-box proteins

F-box proteins are named according to an approximately 50 amino acid domain, which was initially identified in cyclin-F/FBXO1 (Kipreos and Pagano 2000);(Skaar, Pagan et al. 2014). The F-box motif allows the interaction with the SCF-core via SKP1, while the presence of additional protein interaction domains permits a categorization of the 69 human F-boxes into three families. F-box proteins with WD-40 domains are referred to as FBXWs (*n* = 10), F-box proteins with leucine-rich repeats are named as FBXLs (*n* = 21), while all other F-boxes with divers target protein interaction motifs (e.g. tetratricopeptide repeats or proline-rich regions) are classified as FBXOs (*n* = 38) (Kipreos and Pagano 2000);(Jin, Cardozo et al. 2004);(Skaar, Pagan et al. 2014). Described functional domains typically recognize specific substrates by their degron motifs which have been modified by phosphorylation, glycosylation or co-factor binding (Skaar, Pagan et al. 2013). Due to the wide range of substrates that play key roles in cell cycle regulation, apoptosis and proliferation, F-box proteins themselves play essential roles as oncogenes and tumor suppressor genes.

The F-box protein SKP2/FBXL1 has been characterized as classical oncogene because of mediation of the UPS-dependent degradation of the CDK-inhibitor p27, thus promoting S-phase entry (Frescas and Pagano 2008). Overexpression of SKP2 has thereby been associated with tumor progression and poor prognosis in variable cancer types including lymphoma (Latres, Chiarle et al. 2001);(Skaar, Pagan et al. 2014). In contrast, FBXW7 represents a tumor suppressive E3 ligase by targeting proto-oncogenes that function in growth and cell division

pathways (e.g. c-Myc, NOTCH and cyclin-E) for degradation (Welcker and Clurman 2008);(Kitagawa and Kitagawa 2016). Thereby, loss of FBXW7 function by either mutations of FBXW7 or its substrates has been linked to tumorigenesis and cancer progression (Welcker and Clurman 2008).

Although some F-box proteins have been characterized well, the corresponding substrates of the great majority remain elusive. Further studies are required to elucidate the role of the orphan F-boxes as cellular regulators, tumor suppressor genes or oncogenes and their involvement in tumorigenesis.

3.4 Identification of novel deregulated ubiquitylation events in MCL

As described above, MCL represents an aggressive form of B-NHL which is characterized by the t(11;14)(q13;q32) translocation leading to deregulated cell cycle control through cyclin-D1 overexpression (Tsujimoto, Jaffe et al. 1985). Although cyclin-D1 overexpression resembles the hallmark of MCL, transgenic mouse models have shown that it is not sufficient to induce MCL development (Lovec, Grzeschiczek et al. 1994);(Bodrug, Warner et al. 1994). In fact, additional genetic alterations leading to dysregulation of oncogenes and tumor suppressor genes are necessary for the malignant transformation of MCL (Schraders, Pfundt et al. 2005). The underlying pathogenic DNA copy number changes (gain, amplification and deletion) are thereby frequently studied by high resolution comparative genomic hybridization arrays (aCGHs) on a genome-wide scale (Toujani, Dessen et al. 2009);(Bejjani and Shaffer 2006).

An initial CGH array data set analysis in search for genomic changes of ubiquitin-proteasome system (UPS) components, identified 8p23.3 as potential genomic locus of a novel tumor suppressor gene (Baumann 2011). Deletions of 8p23.3, correlating with the genomic localization of *FBXO25* encoding the orphan F-box protein FBXO25, were observed in approximately 29% of MCL patient samples (n = 68) (Schraders, Pfundt et al. 2005), 33% of MCL cell lines (n = 9) (Schraders, Pfundt et al. 2005) and around 8% of DLBCL biopsies (n = 73) (Pasqualucci, Trifonov et al. 2011), while no alteration of the locus could be observed in Burkitt lymphoma (Toujani, Dessen et al. 2009) and FL (Cheung, Shah et al. 2009).

A more stringent analysis of five independent aCGH studies of 189 MCL patient samples (Rubio-Moscardo, Climent et al. 2005);(Schraders, Pfundt et al. 2005);(Flordal Thelander, Ichimura et al. 2007);(Tagawa, Karnan et al. 2005);(Martinez-Climent, Vizcarra et al. 2001) [performed by Roland Rad, Technische Universität München, Germany] unraveled the anatomy of chromosome 8p aberrations in MCL (Figure 6).

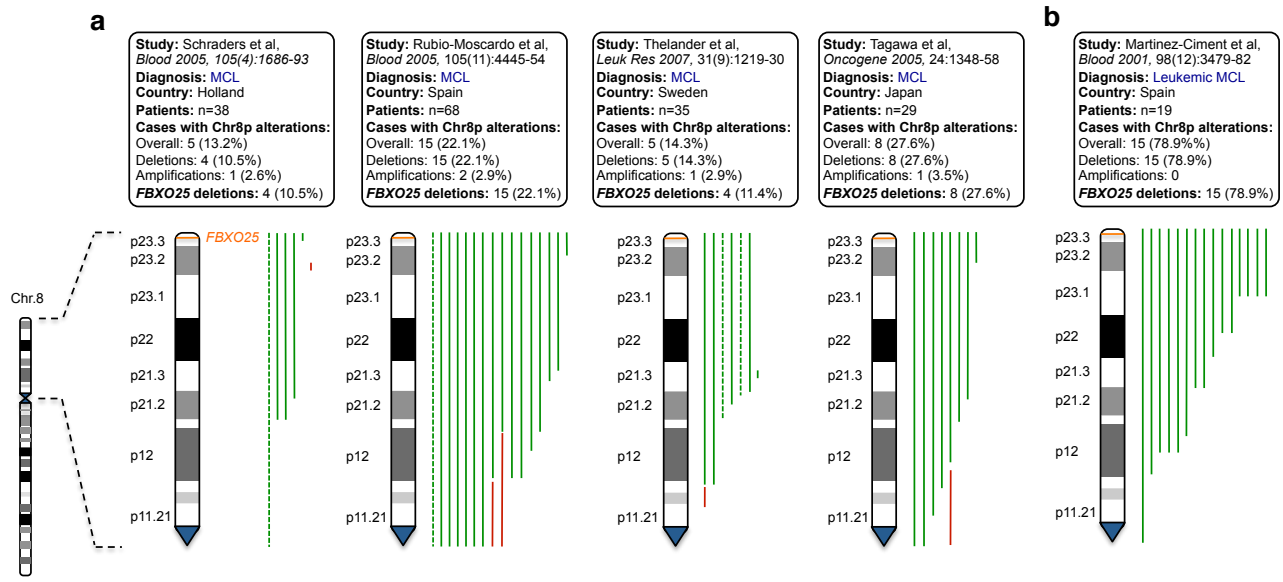

Figure 6: Mantle cell lymphoma derived copy number variations (CNVs) at human chromosome 8p determined by comparative genomic hybridization (CGH). (a) CNV calling on data derived from indicated publications performed with identical criteria for all 170 MCL cases. Red, copy number gain and green, copy number loss, while the criteria for CNV calling were defined as: loss, log2 value <= -0.3; homozygous loss, log2 value <= -1.0; amplification, log2 value >= 0.3 (dotted lines without significant treshhold not included in the calculation of deletion rate). (**b)** CGH on metaphase chromosome spreach of leukemic MCL patient samples. [Data analysis and graphic presentation performed by Roland Rad, Technische Universität München, Germany.]

The dissection of present copy number variations (CNVs) shows *FBXO25* within the minimal common region of deletion (1.2 Mb). Deletion of the *FBXO25* locus was observed in approximately 24% of all samples (*n* = 189), while all deletions were of monoallelic nature, exclusively.

In summary, analyses of CGH array data sets identified 8p23.3 as hotspot region of genomic deletion in MCL and *FBXO25* as candidate for a novel tumor suppressor gene in MCL.

3.5 The human F-box protein FBXO25

The human F-box protein FBXO25 is encoded by the 63 kilobase (kb) *FBXO25* gene located on chromosome 8p23.3. The resulting gene product comprises three different isoforms of 367 amino acids (FBXO25_1; NP_904357), 358 aa (FBXO25_2; NP_904356) and 291 aa (FBXO25_3; NP_036305). A BLASTP based protein alignment of human FBXO25 and the corresponding murine homologue indicates an identity of 89 percent and a similarity of 94% between the protein sequences.

Furthermore, analyses for conserved motifs and domains within the human FBXO25 protein sequence identified a nuclear localization signal (aa 65 - 69), a nuclear export signal (aa 173 - 183) and a F-box motif (aa 228 - 329) (Figure 7).

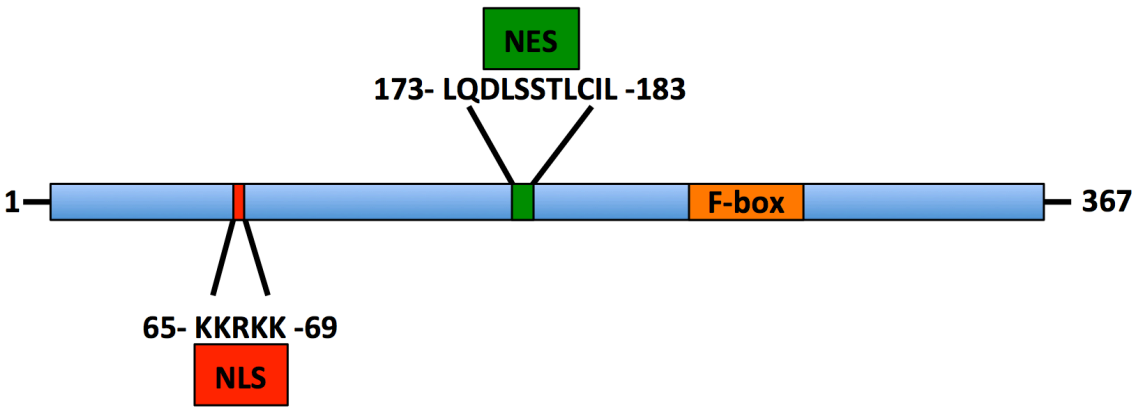

Figure 7: Schematic overview over conserved motifs of the human F-box protein FBXO25. The protein sequence of FBXO25 contains a nuclear localization signal (aa 65 - 69; red bar), a nuclear export signal (aa 173 - 183; green rectangle) and a F-box motif (aa 228 - 329; orange rectangle).

The monopartite SV40 large T antigen-like nuclear localization signal (NLS) within the FBXO25 sequence allows interaction with importin α/β heterodimers, facilitating the translocation of FBXO25 through nuclear pores (Görlich, Kostka et al. 1995);(Lange, Mills et al. 2007). Whereas the presence of a nuclear export signal (NES) indicates the possibility that FBXO25 might be exported back to the cytoplasm. Observed export processes thereby are often controlled by phosphorylation of NES associated serine residues (la Cour, Kiemer et al. 2004); (Dominguez, Montserrat-Sentis et al. 2003);(Zhang and Xiong 2001). The additional bioinformatic identification of a single conserved F-box protein consensus motif within the sequence confirms FBXO25 as part of the F-box protein family (Kipreos and Pagano 2000). The F-box protein-protein interaction domain arbitrates interaction with SKP1 and thus allows for the assembly of a functional SCF^{FBXO25}

complex that should have the ability to mediate ubiquitylation of specific substrates (Kipreos and Pagano 2000);(Randle and Laman 2016).

FBXO25 was initially discovered by two screenings designed to identify homologues of human F-box proteins (Winston, Koepp et al. 1999);(Cenciarelli, Chiaur et al. 1999). Subsequent studies confirmed FBXO25 as active E3 ligase component (Maragno, Baqui et al. 2006);(Teixeira, Yokoo et al. 2010) showing highest expression levels in brain, intestine and kidney (Hagens, Minina et al. 2006);(Maragno, Baqui et al. 2006). Immunofluorescence based tracking approaches demonstrated a predominantly nuclear accumulation of human FBXO25 (Maragno, Baqui et al. 2006);(Manfiolli, Maragno et al. 2008). More detailed analyses on the nuclear FBXO25 distribution by Manfiolli et al. identified FBXO25 associated novel subnuclear structures (FANDs) that were clearly distinguishable from other known nucleoplasmatic compartments (Manfiolli, Maragno et al. 2008). The structural organization of FAND domains is regulated by direct interaction of FBXO25 with β-actin, whereby the FAND domains were functional supposed to be involved in preventing the aggregation of polyglutamine-containing proteins (Manfiolli, Maragno et al. 2008);(Teixeira, Yokoo et al. 2010). Independent of its accumulation in FANDs, FBXO25 regulates the proteasomal degradation of ELK1, thus influencing the induction of the ELK1 target genes *c-FOS* and *EGR1*. Albeit FBXO25 mediates the ubiquitylation of ELK1, the functional role of FBXO25 in the regulation of immediate early genes remained unkonwn (Teixeira, Manfiolli et al. 2013).

More recent studies identified FBXO25 as an E3 ligase component influencing cardiomyocyte differentiation and regeneration of cardiac tissue by mediating the proteasomal degradation of the cardiac specific transcription factors NKX2-5 and TBX5 (Jang, Lee et al. 2011);(Jeong, Jung et al. 2015).

To elucidate the role of *FBXO25* as potential candidate for a novel tumor suppressor gene, a mass spectrometry based screen for interactors of tandem-affinity purified FBXO25 identified the anti-apoptotic HCLS1-associated protein X-1 as potential substrate (Baumann 2011). The functional relevance of a possible FBXO25-HAX1 interaction in the tumorigenesis of B-cell non-Hodgkin lymhoma remained to be demonstrated.

3.6 The HCLS1-associated protein X-1 (HAX1)

HCLS1-associated protein X-1 (HAX1) was initially identified as interactor of Hematopoietic Cell-Specific Lyn Substrate 1 (HCLS1/HS-1), a SRC kinase substrate, which is specifically expressed in hematopoietic cells and regulates signal transduction processes in lymphocytes (Suzuki, Demoliere et al. 1997). The approximately 35 kDa protein HAX1 contains a

transmembrane domain, two predicted BCL-2 homology domains as well as a PEST sequence that allows regulation of HAX1 levels by K48-ubiquitylation dependent proteasomal degradation (Suzuki, Demoliere et al. 1997);(Trebinska, Hogstrand et al. 2014);(Li, Hu et al. 2012). HAX1 is ubiquitously expressed in murin and human tissues and localizes mainly to mitochondria and to a lesser extent to endoplasmatic reticulum (ER) and nuclear membrane (Suzuki, Demoliere et al. 1997);(Kwiecinska, Ottosson-Wadlund et al. 2011).

Functional studies disclose HAX1 as multifunctional protein involved in cellular homeostasis (e.g. calcium homeostasis) (Vafiadaki, Arvanitis et al. 2009), migration (Radhika, Onesime et al. 2004);(Ramsay, Keppler et al. 2007) and the regulation of apoptosis (Yap, Koontz et al. 2011).

3.6.1 HAX1 as a regulator of cellular homeostasis and migration

The protein HAX1 has been described to be involved in a great variety of distinct cellular mechanisms. One of them is the interaction of HAX1 with the human immunodeficiency virus type 1 viral protein R (VPR) and the HIV-1 REV protein (Yedavalli, Shih et al. 2005);(Modem and Reddy 2008). The REV protein normally facilitates the nuclear export of viral mRNA containing a REV response element (RRE), while increased interaction of HAX1 and REV leads to inhibition of REV function and degradation of RRE-containing mRNAs (Modem and Reddy 2008);(Fadeel and Grzybowska 2009). In addition to its indirect effect on the stability of RRE-containing viral mRNAs, HAX-1 has also been reported to directly interact with eukaryotic RNA targets. Thereby, HAX1 interacts with structural hairpin motifs within the 3` untranslated regions (3` UTRs) of transcripts encoding for vimentin and DNA polymerase β (POLB) (Al-Maghrebi, Brule et al. 2002);(Sarnowska, Grzybowska et al. 2007);(Fadeel and Grzybowska 2009). Interaction of HAX1 with the so called "zip-code" element (Morris, Evason et al. 2000) confers instability and leads to a decrease of the corresponding mRNA, a process that has been described to be located in processing bodies (P-bodies), aggregates of mRNAs and proteins that are involved in the post-transcriptional regulation of gene expression (Grzybowska, Zayat et al. 2013);(Zayat, Balcerak et al. 2015). Independent of its specific mRNA regulatory role, interaction of HAX1 with HCLS1, a hematopoietic cell specific homolog of cortactin, underlines a potential role of HAX1 in cell migration (Uruno, Zhang et al. 2003);(Gomathinayagam, Muralidharan et al. 2014). A subsequent functional study confirmed the association between HAX1 and the F-actin binding protein cortactin, thus confirming a direct link of HAX1 with the actin cytoskeleton (Gallagher, Cedzich et al. 2000). In line with these data, HAX1 is described to link the alpha-subunit of the heterotrimeric G protein G13 ($G\alpha_{13}$) to the cytoskeleton, forming a complex with cortactin and Rac1, which allows for $G\alpha_{13}$ mediated migration (Radhika,

Onesime et al. 2004);(Gomathinayagam, Muralidharan et al. 2014). Of note, knock-down of endogenous HAX1 by small interfering RNAs significantly reduced $G\alpha_{13}$ mediated cell migration (Radhika, Onesime et al. 2004). More recent studies unravel a second aspect of HAX1 involvement in cell migration, regulating the internalization and clathrin-mediated endocytosis of $\alpha_V\beta_6$-integrin. siRNA mediated knock-down of HAX1 decreased the internalization rate for $\alpha_V\beta_6$-integrin and led to a block of $\alpha_V\beta_6$-dependent migration, showing that HAX1-dependent integrin endocytosis is required for $\alpha_V\beta_6$-mediated cell motility (Ramsay, Keppler et al. 2007);(Fadeel and Grzybowska 2009). In accordance with the regulation of receptor endocytosis by clathrin, HAX1 is also described to control the membrane abundance of the ABC transporter BSEP (bile salt export protein) by mediating its internalization (Ortiz, Moseley et al. 2004). Thereby, the association of HAX1 with ion channels is not restricted to apical membrane BSEP or endolysosomal two pore channel TPCs (Ortiz, Moseley et al. 2004);(Lam, Galione et al. 2013). HAX1 also represents an essential regulator of divers mediators of ER calcium homeostasis (Simmen 2011);(Gallagher, Cedzich et al. 2000).

An important regulation by HAX1 is the modulation of Ca^{2+} homeostasis via the two main regulators of the sarcoendoplasmic reticulum, SERCA (sarcoendoplasmic reticulum (SR) Ca^{2+} transport ATPase) and its inhibitor PLN (phospholamban) (Yap, Koontz et al. 2011). The SERCA Ca^{2+} transport ATPase regulates the rate of cytoplasmic Ca^{2+} removal and the sarcoendoplasmic Ca^{2+} load, while its interaction with PLN decreases SERCA affinity for Ca^{2+} (Vafiadaki, Arvanitis et al. 2009). Therein HAX1 association with PLN promotes the formation of active inhibitory phospholamban monomers, whereas the HAX1 interaction with SERCA decreases SERCA protein levels, thus reducing ER Ca^{2+} content (Vafiadaki, Arvanitis et al. 2009);(Zhao, Waggoner et al. 2009). The resulting drop in ER Ca^{2+} ions protects mitochondria from depolarization through Ca^{2+} overload and underlines the anti-apoptotic function of HAX1 (Vafiadaki, Arvanitis et al. 2009).

3.6.2 Regulation of apoptosis by HAX1

Apoptosis is a tightly regulated mechanism of cell death that is controlled by repressing and activating the function of cysteine-dependent caspases (Fadeel and Orrenius 2005);(Fadeel and Grzybowska 2009). Caspase activation can occur via the extrinsic receptor-mediated pathway (e.g. by binding of macrophage-secreted TNF-alpha to the TNF-receptor TNFR1 (Wajant 2002)) or via the intrinsic mitochondria-dependent pathway. Activation of the mitochondria-dependent pathway leads to permeabilization of mitochondrial membranes thus resulting in the release of cytochrome C and other pro-apoptotic molecules. Free cytochrome C facilitates the formation of the apoptosome by serving as co-factor for the apoptotic protease activity factor-1 (APAF-1), which

induces activation of the initiator-caspase pro-caspase-9 and downstream effector-caspases thus leading to the death of the affected cell (Fadeel, Ottosson et al. 2008);(Fadeel and Grzybowska 2009).

Due to the presence of two BCL-2 homology domains within its protein sequence, HAX1 was predicted to be involved in the anti-apoptotic regulation of cell survival (Suzuki, Demoliere et al. 1997);(Yap, Koontz et al. 2011). Studies in search for the anti-apoptotic functions of HAX1, describe HAX1 as a direct negative regulator of caspase-cascade dependent cell death by either preventing the activation of initiator-caspase 9 (Han, Chen et al. 2006) or by inhibiting the catalytic activity of caspase 3 (Lee, Lee et al. 2008). In line with the inhibition of caspases 3 and 9 (Han, Chen et al. 2006), HAX1 was additionally described to protect X-linked inhibitor of apoptosis protein (XIAP), another direct caspase-3, -7 and -9 inhibitor, from proteasomal degradation by preventing it from polyubiquitylation, thus finally augmenting its inhibitory effect on caspases (Kang, Jang et al. 2010).

In addition to its inhibitory effect on caspase activation, Hax1 also has been described to interact with the mitochondrial proteases Parl (presenilin-associated, rhomboid-like) and HtrA2/Omi (high temperature regulated A2). Direct interaction of Hax1 and HtrA2 at site of mitochondria allows HtrA2 activation by Parl. The proteolytic active form of HtrA2 subsequently prevents the accumulation of pro-apoptotic Bax protein within the outer mitochondrial membrane, thus anticipating the initiation of apoptosis (Chao, Parganas et al. 2008). After induction of apoptosis HtrA2/Omi proteolytically cleaves HAX1 at mitochondria and initiates the subsequent degradation of IAPs in caspase-dependent apoptosis (Cilenti, Soundarapandian et al. 2004);(Li, Hu et al. 2010). Moreover, HAX1 can be cleaved by granzyme B (GrB), a serine protease secreted from cytotoxic lymphocytes. While cleavage of HAX1 by GrB leads to loss of the inner mitochondrial membrane potential and induction of apoptosis, overexpression of HAX1 protects cells from GrB mediated depolarization (Casciola-Rosen, Garcia-Calvo et al. 2007);(Han, Goldstein et al. 2010).

In summary, HAX1 represents a multifunctional protein which is involved in the regulation of cellular homeostasis (Vafiadaki, Arvanitis et al. 2009), migration (Radhika, Onesime et al. 2004);(Ramsay, Keppler et al. 2007) and apoptosis (Yap, Koontz et al. 2011). Due to its interaction with a multitude of survival regulators, HAX1 represents a promising candidate for a therapeutic relevant key regulator of cellular survival and tumorigenesis.

3.6.3 Disease association of HAX1

Hax1$^{-/-}$ mice are described to survive not longer than 14 weeks due to increased apoptosis of neurons in striatum and cerebellum, and due to a massively reduced cellularity of the lymphatic tissues: spleen, bone marrow and thymus (Chao, Parganas et al. 2008);(Peckl-Schmid, Wolkerstorfer et al. 2010). The bone marrow of *Hax1*$^{-/-}$ mice shows a decrease in pro-B and pre-B cells (Chao, Parganas et al. 2008). The specific loss of these B-cell populations is associated with increased apoptosis rates (Chao, Parganas et al. 2008) as well as migratory defects due to the significant reduced expression levels of the hematopoietic chemokine receptor Cxcr4 in *Hax1*$^{-/-}$ mice (Peckl-Schmid, Wolkerstorfer et al. 2010).

Sequence analyses of human patient samples of Severe Congenital Neutropenia (SCN or Kostman disease), an autosomal recessive trait characterized by loss of mature neutrophil granulocytes in the bone marrow and peripheral blood, identified homozygous *HAX1* mutations as causative aberrations of SCN (Klein 2011);(Klein, Grudzien et al. 2007). Loss of HAX1 expression, due to biallelic mutations in the gene, leads to destabilization of mitochondrial membrane potential and increase mitochondrial-dependent apoptosis of myeloid progenitor cells (Carlsson, Aprikyan et al. 2004);(Boztug and Klein 2009);(Trebinska, Hogstrand et al. 2014). Of note, HAX1 mutations affecting all isoforms are associated with neurological symptoms, while mutations affecting only isoform 1 cause SCN without central nervous system involvement (Germeshausen, Grudzien et al. 2008);(Carlsson, van't Hooft et al. 2008).

Because HAX1 regulates apoptosis and cell migration (Fadeel and Grzybowska 2009), two major pathways involved in tumorigenesis, HAX1 expression has also been analyzed in the context of tumor formation and treatment resistance. Increased HAX1 expression has been reported in lung cancer (Trebinska, Rembiszewska et al. 2010), breast cancer (Trebinska, Rembiszewska et al. 2010), lymphoma (Kwiecinska, Ottosson-Wadlund et al. 2011), leukemia (Kwiecinska, Ottosson-Wadlund et al. 2011), esophageal carcinoma (Sun, Feng et al. 2012) and colon cancer (Li, Jiang et al. 2015). Overexpression of HAX1 in esophageal carcinoma and colorectal cancer increases invasive potential and promotes resistance towards chemotherapy (Li, Hu et al. 2012);(Sun, Feng et al. 2012), thus underlining high HAX1 expression levels as a risk factor for survival (Li, Tang et al. 2013);(Wei, Li et al. 2014). Moreover, HAX1 is particularly overexpressed in B-cell related hematologic malignancies (e.g. B-cell lymphomas) and therein associated with increased proliferation of B-cells (Kwiecinska, Ottosson-Wadlund et al. 2011).

3.7 Protein kinase C delta as regulatory pro-apoptotic kinase

Protein kinase C (PKC) represents a superfamily of twelve serine/threonine protein kinases which play an essential role in the regulation of proliferation, cellular differentiation and apoptosis (Mellor and Parker 1998);(Livneh and Fishman 1997);(Nishizuka 1992);(Zhao, Xia et al. 2012). Among all PKC family members only the isozyme protein kinase C delta (PRKCD) has been described to promote anti-proliferative and apoptotic signaling pathways (Griner and Kazanietz 2007);(Jackson and Foster 2004). PRKCD, a novel PKC, is ubiquitously expressed in mammalian tissues (Leibersperger, Gschwendt et al. 1991). With regard to its domain structure, PRKCD is composed of a N-terminal regulatory domain linked to a C-terminal catalytic domain (Yoshida 2007). Without stimulation, PRKCD is a self-inactivating kinase because a pseudosubstrate motif within the N-terminal regulatory domain blocks the substrate binding pocket in the C-terminal catalytic subunit (Zhao, Xia et al. 2012). Downstream signaling of PRKCD can either be enabled by activating its kinase function via tyrosine phosphorylation and subsequent cleavage of the N-terminal regulatory domain or by its translocation to variable cellular compartments (Yoshida 2007). Although PRKCD represents a central pro-apoptotic regulator, specific phosphorylation- and translocation events can also promote survival (Basu and Pal 2010). Tyrosine phosphorylation at Tyr155 and Tyr332 promote translocation of PRKCD to the endoplasmatic reticulum and facilitate resistance against tumor necrosis factor-related apoptosis-inducing ligand (TRAIL) induced cell death (Lu, Lee et al. 2007).

Studies using the *Prkcd*$^{-/-}$ mouse unravel that loss of Prkcd leads to an autonomous expansion of B-lymphocyte populations, abrogated B-cell tolerance and an overall massively decreased apoptotic response (Miyamoto, Nakayama et al. 2002);(Humphries, Limesand et al. 2006). In line with this, variable apoptotic stimuli including irradiation, genotoxic agents and oxidative stress induce the activation of nuclear and mitochondrial apoptosis pathways dependent on PRKCD (Matassa, Carpenter et al. 2001);(Majumder, Mishra et al. 2001);(DeVries-Seimon, Ohm et al. 2007). Upon etoposide treatment, SRC-like tyrosine kinases as well as the DNA damage responsive kinase C-ABL, phosphorylate PRKCD at tyrosines Y64, Y155 and Y187 thereby facilitating its nuclear translocation (Humphries, Ohm et al. 2008);(Blass, Kronfeld et al. 2002). Subsequent to this translocation event, PRKCD gets cleaved by caspase 3, thus leading to accumulation of the catalytic active fragment within the nucleus (DeVries-Seimon, Ohm et al. 2007). Catalytic active PRKCD irreversibly induces apoptosis by inhibiting the DNA double-strand repair molecule DNA-PK, by activating the genotoxin-activated checkpoint signaling component RAD9 and by inducing the cleavage of the nuclear lamina component lamin B (Steinberg 2004);(Bharti, Kraeft et al. 1998);(Yoshida, Wang et al. 2003);(Cross, Griffiths et al. 2000). The

nuclear accumulation of PRKCD is followed by CRM1-mediated nuclear export of PRKCD and its translocation to mitochondria (DeVries-Seimon, Ohm et al. 2007);(Griner and Kazanietz 2007). Active forms of PRKCD at this cellular compartment lead to a decrease of the mitochomdrial membrane potential that is followed by cyctochrome C release from mitochondria and activation of the apoptotic caspase-cascade (Matassa, Carpenter et al. 2001).

In summary, PRKCD represents an apoptosis regulating kinase that is specifically activated by tyrosine phosphorylation, cleavage and translocation processes. Albeit variable nuclear and mitochondrial targets of PRKCD have been described, a conclusive functional role of the timely regulated translocation events remains to be demonstrated.

4 Aim of the study

MCL represents a heterogeneous, genetically unstable tumor entity with overall poor survival. Although molecular based treatments, e.g. proteasomal inhibition, have improved the therapy of MCL, the underlying deregulated cellular signaling pathways are largely unknown.

In search for deregulated UPS components in MCL, analyses of CGH-array data sets identified a frequent monoallelic deletion of the *FBXO25* gene locus on chromosome 8p23.3, whereupon tandem affinity purification based mass spectrometry analysis for FBXO25 interactors indicated the anti-apoptotic molecule HAX1 as potential interactor of the previously orphan SCF^{FBXO25} E3 ligase. Molecular interactions of FBXO25 as well as conditioned ubiquitylation dependent proteasomal degradation events were characterized biochemically using a broad range of *in vivo* and *in vitro* approaches, thus allowing for an insight into the cellular context of FBXO25. Variable cell culture and animal models were further used to elucidate the physiological role of FBXO25 as well as the effect of deregulations of FBXO25 and its interaction partners on B-cell lymphomagenesis and resistance towards chemotherapeutic treatment. The subsequent analyses of comprehensive MCL patient samples validated the loss of control of the FBXO25 axis within malignant human tumors and aimed to link these deregulations to growth and survival advantages of MCL cells. Moreover, the FBXO25-mediated mechanism derived from MCL was identified as novel regulatory hub in the regulation of B-lymphocyte homing and migration.

Data derived from the present study should provide insight into the molecular background of a previously undescribed ubiquitylation dependent pathway in MCL. The deregulated signaling components are thereby presented as novel biomarkers and therapeutic target structures that could lead to an improved treatment of MCL patients.

5 Material and Methods

5.1 Material

5.1.1 Reagents

Reagent	Provided by
2-Mercaptoethanol	Sigma-Aldrich (Cat. No. M3148)
2-Propanol	Carl Roth (Cat. No. 6752.4)
3x FLAG® Peptide	Sigma-Aldrich (Cat. No. F4799)
Acetic acid glacial	Carl Roth (Cat. No. 3738.5)
Acetone	Carl Roth (Cat. No. 9372.4)
Adefodur developer solution	Adefo Chemistry (Cat. No. 00176)
Adefo-Fix fixer solution	Adefo Chemistry (Cat. No. 00103)
Adenosine 5´-triphosphate	Sigma-Aldrich (Cat. No. A7699)
Agarose NEEO	Carl Roth (Cat. No. 2267.4)
Albumin Fraction V	Carl Roth (Cat. No. 8076.3)
Ammonium persulfat	Sigma Aldrich (Cat. No. 215589)
Ampicillin sodium salt	Sigma-Aldrich (Cat. No. A9518)
Anti-FLAG® M2 Affinity Gel	Sigma-Aldrich (Cat. No. A2220)
Anti-HA Affinity Matrix	Roche (Cat. No. 11815016001)
Aprotinin from bovine lung	Sigma-Aldrich (Cat. No. A1153)
Aqua	B. Braun Melsungen (Cat. No. 0082479E)
Bacto™ Agar	BD (Cat. No. 214010)
Bacto™ Tryptone	BD (Cat. No. 211699)
Bacto™ Yeast Extract	BD (Cat. No. 212750)
BES buffered saline	Sigma-Aldrich (Cat. No. 14280)

Beta-Glycerolphosphate disodium salt hydrate	Sigma-Aldrich (Cat. No. G6376)
Boric acid	Sigma-Aldrich (Cat. No. B7901)
Brilliant Blue R 250	Carl Roth (Cat. No. 3862.1)
Bromphenol Blue	Sigma-Aldrich/Fluka (Cat. No. 18030)
Calcium chloride dihydrate	Sigma-Aldrich (Cat. No. C7902)
Ciprofloxacin	Sigma-Aldrich (Cat. No. PHR1167)
Cycloheximide	Sigma-Aldrich (Cat. No. C7698)
Deoxycholic acid sodium salt	Sigma-Aldrich/Fluka (Cat. No. 30970)
Dimethylsulfoxid	Carl Roth (Cat. No. 4720.2)
Di-Sodium hydrogene phosphate dihydrate	Merck (Cat. No. 1.06580)
DL-Dithiothreitol	Sigma-Aldrich (Cat. No. D0632)
DNA Loading Dye (6x)	ThermoFisher Scientific (Cat. No R0611)
dNTP Mix, 10 mM each	ThermoFisher Scientific (Cat. No R0192)
Dodecylsulfate-Na-salt (in pellets)	SERVA (Cat. No. 20765.03)
Ethanol	Merck (Cat. No. 1.00983)
Ethidium bromide solution	Sigma-Aldrich (Cat. No. E1385)
Ethylenediaminetetraacetic acid	Sigma-Aldrich/Fluka (Cat. No. 03609)
Ethylenediaminetetraacetic acid disodium salt solution	Sigma-Aldrich (Cat. No. E7889)
Etoposide	Sigma-Aldrich (Cat. No. E1383)
FACS Flow	BD (Cat. No. 342003)
Fluoride ion solution (NaF)	Sigma-Aldrich (Cat. No. 47072)
Gelatin, from porcine skin	Sigma-Aldrich (Cat. No. G2500)
GelRed Nucleic Acid Gel Stain	Biotium (Cat. No. 41003)
Glucose	Sigma-Aldrich (Cat. No. G7528)
Glutathione Sepharose™ 4B	GE Healthcare (Cat. No. 17-0756-01)
Glycerol	Sigma-Aldrich (Cat. No. 49767)

Glycin	Carl Roth (Cat. No. 3908.3)
Goat serum	Sigma-Aldrich (Cat. No. G9023)
Hexadimethrine bromide (polybrene)	Sigma-Aldrich (Cat. No. H9268)
Hexanucleotide Mix, 10x conc.	Roche (Cat. No. 11277081001)
Hydrochloric acid 32%	Carl Roth (Cat. No. P074.4)
Hydrochloric acid fuming 37%	Carl Roth (Cat. No. 2607.1)
Imidazole	Sigma-Aldrich (Cat. No. I0125)
Isopropyl β-D-1-thiogalactopyranoside	Sigma-Aldrich (Cat. No. I6758)
Kanamycin sulfate	Sigma-Aldrich (Cat. No. 60615)
Leupeptin	Sigma-Aldrich (Cat. No. L2884)
L-Glutathione reduced	Sigma-Aldrich (Cat. No. G4251)
Lysozyme from chicken egg white	Sigma-Aldrich (Cat. No. L3790)
Magnesium chloride anhydrous	Sigma-Aldrich (Cat. No. M8266)
Magnesium sulfate anhydrous	Sigma-Aldrich (Cat. No. M7506)
Methanol	J. T. Baker (Cat. No. 8045)
N-(2-Hydroxyethyl)piperazine-N`-2-ethane sulfonic acid	SERVA (Cat. No. 25245.04)
Nα-Tosyl-L-lysine chloromethyl ketone hydrochloride	Sigma-Aldrich (Cat. No. T7254)
Ni-NTA Agarose	Qiagen (Cat. No. 1018244)
N,N,N`,N``-tetramethyl-ethylenediamine	Sigma-Aldrich (Cat. No. T7024)
N-p-Tosyl-L-phenylalanine chloromethyl ketone	Sigma-Aldrich (Cat. No. T4376)
Nonidet P-40 substitute (10%)	Roche (Cat. No. 11332473001)
NuPAGE® MES SDS Running buffer (20x)	ThermoFisher Scientific (Cat. No. NP0002)
Okadaic Acid *Prorocentrum sp.*	Calbiochemi (Cat. No. 495604)
Paclitaxel	Sigma-Aldrich (Cat. No. T7191)
Paraformaldehyde, powder	Sigma-Aldrich (Cat. No. 158127)

PBS Dulbecco, powder	Biochrom (Cat. No. L182-10)
Phenylmethanesulfonylfluoride solution	Sigma-Aldrich (Cat. No. 93482)
Ponceau S solution	Sigma-Aldrich (Cat. No. 7170)
Potassium chloride	Sigma-Aldrich/Fluka (Cat. No. 60129)
ProLong® Gold antifade reagent with DAPI	ThermoFisher Scientific (Cat. No. P36935)
Propidium iodide	Sigma-Aldrich (Cat. No. P4170)
Protein A Sepharose™ CL-4B	GE Healthcare (Cat. No. 17-0963-03)
Protein G Agarose, Fast Flow	Sigma-Aldrich (Cat. No. P4691)
Protein G Sepharose™ 4 Fast Flow	GE Healthcare (Cat. No. 17-0618-01)
Puromycin	ThermoFisher Scientific (Cat. No. A1113803)
Rotiphorese® NF-Acrylamide/Bis-solution 40% (29:1)	Carl Roth (Cat. No. A121.1)
Rottlerin	Calbiochem (Cat. No. 557370)
Silver nitrate	Sigma-Aldrich (Cat. No. 20,913-9)
Skim Milk Power	Sigma-Aldrich (Cat. No. 70166)
Sodium acetate	Merck (Cat. No. 1.06268)
Sodium azide	Merck (Cat. No. 1.06688)
Sodium carbonate	Merck (Cat. No. 1.06392)
Sodium chloride	Carl Roth (Cat. No. 3957)
Sodium dihydrogen phosphate monohydrate	Merck (Cat. No. 1.06346)
Sodium fluoride	Sigma-Aldrich (Cat. No. 71519)
Sodium hydroxide solution 45%	Carl Roth (Cat. No. 0993.2)
Sodium orthovanadate	Sigma-Aldrich (Cat. No. S6508)
Sodium phosphate dibasic	Sigma-Aldrich (Cat. No. S7907)
Strep-Tactin® Superflow®	Iba (Cat. No. 2-1206-025)
Strep-tag® elution buffer	Iba (Cat. No. 2-1000-025)

Trichloroacetic acid solution	Sigma-Aldrich/Fluka (Cat. No. 91240)
TRIS	Carl Roth (Cat. No. 5429.2)
Triton™ X-100	Sigma-Aldrich (Cat. No. T8787)
Trypsin inhibitor from soybean	Sigma-Aldrich (Cat. No. T9003)
TWEEN® 20	Sigma-Aldrich (Cat. No. 93773)
UltraPure™ TBE buffer (10x)	ThermoFisher Scientific (Cat. No. 15581)
Water	Sigma-Aldrich (Cat. No. W3500)
Xylene cyanol	Sigma-Aldrich (Cat. No. X4126)

5.1.2 Antibodies

5.1.2.1 List of commercial available primary antibodies

Antibody (clone)	**Source**	**Company**	**Catalog#**	**Application (dilution)**
α/β-tubulin	rabbit; polyclonal	Cell Signaling Technology	2148	WB (1:1000)
B220 (RA3-6B2)	rat; monoclonal	Affymetrix	14-0452	IHC
Caspase-3 (8G10)	rabbit; monoclonal	Cell Signaling Technology	9665	WB (1:1000)
CD20 (EP459Y)	rabbit; monoclonal	Abcam	ab78237	IHC
CD45/B220 (30-F11)	rat; monoclonal	BD Biosciences	561869	FACS
Cleaved caspase-3 (Asp175)	rabbit; polyclonal	Cell Signaling Technology	9661	IHC
Cleaved caspase-3 (5A1E)	rabbit; monoclonal	Cell Signaling Technology	9664	WB (1:1000)
CUL-1 (2H4C9)	mouse; monoclonal	ThermoFisher Scientific	32-2400	WB (1:500)

CXCR4 (12G5)	mouse; monoclonal	BD Pharmingen	555972	FACS
CXCR4 (UMB2)	rabbit; monoclonal	Abcam	ab124824	WB (1:1000)
CXCR4 Lot: GR69382-5	rabbit; polyclonal	Abcam	ab2074	WB (1:1000)
Cytochrome C (7H8.2C12)	mouse; monoclonal	Abcam	ab13575	WB (1:1000)
FBXO25	rabbit; polyclonal	Sigma-Aldrich	AV43118	IHC
FLAG	rabbit; polyclonal	Sigma-Aldrich	F7425	WB (1:1000); IF
FLAG-M2 (M2)	mouse; monoclonal	Sigma-Aldrich	F3165	WB (1:1000); IF
GFP	rabbit; polyclonal	Novus Biologicals	NB600-303	WB (1:2000)
GST (B-14)	mouse; monoclonal	Santa Cruz Biotechnology	sc-138	WB (1:1000)
HA	rabbit; polyclonal	Santa Cruz Biotechnology	sc-805	WB (1:1000)
HA.11 (16B12)	mouse; monoclonal	Covance	MMS-101P	WB (1:1000); IF
HAX1 (52)	mouse; monoclonal	BD Transduction Laboratories	610825	WB (1:500)
HAX1	rabbit; polyclonal	Proteintech Group	11266-1-AP	IHC
Ki-67 (D3B5)	rabbit; monoclonal	Cell Signaling Technology	12202	IHC
p44/42 MAPK (ERK1/2)	rabbit; polyclonal	Cell Signaling Technology	9102	WB (1:1000)
p53	rabbit polyclonal	Cell Signaling Technology	9282	WB (1:1000)
P-p44/42 MAPK (pERK1/2) (T202/Y204)	rabbit; polyclonal	Cell Signaling Technology	9101	WB (1:1000)
PRKCD (D10E2)	rabbit; monoclonal	Cell Signaling Technology	9616	WB (1:1000)
SKP11 p19	rabbit; polyclonal	Santa Cruz Biotechnology	sc-7163	WB (1:500)
Ubiquitin (FK2)	mouse; monoclonal	Enzo	BML-PW8810	WB (1:1000)

5.1.2.2 List of peptides used for production of custom made primary antibodies

All custom made antibodies were produced with Innovagen, Sweden.

Antibody	Peptide sequence (NH_2-aa-$CONH_2$)	Protein coverage (aa)	Company
FBXO25	CGEIFNNEEHEYASK	52-65	Innovagen
FBXO25 pS178	CKDLLQDLS(pS)TL	170-180	Innovagen
HAX1 pS210	CPKSYFK(pS)ISVTKI	204-216	Innovagen

5.1.2.3 List of secondary antibodies

Antibody (clone)	Source	Company	Catalog#	Application (dilution)
Alexa Fluor® 488 anti-mouse IgG	goat	Life Technologies	A11001	IF (1:2000); FACS (1:2000)
Alexa Fluor® 594 anti-mouse IgG	goat	Life Technologies	A11005	IF (1:2000)
Alexa Fluor® 488 anti-rabbit IgG	goat	Life Technologies	A11008	IF (1:2000)
Alexa Fluor® 594 anti-rabbit IgG	goat	Life Technologies	A11012	IF (1:2000)
ECLTM Anti-Mouse IgG, Horseradish Peroxidase linked	sheep	GE Healthcare UK	NA931V	WB (1:5000)
ECLTM Anti-Rabbit IgG, Horseradish Peroxidase linked	donkey	GE Healthcare UK	NA934V	WB (1:5000)
Protein A, Horseradish Peroxidase linked		GE Healthcare UK	NA9120V	WB (1:5000)

5.1.3 Plasmids

Sequences of all plasmids were verified by sequencing reactions using corresponding primers (sequencing performed by Eurofins Genomics, Ebersberg, Germany).

Plasmid	Backbone	Insert	Bacterial Resistance	Cloned/ provided by
gag/pol	not provided	gag/pol	Amp	Tannishtha Reya (Reya, Duncan et al. 2003); addgene #14887
N-SF-TAP-pcDNA3	pcDNA™3.0		Amp	M.Ueffing (Gloeckner, Boldt et al. 2007)
N-SF-TAP-pcDNA3-hCXCR4	pcDNA™3.0	hCXCR4	Amp	U.Baumann; present study
N-SF-TAP-pcDNA3-hCXCR4(R334X)	pcDNA™3.0	hCXCR4(S334X)	Amp	U.Baumann; present study
N-SF-TAP-pcDNA3-hCXCR4(S339fs342X)	pcDNA™3.0	hCXCR4(S339fs342X)	Amp	U.Baumann; present study
N-SF-TAP-pcDNA3-hCXCR4(E343X)	pcDNA™3.0	hCXCR4(E343X)	Amp	U.Baumann; present study
N-SF-TAP-pcDNA3-hFBXO25	pcDNA™3.0	hFBXO25	Amp	U.Baumann (Baumann 2011)
N-SF-TAP-pcDNA3-hFBXO25(S178A)	pcDNA™3.0	hFBXO25_S178A	Amp	U.Baumann; present study
N-SF-TAP-pcDNA3-PRKCD	pcDNA™3.0	PRKCD	Amp	U.Baumann; present study
pBacPAK9	pBacPAK9		Amp	Clontech Laboratories
pBacPAK9-FBXO25	pBacPAK9	hFBXO25	Amp	Ursula Baumann; present study
pcDNA3-FLAG-Hax1	pcDNA™3.0	FLAG-Hax1	Amp	James N. Ihle; unpublished
pcDNA3-FLAG-Hax1(1-123)	pcDNA™3.0	FLAG-Hax1 (1-123)	Amp	James N. Ihle; unpublished
pcDNA3-FLAG-Hax1(1-200)	pcDNA™3.0	FLAG-Hax1 (1-200)	Amp	James N. Ihle; unpublished
pcDNA3-FLAG-Hax1(123-200)	pcDNA™3.0	FLAG-Hax1 (123-200)	Amp	James N. Ihle; unpublished

pcDNA3-FLAG-Hax1(124-279)	pcDNA™3.0	FLAG-Hax1 (124-279)	Amp	James N. Ihle ; unpublished
pcDNA3-FLAG-Hax1(201-280)	pcDNA™3.0	FLAG-Hax1 (201-280)	Amp	James N. Ihle; unpublished
pcDNA3-HA-ubiquitin	pcDNA™3.0	HA-ubiquitin	Amp	Edward T. Yeh (Kamitani, Kito et al. 1997); (addgene #18712)
pcDNA3-Hax1-c2xHA	pcDNA™3.0	Hax1WT-c2xHA	Amp	James N. Ihle (Chao, Parganas et al. 2008)
pcDNA3-Hax1(d1-39)-c2xHA	pcDNA™3.0	Hax1(d1-39)-c2xHA	Amp	James N. Ihle (Chao, Parganas et al. 2008)
pcDNA3-Hax1(d73-100)-c2xHA	pcDNA™3.0	Hax1(d73-100)-c2xHA	Amp	James N. Ihle (Chao, Parganas et al. 2008)
pcDNA3-Hax1(dPEST)-c2xHA	pcDNA™3.0	Hax1(dPEST)-c2xHA	Amp	James N. Ihle (Chao, Parganas et al. 2008)
pcDNA3-Hax1(d129-172)-c2xHA	pcDNA™3.0	Hax1(d129-172)-c2xHA	Amp	James N. Ihle (Chao, Parganas et al. 2008)
pcDNA3-Hax1(d183-235)-c2xHA	pcDNA™3.0	Hax1(d183-235-c2xHA	Amp	James N. Ihle (Chao, Parganas et al. 2008)
pcDNA3-gag-pol	pcDNA™3.0	gag-pol	Amp	Tannishtha Reya (Reya, Duncan et al. 2003); (addgene #14887)
pcDNA3.1 (+) zeo	pcDNA™3.1(+)		Amp	ThermoFisher Scientific
pcDNA3.1-FLAG	pcDNA™3.1	FLAG	Amp	Florian Bassermann
pcDNA3.1-FLAG-FBXO11	pcDNA™3.1	FLAG-FBXO11	Amp	Michele Pagano (Duan, Cermak et al. 2012)
pcDNA3.1-FLAG-FBXO18	pcDNA™3.1	FLAG-FBXO18	Amp	Michele Pagano; unpublished
pcDNA3.1-FLAG-FBXO21	pcDNA™3.1	FLAG-FBXO21	Amp	Michele Pagano; unpublished

pcDNA3.1-HA	pcDNA™3.1	HA	Amp	Florian Bassermann
pcDNA3.1-FLAG-HAX1(S192A)	pcDNA™3.1	FLAG-hHAX1 (S192A)	Amp	Ursula Baumann; present study
pcDNA3.1-FLAG-HAX1(S206A)	pcDNA™3.1	FLAG-hHAX1 (S206A)	Amp	Ursula Baumann; present study
pcDNA3.1-FLAG-HAX1(S210A)	pcDNA™3.1	FLAG-hHAX1 (S210A)	Amp	Vanesa Fernández-Sáiz
pcDNA3.1-FLAG-HAX1(S212A)	pcDNA™3.1	FLAG-hHAX1 (S212A)	Amp	Ursula Baumann; present study
pcDNA4-hFbxo25-ORF1-V5	pcDNA™4/V5	hFBXO25-ORF1	Amp	V.Kalscheuer (Hagens, Minina et al. 2006)
pCMV3-hCXCR4	pCMV3	hCXCR4	Amp	Sino Biologicals (HG11325_M)
pEGFP-C3	pEGFP-C3		Kana	Clontech Laboratories
pEGFP-C3-FBXO25	pEGFP-C3	hFBXO25	Kana	Ursula Baumann; present study
pEGFP-C3-FBXO25(S177/178A)	pEGFP-C3	hFBXO25	Kana	Vanesa Fernández-Sáiz
pEGFP-C3-FBXO25(S178A)	pEGFP-C3	hFBXO25	Kana	Ursula Baumann; present study
pGEX-4T-2	pGEX-4T-2		Amp	GE Healthcare Life Sciences
pGEX-4T-2-FBXO25	pGEX-4T-2	hFBXO25	Amp	Ursula Baumann; present study
pGEX-4T-2-FBXO25(S178A)	pGEX-4T-2	hFBXO25_S178A	Amp	Ursula Baumann; present study
pGEX-4T-2-HAX1	pGEX-4T-2	hHAX1	Amp	Ursula Baumann; present study
pGEX-4T-2-HAX1(S210A)	pGEX-4T-2	hHAX1(S210A)	Amp	Ursula Baumann; present study
pGEX-4T-2-HAX1(200-230)	pGEX-4T-2	hHAX1(200-230)	Amp	Ursula Baumann; present study
pGEX-4T-2-HAX1(200-279)	pGEX-4T-2	hHAX1(200-279)	Amp	Ursula Baumann; present study
pGEX-4T-2-HAX1(230-250)	pGEX-4T-2	hHAX1(230-250)	Amp	Ursula Baumann; present study

pGEX-4T-2-HAX1(250-279)	pGEX-4T-2	hHAX1(250-279)	Amp	Ursula Baumann; present study
pHACE-PKC delta	pHACE	mPKC delta WT	Amp	Bernard Weinstein (Soh and Weinstein 2003); (addgene #16386)
pHACE-PKC epsilon	pHACE	mPKC epsilon	Amp	Bernard Weinstein (Soh and Weinstein 2003); (addgene #21240)
pHACE-PKC eta	pHACE	mPKC eta	Amp	Bernard Weinstein (Soh and Weinstein 2003); (addgene #21244)
pHACE-PKC gamma	pHACE	mPKC gamma WT	Amp	Bernard Weinstein (Soh and Weinstein 2003); (addgene #21236)
pLKO.1_puro	pLKO.1		Amp	Stewart SA. (Stewart, Dykxhoorn et al. 2003); (addgene #8453)
pLKO.1_RFP	pLKO.1		Amp	Ruth Eichner (Eichner, Heider et al. 2016); (derived from addgene #8453)
pLKO.1_RFP_ shHAX1_1	pLKO.1	shHAX1_1	Amp	Ursula Baumann; present study
pLKO.1_RFP_ shHAX1_2	pLKO.1	shHAX1_2	Amp	Ursula Baumann; present study
pLPC_puro	pLPC	FLAG	Amp	Titia de Lange (Dimitrova, Chen et al. 2008); unpublished (derived from addgene #19836)

pLPC_HAX1	pLPC-N-FLAG	hHAX1 WT	Amp	Ursula Baumann; present study
pLPC_HAX1_ S210A	pLPC-N-FLAG	hHAX1 S210A	Amp	Ursula Baumann; present study
pLPC-N-FLAG	pLPC	FLAG	Amp	Titia de Lange; unpublished (addgene #12521)
pLPC-N-FLAG-HAX1	pLPC-N-FLAG	hHAX-1 WT	Amp	Ursula Baumann; present study
pMD2.G	pMD2.G		Amp	Didier Trono; unpublished (addgene #12259)
pMigR1	pMSCV		Amp	Warren S. Pear(Pear, Miller et al. 1998); (addgene #27490)
pMigR1-FBXO25	pMigR1	hFBXO25	Amp	Ursula Baumann; present study
pMigR1-FBXO25(S178A)	pMigR1	hFBXO25_S178A	Amp	Ursula Baumann; present study
pMigR1-FLAG-FBXO25	pMigR1	FLAG-hFBXO25	Amp	Ursula Baumann; present study
pMigR1-FLAG-HAX1	pMigR1	FLAG-hHAX1	Amp	Ursula Baumann; present study
pMigR1-FLAG-HAX1(S206A)	pMigR1	FLAG-hHAX1(S206A)	Amp	Ursula Baumann; present study
pMigR1-FLAG-HAX1(S210A)	pMigR1	FLAG-hHAX1(S210A)	Amp	Ursula Baumann; present study
pMigR1-FLAG-HAX1(S212A)	pMigR1	FLAG-hHAX1(S212A)	Amp	Ursula Baumann; present study
pMigR1-HAX1	pMigR1	hHAX1 WT	Amp	Ursula Baumann; present study
pMigR1-HAX1(S206A)	pMigR1	hHAX1(S206A)	Amp	Ursula Baumann; present study
pMigR1-HAX1(S210A)	pMigR1	hHAX1(S210A)	Amp	Ursula Baumann; present study
pMigR1-HAX1(S212A)	pMigR1	hHAX1(S212A)	Amp	Ursula Baumann; present study
pMigR1-Hax1	pMigR1	mHax1 WT	Amp	Ursula Baumann; present study

pMigR1-PRKCD	pMigR1	PRKCD	Amp	Ursula Baumann; present study
pMLS	pMSCV-LTRmiR30-SV40GFP		Amp	Scott W. Lowe (Dickins, Hemann et al. 2005)
pMLS-sh710Fbxo25	pMLS	shFbxo25 (#710)	Amp	Cornelius Miething (Scuoppo, Miething et al. 2012)
pMLS-sh1524Fbxo25	pMLS	shFbxo25 (#1524)	Amp	Cornelius Miething (Scuoppo, Miething et al. 2012)
pMLS-sh1565Fbxo25	pMLS	shFbxo25 (#1565)	Amp	Cornelius Miething (Scuoppo, Miething et al. 2012)
pMSCV_puro	pMSCV		Amp	Clontech Laboratories
pMSCV-FBXO25	pMSCV-puro	hFBXO25	Amp	Ursula Baumann (Baumann 2011)
psPAX2	psPAX2		Amp	Didier Trono; unpublished (addgene #12260)
pWZL-Neo-Myr-FLAG-PRKCD	pWZL-Neo-Myr-FLAG-DEST	hPRKCD	Amp	William Hahn (Boehm, Zhao et al. 2007); (addgene #20603
VSV.G	pCl	VSV.G envelope	Amp	Tannishtha Reya (Reya, Duncan et al. 2003); (addgene #14888)

5.1.4 Oligonucleotides

All oligonucleotides were synthesized with Eurofins Genomics, Ebersberg, Germany.

5.1.4.1 List of oligonucleotides used for cloning

Primer	Sequence (5`-x-3`)
CXCR4_NheI_fw	5`-GCCGCTAGCTCCATTCCTTTGCCTCTTTTGCAG-3`
CXCR4_XhoI_rv	5`-GCCCTCGAGTTAGCTGGAGTGAAAACTTGAAG-3`
CXCR4_R334X_fw	5`-CTCTCCAAAGGAAAGTGAGGTGGACATTCATC-3`
CXCR4_R334X_rv	5`-GATGAATGTCCACCTCACTTTCCTTTGGAGAG-3`
CXCR4_S339fs342X_fw	5`-GGTGGACATTCATGTTTCCACTGAG-3`
CXCR4_S339fs342X_rv	5`-CTCAGTGGAAACATGAATGTCCACC-3`
CXCR4_E343X_fw	5`-CATCTGTTTCCACTTAGTCTGAGTCTTC-3`
CXCR4_E343X_rv	5`-GAAGACTCAGACTAAGTGGAAACAGATG-3`
FBXO25_BamHI_fw	5`-CCTGGATCCCCATTTTTGGGTCAGGACTGG-3`
FBXO25_BamHI_rv	5`-GGTGGATCCTTAAAACTTGAAGAGGTCGATGAAGTGC TGCGG-3`
FBXO25_EcoRI_rv	5`-GGTGAATTCTTAAAACTTGAAGAGGTCGATGAAGTGCT GCGG-3`
FBXO25_FLAG_BamHI _fw	5`-CAAGGATCCTAGCCACCATGGATTATAAAGATGATGAT GATAAAGGCCCATTTTTGGGTCAGGACTGG-3`
FBXO25_FLAG_XhoI_ fw	5`-CAACTCGAGTAGCCACCATGGATTATAAAGATGATGAT GATAAAGGCCCATTTTTGGGTCAGGACTGG-3`
FBXO25_HA_NheI_fw	5`-CCTGCTAGCGCCACCATGTACCCCTACGACGTGCCCG ACTACGCCCCATTTTTGGGTCAGGACTGG-3`
FBXO25_NES_S178A_ fw	5`-CTTCTGCAAGACCTAAGCGCTACCCTCTGCATTC-3`
FBXO25_NES_S178A_ rv	5`-GAATGCAGAGGGTAGCGCTTAGGTCTTGCAGAAG-3`
FBXO25_NheI_ATG_fw	5`-CCTGCTAGCATGCCATTTTTGGGTCAGGACTGG-3`
FBXO25_NheI_fw	5`-CCTGCTAGCCCATTTTTGGGTCAGGACTGG-3`
FBXO25_SalI_rv	5`-GGTGTCGACTTAAAACTTGAAGAGGTCGATGAAGTGCT GCGG-3`
FBXO25_XhoI_rv	5`GGACTCGAGTTAAAACTTGAAGAGGTCGATGAAGTGCTGC GG-3`
FBXO25_XhoI_ATG_fw	5`-CCGCTCGAGGCCACCATGCCATTTTTGGGTAGGACT GG-3`
FBXO25_XhoI_fw	5`-GGCCTCGAGCCATTTTTGGGTCAGGACTGG-3`

HAX1_200-230_rv	5`-GGACTCGAGCACCACAGTCCGGCGCTCCTCC-3`
HAX1_200-279_fw	5`-CCTGGATCCCTACAGCCCCAGCCCAAATCCTA-3`
HAX1_200-279_rv	5`-GGACTCGAGCTACCGGGACCGGAACCAACG-3`
HAX1_230-250_fw	5`-CCTGGATCCGTGGACAGTGAGGGCCGGACAG-3`
HAX1_230-250_rv	5`-GGACTCGAGCCTAGGACTGCTATCTGCTTCG-3`
HAX1_250-279_fw	5`CCTGGATCCAGGGGTGATCCAGAATCACCAAGACC-3`
HAX1_BamHI_ATG_fw	5`-CAAGGATCCATGAGCGTCTTTGATCTTTTCCGA-3`
HAX1_BamHI_fw	5`-GGCGGATCCAGCCTCTTTGATCTCTTCCGGGGC-3`
HAX1_EcoRI_rv	5`-GGCGAATTCCTACCGGGACCGGAACCAACG-3`
HAX1_HindIII_rv	5`-GGTAAGCTTCTATCGGGACCGAAACCAACGTCC-3`
HAX1_KspAI_fw	5`-GGTGTTAACCTATCGGGACCGAAACCAACGTCC-3`
HAX1_NotI_fw	5`-CAAGGCGGCCGCGCCACCATGAGCGTCTTTGATCTTTT CCG-3`
HAX1_NotI_rv	5`-GGCGGCGGCCGCCTACCGGGACCGGAACCAACG-3`
HAX1_S192A_fw	5`-CTTGATTCCCAGGTTGCCCAGGAGGGTCTTG-3`
HAX1_S192A_rv	5`-CAAGACCCTCCTGGGCAACCTGGGAATCAAG-3`
HAX1_S206A_fw	5`-GCCCCAGCCCAAAGCCTATTTCAAGAG-3`
HAX1_S206A_rv	5`-CTCTTGAAATAGGCTTTGGGCTGGGGC-3`
HAX1_S210A_fw	5`-CCCAAATCCTATTTCAAGGCCATCTCTGTGACCAAGATC AC-3`
HAX1_S210A_rv	5`-GTGATCTTGGTCACAGAGATGGCCTTGAAATAGGATTTG GG -3`
HAX1_S212A_fw	5`-CTATTTCAAGAGCATCGCTGTGACCAAGATCAC-3`
HAX1_S212A_rv	5`-GTGATCTTGGTCACAGCGATGCTCTTGAAAATAG-3`
mFbxo25_HindIII_fw	5`-CAAAAGCTTGCCACCATGCCATTTTTGGGTAGGATCGG-3`
mFbxo25_NotI_rv	5`-GGTGGCGGCCGCTCAGAACTTGAAGAGGTCGATGAAG TGCTGCGG-3`
mHax1_HindIII_fw	5`-CAAAAGCTTGCCACCATGAGCGTCTTTGATCTTTTCCG-3`
mHax1_NotI_rv	5`-GGTGGCGGCCGCCTATCGGGACCGAAACCAACGTCC-3`
patientHAX1_BglII_fw	5`-GCCAGATCTATGGACCCCATCCTAGAAC-3`
patientHAX1_EcoRI_rv	5`-GCCGAATTCCTCACTGTCCACCACAGTCC-3`
patientHAX1_EcoRV_fw	5`-GCCGATATCATGGACCCCCATCCTAGAAC-3`
patientHAX1_EcoRV_rv	5`-GCCGATATCCTCACTGTCCACCACAGTCC-3`

5.1.4.2 List of oligonucleotides used for sequencing

Primer	Sequence (5`-x-3`)
CMVfor	5`-CGCAAATGGGCGGTAGGCGTG-3`
MSCV-MCS-5	5`-CGTTCGACCCCGCCTCGATCC-3`
pBacPAK_fw	5`-ACCATCTCGCAAATAAATAAG-3`
pBacPAK_rv	5`-ACAACGCACAGAATCTAGCG-3`
pEGFP_fw	5`-GCAGAGCTGGTTTAGTGAAC-3`
pEGFP_rv	5`-CGTCGCCGTCCAGCTCGACCAG-3`
pGEX for	5`-ATAGCATGGCCTTTGCAGG-3?
pGEX_fw	5`-GGGCTGGCAAGCCACGTTTGGTG-3`
pGEX_rv	5`-CCGGGAGCTGCATGTGTCAGAGG-3`
pLKO1	5`-GACTATCATATGCTTACCGT-3`
pLPC_fw	5`-TAGGCGTGTACGGTGGGA-3`
pLPC_rv	5`-CTTGCCAAACCTACAGGT-3``
pMSCV_5`	5`-CCCTTGAACCTCCTCGTTCGACC-3`
pMSCV_3`	5`-GAGACGTGCTACTTCCATTTGTC-3`
T7(fw)	5`-TAATACGACTCACTATAGGG-3`

5.1.4.3 List of oligonucleotides for quantitative PCR

Primer	Sequence (5`-x-3`)
*ACTB*_MCLpatient_fw	5`-AGGTGCACAGTAGGTCTGAACAGA-3`
*ACTB*_MCLpatient_rv	5`-AAGTGCAAAGAACACGGCTAAGT-3`
*ARPP_P0*_fw	5`-GCACTGGAAGTCCAACTACTTC-3`
*ARPP_P0*_rv	5`-TGAGGTCCTCCTTGGTGAACAC-3`
*Cxcr4*_1_fw	5`-AGCATCGTGCACAAGTGGATCTC-3`
*Cxcr4*_1_rv	5`-TCAGGCAACAGTGGAAGAAGGC-3`
*Cxcr4*_2_fw	5`-TCAGTGGCTGACCTCCTCTT-3`(Aboumrad, Madec et al. 2007)
*Cxcr4*_2_rv	5`-CTTGGCCTTTGACTGTTGGT-3`(Aboumrad, Madec et al. 2007)
*CXCR4*_fw	5`-TCCTGGCTTTCTTCGCCTGTTG-3`
*CXCR4*_rv	5`-AGGAGGATGAAGGAGTCGATGC-3`
*FBXO25*_fw	5`-TGAGTGTGAATACGCAGCC-3`
*FBXO25*_rv	5`-GCCTTTCCTTTGTGCTTTCC-3`
*FBXO25*_MCLpatient_fw	5`-GTTGCTGTTGTGTTTTCCTTTC-3`
*FBXO25*_MCLpatient_rv	5`-GAGACTGCTGCATCCCACT-3`

*GAPDH*_fw	5`-GAAGGTGAAGGTCGGAGTC -3`
*GAPDH*_rv	5`-GAAGATGGTGATGGGATTTC -3`

5.1.4.4 List of amplification-/sequencing-oligonucleotides for human patient samples

Primer	**Sequence (5`-x-3`)**
*FBXO25*_exon4_fw	5`-GCTCAGCTTTTTTCCGTCTT-3`
*FBXO25*_exon4_rv	5`-CTCCTTGCACCAAATTTCTAA-3`
*FBXO25*_exon5-partA_fw	5`-TGTTGCTTAACTGTATCAATCCAT-3`
*FBXO25*_exon5-partA_rv	5`-GCCAGGCGAGAATAGTTTCTAA-3`
*FBXO25*_exon5-partB_fw	5`-CTGCAAGACCTAAGCTCTACCC-3`
*FBXO25*_exon5-partB_rv	5`-GAGTGTAATAACTCTTATGCCGAGAT-3`
*FBXO25*_exon6_fw	5`-GTTGCTGTTGTGTTTTCCTTTC-3`
*FBXO25*_exon6_rv	5`-GAGACTGCTGCATCCCACT-3``
*FBXO25*_exon7-partA_fw	5`-TCGGGATTCTGAATGGAGTT-3`
*FBXO25*_exon7-partA_rv	5`-CTGCAGTGCCGACAGAAAT-3`
*FBXO25*_exon7-partB_fw	5`-CATTTGATCCTTTCAGAAAAAGGT-3`
*FBXO25*_exon7-partB_rv	5`-TGTTTCACCAAAATTTAATCCTGA-3`
*FBXO25*_exon8_fw	5`-CTAGAGTGTGGCTGGTGGTG-3`
*FBXO25*_exon8_rv	5`-GCACAGACAGCAGGATTCAC-3`
*HAX1*_exon5_fw	5`-ATGGACCCCCATCCTAGAAC-3`
*HAX1*_exon5_rv	5`-CTCACTGTCCACCACAGTCC-3`

5.1.5 Sequences of shRNAs

ShRNA mediated silencing of human *FBXO25* and human *PRKCD* was performed using SMARTvector 2.0 lentiviral particles obtained from ThermoFisher/Dharmacon. ShRNA mediated silencing of murine *Fbxo25* was based on retroviral pMLS-constructs provided by Cornelius Miething (Scuoppo, Miething et al. 2012). Silencing of human *HAX1* gene expression was based on lentiviral pLKO.1-constructs (Moffat, Grueneberg et al. 2006). All shRNA sequences are listed below.

Name	**Sequence (5`-x-3`)**	**Provided by**
*FBXO25*_01	5`-CCGGTATAGGATGTTGTTC-3`	ThermoFisher/Dharmacon (Cat. No. SH-019192-01)

*FBXO25*_02	5`-TCGGCAAATCCAAATATTG-3`	ThermoFisher/Dharmacon (Cat. No. SH-019192-02)
*FBXO25*_03	5`-CCTTCGCTGGGTAATGTTT-3`	ThermoFisher/Dharmacon (Cat. No. SH-019192-03)
Fbxo25(sh710)	5`-CCCAGGTGACAAAGCAGGTAA ATAGTGAAGCCACAGATGTATTTAC CTGCTTTGTCACCTGGATG-3`	Cornelius Miething (Scuoppo, Miething et al. 2012)
Fbxo25(sh1524)	5`-ATACAGTAATTGGGATGAAGAAT AGTGAAGCCACAGATGTATTCTTC ATCCCAATTACTGTAGT-3`	Cornelius Miething (Scuoppo, Miething et al. 2012)
Fbxo25(sh1565)	5`-CTACATTATGCAGAATATTTATT AGTGAAGCCACAGATGTAATAAAT ATTCTGCATAATGTATT-3`	Cornelius Miething (Scuoppo, Miething et al. 2012)
*HAX1*_1_pLKO.1_fw	5`-CCGGAACAGCCCAAATCCTATT TCACTCGAGTGAAATAGGATTTGG GCTGTTTTTTTG-3`	Ursula Baumann; present study
*HAX1*_1_pLKO.1_rv	5`-AATTCAAAAAAACAGCCCAAATC CTATTTCACTCGAGTGAAATAGGAT TTGGGCTGTT-3`	Ursula Baumann; present study
*HAX1*_2_pLKO.1_fw	5`-CCGGAATCAAGATCATTGTCCT CTCCTCGAGGAGAGGACAATGATC TTGATTTTTTTG-3`	Ursula Baumann; present study
*HAX1*_2_pLKO.1_rv	5`-AATTCAAAAAAATCAAGATCATT GTCCTCTCCTCGAGGAGAGGACAA TGATCTTGATT-3`	Ursula Baumann; present study
*PRKCD*_01	5`-TATATCAGGGTTTCGAGA-3`	ThermoFisher/Dharmacon (Cat. No. SH-003524-01)
*PRKCD*_02	5`-TGCAAACAGTCTATGCGCA-3`	ThermoFisher/Dharmacon (Cat. No. SH-003524-02)
*PRKCD*_03	5`-GCGACAAGAACCTCATCGA-3`	ThermoFisher/Dharmacon (Cat. No. SH-003524-03)
Scrambled_control_ pLKO.1_fw	5`-CCGGCCTAAGGTTAAGTCGCCC TCGCTCGAGCGAGGGCGACTTAAC CTTAGGTTTTTG-3`	Ruth Eichner; Technische Universität München; Germany
Scrambled_control_ pLKO.1_rv	5`-AATTCAAAAACCTAAGGTTAAGT CGCCCTCGCTCGAGCGAGGGCGA CTTAACCTTAGG-3`	Ruth Eichner; Technische Universität München; Germany

5.1.6 Cell culture

5.1.6.1 Cell lines

Cell line	Description	Provided by
COS-7	monkey kidney fibroblast-like cells	ATCC (CRL-1651™)
Eμ-Myc lymphoma cells	cells derived from the Eμ-myc lymphoma model (Harris 1988)	Susanne Kratzat; Technische Universität München; Germany
GP-293	retrovirus producer cell line based on human enbryonic kidney cells	Clontech Laboratories (#631505)
Granta-519	human B cell lymphoma (MCL)	Martin Dreyling; University Hospital Munich; Germany
HEK293T	human embryonic kidney cells	ATCC (CRL-3216™)
High Five™	insect cells derived from *Trichoplusia ni*	ThermoFisher Scientific
Jeko-1	human mantle cell lymphoma	Martin Dreyling; University Hospital Munich; Germany
JVM-2	human mantle cell lymphoma	ATCC (CRL-3002™)
MEF *Hax1*$^{-/-}$	murin embryonic fibroblast; *Hax-1* knock-out	James N. Ihle (Chao, Parganas et al. 2008)
MEF *Hax1* WT	murin embryonic fibroblast; *Hax1* WT; control for MEF *Hax1*$^{-/-}$	James N. Ihle (Chao, Parganas et al. 2008)
MEF *p53*$^{-/-}$	murin embryonic fibroblast; *p53* knock-out	Andreas Villunger (Olsson, Manzl et al. 2007)
MEF *p53* WT	murin embryonic fibroblast; *p53* WT; control for MEF *p53*$^{-/-}$	Andreas Villunger (Olsson, Manzl et al. 2007)
MEF *Prkcd*$^{-/-}$	murin embryonic fibroblast; *Prkcd* knock-out	Michael Leitges (Leitges, Mayr et al. 2001)
MEF *Prkcd* WT	murin embryonic fibroblast; *Prkcd* WT; control for MEF *Prkcd*$^{-/-}$	Michael Leitges (Leitges, Mayr et al. 2001)
NIH/3T3	murin embryonic fibroblasts	ATCC (CRL-1658™)
Phoenix-ECO	retrovirus producer cell line based on human enbryonic kidney cells	ATCC (CRL-3214™)
Rec-1	human mantle cell lymphoma	ATCC (CRL-3004™)
Sf21	insect cells derived from *Spodoptera frugiperda*	ThermoFisher Scientific
SU-DHL-8	human B-lymphocyte derived from metastatic site	ATCC (CRL-2961™)

5.1.6.2 Media, reagents and supplements for cell culture

Reagent	Provided by
2-Mercaptoethanol 50mM	ThermoFisher Scientific/Gibco® (Cat. No. 31350)
ACK Lysing Buffer	ThermoFisher Scientific/Gibco® (Cat. No. A10492)
AMD3100 octahydrochloride hydrate	Sigma-Aldrich (Cat. No. A5602)
Amphotericin B (250µg/ml)	PAA (Cat. No. P11-001)
Express Five® SFM (1x)	ThermoFisher Scientific/Gibco® (Cat. No. 10486)
Dulbecco´s Modified Eagle Medium (DMEM)	ThermoFisher Scientific/Gibco® (Cat. No. 41966)
Dulbecco´s Phosphate Buffered Saline (1x DPBS)	ThermoFisher Scientific/Gibco® (Cat. No. 14190)
Etoposide	Sigma-Aldrich (Cat. No. E1383)
FBS Superior standardized	Biochrom (Cat. No. S0615)
Gentamicin (50mg/ml)	ThermoFisher Scientific/Gibco® (Cat. No. 15750)
Grace´s Insect Medium (1x)	ThermoFisher Scientific/Gibco® (Cat. No. 11605)
Hank´s Balanced Salt Solution (10x)	ThermoFisher Scientific/Gibco® (Cat. No. 14065)
HEPES Buffer Solution (1M)	ThermoFisher Scientific/Gibco® (Cat. No. 15630)
L-Glutamine (200mM)	Biochrom (Cat. No. 0283)
Matrigel™ Basement Membrane Matrix	BD Biosciences (Cat. No. 354234)
MG132	Tocris (Cat. No. 1748)
MitoTracker® Orange CMTMRos	ThermoFisher Scientific (Cat. No. M-7510)
NEM NEAA (100x)	ThermoFisher Scientific/Gibco® (Cat. No. 11140)
Newborn Calf Serum	Biochrom (Cat. No. S0125)
Opti-MEM® I (1x)	ThermoFisher Scientific/Gibco® (Cat. No. 11058)
Paclitaxel	Sigma-Aldrich (Cat. No. T7191)
Pen/Strep (Penicillin/Streptomycin)	ThermoFisher Scientific/Gibco® (Cat. No. 15140)
Recombinant Mouse IL-3	R&D Systems (Cat. No. 403-ML)
Recombinant Mouse IL-6	R&D Systems (Cat. No. 406-ML)

Rottlerin	Calbiochem (Cat. No. 557370)
RPMI Medium 1640 (1x) with GlutaMAX™	ThermoFisher Scientific/Gibco® (Cat. No. 61870)
SCF/c-kit ligand	R&D Systems (Cat. No. 455-MC)
Sdf-1	R&D Systems (Cat. No. 460-SD)
Sf-900™ II SFM (1x)	ThermoFisher Scientific/Gibco® (Cat. No. 10902)
Trypan Blue Stain (0.4%)	ThermoFisher Scientific/Gibco® (Cat. No. 15250)
Trypsin/EDTA Solution (10x)	Biochrom (Cat. No. L2153)

5.1.6.3 Reagents for lipofection

Reagent	**Provided by**
Amaxa™ Cell Line Nucleofector™ Kit R	Lonza (Cat. No. VCA-1001)
Amaxa™ Cell Line Nucleofector™ Kit V	Lonza (Cat. No. VCA-1003)
Lipofectamine® 2000 Reagent	ThermoFisher Scientific (Cat. No. 11668027)
X-tremeGENE 9	Roche (Cat. No. 06365779001)

5.1.7 Enzymes

Enzyme	**Provided by**
AgeI (BshTI)	ThermoFisher Scientific (Cat. No. ER1461)
Antarctic Phosphatase	New England Bioloabs (Cat. No. M0289)
BamHI	ThermoFisher Scientific (Cat. No. ER0051)
Benzonase® Nuclease	Sigma-Aldrich (Cat. No. E1014)
EcoRI	ThermoFisher Scientific (Cat. No. ER0271)
EcoRV	New England Bioloabs (Cat. No. R0195)
HindIII	ThermoFisher Scientific (Cat. No. ER0501)
KspAI	ThermoFisher Scientific (Cat. No. ER1031)
NheI	ThermoFisher Scientific (Cat. No. ER0972)
NotI	ThermoFisher Scientific (Cat. No. ER0592)
PfuUltra II Fusion HS DNA Polymerase	Agilent Technologies (Cat. No. 60067451)
Proteinase K	Qiagen (Cat. No. 1019499)

RNaseOUT™ Recombinant Ribonuclease Inhibitor	Invitrogen™ (Cat. No. 100000840)
SalI	ThermoFisher Scientific (Cat. No. ER0645)
SuperScript® III Reverse Transcriptase	Invitrogen™ (Cat. No. 1808044)
XhoI	ThermoFisher Scientific (Cat. No. ER0695)

5.1.8 Bacteria strains

Strain	Provided by
BL21 (DE3) competent cells	Agilent Technologies (Cat. No. 200131)
NEB 5-alpha competent *E. coli*	New England Biolabs® (Cat. No. C2987)
XL1-Blue competent cells	Agilent Technologies (Cat. No. 200249)

5.1.9 Strains of mice

Strain	Genotype	Provided by
C57BL/6 Inbred Mice	C57BL/6JOlaHsd	Harlan Laboratories
NOD SCID mice	NOD.CB17-Prkdc^{scid}/NCrCre	Charles River
NOD SCID mice	NOD.CB17-Prkdc^{scid}/NCrHsd	Harlan Laboratories

5.1.10 Tumor samples

Lymph node samples from mantle cell lymphoma patients (146 human subjects in total) were divided into three cohorts according to providing institutions. Specimens from cohort 1 (45 human samples) were obtained from the archives of the Department of Pathology of Technische Universität München (Martina Rudelius), Germany. Lymph node samples from cohort 2 (81 human samples) were provided by the archives of the lymph node registry of the German Low Grade Lymphoma Study Group (GLSG) (Wolfram Klapper), Germany. Specimens from cohort 3 (20 human samples) were obtained from the archives oft the Department of Pathology of the University of Würzburg (Andreas Rosenwald), Germany.

5.1.11 Inhibitors for protein analysis

Reagent	Final concentration	Provided by
Aprotinin from bovine lung	1 µg/ml	Sigma-Aldrich (Cat. No. A1153)
beta-Glycerolphosphate disodium salt hydrate	10 mM	Sigma-Aldrich (Cat. No. G6376)
DL-Dithiothreitol	1 mM	Sigma-Aldrich (Cat. No. D0632)
Leupeptin	1 µg/ml	Sigma-Aldrich (Cat. No. L2884)
Nα-Tosyl-L-lysine chloromethyl ketone hydrochloride	5 µg/ml	Sigma-Aldrich (Cat. No. T7254)
N-p-Tosyl-L-phenylalanine chloromethyl ketone	10 µg/ml	Sigma-Aldrich (Cat. No. T4376)
Okadaic Acid *Prorocentrum sp.*	10 nM	Calbiochem (Cat. No. 495604)
Phenylmethanesulfonylfluoride solution	100 µM	Sigma-Aldrich (Cat. No. 93482)
Sodium orthovanadate	100 µM	Sigma-Aldrich (Cat. No. S6508)
Trypsin inhibitor from soybean	10 µg/ml	Sigma-Aldrich (Cat. No. T9003)

5.1.12 List of purified proteins for ubiquitylation and kinase reactions

Protein	Provided by
PRKCD active	SignalChem (Cat. No. P64-10G-05)
UbcH5A	Boston Biochem (Cat. No. E2-616)
UbcH5B	Boston Biochem (Cat. No. E2-622)
UbcH5C/UBE2D3	Boston Biochem (Cat. No. E2-627)
UBE1	Boston Biochem (Cat. No. E-305)
Ubiquitin	Boston Biochem (Cat. No. U-100H)
Ubiquitin Aldehyde human	Sigma-Aldrich (Cat. No. SRP6024)

5.1.13 Standards for DNA and protein electrophoresis

GeneRuler 1 kb DNA Ladder	ThermoFisher Scientific (Cat. No. SM0311)
PageRuler Plus Prestained Protein Ladder	ThermoFisher Scientific (Cat. No. 26620)

5.1.14 Buffers

All listed buffers were prepared with *aqua dest.*, unless specified otherwise.

Coomassie Destaining (1x):	45% MeOH (v/v) 10% acetic acid glacial (v/v)

Coomassie Staining (1x):	45% MeOH (v/v) 10% acetic acid glacial (v/v) 0.25% Coomassie Brilliant Blue R250 (w/v)

DNA Loading Dye (6x):	30% glycerol (v/v) 0.25% Bromphenol Blue (w/v) 0.25% xylene cyanol (w/v)

FACS Buffer (1x):	Dulbecco PBS (1x) 5% fetal bovine serum (v/v)

FFPE Protein Extraction Buffer (1x):	100 mM Tris (pH 6.8) 2% SDS (w/v) 20% glycerol (v/v) 4% β-mercaptoethanol (v/v)

GST Elution Buffer (1x):	35 mM glutathione 100 mM Tris (pH 8.0) 120 mM NaCl

IF-Blocking Buffer (1x):	Dulbecco PBS (1x) 0.5% Tween 20 (v/v) 5% goat serum (v/v)

IF-Washing Buffer (1x):	Dulbecco PBS (1x) 0.5% Tween 20 (v/v)s

HF2+ Buffer (1x):	HBSS (1x) 5% heat-inactivated FBS (v/v) 1% Pen/Strep (v/v) 1% NEAA (v/v) 10 µM β-mercaptoethanol 1 mM HEPES

Kinase Assay Buffer (1x):	80 mM HEPES (pH 7.4) 10 mM $MgCl_2$ 50 µM ATP 1 µCi [γ-^{32}P] ATP (Hartmann Analytic) 1 mM DTT

Laemmli Buffer (5x):	300 mM Tris (pH 6.8) 50% glycerol (v/v)

	10% SDS (w/v) 5% β-mercaptoethanol (v/v) 0.01 % Bromphenol Blue (w/v)

LB Medium (1x):	1% Bacto Tryptone (w/v) 0.5% Bacto Yeast Extract (w/v) 170 mM NaCl opptional: 1.5% Bacto Agar (w/v)

Lysis Buffer (1x):	50 mM Tris (pH 7.5) 250 mM NaCl 0.1% Triton X-100 1 mM EDTA 50 mM NaF + protease inhibitors

NETN Buffer (1x):	20 mM Tris (pH 8.0) 100 mM NaCl 0.5% NP40 1 mM EDTA 2 mM PMSF + protease inhibitors

Ponceau Staining Solution (1x):	0.1% Ponceau S (w/v) 5% acetic acid glacial (v/v)

Proteinase K Buffer (1x):	100 mM Tris (pH 8.5) 5 mM EDTA 0.2% SDS 200 mM NaCl

SDS-Page Seperating Gel Buffer (1x):	Dulbecco PBS (1x) 1.5 mM Tris (pH 8.8)

SDS-Page Stacking Gel Buffer (1x):	Dulbecco PBS (1x) 0.5 mM Tris (pH 6.8)

SDS-Running Buffer (1x):	25 mM Tris 192 mM glycine 0.1% SDS

SDS-Transfer Buffer (1x):	48 mM Tris 39 mM glycine 20% methanol (v/v)

SOC Medium (1x):	2% Bacto Tryptone (w/v) 0.5% Bacto Yeast Extract (w/v) 10 mM NaCl 2.5 mM KCl 10 mM $MgCl_2$ 10 mM $MgSO_4$ 20 mM glucose

TBE Buffer (1x):	100 mM Tris 90 mM boric acid 1 mM EDTA

Ubiquitylation (*in vitro*) Assay Buffer (1x):	50 mM Tris (pH 7.6) 5 mM $MgCl_2$ 0.6 mM DTT 2 mM ATP 1.5 ng/µl E1 (Boston Biochem) 10 ng/µl Ubc3 (Boston Biochem) 10 ng/µl Ubc5 (Boston Biochem) 2.5 µg/µl ubiquitin 1 µM ubiquitin aldehyde

Ubiquitylation-Denaturing Buffer (1x):	50 mM Tris (pH 7.5) 250 mM NaCl 0.1% Triton X-100 (v/v) 1 mM EDTA 50 mM NaF 0.1% NP40 1% SDS + protease inhibitors

Ubiquitylation-Quenching Buffer (1x):	50 mM Tris (pH 7.5) 250 mM NaCl 1.1% Triton X-100 (v/v)

	1 mM EDTA 50 mM NaF + protease inhibitors

Wester Blot Blocking Buffer (1x):	Dulbeccos PBS (1x) 0.1% Tween 20 5% skim milk powder (w/v)

Western Blot Washing Buffer (1x):	Dulbeccos PBS (1x) 0.1% Tween 20 (v/v)

5.1.15 Commercial available kits for molecular biology

AllPrep® DNA/RNA FFPE Kit	Qiagen (Cat. No. 80234)
DC™ Protein Assay	Bio-Rad (Cat. No. 5000116)
GeneJET Gel Extraction Kit	ThermoFisher Scientific (Cat. No. K0692)
GeneJET PCR Purification Kit	ThermoFisher Scientific (Cat. No. K0702)
LightCycler® 480 High Resolution Melting Master	Roche (Cat. No. 04909631001)
LightCycler® 480 SYBR Green I Master	Roche (Cat. No. 04707516001)
peqGOLD Plasmid Miniprep Kit I	Peqlab (Cat. No. 12-6942-02)
Pre-Diluted Proteins Assay Standard BSA	ThermoFisher Scientific (Cat. No. 23208)
Qiagen Plasmid Maxi Kit	Qiagen (Cat. No. 12165)
QIAshredder™	Qiagen (Cat. No. 79656)
QuikChange® Site-Directed Mutagenesis Kit	Stratagene (Cat. No. 200518)
Rapid DNA Dephos & Ligation Kit	Roche (Cat. No. 04898125001)
RNeasy® FFPE Kit	Qiagen (Cat. No. 73504)
RNeasy® Mini Kit	Qiagen (Cat. No. 74106)
SuperSignal® West Pico Sensitivity Substrate	ThermoFisher Scientific (Cat. No. 34080)
SuperSignal® West Femto Sensitivity Substrate	ThermoFisher Scientific (Cat. No. 34096)

5.1.16 Software and database tools

ApE plasmid Editor 2.0

BLAST Basic Local Alignment Search Tool

CellQuest™ Pro

COSMIC v73 cell line project

COSMIC v73 whole genomes

FlowJo Single Cell Analysis Software v10

GEO Gene Expression Omnibus NCBI

GraphPad Prism 6

ImageJ 1.49 imaging software

MacVector 13.5.5

Oncomine™

PrimerX

QuantPrime BMC Bioinformatics

TillVision microscope imaging software

5.1.17 Machinery

Device	**Provided by**
Analytic balance ABJ 220	Kern & Son
Aqualine water bath	Lauda-Brinkmann
Axiovert 40 CFL with HBO50	Carl Zeiss
Centrifuge 5417R with rotor F453011	Eppendorf
Centrifuge 5424 with rotor FA452411	Eppendorf
Concentrator plus	Eppendorf

Digital Sonifier® 250D	Branson-Emerson
E-Box VX2 Imager	Vilber
FACSCalibur	BD
FluoView FV 10i with filter sets 15, 25 and 71	Olympus
Fridges and lab freezers	Liebherr
Heracell 150i CO_2 incubator	Thermo Scientific
Herafreeze	Thermo Scientific
HeraSafe KS safety cabinet	Thermo Scientific
Hypercassette™	Amersham Biosciences
Incubator for bacteria	Memmert
Innova® 40 shaker for bacteria	New Brunswick Scientific
IX Inverted Fluorescence Microscope	Olympus
LightCycler® 480 system	Roche
LS4800 liquid nitrogen tank	Taylor-Wharton Lab Systems
Magnetic thermo stirrer bacis RCT	IKA Laboratory Equipment
Micro PET system	Siemens preclinical solutions
Microwave	Samsung
Mini-PROTEAN Tetra cell SDS electrophoresis system	Bio-Rad Laboratories
Mini-Sub® Cell GT system for agarose electrophoresis	Bio-Rad Laboratories
Multifuge 3SR+	Thermo Scientific
NanoPhotometer	Implen
Neubauer chamber	Marienfeld
Novex® Mini cell system for precast NuPAGE gels	ThermoFisher Scientific
Nucleofector™	Lonza

Peqstar 2x gradient PCR cycler	Peqlab Biotechnology
Pipetman neo (P2N, P10N, P20N, P100N, P200N and P1000N)	Gilson®
Polymax 1040 shaker	Heidolph Instruments
PowerPac™ Basic	Bio-Rad Laboratories
PowerPac™ HC	Bio-Rad Laboratories
Precision balance 572-37	Kern & Son
Scanner V750 Pro	Epson
SevenCompact pH/Ion pH-meter	Mettler-Toledo
Sorvall® RC-5B with rotors SS-24 and GS-3	Du Pont Instruments
SRX-101A developer	Konica-Minolta
Thermal printer P95	Mitsubishi
Thermo block MBT250	Kleinfeld Labortechnik
Thermomixer compact	Eppendorf
Tube rotator wheel RPM	Fröbel Labortechnik
Tumbling roller mixer RM5	Neolab

5.1.18 Consumables

3mm CHR paper (Whatman™)	GE Healthcare
Cell culture flasks	Greiner Bio-One
Cell culture plates	Biochrom/Falcon®
Cell scraper	Sarstedt
CL-XPosure™ Films	ThermoFisher Scientific
Cryo tubes	Sardtedt
Graduated tubes	Greiner Bio-One
Hypodermic needles	Braun

Immobilon®-P PVDF transfer membrane	Millipore (Cat. No. IPVH00010)
Lab-Tek® Chamber Slides	Nunc®/Sigma-Aldrich
Pipette tips	Sarstedt
SafeSeal tubes	Sarstedt
Serological pipettes	Greiner Bio-One
S-Monovette®	Sarstedt
Syringe filters	TPP/Biochrom
Syringes	Braun
UVette® routine pack	Eppendorf

5.2 Methods

5.2.1 DNA based methods

5.2.1.1 Agarose gel electrophoresis

Agarose gel electrophoresis was performed to analyze the integrity and length of circular and linear DNA. Therefore, agarose (1%; w/v) was mixed with 1-fold TBE buffer (100 mM Tris, 90 mM boric acid, 1 mM EDTA) and boiled to dissolve the contained agarose. Afterwards, DNA intercalating ethidium bromide was added to allow visualization of DNA. When an electric field was applied to the agarose gels loaded with samples, DNA with its negatively charged phosphate backbone migrated towards the positive electric pole, thus leading to a size dependent separation of DNA fragments in the agarose matrix (Zimm and Levene 1992). DNA was visualized under an UV-light source.

5.2.1.2 Polymerase chain reaction

DNA fragments of interest were amplified by polymerase chain reaction (PCR) (Saiki, Gelfand et al. 1988). Therfore, 100 ng of template DNA were mixed with 0.2 µM of each target-sequence compatible primer, 0.8 mM dNTPs (200 µM each dNTP) and PfuUltra II Fusion HS DNA Polymerase (Agilent Technologies) within the provided buffer system. DNA double strands were separated at 95 °C, primers were annealed to their target sites at 60 °C - 65 °C (dependent on the calculated melting temperature of the oligonucleotides), subsequent elongation of DNA fragments was carried out at 72 °C (2 kb/min dependent on target sequence length). Target DNA sequences were amplified exponentially by 30 repetitions of the described cycling process. DNA amplicons were analyzed by agarose gel electrophoresis.

5.2.1.3 Molecular cloning

To clone specific cDNAs of interest into expression vectors, the target cDNA was amplified by PCR using oligonucleotides with 5`-overhangs that can be recognized and cleaved by specific restriction endonucleases. Restriction sites were selected due to their presence in the multiple cloning site (MCS) of the selected target vector. PCR amplicon and target vector were restricted with the corresponding enzymes, subsequently products were purified by a preparative agarose

gel. Extraction from agarose matrix was performed using the GeneJET Gel Extraction Kit (ThermoFisher Scientific) according to manufacturer`s instructions. Restriction overhangs from purified cDNA and vector were ligated using the Rapid DNA Dephos & Ligation Kit (Roche), according to manufacturer`s protocol. Newly ligated expression vectors were subsequently transformed into NEB 5-alpha competent cells (see 5.2.11.1), checked for positivity by test restriction and sent for sequencing.

5.2.1.4 Sequencing of vector DNA

For sequencing, plasmid concentration was adjusted to 60 - 100 ng/µl. Sequencing reactions were performed by Eurofins Genomics, Ebersberg, Germany, using promotor- or gene-specific oligonucleotides.

5.2.1.5 Modification of DNA sequences by mutagenesis PCR

Mutagenesis PCR was performed to introduce site-directed mutations into vector DNA. Therefore, the underlying vector was amplified using 40 - 45 nucleotide oligomers that cover the desired base mutations within their center. Base triplets encoding for serine residues were mutated to triplets encoding for alanine in order to obtain cDNA information for proteins with selectively mutated phosphorylation sites.

Composition and processing of PCR reactions was performed according to the QuikChange Site-Directed Mutagenesis Kit (Stratagene). The original plasmid DNA was digested by DpnI, a restriction endonuclease that specifically recognizes bacterial methylated sites within the template DNA. The remaining newly amplified plasmids were transformed into NEB 5-alpha competent cells (see 5.2.11.1). Subsequently, sequence integrity was check by sequencing reactions and sequence analyses.

5.2.2 RNA based methods

5.2.2.1 RNA extraction from cultured cells

RNA from cultured cells was extracted using the RNeasy Mini Kit in combination with the QIAshredder (both Qiagen), according to the manufacturer`s instructions.

Concentration of the eluted RNA samples was measured against RNAse free water as blank using a NanoPhotometer (Impel).

5.2.2.2 cDNA synthesis

For synthesis of complementary DNA (cDNA), 1 µg of extracted RNA was mixed with 1 µl of Hexanucleotide Mix (Roche) and incubated for 5 minutes at 70 °C in order to enable binding of hexamers to their complementary RNA target sequences. Subsequently, RNA was reversely transcribed into cDNA using the SuperScript III Reverse Transcriptase/ RNase OUT system (Invitrogen).

As preparation for quantitative PCR analysis, processed cDNA was diluted in a ratio of 1:20 with PCR grade water.

5.2.2.3 Quantitative PCR analysis

50 ng of total cDNA were processed in quantification runs at the LightCycler 480 system (Roche), using the SYBR Green I Master (Roche). Priming oligonucleotides for housekeeping genes (*ARPP_P0* and *GAPDH*) and target genes (*HAX1*, *FBXO25 and CXCR4*) were selected to compass at least two exons in order to prevent amplification of genomic DNA, using Primer X software for oligonucleotide designs. cDNA values for *HAX1*, *FBXO25, CXCR4* and the corresponding housekeeping gene were collected as triplicates for each sample and analyzed by their target/reference Cp values via the $2^{-\Delta\Delta Cp}$ method (Livak and Schmittgen 2001).

Primer sequences for *HAX1*, *FBXO25*, *CXCR4*, *ARPP_P0* and *GAPDH* are indicated in the material part *5.1.4.3.*

5.2.3 Protein based methods

5.2.3.1 SDS-PAGE

SDS polyacrylamide gel electrophoresis (SDS-PAGE) was used to separate proteins according to their molecular weight (Shapiro, Viñuela et al. 1967, Laemmli 1970). In the initial step, protein containing samples were denatured by boiling with Laemmli buffer (Laemmli 1970) (300 mM Tris, 50% glycerol, 10% SDS, 5% β-mercaptoethanol, 0.01% Bromphenol Blue). Binding of the

buffer component SDS to the polypeptide chain provides negative charges to proteins, thus allowing for migration within an electric field. Samples were loaded onto a stacking/separating gel system and placed into a glycine containing buffer (25 mM Tris, 192 mM glycine, 0.1% SDS). Within the pH 6.8 stacking gel negatively charged proteins are assembled in a horizontal line between negative clorie ions and dipolar glycine ions, whereupon pH change to pH 8.8 leads to negative charged glycine that passes migrating proteins thus leading to the separation of proteins according to their molecular weight.

In frame of the present study, all SDS-PAGEs comprised an acrylamide content of 10% within the separating gel part.

5.2.3.2 Immunoblotting

Separated proteins were transferred to a polyvinylidenfluoride (PVDF) membrane using the wet blot technique (Burnette 1981). Amount of transferred proteins was visualized by Ponceaus S staining. After destaining with Washing buffer (PBS, 0.1% Tween 20) and blocking with 5% milk in Washing buffer, membranes were incubated with the corresponding primary antibodies (see 5.1.2.1) for 90 minutes at room temperature. After removal of spare primary antibodies by three repeated washing steps, membranes were incubated with the corresponding horseradish peroxidase (HRP) conjugated secondary antibodies. After 1 hour, non-bound HRP conjugates were removed by two washing steps. HRP-linked to membranes was incubated with enhanced chemiluminescence (ECL) substrate leading to oxidation of luminol and emission of light (Veitch 2004). Emitted light signals were detected by photosensitive films. When specified, the intensity of immunoblotting bands was quantified using ImageJ.

5.2.3.3 Preparation of whole cell lysates

Fresh or frozen eukaryotic cells were resuspended in an appropriate volume of Lysis buffer (250 mM NaCl, 50 mM Tris, 0.1% Triton X-100, 1 mM EDTA, 50 mM NaF) supplemented with inhibitors listed in part 5.1.11 to avoid enzymatic modification or cleavage of contained proteins. After 20 minutes incubation on ice to break up cellular compartments, cellular debris were removed by centrifugation for 20 minutes at full speed in a cold centrifuge. Protein concentrations in cell lysates were determined by the Lowry-based (Lowry, Rosebrough et al. 1951) DC Protein Assay (Biorad). Subsequently, protein extracts were analyzed by SDS-PAGE.

5.2.3.4 Affinity purification

Affinity purification (AP) represents a separation method based on the specific binding interaction between molecules (Skerra and Schmidt 2000, Puig, Caspary et al. 2001). Molecules of interest were fused to a specific tag (e.g. glutathione-s-transferase; GST (Swaffield and Johnston 2001)) and expressed in prokaryotic or eukaryotic cells (Terpe 2003). Lysates of these cells were incubated with the particular ligand of the tag (e.g. glutathione) that has been chemically immobilized to solid phase agarose beads. Target proteins and their potential interaction partner were bound to the ligand immobilized on beads. The high mass of the agarose/sepharose beads allows for separation by centrifugation, thus leading to extraction of target proteins and their interactors from cell lysates. When required, proteins could be eluted from beads by denaturation or high concentrations of competitive interacting factors.

5.2.3.4.1 Immunoprecipitation

Immunopurification resembles a subform of AP when purification is based on the interaction of antibodies to their specific antigens (Kaboord and Perr 2008). Cell lysates containing the tagged target proteins (e.g. FLAG-tagged (Hopp, Prickett et al. 1988)) were therefore incubated with the corresponding antibodies crosslinked to agarose beads. Proteins bound to beads were separated by centrifugation and washed to remove non-specifical bound contaminants. When required, elution was performed by addition of high concentrations of competitive antigens (e.g. 3 x FLAG-peptide).

5.2.4 Modification of cellular protein levels

5.2.4.1 Transient overexpression of proteins

Transient overexpression of proteins was achieved by transfecting cells with plasmids encoding the information for the specific target protein.

5.2.4.1.1 Calcium phosphate transfection

Calcium phosphate transfection represents a cost effective method for transfection of HEK293T cells (Kingston, Chen et al. 2003). Combination of $CaCl_2$ with BES buffered saline leads to the formation of a precipitate of positive calcium ions and negatively charged phosphate ions that bind the added plasmid DNA (10 µg per 55 cm^2 cell monolayer). When added to cells, complexes were adsorbed to cellular membranes and taken up. To allow optimal growth conditions, medium was exchanged 4 hours after transfection. Transfection efficiency was estimated by analyzing GFP-positive cells, 24 hours after transfecting an EGFP-encoding control plasmid.

5.2.4.1.2 Transfection using Lipofectamine 2000

Mouse embryonic fibroblasts (MEF), COS-7 and packaging lines for virus production (GP-293, Phoenix-ECO) were transfected using Lipofectamine 2000 (ThermoFisher Scientific), according to manufacturer`s protocol. During the lipofection process, plasmids were inserted into liposomes and endocytosed by targeted cells (Felgner, Gadek et al. 1987). To reduce the toxicity of Lipofectamine 2000, media was exchanged 4 hours post transfection.

5.2.4.1.3 Transfection using X-tremeGENE 9

COS-7 and MEFs for immunofluorescence studies were transfected using X-tremeGENE 9 (Roche), according to the provided protocol. Medium was exchanged after 4 hours to reduce toxicity induced effects of the transfection reagent.

5.2.4.1.4 Transfection by nucleofection

Mantle cell lymphoma cell lines were transfected by nucleofection, a combination of electroporation with cell type optimized lipofection reagents (Maasho, Marusina et al. 2004). Amaxa Cell Line Nucleofector Kit R (Lonza) was used to transfect Granta-519 (electroporation setting D-023) and JVM-2 (electroporation setting A-023). Amaxa Cell Line Nucleofector Kit V (Lonza) was used to transfect Rec-1 (electroporation setting X-001) and Jeko (electroporation setting T-002). Electroporation was performed using the Amaxa Nucleofector device (Lonza).

5.2.4.2 Construction of stable overexpressing cell lines

Stable overexpression was obtained by transducing cell lines with retroviruses carrying RNA information for the target proteins, thus leading to stable integration of the encoding DNA into the genome of targeted cell lines (Cepko and Pear 2001).

5.2.4.2.1 Production of viruses

For production of ecotrophic retroviruses, Phoenix-ECO cells containing information for gag (coding for capsid proteins), env (coding for viral envelope proteins) and pol (encoding for viral enzymes), were transfected with the corresponding retroviral plasmid (10 μg per 55 cm^2 cell surface) using Lipofectamine 2000.

For production of amphotrophic retroviruses, GP-293T cells were transfected with VSV.G, gag/pol and the selected retroviral target protein encoding plasmid (each 5 μg per plasmid per 55 cm^2 cell surface) using Lipofectamine 2000.

Active retroviruses secreted to the culture media were harvested after 48/72 hours and purified from cells by filtration through a 0.45 μm Whatman filter.

5.2.4.2.2 Infection of target cells

Target cells, plated onto 6-wells (40% - 50% confluency for adherent cells; 5 x 10^5 cells/ml for suspension cells), were treated with 2.0 ml of the previously harvested virus supernatant. Positive charged polybrene was added to a final concentration of 8 μg/ml to support binding of viral glycoproteins to cellular membranes (Davis, Rosinski et al. 2004). The retrovirus infection efficiency was additional enhanced by centrifuging the culture plates for 1 hour at 1000 rpm. Exchange of polybrene containing media was carried out 7 hours after the last spin infection.

5.2.4.2.3 Selection of virus infected cells

Successful transduced cells were selected 48 hours post spin infection due to GFP-positivity or their resistance towards puromycin. GFP positive cells were purified by FACS sorting, whereupon puromycin selection (2.0 μg/ml) was continued for three days to deaden non-transduced cells (Darken 1964).

5.2.4.3 Construction of stable knock-down cell lines

Expression of selected target genes was silenced by RNA interference using short hairpin RNA (shRNA) (Shi, Djikeng et al. 2000);(Paddison, Caudy et al. 2004).

5.2.4.3.1 Production of viruses

For production of murine infectious *Fbxo25* knock-down retroviruses, Phoenix-ECO cells were transfected with retroviral MLS-based constructs (Scuoppo, Miething et al. 2012). Retroviruses secreted to the culture media were harvested after 48/72 hours and purified from cells by filtration through a 0.45 μm Whatman filter.

SMARTvector 2.0 lentiviral particles for silencing of human *FBXO25* and *PRKCD* were obtained from ThermoFisher/Dharmacon.

For production of lentiviruses targeting the expression of human *HAX1*, HEK293T cells were transfected with psPAX2, pMD2.G and the selected lentiviral pLKO.1-based targeting vector (5 μg per plasmid per 55 cm^2 cell surface) using Lipofectamine 2000. Active retroviruses secreted to the culture media were harvested after 48/72 hours and purified from cells by filtration through a 0.45 μm Whatman filter.

Sequences of all shRNA constructs are listed under 5.1.5.

5.2.4.3.2 Infection and selection of target cells

Infection of murine target cells was performed according to 5.2.4.2.2. Infection reactions for the SMARTvector 2.0 (ThermoFisher/Dharmacon) were performed according to manufacturer`s instructions. Knock-down cells were selected by virus induced puromycin resistance (2.0 μg/ml final). For knock-down of *HAX1* gene expression, MCL cell lines were plated onto 6-wells (5 x 10^5 cells/m) and treated with 2.0 ml of the previously harvested lentivirus containing supernatant. Positive charged polybrene was added to a final concentration of 8 μg/ml. Lentiviral infection efficiency was additional enhanced by centrifuging the culture plates for 1.5 hours at 1000 rpm. Exchange of polybrene containing medium was carried out 6 hours after the last spinning process. Successful selected MCL cells were selected due to their resistance towards puromycin (pLKO.1_puro) or their RPF-positivity (pLKO.1_RFP). Efficiency of the corresponding knock-downs was validated by qPCR and immunoblotting.

5.2.5 Purification of proteins for *in vitro* assays

5.2.5.1 Purification of bacteria derived GST-proteins

BL21 (DE3) cells (Agilent Technologies) were transfected, cultured and induced as described under 5.2.11.3 to allow for GST protein production (Harper and Speicher 2011).

Previously frozen bacterial pellets were resuspended in 4-fold volume of NETN buffer (20 mM Tris, 100 mM NaCl, 0.5% NP40, 1 mM EDTA, 2 mM PMSF) supplemented with enzymatic inhibitors. Hydrolysis of bacterial cell walls was supported by addition of lysozyme to a final concentration of 100 µg/ml final (30 minutes on ice) and subsequent microtip sonication with 10 pulses for 1.0 second each at 54% amplitude. Cellular debris were removed by full speed centrifugation and collected supernatants were incubated with Glutathione Sepharos 4B (GE Healtcare) for 60 minutes on a rotating wheel (4 °C). Beads were washed four times with bacterial lysis buffer and stored in NETN buffer at 4 °C for further use in GST pulldown assays.

5.2.5.2 Purification of insect cell derived proteins

SCF components for *in vitro* ubiquitylation assays were produced in High Five insect cells and purified by GST- or hexahis-tags.

5.2.5.2.1 Culture and transfection of Sf21 insect cells

Sf21 insect cells derived from *Spodoptera frugiperda* (ThermoFisher Scientific) were maintained in Grace´s Insect Medium supplemented with 10% heat-inactivated FBS and 10 µg/ml gentamycin at 27 °C. Sf21 cells seeded with a density of approximately 4 x 10^5 cells/ml were passaged when reaching a density of 2 x 10^6 cells/ml.

cDNAs encoding human FBXO25, FBXO9, CUL1, ROC1-His_6 and SKP1_GST were inserted into the baculoviral pBacPAK9 expression vector (Clontech). 1 x 10^6 Sf21 cells were cotransfected with linearized BacPAK6 DNA and the corresponding cDNA encoding construct using Bacfectin (Clontech) according to the provided protocol. First baculovirus was harvested from culture supernatant five days post transfection.

5.2.5.2.2 Amplification of viruses using Sf21 cells

In order to amplify the first baculoviruses, 50 ml Sf21 suspension cultures (4 x 10^5 cells/ml) were treated with 100 µl of each virus. Passage two virus stocks were filtered after 6 days (0.45 µm filters) and stored at 4 °C.

5.2.5.2.3 Protein production in High Five™ cells

High Five insect cells derived from *Trichoplusia ni* (ThermoFisher Scientific) were maintained in Express Five SFM supplemented with 10 mM L-glutamine and 10 µg/ml gentamycin at 27 °C. High five cells seeded with a density of approximately 2 x 10^4 cells/ml were passaged when reaching a density of 3 x 10^6 cells/ml.

Passage two viruses for CUL1-ROC1-His_6 were mixed together as well as viruses for FBXO-SKP1-GST, to allow for later purification. 100 ml of robust growing High Five cells were mixed with 5 ml of each virus combination and incubated for 6 days at 27 °C. Cellular pellets expressing the target proteins were collected by centrifugation and stored at -80 °C.

5.2.5.2.4 Purification of GST-proteins

Pellets from High Five cells expressing FBXO-SKP1-GST were resuspended in lysis buffer (250 mM NaCl) supplemented with the protease inhibitor cocktail. After 20 minutes, insect cell debris were removed through full speed centrifugation and collected supernatants were incubated with Glutathione Sepharos 4B (GE Healthcare) for 60 minutes on a rotating wheel (4 °C). Beads were washed three times with lysis buffer. Subsequent elution of FBXO-SKP1-GST proteins was performed using a 35 mM reduced glutathione containing buffer (35 mM glutathione, 100 mM Tris, 120 mM NaCl). All eluted proteins were snap frozen in liquid nitrogen and stored as aliquots for further use at -80 °C.

5.2.5.2.5 Purification of proteins by His_6-tag

Pellets from High Five cells expressing CUL1-ROC1-His_6 were resuspended in lysis buffer (250 mM NaCl) supplemented with the protease inhibitor cocktail (except DL-dithiothreitol). The lysis buffer was additionally supplemented with 10 mM imidazole to later avoid binding of endogenous proteins with histidine clusters to Ni-NTA agarose. After 20 minutes, insect cell debris

were removed through full speed centrifugation and collected supernatants were incubated with Ni-NTA agarose (Qiagen) for 90 minutes on a rotating wheel (4 °C). Beads were washed three times with lysis buffer (containing 15 mM imidazole) and subsequently eluted with lysis buffer containing 250 mM imidazole. All eluted proteins were snap frozen in liquid nitrogen and stored as aliquots for further use at -80 °C.

5.2.6 Cell culture and drug treatments

5.2.6.1 Cell culture

COS-7, GP-293, NIH/3T3 and Phoenix-ECO cells were cultured in DMEM supplemented with 10% FBS and 1% penicillin-streptomycin. HEK293T were maintained in DMEM supplemented with 10% BS and 1% penicillin-streptomycin. *Hax1*$^{-/-}$ MEFs and their wildtype counterparts, *p53*$^{-/-}$ MEFs and their wildtype counterparts as well as *Prkcd*$^{-/-}$ MEFs and their wildtype counterparts were maintained in DMEM containing 10% heat-inactivated FBS and 1% penicillin-streptomycin. Mantle cell lymphoma lines Granta-519, JVM-2 and Rec-1 and the B-cell lymphoma line SU-DHL-8 were cultured in RPMI-1640 enriched with 10% heat-inactivated FBS and 1% penicillin-streptomycin. Cells from the MCL line Jeko were maintained in RPMI-1640 with 20% heat-inactivated FBS and 1% penicillin-streptomycin. Eμ-Myc lymphoma cells were cultured in RPMI-1640 with 10% heat-inactivated FBS, 1% penicillin-streptomycin, 1% non-essential amino acids and 100 μM β-mercaptoethanol. All cells cultured under 37 °C and 5% CO_2 were tested for mycoplasm contamination by a PCR based method.

5.2.6.2 Drug treatments

5.2.6.2.1 Inhibition of protein *de novo* synthesis

Half life of proteins was analyzed by adding the polypeptide biosynthesis inhibitor cycloheximide (100 μg/ml) to cell cultures. The *de novo* synthesis of proteins by ribosomes was thereby inhibited by a blockade of translational elongation (Schneider-Poetsch, Ju et al. 2010).

5.2.6.2.2 Inhibition of proteasomal degradation

Proteasomal degradation was inhibited by addition of 10 μM MG132 for 4 hours to cell culture medium. MG132 represents a peptide aldehyde inhibitor that blocks the chymotrypsin-like activity of the 20S-proteasome core, thus leading to stabilization of proteolytic degraded proteins (Rock, Gramm et al. 1994);(Myung, Kim et al. 2001).

5.2.6.2.3 Induction of apoptotic signaling pathways

Apoptosis was induced by addition of 1 μg/ml etoposide or 1 μg/ml paclitaxel to cell culture medium.

Etoposide is a topoisomerase inhibitor that complexes DNA with topoisomerase II, thus leading to DNA strand breaks and subsequent induction of apoptotic signaling (Pommier, Leo et al. 2010).

Paclitaxel is a *taxus brevifolia* derived agent that inhibits depolymerization of alpha- and beta-tubulin heterodimers (Schiff, Fant et al. 1979). The induced changes in microtubule dynamics disturb proper spindle formation and alignment of chromosomes, thus leading to apoptosis (Jordan, Wendell et al. 1996, Torres and Horwitz 1998)

5.2.6.2.4 Inhibition of PRKCD

Inhibition of the kinase PRKCD was achieved by addition of 10 μM rottlerin to cell culture media.

5.2.6.2.5 Inhibition of CXCR4

CXCR4 surface expression and activity was inhibited by addition of AMD3100/Plerixafor to the cell culture media for 4 hours. The CXCR4 antagonist AMD3100 was added in a final concentration of 5 μg/ml, inducing the internalization of CXCR4 (Cashen, Nervi et al. 2007).

5.2.6.2.6 Activation of CXCR4 downstream signaling

Cxcr4-mediated downstream signaling in murine cells was activated by addition of its natural ligand Sdf-1 to the cell culture medium for 4 hours. Sdf-1 was added in a final concentration of 100 ng/ml, leading to activation of Cxcr4 signaling e.g. via phosphorylation and activation of Erk1/2 (Aboumrad, Madec et al. 2007).

5.2.7 Fluorescence imaging studies

Fluorescence studies were performed to determine the subcellular localization of proteins of interest. All images were obtained using a IX Inverted Fluorescence Microscope (Olympus) with TillVision imaging software. Following excitation wavelenght were used: 400 nm (DAPI), 490 (FITC) and 585 (TR). All microscopy studies were performed on Lab-Tek chamber slides (Nunc).

5.2.7.1 Imaging by direct fluorescence

Plasmids encoding GFP fusion proteins were transfected into COS-7 or MEF cells using X-tremeGENE (Roche). After indicated times, cells were washed with 1 x PBS and mounted with ProLong Gold antifade reagent with DAPI (ThermoFisher Scientific).

5.2.7.2 Indirect immunofluorescence

Plasmids encoding tagged versions of the proteins of interest were transfected into COS-7 or MEF cells using X-tremeGENE (Roche). After indicated times, cells were permeabilized with ice cold methanol and unspecific binding sites were blocked by addition of 5% BSA in IF buffer (1 x PBS supplemented with 0.5% Tween 20). Primary antibodies to HA (mouse) and FLAG (rabbit) were diluted 1:500 in IF buffer and applied on permeabilized cells for 1.5 hours at room temperature. Unbound primary antibodies were removed by three washing steps with IF buffer (5 minutes each). Alexa Fluor 488 conjugated anti-mouse/anti-rabbit and Alexa Fluor 594 conjugated anti-mouse in a dilution of 1:1000 in IF buffer were utilized to mark proteins with fluorescence labels. Secondary antibodies were removed after 45 minutes by three washing steps. Subsequently, cells were mounted with ProLong Gold antifade reagent with DAPI. Staining of

mitochondria was performed by addition of MitoTracker Orange CMTMRos (ThermoFisher Scientific) for 15 minutes before fixation to cell culture media.

5.2.8 Flow cytometry

Fluorescence activated cell sorting (FACS) allows for the quantification of fluorochromes, attached to specific cellular targets, on a single cell level. Therefore, cellular target structures were stained with fluorochrome-conjugated antibodies or fluorescence molecules that can be excited with a specific laser wave length thus leading to light signals detectable by FACS machine sensors. For measurement of apoptotic cells, 1 µg/ml propidium iodide (PI) was added to harvested and washed cells. PI thereby intercalates into the DNA of dead cells while it cannot stain live cells due to the integrity of plasma membranes (Riccardi and Nicoletti 2006);(Rieger, Nelson et al. 2011). PI positivity was detected in the red FL3 channel.

Cells for the analysis of CXCR4 surface expression were collected by centrifugation and washed once with 1 x PBS. Subsequently, cells were fixed in 2% paraformaldehyde (without methanol) for 60 minutes at 4 °C to avoid permeabilization and allow for specific detection of cell surface CXCR4. Cells were stained with primary antibodies directed against CXCR4 or an IgG control using 5% BSA in 1 x PBS as solution to dilute the primary antibodies. After 90 minutes of incubation at room temperature cells were washed once with 1 x PBS and incubated with an Alexa Fluor 488 conjugated anti-mouse secondary antibody diluted in 5% BSA in 1 x PBS for 60 minutes at room temperature. Non-bound secondary antibodies were removed by a 1 x PBS washing step and cells were subjected to flow cytometric analysis detecting FITC-positivity in the green FL1 channel. Collected data sets were analyzed using the FlowJo Single Cell Analysis Software v10.

5.2.9 Ubiquitylation assays

Ubiquitylation of specific substrates was reconstituted by *in vivo* and *in vitro* ubiquitylation assays.

5.2.9.1 In vivo ubiquitylation

The *in vivo* assay was used to reconstruct the ubiquitylation of a specific substrate within the cellular context. For this purpose HEK293T cells were transfected with plasmids encoding HA-

tagged ubiquitin, FLAG-tagged substrate, GFP-tagged F-box proteins or respective controls. 20 hours after transfection cells were treated with 10 µM MG132 for 4 hours to block proteasomal protein degradation, thus achieving a cellular enrichment of the ubiquitylated substrates. After harvesting, cell pellets were resuspended in 100 µl of lysis buffer (250 mM NaCl) and incubated for 20 minutes on ice. Supernatants were denatured by addition of 6 mM EDTA, 0.1% NP-40 and 1% SDS and subjected to a heating step to 95 °C that allows only for the preservation of covalent protein-protein interactions. 1% SDS contained in the lysis buffer was subsequently quenched by addition of 900 µl of 10% Triton X-100 (final 1%), thus adapting the buffer conditions for antibody based assays. FLAG-tagged substrate was immunoprecipitated according to section 5.2.3.4.1 and ubiquitylation status was analyzed using SDS-PAGE based immunoblotting (compare sections 5.2.3.1 and 5.2.3.2).

5.2.9.2 In vitro ubiquitylation

The *in vitro* assays were used to reconstitute specific ubiquitylation reactions in a cell free system under controlled conditions. All required SCF-components were purified from High Five insect cells (see chapter 5.2.5), while FLAG-tagged HAX1 was immunoprecipitated from transfected HEK293T cells as described in sector 5.2.4.1.1. Concentration of eluted proteins was determined by SDS-PAGE and subsequent Coomassie staining using a BSA protein standard as reference. All ubiquitylation reactions were performed in a volume of 10 µl containing 50 mM Tris pH 7.6, 5 mM MgCl2, 0.6 mM DTT, 2 mM ATP, 1.5 ng/µl E1 (Boston Biochem), 10 ng/µl Ubc3 (Boston Biochem), 10 ng/µl Ubc5 (Boston Biochem), 2.5 µl ubiquitin (Boston Biochem), 1 µM ubiquitin aldehyde (Sigma-Aldrich), 2 µl purified FLAG-tagged HAX-1 and approximately 500 ng of SCF complexes composed of SKP1-FBXO25 or SKP1-FBXO9 with CUL1-ROC1. Ubiquitylation reactions were incubated at 30 °C for 0, 30, 60, 90 and 120 minutes, while corresponding reaction was stopped by addition of 10 µl 2.5 x Laemmli buffer. Ubiquitylation status of HAX1 was analyzed by SDS-PAGE and immunoblotting (compare sections 5.2.3.1 and 5.2.3.2).

5.2.10 Kinase assay

For *in vitro* kinase assays, active PRKCD (SignalChem) and purified substrates (FLAG-FBXO25 wildtype, FLAG-FBXO25^{S178A}, FLAG-HAX1 wildtype and FLAG-HAX1^{S210A} were transferred into the kinase reactions containing 80 mM HEPES (pH 7.4), 10 mM $MgCl_2$, 50 µM

ATP, 1 µCi [γ-^{32}P]ATP (Hartmann Analystics) and 1mM dithiothreitol. All kinase reactions were carried out at 30 °C for 10 minutes (Bassermann, von Klitzing et al. 2007). Phosphorylation of proteins was analyzed by SDS-PAGE and subsequent detection of radioactive γ-^{32}P signals on x-ray films.

5.2.11 Bacteria based methods

All bacteria were propagated at 37 °C in LB medium. If required, selection antibiotics Ampicillin (50 µg/ml) or Kanamycin (20 µg/ml) were added to the bacterial culture medium. Liquid cultures at 37 °C were kept under continuous shaking to avoid bacterial growth arrest by lack of oxygen.

For long term storage, bacteria cultures were mixed with glycerol (1:1 ratio) and stored at -80 °C.

5.2.11.1 Transformation of competent bacteria

Plasmids were transformed into chemical competent *E. coli* cells in order to amplify the corresponing vector DNA. Therefore, NEB 5-alpha cells (New England Biolabs) were incubated with plasmids of interest for 30 minutes on ice. Heat shock for 45 seconds at 42 °C and immediate cool down led to incorporation of vector DNA by bacterial cells. After recovery in SOC medium (Super Optimal Broth Medium), cells were plated on LB agar containing a selection antibiotic, thus allowing only for the growth of *E. coli* transformed with functional plasmids.

5.2.11.2 Extraction of plasmid DNA

Amplified plasmid DNA from NEB 5-alpha *E. coli* was purified using peqGOLD Plasmid Miniprep Kit I (Peqlab) or Qiagen Plasmid Maxi Kit (Qiagen), according to supplied protocols.

5.2.11.3 Production of GST-tagged proteins

To produce glutathione-s-transferase (GST) tagged proteins, corresponding cDNAs were cloned into pGEX-4T-2. For initiation of protein production, pGEX-4T-2 vectors were transformed

into BL21 (DE3) *E. coli* (Agilent Technologies) and grown over night at 37 °C in LB medium supplemented with 50 μg/ml Ampicillin. Overnight cultures were diluted (1:10 ratio) in antibiotic free LB medium, to allow for higher proliferation efficiency, and grown to the exponential phase with an OD_{600} of 0.5. Subsequent addition of 1 μM isopropyl β-D-1-thiogalactopyranoside (IPTG) to cultures led to inactivation of the *lac* repressor and initiation of protein production (Hansen, Knudsen et al. 1998). Induced BL21 (DE)3 cells were pelleted after 3 hours and stored at -80 °C.

5.2.12 Studies in mice

All animal experiments were performed in agreement with the local ethical guidelines and approved by the District Gorvernment of Upper Bavaria.

5.2.12.1 The transgenic Eμ-Myc lymphoma mouse model

Rearrangements of the *c-Myc* proto-oncogene into the heavy- and light-chain immunoglobulin loci (*IgL*) have been frequently detected in a wide range of lymphoid neoplasms (Dang 2012);(Ott, Rosenwald et al. 2013). However, the *c-Myc* activating translocation alone does not lead to lymphomagenesis (Sander, Calado et al. 2012), thus presenting an interesting background to study the effect of various genetic alterations on lymphomagenesis.

In the here used Eμ-myc transgenic mouse model, the c-Myc gene has been fused to the immunoglobulin heavy chain enhancer (Harris 1988), thus leading to high proliferation rates of pre-B cells (Langdon, Harris et al. 1986) and higher incidence of lymphomas of B-lineage cells (Adams, Harris et al. 1985).

5.2.12.2 Transplantation of primary Eμ-Myc lymphoma cells into C57BL/6 mice

5.2.12.2.1 Transduction and transplantation of primary Eμ-Myc lymphoma cells

Pre-established Eμ-Myc lymphoma cells from the Eμ-myc transgenic mouse model (Harris 1988) were a gift of Susanne Kratzat, Technische Universität München, Germany. Cells were infected twice with retroviruses encoding for Fbxo25 with an IRES-linked GFP cassette or control, respectively. 48 hours after the last spin infection, cells were sorted for GFP positivity and propidium iodide negativity in order to select for infected (GFP positive) and non-dead (PI negative)

cells. After removal of PI by repeated washing steps, cells were resuspended in HF2+ buffer (1x HBSS supplemented with 5% heat-inactivated FBS, 1% Pen/Strep, 1% NEAA, 10 μM β-mercaptoethanol, 1 mH HEPES). Afterwards, 5.5 x 10^3 cells in HF2+ buffer were transplanted into the tail vain of one C57BL/6JOla mouse (Harlan), each.

All transplanted female mice were 10 weeks of age and housed, fed and bred equally. The distribution of mice in the two experimental groups (Fbxo25 overexpression and control groups) was conducted randomly.

5.2.12.2.2 Analysis of transplanted mice

Disease state of the transplanted mice was specified by the presence of palpable lymph nodes and the impairment of the general health status. Time point of sacrifice was determined by an independent member of the mouse care facility with no insight into the experimental design.

In a first experimental step, the spleen weight of sacrificed mice was determined. Next, enlarged lymph nodes were removed from mice and separated into two parts. One part for IHC analysis was fixed in 4% paraformaldehyde (methanol stabilized) and stored at 4 °C. The remaining part of the lymph node was passed through a 70 μm cell straine r in order to obtain a single cell suspension suitable for lysis and analysis of protein levels. Hemoglobin that interferes with protein concentration measurements was removed by lysing erythrocytes using the ACK lysis buffer (ThermoFisher Scientific). Protein levels were determined by SDS-PAGE and immunoblotting.

5.2.12.2.2.1 Lymph node analysis by immunohistochemistry

All IHC stainings and subsequent analyses of lymph nodes were performed by Martina Rudelius, Julius-Maximilians University, Würzburg, Germany.

Samples from transplanted mice were stained for FBXO25 (Sigma-Aldrich, #AV43118), HAX1 (Proteintech, #11266-1-AP), B220 (Affymetrix, #14-0452) as marker for B cells and cleaved caspase 3 (Cell Signaling Technology, #9661) as marker for apoptotic cells. The staining process was performed as described previously (Volkmann, Reuning et al. 2013).

5.2.12.2.2.2 Analysis of survival data

Survival data of the of mice transplanted with Eμ-Myc lymphoma cells were analyzed according to the Kaplan-Meier method (Kaplan and Meier 1958). Statistical significance of the collected data was determined by the Mantel-Cox test using GraphPad Prism 6 as evaluation software.

5.2.12.3 Transplantation of transduced HSPCs into irradiated C57BL/6 mice

5.2.12.3.1 Transduction and transplantation of HSPCs

Hematpoietic stem cell progenitor cells (HSPCs) were prepared from a mixture of Eμ-myc E12.5 to E14.5 fetal livers (McCurrach 2001) [performed by Susanne Kratzat, Technische Universität München, Germany]. HSPCs were pre-stimulated in BBMM (IMDM supplemented with 20% heat-inactivated FBS and 1% BSA) containing 10 ng/ml murine IL-3, 10 ng/ml murine IL-6 and 50 ng/ml SCF (R&D Systems) (Miething, Feihl et al. 2006). After 24 hours of pre-stimulation, stem cell progenitor cells were retrovirally transduced with MLS_shFbxo25 or MLS_control (series of four independent spin infections each) (Scuoppo, Miething et al. 2012). 12 hours after the last spin infection, 8 x 10^6 HSPCs were injected into the tail vain of sublethal irradiated (550 rad) C57BL/6JOla mice (Harlan). To avoid infections due to the transplantation process, mice were treated with 100 mg/l ciprofloxacin in the drinking water. Antibiotic treatment was started 5 days before injection and was finished 8 days post transplantation.

All transplanted female mice were 8 weeks of age and housed, fed and bred equally. The distribution of mice in the two experimental groups (MLS_shFbxo25 versus MLS_control) was conducted randomly.

5.2.12.3.2 Analysis of engraftment

Engraftment of hematopoietic stem cell progenitor cells was measured by FACS analysis. Blood taken from mice at day 28 post transplantation was processed by ACK lysis buffer (ThermoFisher Scientific) in order to remove erythrocytes. Remaining blood cells were stained for CD45/B220 (BD Biosiences, #561869) surface expression to select for hematopoietic cells of the B cell lineage. Afterwards, GFP-positivity of CD45+/B220+ cells was measured by flow cytometry.

5.2.12.3.3 Analysis of transplanted mice

Mice were examined regularly by palpation of the lymph nodes. Disease state of the transplanted mice was specified by the presence of palpable lymph nodes or paralysis (Scuoppo, Miething et al. 2012). Time point of sacrifice was determined by an independent member of the mouse care facility with no insight into the experimental design.

Spleen weight was determined after euthanasia of mice. In a next step, enlarged lymph nodes were removed from mice and separated into two parts. The first part was fixed in 4% paraformaldehyde (methanol stabilized) and stored at 4 °C for further use in IHC. The second part of the lymph nodes was passed through a 70 μm mesh in order to obtain a single cell suspension. Afterwards, single cell suspension was cleared from erythrocytes using the ACK lysis solution (ThermoFisher Scientific). Protein levels were accessed by SDS-PAGE and subsequent immunoblotting analyses.

5.2.12.3.3.1 Lymph node analysis by immunohistochemistry

All IHC stainings and subsequent analyses of samples from mice transplanted with HSPCs were performed by Martina Rudelius, Julius-Maximilians University, Würzburg, Germany. Samples from transplanted mice were stained for FBXO25 (Sigma-Aldrich, #AV43118), HAX1 (Proteintech, #11266-1-AP), B220 (Affymetrix, #14-0452) as marker for B-cells and cleaved caspase 3 (Cell Signaling Technology, #9661) as marker for apoptotic cells. The staining process was performed as described previously (Volkmann, Reuning et al. 2013).

5.2.12.3.3.2 Analysis of survival data

Survival data for the *de novo* lymphomagenesis in C57BL/6 mice were analyzed according to the Kaplan-Meier method (Kaplan and Meier 1958). Statistical significance of the collected data was determined by the Mantel-Cox test using GraphPad Prism 6.

5.2.12.4 Xenograft transplantation model

The mantle cell lymphoma line Granta-519 has been reported to be a suitable line for a xenogeneic transplantation approach (Palmieri, Falcone et al. 2010).

5.2.12.4.1 Transduction and transplantation of Granta-519 cells

In case of the FBXO25 knock-down approach, Granta-519 cells were infected twice with lentiviral shRNA particles targeting human *FBXO25* or corresponding scrambled controls (ThermoFisher/Dharmacon). For targeting *FBXO25* expression, a mixture of all 3 lentiviral particles was added to the infection reaction (supported by 6 μg/ml polybrene).

In case of the HAX1^{S210A} overexpression setting, Granta-519 cells were transduced twice with retroviruses derived from pLPC_puro or pLPC_HAX1_S210A (supported by 6 μg/ml polybrene). All cells were selected with 1 μg/ml puromycin for 3 days to remove non-infected cells. After selection, 8 x 10^6 Granta-519 cells were resuspended in 50 μl 1 x PBS, mixed with 150 μl of Matrigel™ Basement Membrane Matrix (BD Biosciences) and injected subcutaneously into the flanks of female NOD.CB17-Prkdc^{scid}/NCrHsd mice 8 weeks of age (Harlan). To avoid influences of residual mouse immunity on the tumor growth, both experimental conditions (shFBXO25/shcontrol or HAX1_S210A/control) were administered to each mouse.

5.2.12.4.2 PET imaging of xenograft mice

FDG-PET imaging and analysis of PET data were performed by the department of nuclear medicine, Technische Universität München, Germany.

PET analysis was performed at day 26 and day 28 post transplantation, when first xenograft tumors reached the maximal diameter of 15 mm, the pre-defined guide value for terminal disease. The FDG radiotracker was applied by tail vain injection at an activity dose of 5 to 10 MBq, whereby accumulation of the injected radiotracker was allowed for approx. 60 minutes.

The metabolic tumor volume (mm^3) was defined from acquired PET images by placing a semi-automated three-dimensional region of interest (isocontour 50%) around the maximal activity of the tumor (Li, Thorstad et al. 2008).

5.2.12.4.3 Analysis of explanted tumors

Direct after euthanasia of mice, metric tumor volume was calculated by measurement of length (L) and approximately width (W) by calipers and subsequent application of the equation: $V=(L \times W^2) \times 0.5$ (Tomayko 1989).

Tumors were separated into two parts. The first part of the xenograft tumor was passed through a 70 μm cell strainer in order to obtain a single cell suspension suitable for lysis and analysis of protein levels. After removal of erythrocytes by ACK lysis, cell extracts were analyzed

by SDS-PAGE and immunoblotting. The remainig part of the tumor was immunohistochemically analyzed by Martina Rudelius, Julius-Maximilians University, Würzburg, Germany. Samples were stained for FBXO25 (Sigma-Aldrich, #AV43118), HAX1 (Proteintech, #11266-1-AP), CD20 (Abcam, #ab78237) as marker for human B-cells and cleaved caspase 3 (Cell Signaling Technology, #9661) as marker for apoptotic cells. The staining process was performed as previously described (Volkmann, Reuning et al. 2013).

5.2.13 Analysis of human MCL tumor samples

All human MCL tumor samples were analyzed with informed consent in accordance with the review board at the medical faculty at Technische Universität München, Germany.

5.2.13.1 Quantification of DNA levels based on FFPE fixed tumor samples

For DNA extraction, one 10 µm slice of each formalin-fixed paraffin-embedded tumor sample was deparaffinized by a 30 minute incubation with 1 ml xylene and subsequent removal of the paraffin-containing xylene supernatant after a 5 minute centrifugation step at 13000 rpm in a table top centrifuge. Samples were dehydrated and cleared with two 100% ethanol washing steps, each with an incubation time of 30 minutes. The ethanol containing supernatant was removed by a 5 minute centrifugation step at 13000 rpm in a table top centrifuge. Tubes were sealed with laboratory film and dried for 1 hour at 45 °C to achieve a complete desiccation of the contained tumor material. The dried tissue was resuspended in 200 µl Proteinase K buffer (100 mM Tris pH 8.5, 5 mM EDTA, 0.2% SDS, 200 mM NaCl) supplemented with 200 µg of Proteinase K (Qiagen) and stored over night at 55 °C in order to digest all of the contained tumor tissue. Proteinase K was inactivated by a 5 minute incubation step at 95 °C, while potential remaining tissue fragments were removed via short spin in a table top centrifuge. DNA containing buffer was store at 4 °C.

For quantification of *FBXO25* and *ACTB* DNA levels in supplied human MCL patient samples, 40 ng of total DNA were processed in quantification runs at the LightCycler 480 system (Roche), using the SYBR Green I Master (Roche). DNA values for *FBXO25* and *ACTB* were collected as triplicates for each sample and analyzed by their target/reference ratio.

Sequences of primers for the amplification of *FBXO25* exon 6 and *ACTB* are listed under 5.1.4.3.

5.2.13.2 Quantification of mRNA expression levels in FFPE fixed tumor samples

For quantification of *FBXO25* and *ARPP_P0* expression levels in human MCL tumor samples, total RNA from formalin-fixed paraffin-embedded tissue was extracted using the AllPrep DNA/RNA FFPE kit (Qiagen). Extraction was performed according to the manufacturer´s protocol. 1 µg of total RNA was reversely translated to cDNA using the SuperScript III/RNase OUT system (Invitrogen) according to manufacturer´s protocol. 10 ng of total cDNA were processed in quantification runs at the LightCycler 480 system (Roche), using the SYBR Green I Master (Roche). cDNA values for *FBXO25* and *ACTB* were collected as triplicates for each sample and analyzed by their target/reference Cp values via the $2^{-\Delta\Delta Cp}$ method (Livak and Schmittgen 2001).

Primer sequences for *FBXO25* and *ACTB* are indicated within the material part *5.1.4.3*.

5.2.13.3 Immunohistochemistry

FBXO25 and HAX1 protein levels in FFPE tumor samples were determined by immunohistochemistry (IHC).

All IHC stainings and subsequent analyses of stained samples were performed by Martina Rudelius, Julius-Maximilians University, Würzburg, Germany.

Purity of tumor samples on tissue microarrays (TMA) of patient cohort 1 to 3 was determined by histological and immunohistochemical validation before the staining process. Samples on TMAs were stained for FBXO25 (Sigma-Aldrich, #AV43118) and HAX1 (Proteintech, #11266-1-AP), the staining process was performed as described previously (Volkmann, Reuning et al. 2013). FBXO25 and HAX1 protein levels in the IHC stained samples were quantified using the H-score (Kraus, Dabbs et al. 2012). The H-score represents a semi-quantitative immunohistochemical assay by which the percentage of FBXO25/HAX1 positive cells get multiplied by a value correlating to the level of staining intensity (0: none; 1: weak; 2: moderate and 3: strong)(Kraus, Dabbs et al. 2012). H-scores depict values between 0 (0% positive cells with none staining intensity) and 300 (100% positive cells with strong staining intensity). Cutoff values for $FBXO25_{low}$/$FBXO25_{high}$ and $HAX1_{low}$/$HAX1_{high}$ were calculated using the Cutoff Finder (Budczies, Klauschen et al. 2012). Cutoff values were set the following: FBXO25 = 130 and HAX1 = 170.

5.2.13.4 Concordance analysis between IHC, DNA and mRNA data sets

To analyze the concordance between FBXO25 IHC and DNA quantification as well as between FBXO25 IHC and RNA quantification, samples for each method were classified into two

groups: (i) for FBXO25 IHC: $FBXO25_{high}$ and $FBXO25_{low}$ (as indicated in the IHC part), whereby $FBXO25_{high}$ was assigned as 1 and $FBXO25_{low}$ was assigned as 0; (ii) for *FBXO25* DNA quantification: $FBXO25_{high}$ (indicative for two copies of the genomic *FBXO25* locus) and $FBXO25_{low}$ (indicative for one copy of the genomic *FBXO25* locus), while normalized *FBXO25*/*ACTB* ratios > 0.61 were scored as high (assigned as 1), and ratios ≤0.61 were scored as low (assigned as 0); (iii) for *FBXO25* mRNA expression: $FBXO25_{high}$ and $FBXO25_{low}$, while normalized *FBXO25*/*RPPA_P0* ratios > 0.65 were scored as high (assigned as 1), and ratios ≤0.65 were scored as low (assigned as 0). Concordance was assumed when values for FBXO25 IHC and DNA quantification or FBXO25 IHC and RNA quantification were both assigned as 1 or 0. Values for overall concordance between FBXO25 IHC and *FBXO25* DNA/RNA were indicated as percentages.

5.2.13.5 Extraction and analysis of proteins from FFPE fixed tumor samples

Extraction of proteins from FFPE tumor samples was performed according to the protocol published by Nirmalan et al. (2009) (Nirmalan, Harnden et al. 2009).

Two 10 µm slices of selected patient samples were deparaffinized by two 5 minute incubation steps with 1 ml of xylene. Paraffin containing supernatants were removed after centrifugation at maximum speed for 5 minutes. Tissue samples were rehydrated using a decreasing ethanol gradient (100% EtOH – 90% EtOH – 70% EtOH – 70% EtOH). Each of the ethanol rehydrating steps was performed for 5 minutes at room temperature, while afterwards the ethanol containing solution was removed by centrifugation at maximum speed for 5 minutes. For lysis, tissue fractions were resuspended in 100 µl of FFPE Protein Extraction Buffer (100 mM Tris pH 6.8, 2% SDS, 20% glycerol, 4% β-mercaptoethanol) and boiled for 20 minutes at 105 °C. After a 5 minute cool-down on ice, cellular debris were removed by a 30 minutes centrifugation at maximum speed. (Nirmalan, Harnden et al. 2009)

While protein concentrations of FFPE extracts could not be determined by the Bio-Rad DC/Lowry protein assay, a test SDS-PAGE with 10 µl of each extracted sample was set up. Loading of subsequent SDS-PAGEs was normalized according to the Ponceaus S staining of the test SDS-PAGE membrane.

5.2.13.6 Sequencing of MCL tumor samples

DNA from FFPE tumor samples was extracted using the AllPrep DNA/RNA FFPE kit (Qiagen). *FBXO25* exons 4 to 8 and *HAX1* exon 5 were amplified using the LightCycler 480 High

Resolution Melting Master (Roche). Extraction and amplification of DNA was performed according to the corresponding protocol.

Amplified tumor DNA was purified from components of the amplification reaction via the GeneJET PCR purification Kit (TermoFisher Scientific). DNA was sequenced using the same primers as used for amplification of DNA elements, sequences of corresponding primers are listed in the material part 5.1.4.4. Sequencing reactions were performed with Eurofins Genomics, Ebersberg, Germany.

Sequencing results from tumor samples were aligned (MacVector 13.5.5) to the wildtype reference sequences of *FBXO25* and *HAX1* obtained from the NCBI database. The somatic origin of all identified mutations was verified by sequencing the corresponding patient DNA from normal, tumor-surrounding tissue.

5.2.14 CHG array data analysis

Analyses of comparative genomic hybridization (CGH) data sets were performed to identify copy number variations (CNVs) at the human chromosome 8p in mantle cell lymphoma. Previously published data sets for 170 MCL patients were accessed and CNV calling was performed according to identical criteria for all studies. Criteria for copy number variation calling were assigned as follows: heterozygous loss, log2 value ≤ -0.3; homozygous loss, log2 value ≤ -1.0; amplification, log2 value ≥ 0.3. The minimal number of sequential probes/BAC clones for calling of a specific region was set as $n = 3$.

5.2.15 Statistics

Statistical analyses of relative results were performed by Mantel-Cox test, unpaired *t*-test or one-way analysis of variance (one-way ANOVA), according to assumptions of the corresponding test. All statistical calculations were executed using GraphPad Prism 6 software. Error bars shown in the figures represent the mean +/- standard deviation (SD) or the mean +/- standard error of the mean (SEM). When a statistic significant difference was present, *P* values were represented in the figure legends. Distribution of *P* values was the following: * $P < 0.05$; ** $P < 0.01$ and *** $P < 0.001$.

6 Results

The present study was performed in cooperation with the co-author Vanesa Fernández-Sáiz, Technische Universität München, Germany and other collaborators. Contributions of these collaborators to the presented data sets are indicated within text and figure legends. Initial data of the presented project, including mass spectrometry based analysis of tandem affinity purified FBXO25, were already presented within my master`s thesis "Characterization of the SCF-FBXO25-E3-ubiquitin-ligase" (Baumann 2011). Previous published results are additionally indicated in text and figure legends.

6.1 FBXO25 targets HAX1 in response to apoptotic stimulation

6.1.1 FBXO25 is an interactor of the unstable apoptosis regulator HAX1

The analysis of public available comparative genomic hybridization array (aCGH) data sets from different human B-cell lymphoma entities identified a frequent deletion of the genomic locus 8p23.3 (Schraders, Pfundt et al. 2005);(Pasqualucci, Trifonov et al. 2011), correlating with the genomic localization of the human F-box protein FBXO25. Deletions of 8p23.3 were present at high frequencies in MCL patient samples (up to 29%) (Schraders, Pfundt et al. 2005) and DLBCL biopsies (approx. 8%), while no alteration of the locus could be identified in Burkitt lymphoma (Toujani, Dessen et al. 2009) and FL (Cheung, Shah et al. 2009). A more stringent analysis of aCGH studies of human MCL (189 cases in total) (Schraders, Pfundt et al. 2005);(Rubio-Moscardo, Climent et al. 2005);(Flordal Thelander, Ichimura et al. 2007);(Tagawa, Karnan et al. 2005);(Martinez-Climent, Vizcarra et al. 2001) identified *FBXO25* within a 1.2 Mb minimal common region of deletion of 8p23.3 and confirmed a high frequency of *FBXO25* deletions (mean, 24.3%) in the studied human MCL samples (for methodology compare 5.2.14). Moreover, aCGH data analyses unraveled an exclusively monoallelic nature of the observed *FBXO25* deletions, giving rise to *FBXO25* as a potential new haploinsufficient tumor suppressor gene.

In order to identify the corresponding substrate(s) of the previously orphan F-box protein FBXO25, cDNA of FBXO25 was cloned into N-SF-TAP-pcDNA3.0. Tandem-Strep-single-FLAG-tagged FBXO25 and the corresponding empty vector control were transiently expressed in human embryonic kidney (HEK)293T cells and purified by a tandem affinity purification approach (Figure 8a) (Baumann 2011). Purified baits and their potential interactors were analyzed by mass spectrometry [mass spectrometry was performed by Simon Lemeer, Technische Universität München, Germany]. Mass spectrometric analysis using FBXO25 as bait identified peptides

derived from the SCF core components SKP1 and CUL1 as well as 11 unique peptides corresponding to the HCLS1-associated protein X-1 (HAX1) (Figure 8b). [FBXO25 purification and mass spectrometric analysis were previously part of the master`s thesis "Characterization of the SCF-FBXO25-E3-ubiquitin-ligase" (Baumann 2011).]

a

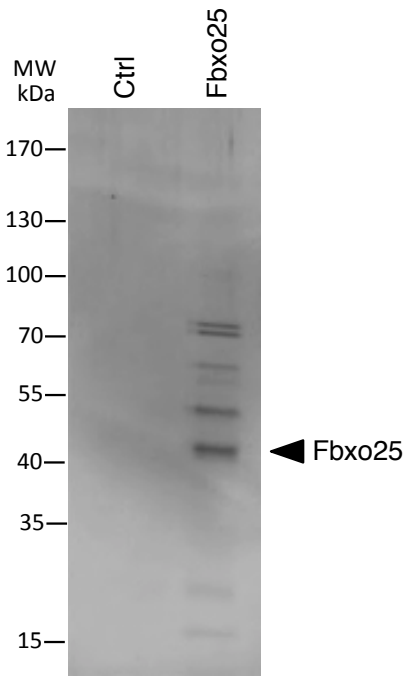

b

HCLS1 associated protein X-1 (Hax-1)0000 IPI00641973

Sequence	Mascot Ion score	Modifications	Start	Stop
(K)ITKPDGIVEER(R)	51,28		224	234
(K)ITKPDGIVEERR(T)	33,17		224	235
(K)YPDSHQPR(I)	44,78		140	147
(R)DPFFGGmTR(D)	37,69	Oxidation (+16)	21	29
(R)DSmLKYPDSHQPR(I)	29,53	Oxidation (+16)	135	147
(R)GFFGFPGPR(S)	48,17		9	17
(R)IFGGVLESDAR(S)	63,48		148	158
(R)LREGQTLR(D)	44,01		127	134
(R)RTVVDSEGRTETTVTR(H)	29,1		235	250
(R)TREDNDLDSQVSQEGLGPVLQPQPK(S)	48,49		189	213
(R)TVVDSEGRTETTVTR(H)	43,04		236	250

Figure 8: Purification of FBXO25 and mass spectrometric analysis for interactors. (**a**) Tandem-Step-single-FLAG-tagged FBXO25 was transiently expressed in HEK293T cells ($5x10^9$ cells) and purified by a tandem affinity approach comprising immobilization on Strep-Tactin beads and elution with 2.5 mM desthiobiotin followed by immobilization on anti-FLAG M2 agarose and elution with 3x FLAG peptide. As control, whole cell lysates from HEK293T cells ($5x10^9$ cells) transfected with an empty vector control were purified as indicated above. The depicted silver stained SDS-gel corresponds to 5% of the final 3x FLAG peptide eluted proteins. [data previously published in "Characterization of the SCF-FBXO25-E3-ubiquitin ligase" (Baumann 2011)]. (**b**) Sequences of unique peptides corresponding to HAX1 identified by mass spectrometric analysis within the FBXO25 sample [data provided by Simon Lemeer, Technische Universität München, Germany]

Proteins known to be degraded by the ubiquitin-proteasome system are, in the majority of cases, characterized by their short half-life time (Ciechanover, Orian et al. 2000). To test whether HAX1 is an unstable protein, which might be even a specific substrate of the UPS E3 ligase FBXO25, U-2 OS cells were treated with 100 µg/ml cycloheximide to inhibit *de novo* synthesis of proteins by blocking translational elongation at ribosomes. Analysis of whole cell lysates showed HAX1 as unstable protein with a half-life of approximately two hours (Figure 9a). The comparison with PLK1, a molecule described to be unstable and UPS-degraded, emphasizes HAX1 as potential novel substrate of the orphan E3 ubiquitin ligase SCF^{FBXO25} (Figure 9a). [Analysis of HAX1 after cycloheximide addition was previously part of the master`s thesis "Characterization of the SCF-FBXO25-E3-ubiquitin-ligase" (Baumann 2011).] HAX1 has previously been implicated in pro-survival signaling (Klein, Grudzien et al. 2007), hypothesizing that the anti-apoptotic molecule is degraded after induction of apoptosis. To test this hypothesis, U-2 OS cells were treated with 1 µg/ml paclitaxel in order to induce apoptosis by inhibiting beta-tubulin dependent formation of the mitotic spindle. Analysis of U-2 OS whole cell lysates showed a clear drop of HAX1 levels after 10 to 24 hours of paclitaxel treatment, underlining that HAX1 is degraded after induction of apoptosis (Figure 9b).

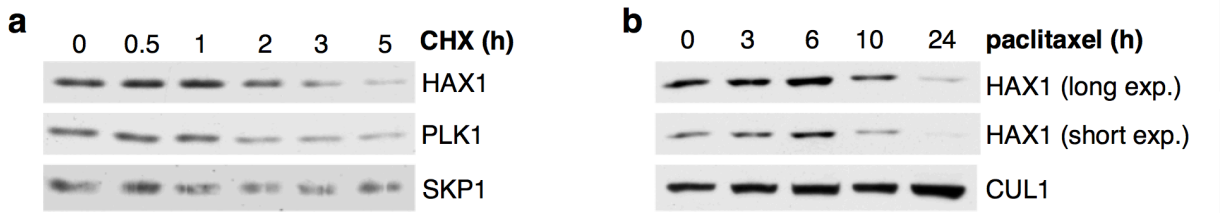

Figure 9: HAX1 is an unstable protein that is degraded after induction of apoptosis. (**a**) U-2 OS cells were treated with cycloheximide for 0, 0.5, 1, 2, 3 and 5 hours (h) to inhibit *de novo* protein synthesis. Whole cell lysates were seperated by SDS-PAGE and protein levels were analyzed by immunoblotting using antibodies directed against HAX1, the known UPS substrate PLK1 and SKP1. SKP1 levels serve as loading control. [data previously published in "Characterization of the SCF-FBXO25-E3-ubiquitin ligase" (Baumann 2011)]. (**b**) U-2 OS cells were treated with paclitaxel for 0, 3, 6, 10 and 24 hours (h) to induce apoptosis. Whole cell lysates were seperated by SDS-PAGE and protein levels of HAX1 and CUL1 were accessed by immunoblotting using the corresponding antibodies. CUL1 levels serve as loading control of the SDS-PAGE. Exp., exposure.

In summary, MS-based analysis identified HAX1 as potential novel interactor of the SCF^{FBXO25} E3 ligase complex. Moreover, HAX1 itself represents an unstable molecule that is degraded after induction of apoptosis.

6.1.2 FBXO25 specifical interacts with HAX1 and forms an intact SCF-complex

FBXO25 has previously been described as an evolutionary conserved F-box protein that forms an intact SCF complex (Hagens, Minina et al. 2006). In line with this study, mass spectrometric analysis in search for FBXO25 interactors identified peptides corresponding to the SCF core components CUL1 and SKP1 as well as peptides corresponding to the potential substrate HAX1 within samples of affinity purified FBXO25. To verify these interactions, GFP-tagged FBXO25 was overexpressed in HEK293T cells in the presence or absence of co-overexpressed FLAG-tagged HAX1. Immunoprecititation of HAX1 by an anti-FLAG resin (see 5.2.3.4.1) showed a specific co-immunopreciptiation of FLAG-HAX1 with GFP-tagged FBXO25 and the SCF core components CUL1 and SKP1, whereupon no significant interaction could be detected within control samples (Figure 10a). In order to validate the immunoprecipitation results in a *vice versa* setting, FLAG-tagged FBXO25 was transiently overexpressed in HEK293T cells. The results of the immunoprecipitation study showed a clear interaction of FLAG-tagged FBXO25 with the SCF subunits SKP1 and CUL1 as wells as with endogenous HAX1, the potential substrate of SCF^{FBXO25} (Figure 10b).

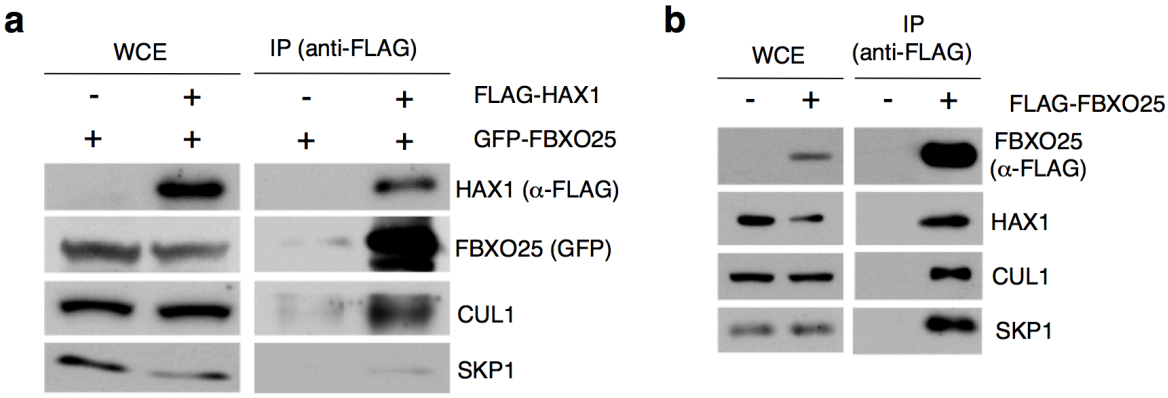

Figure 10: FBXO25 and HAX1 co-immunoprecipitate with the SCF core components SKP1 and CUL1. (**a**) HEK293T cells were transfected with the indicated constructs of FLAG-HAX1 and GFP-FBXO25. Proteins of whole cell lysates of untreated cells were immunoprecipitated with anti-FLAG resin, separated by SDS-PAGE and probed with antibodies directed against FLAG (HAX1), GFP (FBXO25), CUL1 and SKP1. (**b**) HEK293T cells were transfected with the indicated construct of FLAG-FBXO25. Proteins of whole cell lysates of untreated cells were immunoprecipitated with anti-FLAG resin and probed with antibodies directed against FLAG (FBXO25), HAX1, CUL1 and SKP1.

HAX1 showed a clear interaction with FBXO25 and the SCF components SKP1 and CUL1. To further evaluate the specificity of the HAX1/FBXO25 interaction and to preclude a general interaction of HAX1 with F-box proteins, variable F-boxes were tested with regard to their potential

interaction with HAX1. For that purpose, FLAG-tagged FBXO11, FBXO18, FBXO21, FBXO25 and an empty vector control were transiently transfected into HEK293T cells and all samples were treated with 1 µg/ml paclitaxel for 24 hours before harvesting. Immunopreciptitation of the overexpressed F-box proteins uncovered a clear interaction of FBXO25 with endogenous HAX1. In contrast, no co-immunoprecipitation of HAX1 could be observed for FBXO11, FBXO18, FBXO21 and the empty vector control (Figure 11).

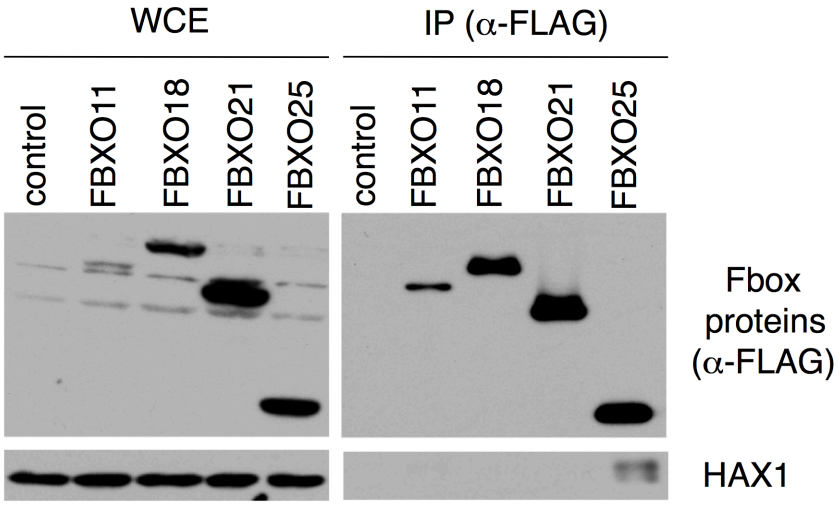

Figure 11: HAX1 specifically interacts with FBXO25. HEK293T cells were transiently transfected with empty vector control or the indicated constructs of FLAG-tagged F-box proteins. After transfection, cells were treated for 24 hours with 1 µg/ml paclitaxel. Whole cell lysates were immunoprecipitated using an anti-FLAG resin and separated by SDS-PAGE. Subsequently, immunoprecipitates were probed with antibodies to FLAG (F-box proteins) and endogenous HAX1.

In summary, FBXO25 forms an intact SCF-complex by immunoprecipitating with the SCF core components SKP1 and CUL1. Moreover, HAX1 interacts with FBXO25 on protein levels, an interaction that is specific for FBXO25 and is not verifiable with FBXO11, FBXO18 and FBXO21.

6.1.3 FBXO25 targets HAX1 in response to apoptotic stimulation

Previous experiments identified the anti-apoptotic HAX1 as an unstable molecule that is degraded after induction of apoptosis (Figure 9). In this context FBXO25 was hypothesized to function as the E3 ubiquitin ligase of HAX1 in response to apoptotic stimulation, leading to a potential increased interaction of FBXO25 and HAX1 after induction of apoptosis. To test this hypothesis, HEK293T cells were treated with 1 µg/ml etoposide, inducing apoptosis via DNA

double strand breaks, or solvent for 24 hours. Subsequently, whole cell lysates were immunoprecipitated with an anti-FBXO25 antibody or corresponding control IgG. In line with the initial hypothesis, HAX1 demonstrated increased binding to FBXO25 after exposure to apoptotic stimulation, suggesting an increased SCF^{FBXO25} mediated degradation of HAX1 (Figure 12). The elevated levels of the apoptotic effector cleaved caspase 3 (CC3) within the whole cell extracts served as controls for the induction of apoptosis by etoposide.

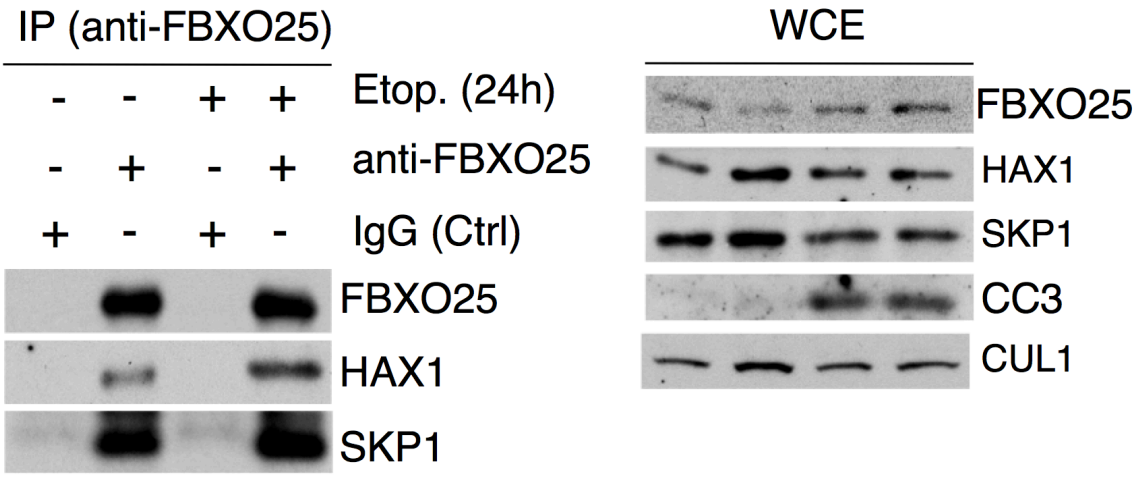

Figure 12: HAX1 shows increased binding to FBXO25 after induction of apoptosis. HEK293T cells were treated with etoposide (Etop.) or solvent for 24 hours (h). Whole cell extracts (WCE) represent the input levels of proteins used in the immunoprecipitation assay, whereat cleaved caspase 3 (CC3) serves as marker for apoptosis and CUL1 serves as loading control. Immunoprecipitated proteins were separated by SDS-PAGE and probed with antibodies directed against FBXO25, HAX1 and SKP1.

With regard to FBXO25 as the potential E3 ubiquitin ligase of the cell survival-promoting molecule HAX1, knock-down of FBXO25 should result in an increase of overall HAX1 levels and induce a stabilization of HAX1 after application of variable apoptotic stimuli. In order to validate the effects of a RNAi mediated Fbxo25 knock-down on Hax1 protein levels, NIH/3T3 fibroblasts were transduced retrovirally with constructs encoding shFbxo25 or a non-targeting vector control. Immunoblotting, using Cul1 as a loading control, showed a significant decrease of endogenous Fbxo25 levels in cells treated with shFbxo25 (Figure 13). Lysates of untreated NIH/3T3 cells reveal a slight increase in the overall levels of Hax1 after reduction of Fbxo25 levels (first lanes of both panels). The subsequent treatment of control cells with 100 µg/ml of the protein *de novo* synthesis inhibitor cycloheximide in combination with 1 µg/ml of the apoptosis inducing agent paclitaxel revealed a clear destabilization of Hax1 within 4 to 6 hours of treatment. In contrast, Fbxo25

depleted cells showed a stable Hax1 expression level after treatment with cycloheximide and paclitaxel. The effect seen for Hax1 levels could not be observed for Plk1, another UPS degraded molecule, thus underlining a specific effect of Fbxo25 depletion on Hax1 expression levels. Moreover, additional application of the proteasomal inhibitor MG132 prevented the degradation of Hax1 in both cellular settings (compare lanes 5 to 7 of both panels), further illustrating the proteasome-dependent degradation of Hax1 (Figure 13).

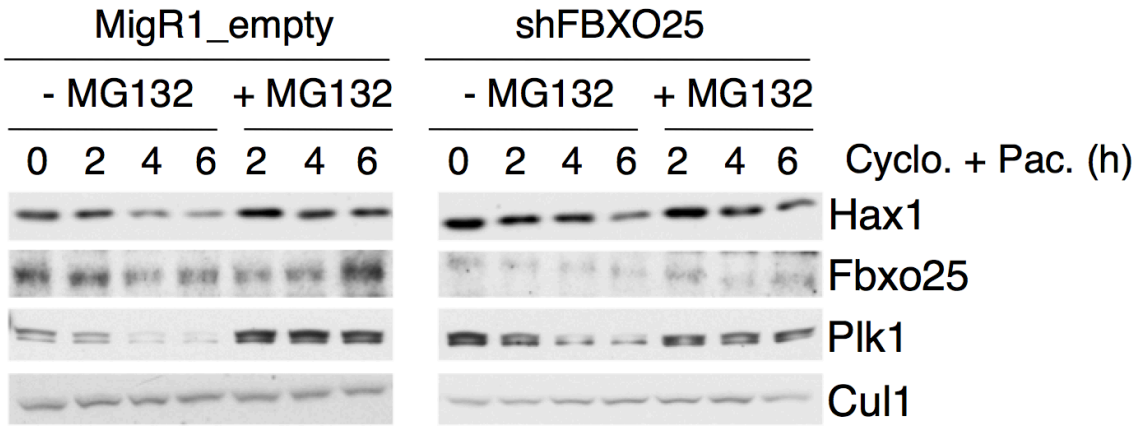

Figure 13: Fbxo25 depletion stabilizes Hax1 protein levels. Immunoblot analysis of NIH/3T3 fibroblasts in which Fbxo25 was silenced by retroviral transduction with shRNA targeted against Fbxo25 (shFbxo25) or control vector (MigR1_empty). Before harvesting, cells were treated with cycloheximide (Cyclo.), paclitaxel (Pac.) and MG132 for 0, 2, 4 or 6 hours (h) as indicated. Whole cell lysates were separated by SDS-PAGE and analyzed with antibodies recognizing Hax1, Fbxo25, Plk1 and Cul1.

An independent experimental approach in C57BL/6 wildtype MEFs reinforced the observed stabilizing effect of Fbxo25 depletion on Hax1 expression levels after variable apoptotic stimuli including etoposide, doxorubicine and serum deprivation [performed by Vanesa Fernández-Sáiz, Technische Universität München, Germany; data not shown].

To test the biological importance of SCF^{FBXO25}-mediated proteolysis of HAX1, effects of Fbxo25 silencing or forced overexpression of Fbxo25 were tested in C57BL/6 *Hax1*$^{-/-}$ MEFs or their corresponding wildtype counterparts (Chao, Parganas et al. 2008) (Figure 14). Knock-down of Fbxo25 in wildtype MEFs impaired the apoptotic response towards etoposide (1 µg/ml), demonstrated by inhibition of Parp1 cleavage and stabilized cellular Hax1 expression levels (upper panel, left part). In contrast, knock-down of Fbxo25 in *Hax1*$^{-/-}$ MEFs did not affect the apoptotic response towards etoposide (upper panel, right side). Forced expression of GFP-tagged Fbxo25 in

C57BL/6 MEFs accelerated the drop of Hax1 protein levels and increased the level of Parp1 cleavage as marker for the apoptotic response (lower panel, left part). Overexpression of GFP-Fbxo25 in *Hax1*$^{-/-}$ MEFs did not affect apoptotic response to etoposide illustrated by unchanged levels of Parp1 and cleaved Parp1 (lower pannel, right part). [The presented experiments of Fbxo25 modification within wildtype or *Hax1*$^{-/-}$ MEFs were performed by Vanesa Fernández-Sáiz, Technische Universität München, Germany]

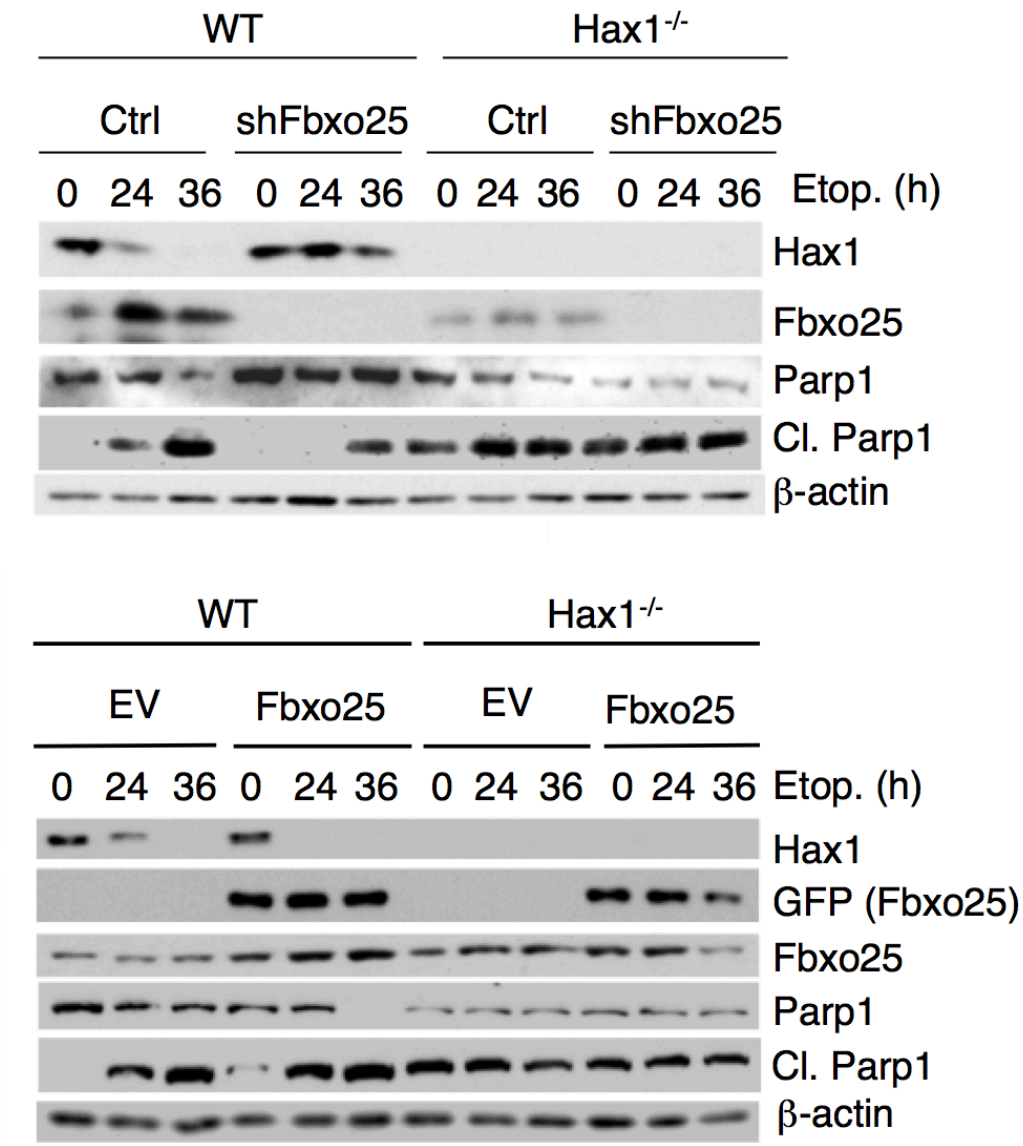

Figure 14: Fbxo25 mediated apoptosis induction is dependent on Hax1. Immunoblot analyses of C57BL/6 *Hax1*$^{-/-}$ or wildtype MEFs. MEFs were transduced with shRNA constructs directed against scrambled control (Ctrl) or Fbxo25 mRNA (shFbxo25) [upper panel] or transfected with GFP-tagged Fbxo25 (Fbxo25) or the corresponding empty vector control (EV). MEFs were treated with etoposide (Etop.) for 0, 24 and 36 hours (h) as indicated and whole cell lysates were analyzed by immunoblotting. [data provided by Vanesa Fernández-Sáiz, Technische Universität München, Germany].

In summary, FBXO25 targets HAX1 in response to apoptotic stimulation, whereupon silencing of Fbxo25 precluded the proteasomal degradation of Hax1 in a NIH/3T3 model. Moreover, Fbxo25 can exert its pro-apoptotic activity only in the presence of Hax1 as demonstrated by silencing or forced expression of Fbxo25 in *Hax1*$^{-/-}$ MEFs versus the corresponding C57BL/6 wildtype MEFs.

6.1.4 Targeting of HAX1 requires the cytoplasmatic translocation of FBXO25

Two proteins that interact on the immunoblotting level are predicted to show also co-localization within cells. In order to test this hypothesis, C57BL/6 wildtype MEFs were transfected with constructs encoding FLAG-Fbxo25 and HA-Hax1. Subsequent to fixation with methanol, cells were stained for FLAG and HA in an immunofluorescence approach (for detailed information see 5.2.7.2). The analysis of the subcellular localization of Fbxo25 and Hax1, using a fluorescence microscope, revealed that Hax1 mostly localized to mitochondria, whereas the majority of Fbxo25 localized to the nucleus (Figure 15, upper panel). To test a potential change of subcellular localization of these proteins after induction of apoptosis, MEFs were treated with 1 µg/ml etoposide for 20 hours. Etoposide treatment induced a translocation of Fbxo25 from nucleus to the cytoplasm, where Fbxo25 co-localized with Hax1 at site of mitochondria (Figure 15, lower panel).

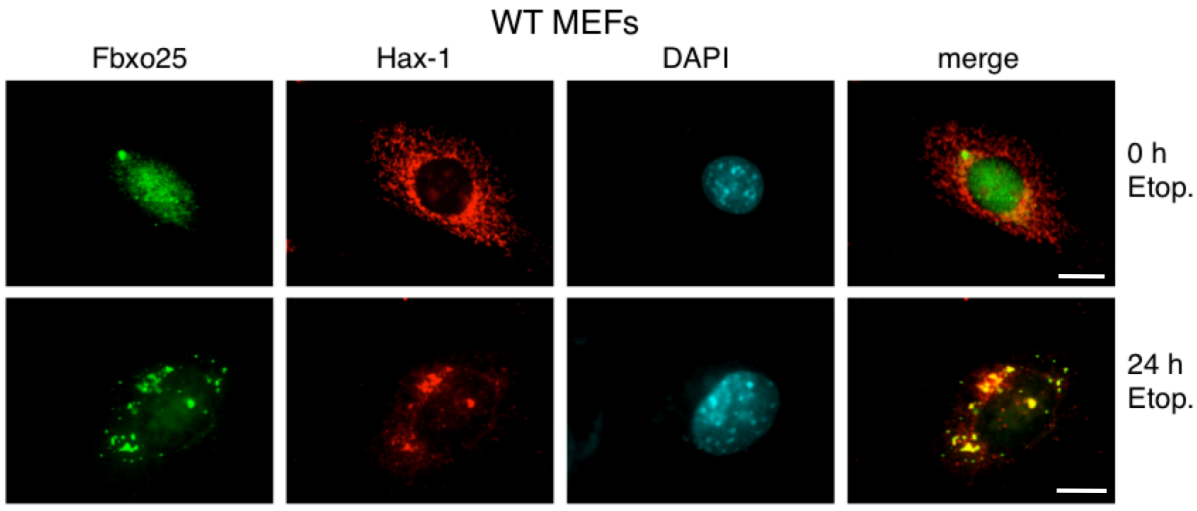

Figure 15: After induction of apoptosis Fbxo25 translocates to mitochondria to co-localize with Hax1. C57BL/6 wildtype MEFs were transiently transfected with constructs encoding FLAG-Fbxo25 and HA-Hax1 and treated for 20 hours with etoposide (Etop.) or solvent. After the treatment period, cells were fixed with methanol and incubated with antibodies directed against FLAG and HA. The primary anti-FLAG antibody was stained in green (Fbxo25) and HA was stained in red (Hax1). DNA was stained with DAPI (blue). Scale bars denote 10 µm.

While many regulatory processes in apoptosis are dependent on TP53 (Fridman and Lowe 2003), the dependency of Fbxo25 shuttling and co-localization with Hax1 on the presence of p53 should be elucidated. For this purpose *p53*$^{-/-}$ MEFs were transfected with constructs encoding FLAG-tagged Fbxo25 and HA-tagged Hax1 and treated with 1 µg/ml etoposide or solvent for 20 hours. In line with the data derived from wildtype MEFs, etoposide treatment induced a similar translocation of Fbxo25 form nucleus to mitochondria and a local co-localization with Hax1 (Figure 16). Indirect immunofluorescence studies (Figure 16) and immunoblotting (performed by Vanesa Fernández-Sáiz, Technische Universität München, Germany; data not shown) underlined the observed autonomy of the Fbxo25 mediated degradation process of Hax1 from p53.

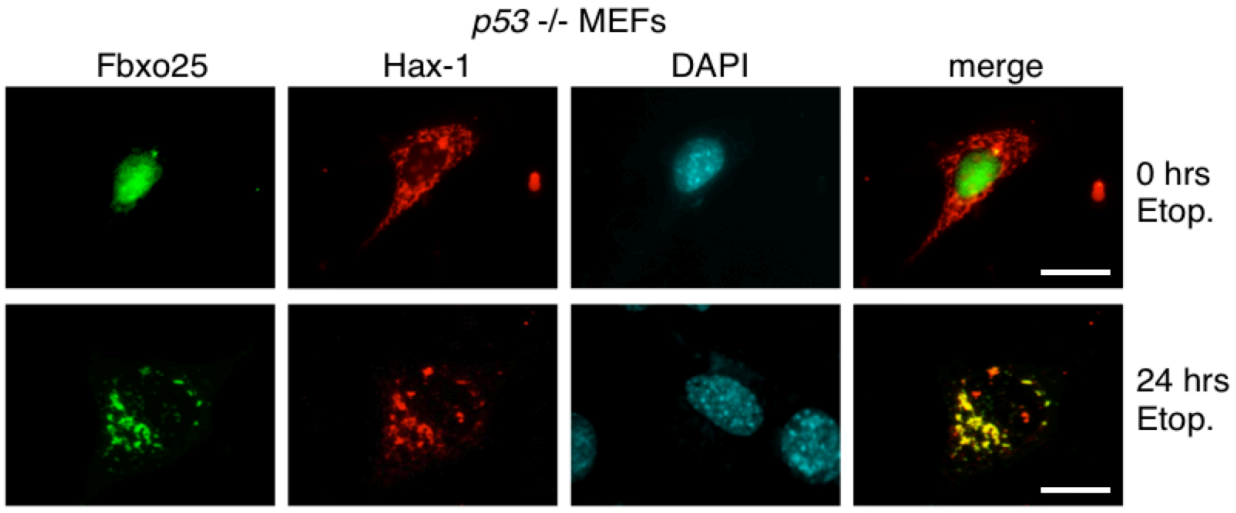

Figure 16: Fbxo25 translocates to mitochondria to co-localize with Hax1 in a p53 independent mechanism. *p53*$^{-/-}$ MEFs were transiently transfected with constructs encoding FLAG-Fbxo25 and HA-Hax1 and treated for 20 hours with etoposide (Etpo.) or solvent. After treatment, cells were fixed with methanol and incubated with antibodies directed against FLAG and HA. FLAG was stained in green (Fbxo25) and HA was stained in red (Hax1). DNA was stained with DAPI (blue). Scale bars denote 10 µm.

In summary, apoptotic stimulation leads to the translocation of Fbxo25 from the nucleus to site of mitochondria leading to a co-localization of Fbxo25 and Hax1. Moreover, studies in *p53*$^{-/-}$ MEFs show the independency of the Fbxo25 shuttling process from the presence of functional p53.

6.2 FBXO25 mediated degradation of HAX1 requires phosphorylation of FBXO25 and HAX1

6.2.1 Degradation of HAX1 requires the phosphorylation of a conserved NES motif within the FBXO25 sequence

The presence of a conserved monopartite SV40 large T antigen-like nuclear localization signal (NLS) within the FBXO25 sequence facilitates a translocation of FBXO25 through nuclear pores and an accumulation within the nucleoplasm (Lange, Mills et al. 2007);(Görlich, Kostka et al. 1995). The previously observed nuclear-cyctoplasmic shuttling process of FBXO25 propounded the additional presence of a nuclear export signal (NES). Sequence analyses uncovered the presence of an evolutional conserved NES (-LQDLSSTLCIL-) within the sequence of FBXO25, spanning amino acids 173 to 183 (Figure 17).

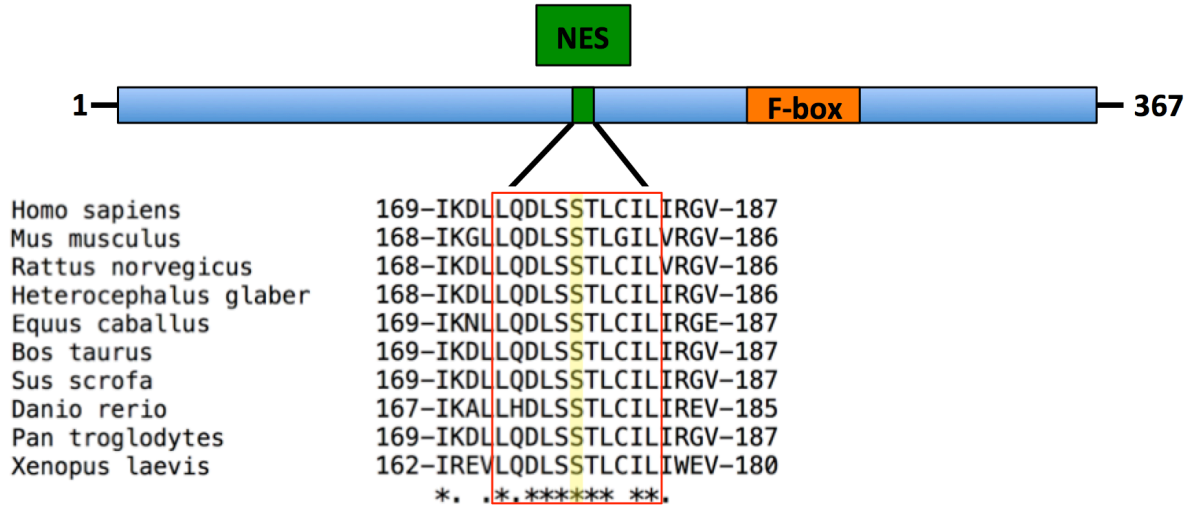

Figure 17: FBXO25 possesses an evolutionary conserved nuclear export signal (NES). Alignment of the amino acid region containing the conserved nuclear export signal (NES) sequence in FBXO25 homologs (red frame) with a conserved serine residue at position 178 of human FBXO25 (marked in yellow).

The identifed NES-sequence contains a conserved serine residue at position 178 that exhibits a high probability of phosphorylation (Figure 17, yellow marked bar). In order to test the dependency of the translocation process on phosphorylation of Ser178 in FBXO25, the serine residue was mutated to alanine using a site directed mutagenesis approach on cDNA level (see 5.2.1.5). COS-7 cells were subsequently transfected with FLAG-tagged constructs of FBXO25 wildtype or the FBXO25^{S178A} mutant and treated for induction of apoptosis with 1 µg/ml etoposide or solvent for 24 hours. Etoposide treatment of COS-7 cells expressing the FBXO25 wildtype

showed the previously observed translocation of FBXO25 to the cytoplasm to co-localize with HAX1 (Figure 18a). [Analysis of the localization of the FBXO25 wildtype +/- induction of apoptosis (Figure 18a) was previously part of the master`s thesis "Characterization of the SCF-FBXO25-E3-ubiquitin-ligase" (Baumann 2011).] The percentage of cells with nuclear staining of FBXO25 decreased significant after treatment of etoposide (n = 4; P < 0.001) (Figure 18b). In contrast, the FBXO25 form mutated at the residue 178 (FBXO25^{S178A}) retained nuclear localization after treatment with etoposide (Figure 18c). The percentage of cells with nuclear staining of FBXO25 did not significantly change after treatment with etoposide as compared to solvent (n = 4) (Figure 18d).

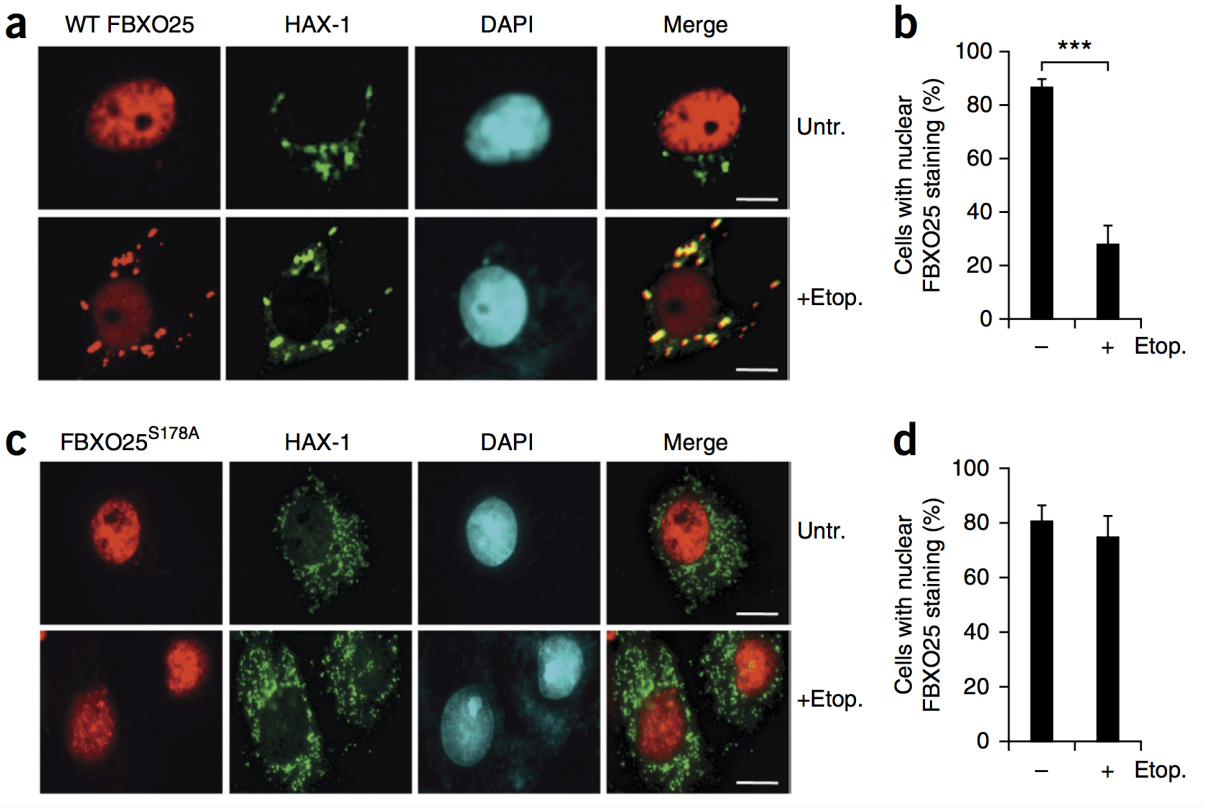

Figure 18: Phosphorylation of a conserved NES motif in FBXO25 enables the nuclear export of FBXO25 after apoptotic stimulation. (**a**) Immunofluorescence study of COS-7 cells transfected with FLAG-FBXO25 wildtype and HA-tagged HAX1. Cells were treated with etoposide (Etop.) or solvent (Untr.) for 24 hours, followed by methanol fixation and incubation with antibodies directed against FLAG or HA. FLAG (FBXO25) was stained in red and HA (HAX1) was stained in green. DNA was counter-stained with DAPI (blue). Scale bars denote 10 µm. [Analysis of the localization of the FBXO25 wildtype +/- induction of apoptosis was previously part of the master`s thesis "Characterization of the SCF-FBXO25-E3-ubiquitin-ligase" (Baumann 2011).] (**b**) Quantification of cells in **a** with nuclear immunofluorescence staining for FBXO25 treated with solvent or etoposide (each count 100 cells, $n$ = 4, mean ± standard deviation). ***$P$ < 0.001, Student`s t test. (**c**) Immunofluorescence imaging of COS-7 cells transfected with the FLAG-FBXO25^{S178A} mutant and HA-tagged HAX1. Cells were treated with etoposide (Etop.) or solvent (Untr.) for 24 hours, followed by methanol fixation and incubation with antibodies directed against FLAG or HA. FLAG (FBXO25^{S178A}) was stained in red and HA (HAX1) was stained in green. DNA was stained with DAPI (blue). Scale bars denote 10 µm. (**d**) Quantification of cells in **a** with nuclear immunofluorescence staining for FBXO25^{S178A} treated with solvent or etoposide (each count 100 cells, n = 4, mean ± standard deviation).

To further verify that FBXO25 translocates to mitochondria after induction of apoptosis by etoposide, COS-7 cells were transfected with FLAG-FBXO25 wildtype and treated with etoposide or solvent for 24 hours. Visualization of mitochondria by mitotracker staining revealed a clear mitochondrial pattern and showed translocation of FBXO25 to these organelles upon induction of apoptosis (Figure 19a). In contrast, the FBXO25^{S178A} NES mutant retained nuclear localization and did not show co-localization with the mitotracker signal after etoposide treatment (Figure 19b).

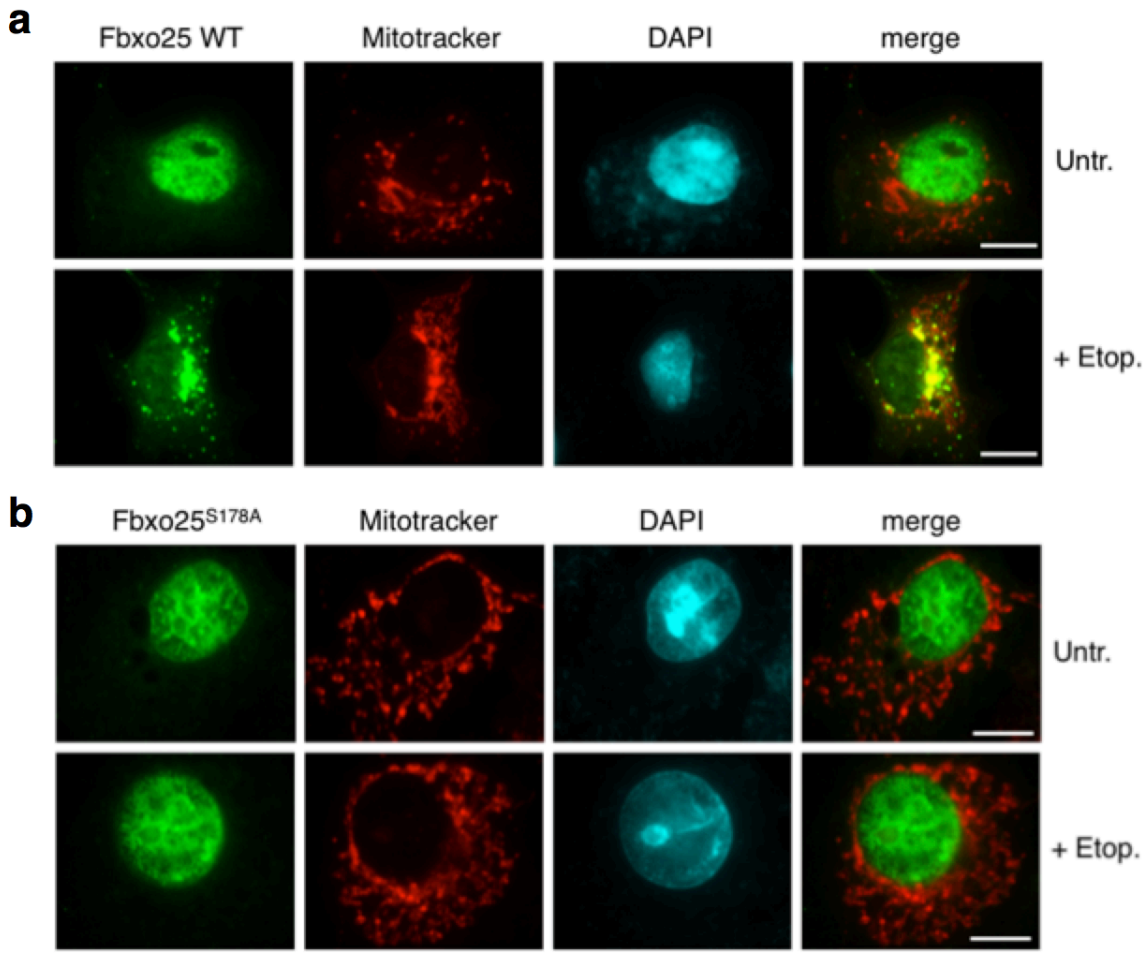

Figure 19: Phosphorylation of a conserved NES motif in FBXO25 enables mitochondrial translocation of FBXO25 after apoptotic stimulation. (**a**) Immunofluorescence study of COS-7 cells transfected with FLAG-FBXO25 wildtype. Cells were treated with etoposide (Etop.) or solvent (Untr.) for 24 hours, followed by mitotracker staining (red). Cells were fixed with methanol and incubated with an antibody directed against FLAG. FLAG (FBXO25) was stained in green and DNA was stained with DAPI (blue). Scale bars denote 10 µm. (**b**) Immunofluorescence imaging of COS-7 cells transfected with the FLAG-FBXO25^{S178A} mutant and treated with etoposide (Etop.) or solvent (Untr.) for 24 hours, followed by mitotracker staining (red). Cells were fixed with methanol and incubated with an antibody directed against FLAG. FLAG (FBXO25^{S178A}) was stained in green and DNA was stained with DAPI (blue). Scale bars denote 10 µm.

Overexpression of Fbxo25 has been shown to induce an increased apoptotic response in MEFs (Figure 14). To further evaluate the effects of forced expression of Fbxo25^{S178A} on apoptotic signaling pathways, MEFs were transfected with Fbxo25 wildtype, Fbxo25^{S178A} or an empty vector control and treated with 1 µg/ml etoposide for 0 or 48 hours (Figure 20a). In untreated control cells, forced expression of the Fbxo25 WT increased the level of phospho-Fbxo25, phosphorylated at serine Ser178 and induced lower levels of Hax1 as well as an increase of cleaved caspase 3, a marker of apoptosis. In contrast, forced expression of the Fbxo25^{S178A} mutant led to a clear stabilization of Hax1 and did not induce higher rates of apoptosis as compared to empty vector control. After treatment with etoposide, Fbxo25 wildtype expressing cells demonstrated lower Hax1 levels, compared to control, and showed a distict accumulation of cleaved caspase 3. In line with the oberservation in solvent treated cells, expression of Fbxo25^{S178A} neither destabilized Hax1 nor led to an increased sensitivity of MEFs towards apoptotic stimulation as represented by cleaved caspase 3 levels comparable to empty vector control. Fluorescence activated cell sorting (FACS) analyses of MEFs transfected with Fbxo25 wildtype showed an increased rate of propidium iodide (PI) positive, apoptotic cells, whereas no effect could be observed in cells overexpressing the Fbxo25^{S178A} NES mutant (Figure 20b) (for methodology compare 5.2.8). After treatment with etoposide for 24 and 48 hours, the Fbxo25 wildtype overexpressing cells showed a significant increase in apoptotic cells as compared to empty vector control cells or cells expressing Fbxo25^{S178A}. Forced expression of Fbxo25^{S178A} demonstrated no significant change in apoptotic rates compared to control cells.

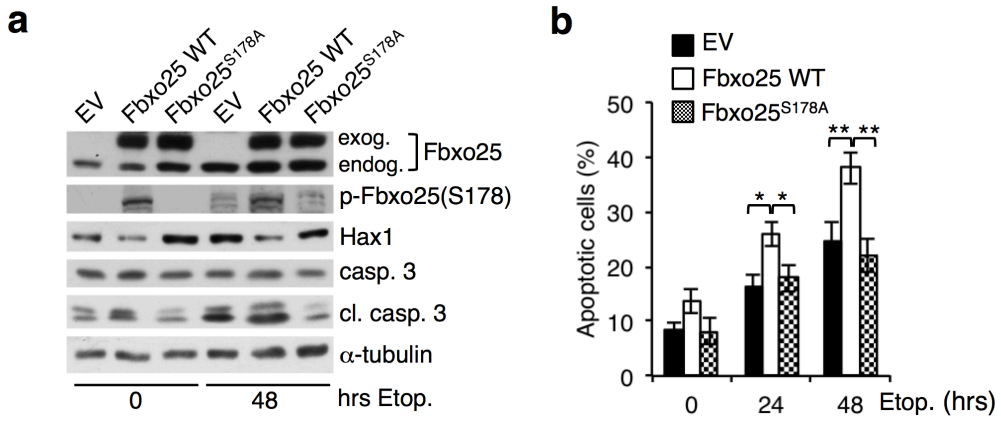

Figure 20: Fbxo25^{S178A} stabilizes Hax1 and prevents the increased sensitivity to apoptotic stimulation as compared to Fbxo25 wildtype. (**a**) C57BL/6 MEFs were transfected with constructs encoding Fbxo25 wildtype (Fbxo25 WT), Fbxo25^{S178A} or empty vector control (EV) and treated with etoposide (Etop.) for 0 or 48 hours (hrs.). Whole cell lysates were immunoblotted with antibodies raised against Fbxo25, phosphorylated Fbxo25 (p-Fbxo25) at serine 178, Hax1, caspase 3 (casp. 3), cleaved caspase 3 (cl. casp. 3) and alpha-tubulin (α-tubulin). Fbxo25 immunoblotting shows two bands, representing the lower endogenous (endog.) Fbxo25 and the upper exogenous (exog.) Fbxo25 signal caused by forced expression of Fbxo25 forms. (**b**) C57BL/6 MEFs were transfected as indicated in **a** and treated with etoposide (Etop.) for 0, 24 and 48 hours (hrs). Rates of apoptotic cells (%) were determined by propidium iodide (PI) FACS analyses. Values are each averaged with with data sets from two additional performed, independent experiments ($n = 3$, mean ± standard deviation). * represents $P < 0.05$, ** represents $P < 0.01$, as calculated by one-way analysis of variance (ANOVA).

6.2.2 Degron-phosphorylation of HAX1 enables the FBXO25-mediated degradation of HAX1

SCF complexes have been described to recognize their substrates by the corresponding F-box protein after modification of the substrate with post-translational modification, usually by phosphorylation of a specific degron motif within the substrate sequence (Petroski and Deshaies 2005);(Fernandez-Saiz, Targosz et al. 2013);(Skaar, Pagan et al. 2013). In order to identify the amino acid residue(s) in HAX1 that are relevant for FBXO25 interaction, FBXO25/HAX1 interaction was mapped by GST pulldown experiments (Figure 21a). GST-tagged fragments of HAX1 or GST-tag alone were purified from induced BL21 bacteria [performed by Ursula Baumann, present study] (see 5.2.5.1) and incubated with whole cell lysates of HEK293T cells transfected with GFP-tagged FBXO25. Pulldown of GFP-FBXO25 with the GST-tagged HAX1 fragments identifed the C-terminal HAX1 region of amino acids 201 to 230 as essential for the interaction with FBXO25 [pulldown and immunoblotting performed by Vanesa Fernández-Sáiz, Technische Universität München, Germany]. The subsequent sequence analysis identified three evolutional conserved serine residues at positions Ser206, Ser210 and Ser212 of HAX1, of which serine 210 showed the highest probablity of phosphorylation (Figure 21b).

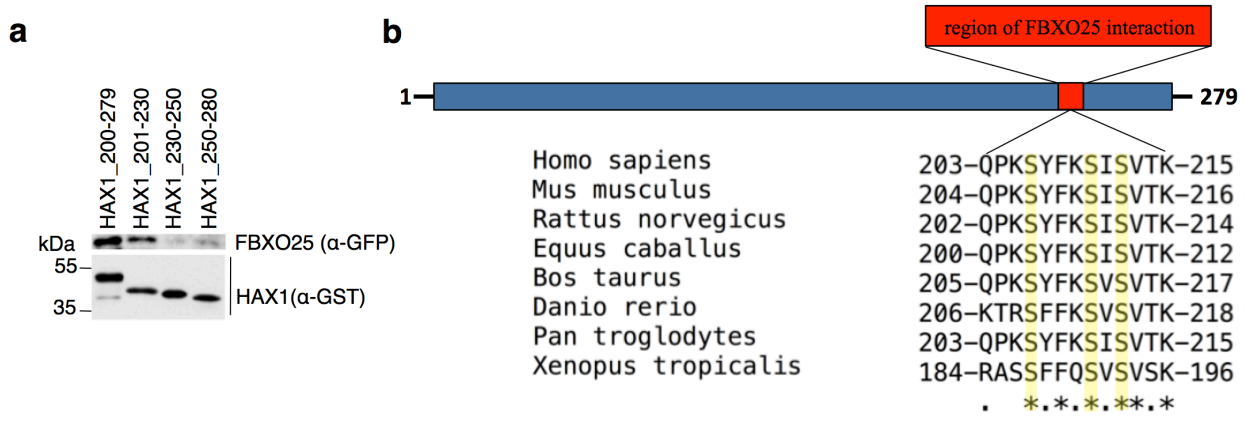

Figure 21: Mapping of the FBXO25 specific phospho-degron within the HAX1 sequence. (**a**) HEK293T cells were transfected with a construct encoding GFP-tagged FBXO25. Whole cell lysates were incubated with the indicated GST-fused fragments of HAX1. Protein complexes were immobilized on glutathione sepharose, resolved by SDS-PAGE and analysed by immunoblotting using antibodies directed against GFP (FBXO25) and GST (HAX1) [data provided by Vanesa Fernández-Sáiz, Technische Universität München, Germany]. (**b**) Alignment of the narrowed amino acid region predicted to contain the potential FBXO25-specific phospho-degron in HAX1 homologs. Yellow bars mark the conserved serine residues Ser206, Ser210 and Ser212 of HAX1.

To further evaluate the impact of the phosphorylation of conserved serine residues in HAX1 on the FBXO25 interaction, HAX1 Ser206 and Ser210 were mutated to alanine, leading to an inhibition of phosphorylation at theses sites. Subsequently, C57BL/6 wildtype MEFs were transfected with constructs encoding FLAG-tagged Hax1 wildtype, Hax1^{S206A}, Hax1^{S210A} or empty vector control and treated with 1 µg/ml etoposide for 24 hours to increase the interaction with Fbxo25 (as observed in Figure 12). Hax1^{S201A} showed slightly increased expression in the whole cell extract and failed to bind Fbxo25 in an immunoprecipitation assay (Figure 22). Moreover, Hax1^{S210A} also missed to interact with Cul1, thus demonstrating protection from the recruitment to the SCF^{Fbxo25} complex. In contrast, no differences in expression and interaction could be observed for Hax1^{S206A} as compared to the Hax1 wildtype.

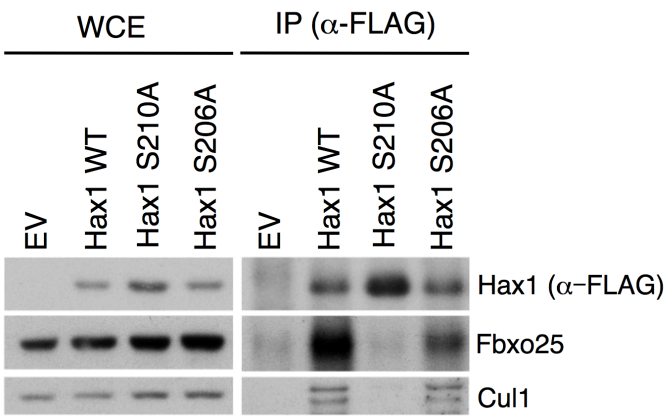

Figure 22: Hax1^{S210A} fails to bind Fbxo25 and Cul1. C57BL/6 wildtype MEFs were transfected with constructs encoding FLAG-tagged Hax1 wildtype, Hax1^{S206A}, Hax1^{S210A} or empty vector control (EV) and treated with etoposide for 24 hours. Whole cell extracts (WCE) were immunoprecipitated with anti-FLAG resin. Immunoprecipitated proteins were separated by SDS-PAGE and immunoblotted using antibodies directed against FLAG (Hax1), Fbxo25 and Cul1.

The missing interaction of Hax1^{S210A} with Fbxo25 hypothesizes a potential stabilization of Hax^{S210A} after induction of apoptosis. To test the stability of Hax1 mutants, C57BL/6 MEFs were virally transduced with FLAG-tagged Hax1 wildtype, Hax1^{S210A}, Hax1^{S212A} or control and treated with 1 µg/ml etoposide or solvent for 24 hours to induce apoptosis. Etoposide treatment induced a robust phosphorylation of Hax1 at Ser210 and led to a clear decrease in Hax1 wildtype and Hax1^{S212A} levels, whereas Hax1^{S210A} remained stable after induction of apoptosis as shown by immunoblotting (Figure 23a) and the corresponding quantification of protein levels (Figure 23b). Moreover, expression of Hax1^{S210A} protected MEFs from apoptosis as demonstrated by decreased levels of cleaved caspase 3 when compared to samples of Hax1 wildtype and Hax1^{S212A} (Figure 23a). An additional performed FACS analysis indicated that Hax1^{S210A} protected cells from apoptosis to a substancial higher extent than Hax1 wildtype or Hax1^{S212A} (Figure 23c).

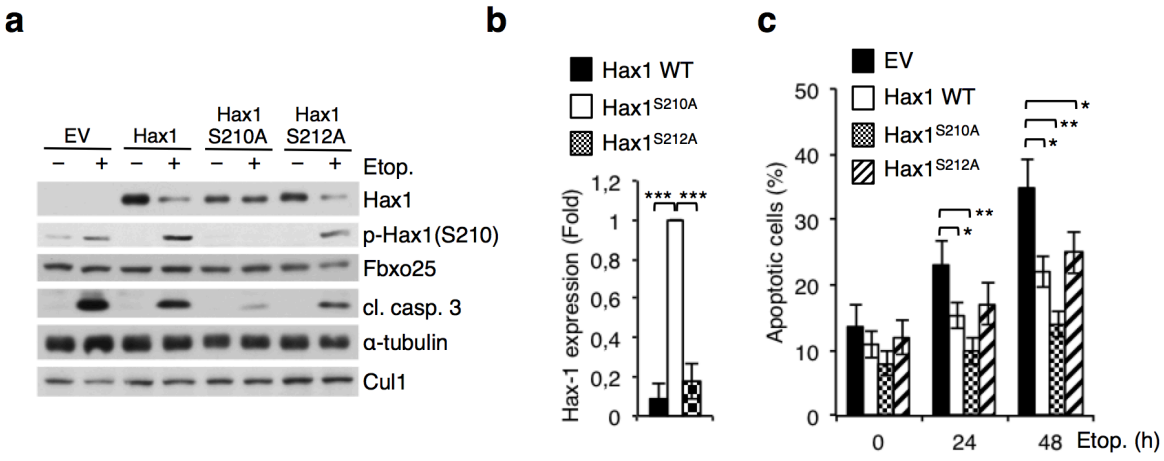

Figure 23: Hax1^{S210A} retains stability after etoposide treatment and protects cells from apoptosis. (**a**) C57BL/6 MEFs were virally transduced with constructs encoding FLAG-Hax1 wildtype, Hax1^{S210A}, Hax1^{S212A} or empty vector control (EV) and treated with etoposide (Etop.) or solvent for 24 hours. Whole cell lysates were separated by SDS-PAGE and probed with antibodies directed against FLAG (Hax1), phospho S210 Hax1 (p-Hax1S210), Fbxo25, cleaved caspase 3 (cl. casp. 3), alpha-tubulin and cullin 1 (Cul1). (**b**) Quantification of Hax1 protein expression at the 24 hour etoposide treatment timepoint. Values for the Hax1^{S210A} mutant were set as 1. Values are averaged with the data from an additional, independent experiment (n = 2, mean ± standard deviation). ***$P < 0.001$, one-way ANOVA. (**c**) FACS analysis for propidium iodide (PI) positive apoptotic cells as seen in **a**. Values are averaged with the data from two additional, independent experiments (n = 3, mean ± standard deviation). *$P < 0.05$, **$P < 0.01$, one-way ANOVA.

6.3 PRKCD phosphorylates nuclear FBXO25 and mitochondrial HAX1

6.3.1 PRKCD sequentially shuttles to nucleus and mitochondria after induction of apoptosis

Serine 178 in FBXO25 and serine 210 in HAX1 have been predicted as protein kinase C (PKC) phospho-acceptor sites. Among the known members of the PKC family, protein kinase C delta (PRKCD) resembles the only isoform with described pro-apoptotic activity (Griner and Kazanietz 2007). Previous studies described a sequential translocation of PRKCD to nucleus and mitochondria (DeVries-Seimon, Ohm et al. 2007);(Griner and Kazanietz 2007), but the function of these translocation events remained absent. To reproduce the published data on PRKCD translocation, C57BL/6 MEFs were transfected with HA-PRKCD and FLAG-Fbxo25 wildtype or

FLAG-Hax1 wildtype and treated with 1 µg/ml etoposide for 0, 4 and 20 hours. Immunofluorescence studies demonstrated nuclear translocation of PRKCD and co-localization with nuclear Fbxo25 after 4 hours of etoposide treatment followed by mitochondrial translocation and interaction with Hax1 after 20 hours of treatment, allowing for successive interaction with Fbxo25 and Hax1 (immunofluorescence studies Figure 24a, quantification of PRKCD Figure 24b).

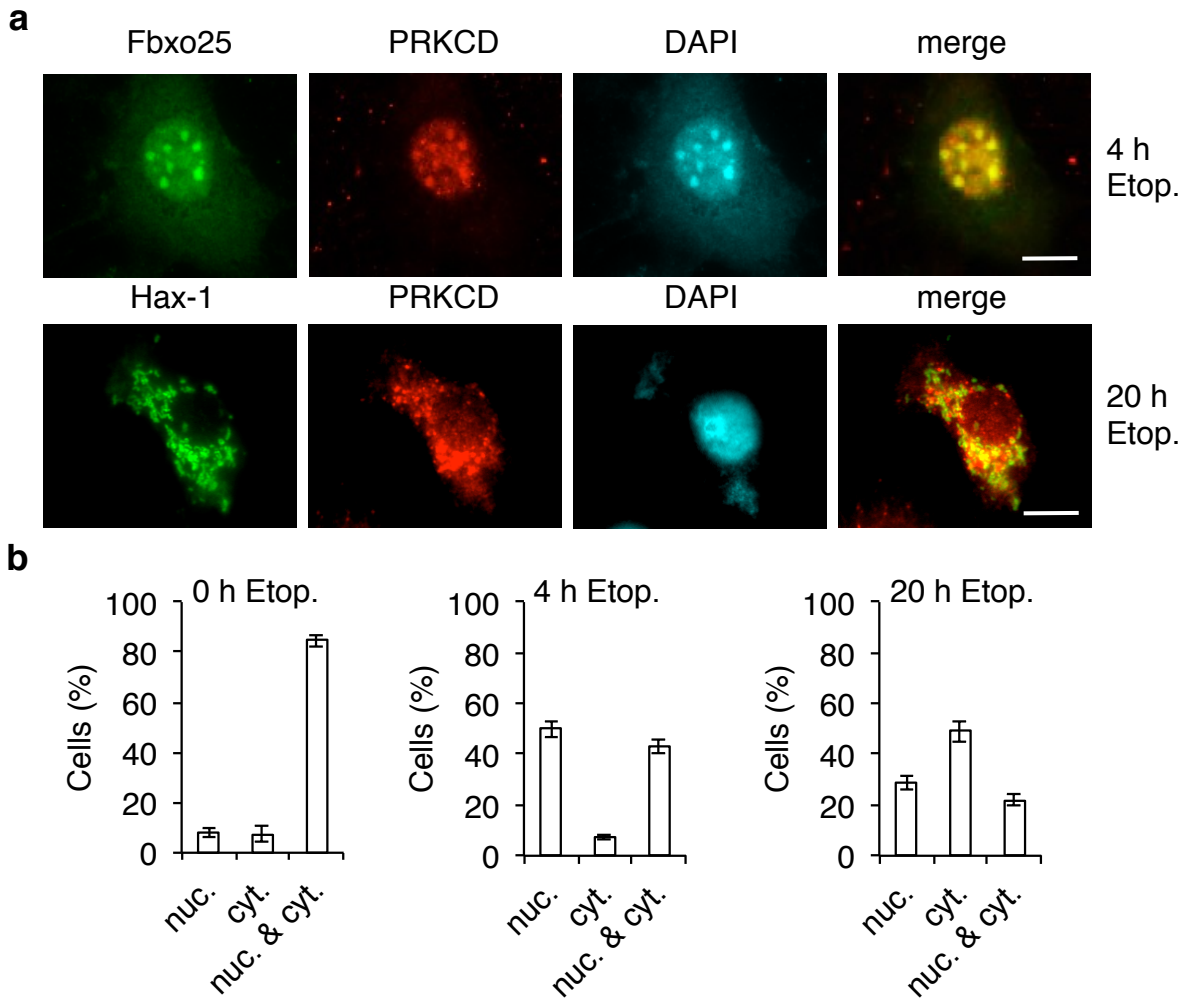

Figure 24: PRKCD consecutively shuttles to the nucleus and cytoplasm in response to apoptotic stimulation to sequentially interact with Fbxo25 and Hax1. (**a**) C57BL/6 MEFs were transiently transfected with plasmids encoding HA-PRKCD and FLAG-Fbxo25 or FLAG-Hax1 and treated with etoposide (Etop.) for 4 and 20 hours (h). Afterwards, cells were fixed with methanol and incubated with anti-FLAG antibody (green) and anti-HA antibody (red). DNA was stained with DAPI (blue). Scale bars denote 10 µm. (**b**) Quantification of cells shown in **a** with regard to nuclear (nuc.) and cytoplasmic (cyt.) PRKCD immunofluorescence staining after treatment with etoposide (Etop.) for 0, 4 and 20 hours. Each quantification approach comprised 100 cells (n =3; ± standard deviation).

6.3.2 PRKCD mediates the nuclear export of FBXO25

Co-immunoprecipitation studies in HEK293T cells transfected with FLAG-tagged FBXO25 and HA-tagged PKC isoforms PRKCD, PRKCG, PRKCH and PRKCE demonstrated an exclusive interaction of FBXO25 with PRKCD [performed by Vanesa Fernández-Sáiz, Technische Universität München, Germany; data not shown]. To further evaluate how far the nuclear translocation of PRKCD mediates the subsequent phosphorylation-dependent nuclear export of FBXO25, *Prkcd*$^{-/-}$ MEFs (Leitges, Mayr et al. 2001) were transfected with FLAG-tagged Fbxo25 wildtype and treated with 1 µg/ml etoposide or solvent for 24 hours. Subcellular localization analyses using immunofluorescence microscopy revealed a clear nuclear retention of FBXO25, preventing translocation to mitochondria in response to etoposide treatment in *Prkcd*$^{-/-}$ MEFs (Figure 25a), an observation that stands in clear contrast to the shuttling process observed in wildtype MEFs (Figure 15). The additionally performed quantification of *Prkcd*$^{-/-}$ cells with nuclear retention of Fbxo25 after etoposide treatment (Figure 25b) underlined the dependency of Fbxo25 nuclear export on the presence of Prkcd.

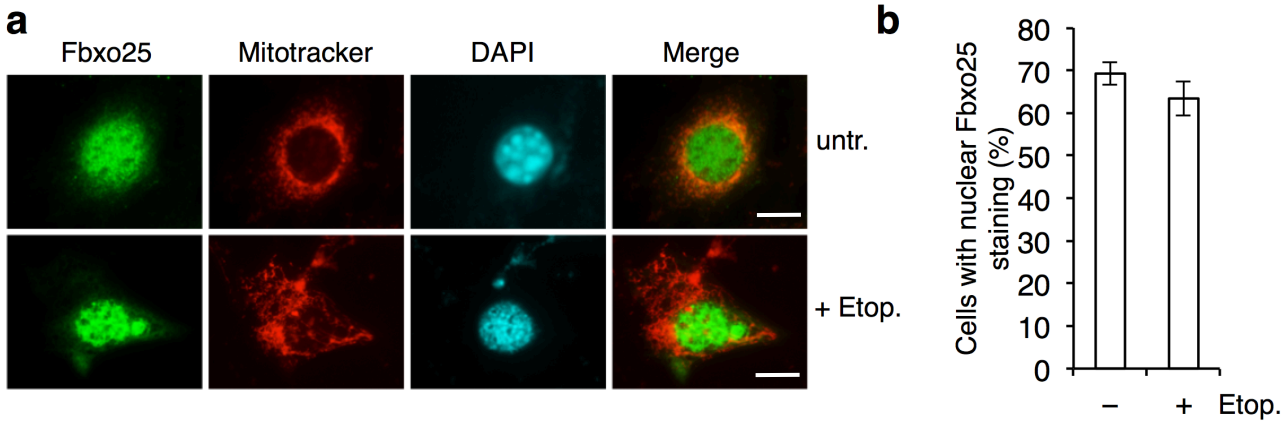

Figure 25: PRKCD is required for the phosphorylation-dependent nuclear export of FBXO25. (**a**) Imaging of *Prkcd*$^{-/-}$ MEFs, transiently transfected with FLAG-Fbxo25 wildtype and treated with etoposide (Etop.) or solvent (untr.) for 24 hours. Cells were fixed with methanol and stained with an antibody directed against FLAG (green). Mitochondria were visualized by Mitotracker staining (red). DNA was stained with DAPI (blue). Scale bars denote 10 µm. (**b**) Quantification of cells with nuclear staining of Fbxo25 after treatment with etoposide (Etop.) or solvent for 24 hours. Each quantification approach comprised 100 cells (n =3; ± standard deviation).

6.3.3 Loss of PRKCD stabilizes HAX1 and blocks apoptosis

The lack of Prkcd caused the nuclear retention of Fbxo25 and prevented the mitochondrial translocation of Fbxo25 after induction of apoptosis (Figure 25). To further investigate the

functional role of Prkcd in the degradation of Hax1, *Prkcd*$^{-/-}$ MEFs (Leitges, Mayr et al. 2001) and their wildtype counterparts were treated with 1 µg/ml etoposide for 0, 12, 24 and 48 hours. After induction of apoptosis, wildtype MEFs showed an increase in the phosphorylation of Fbxo25 at serine 178 and Hax1 at serine 210 leading to an decrease of Hax1 protein levels and an increase of the apoposis marker cleaved caspase 3 (Figure 26a, left panel). The elevated levels of Fbxo25 in immunoblotting after treatment with etoposide thereby might result from a higher solubility of Fbxo25 in the used lysis buffer after cytoplasmatic translocation. In contrast to the observation in C57BL/6 wildtype MEFs, phosphorylation of Fbxo25 serine 178 and Hax1 serine 210 was largely not detectable in *Prkcd*$^{-/-}$ MEFs and Hax1 was not visibly degraded after induction of apoptosis. Moreover, stabilization of Hax1 in *Prkcd*$^{-/-}$ MEFs attenuated the apoptotic response in these cells as represented by lack of an increase of cleaved caspase 3 levels (Figure 26a, right panel). In line with the previous observation, loss of Prkcd anticipated apoptosis in *Prkcd*$^{-/-}$ MEFs, an effect significantly demonstated after 48 hours treatment with etoposide (Figure 26b), supporting the hypothesis that persistent expression levels of Hax1 promote the survival of cells deficient of Prkcd.

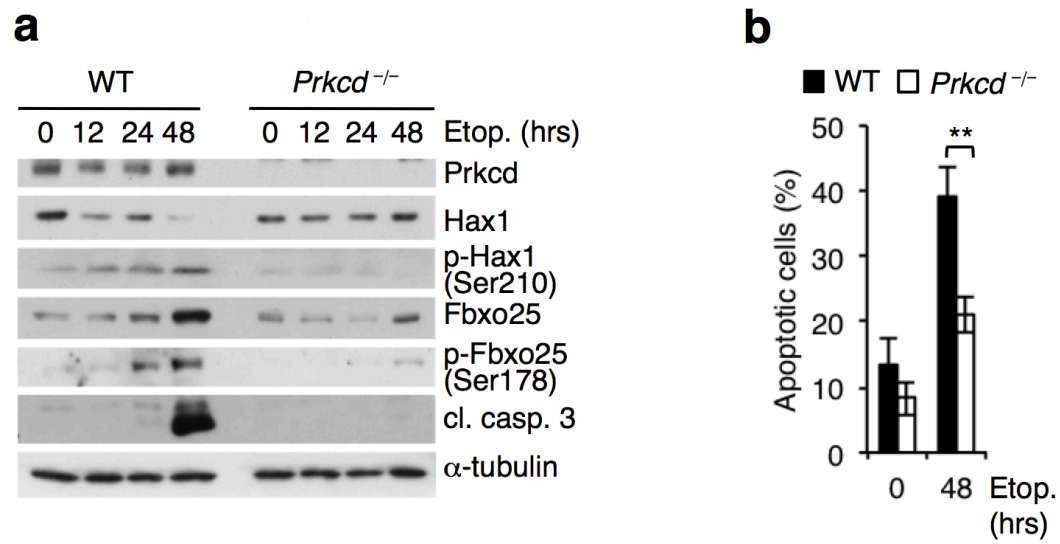

Figure 26: Loss of Prkcd inhibits phosphorylation-dependent degradation of Hax1 and blocks apoptosis. (**a**) C57BL/6 wildtype MEFs or *Prkcd*$^{-/-}$ MEFs were treated with etoposide (Etop.) for 0, 12, 24 and 48 hours (hrs.). Whole cell extracts were separated by SDS-PAGE and analysed by immunoblotting using antibodies directed against Prkcd, Hax1, phospho Hax1 at serine 210 (p-Hax Ser210), phospho Fbxo25 at serine 178 (p-Fbxo25 Ser178), cleaved caspase 3 (cl. casp. 3) and alpha-tubulin (α-tubulin). (**b**) Propidium iodide (PI) based FACS analysis to determine the percentage of apoptotic cells observed in **a** after 0 and 48 hours of etoposide treatment. All values were averaged with data from two additional, independent experiments ($n = 3$, mean ± standard deviation). $^{**}P < 0.01$, Student`s *t* test.

6.3.4 PRKCD moderates the interaction of FBXO25 and HAX1

PRKCD has so far been identifed as an essential factor for the phosphorylation of FBXO25 at serine 178, leading to its nuclear export as well as for the phosphorylation of HAX1 at serine 210, allowing for the subsequent degradation of HAX1. To further investigate to which extent the acitivity of PRKCD contributes to the interaction of FBXO25 and HAX1, HEK293T cells were transfected with FLAG-tagged FBXO25 and treated with 1 µg/ml etoposide and 10 µM of the PRKCD inhibitor rottlerin or solvent for 12 hours. Whole cell extracts were immunoprecipitated using an anti-FLAG resin and interactors of FBXO25 were probed with specific antibodies. Whole cell extracts demonstrate a robust phosphorylation of serine 178 of FBXO25 and serine 210 of HAX1 which disappeared completely after treatment with the PRKCD inhibitor rottlerin (Figure 27, left lanes). FLAG-immunoprecipitation in etoposide only treated cells unraveled a strong interaction of FBXO25 with phosphorylated HAX1 (Ser210) and the SCF-core component CUL1 (Figure 27, right panel). The additional administration of rottlerin inhibited the kinase activity of PRKCD and diminished the interaction of FBXO25 with HAX1 to background level. Of note, interaction of FBXO25 with CUL1 remained largely unaffected, thus underlining that inhibition of PRKCD affected only the specific interaction of FBXO25 with HAX1, but did not affect the formation of an intact SCF^{FBXO25} complex.

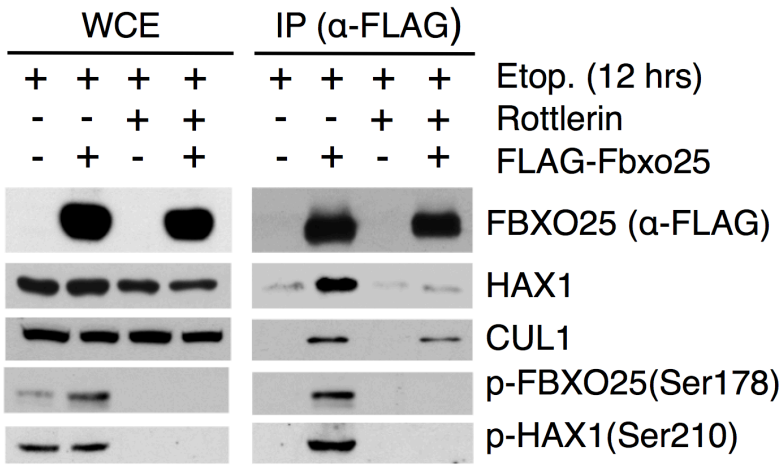

Figure 27: PRKCD moderates the phosphorylation and interaction of FBXO25 and HAX1. HEK293T cells were transiently transfected with plasmids encoding FLAG-FBXO25 wildtype. Cells were treated with etoposide (Etop.) and the PRKCD inhibitor rottlerin or solvent for 12 hours (hrs.). Whole cell extracts (WCE) were subjected to immunoprecipitation (IP) using an anti-FLAG resin. Whole cell extracts and immunoprecipitates were separated by SDS-PAGE and immunoblotted using antibodies directed against FLAG (FBXO25), HAX1, cullin 1 (CUL1), phospho Ser178 FBXO25 (p-FBXO25) and phospho Ser210 HAX1 (p-HAX1).

6.3.5 PRKCD phosphorylates FBXO25 and HAX1

Studies performed by Vanesa Fernández-Sáiz, Technische Universität München, Germany demonstrated a direct interaction of FBXO25 and HAX1 with PRKCD that could not be detected with other PKC isoforms (data not shown). In line with this observation, PRKCD mediates the phosphorylation of FBXO25 (Ser178) and HAX1 (Ser210) and the interaction of both molecules. In order to investigate whether FBXO25 and HAX1 are directly phosphorylated by PRKCD or if the phosphorylation event is indirecty regulated by PRKCD, FBXO25 wildtype and FBXO25^{S178A} as well as HAX1 wildtype and HAX1^{S210A} were purified as GST-fusion proteins [performed by Ursula Baumann, present study] and subjected to an *in vitro* kinase assay [performed by Vanesa Fernández-Sáiz, Technische Universität München, Germany] (see 5.2.10). An autoradiography assay using gamma-ATP identified a robust phosphorylation of FBXO25 wildtype in the presence of purified PRKCD that was massively reduced through mutation of FBXO25 serine 178 to alanine (Figure 28a). Moreover, PRKCE another isoform of the PKC family failed to phosphorylate the FBXO25 wildtype. An equally performed *in vitro* kinase assay for HAX1 wildtype and HAX1^{S210A} illustrated a PRKCD-specific phosphorylation of the HAX1 wildtype that could be abrogated by mutating serine 210 in HAX1 to alanine (Figure 28b). [Data of the *in vitro* kinase assays for FBXO25 and HAX1 were provided by Vanesa Fernández-Sáiz, Technische Universität München, Germany.] Additional studies for the function of PRKCD demonstrated that PRKCD exterted its pro-apoptotic activity only in the presence of FBX025 and HAX1. Forced expression of PRKCD failed to increase the rates of apoptosis when *Fbxo25* or *Hax1* were silenced genetically in MEFs [studies performed by Vanesa Fernández-Sáiz, Technische Universität München, Germany; data not shown].

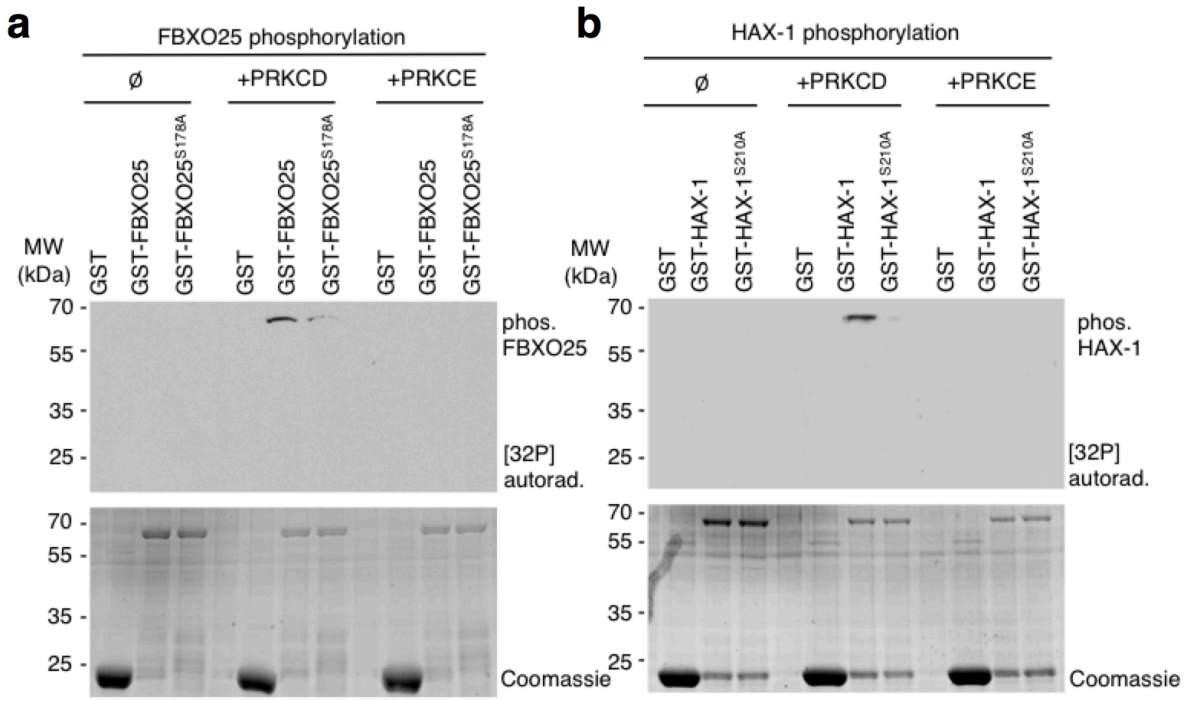

Figure 28: PRKCD phosphorylates FBXO25 and HAX1 *in vitro*. (**a**) Equal amounts of GST-control, GST-FBXO25 or GST-FBXO25^{S178A} were transferred to an *in vitro* kinase reaction to test for the phosphorylation of FBXO25 wildtype and mutant by PRKCD and PRKCE in the presence of [^{32}P]ATP. Phosphorylated proteins were visualized by autoradiograpy. Usage of same mounts of all proteins was verified by Coomassie staining. (**b**) *In vitro* kinase assay for GST-control, GST-HAX1 and GST-HAX1^{S210A} as substrates. The experiment was performed as desribed in **a**. [Data provided by Vanesa Fernández-Sáiz, Technische Universität München, Germany]

In summary, PRKCD subsequently phosphorylates FBXO25 within the nucleus and HAX1 at site of mitochondria. The phosphorylation of FBXO25 at serine 178 within the NES sequence induces a translocation of nuclear FBXO25 to mitochondria. PRKCD dependent phosphorylation of the HAX1 degron at serine 210 enables recruitment of mitochondrial HAX1 to the SCF^{FBX025} complex and facilitates a subsequent degradation via the proteasome system.

6.4 FBXO25 mediated ubiquitylation of HAX1 is dependent on PRKCD

6.4.1 FBXO25 ubiquitylates HAX1 *in vivo* and *in vitro*

The recruitment of HAX1 to the SCF^{FBXO25} E3 ubiquitin ligase complex after induction of apoptosis proposes degradation of HAX1 by the ubiquitin-proteasome system (UPS) regulated by a FBXO25-dependent ubiquitylation of HAX1. In order to test whether HAX1 is ubiquitylated via the SCF^{FBXO25} E3 ubiquitin ligase, the ubiquitylation reaction of HAX1 was rebuilt in an *in vivo* approach under denaturing conditions (see 5.2.9.1). HEK293T cells were transfected with plasmids encoding HA-tagged ubiquitin, FLAG-tagged HAX1 wildtype, GFP-tagged FBXO25 or the control F-box protein GFP-FBXO9 and treated with 1 µg/ml paclitaxel to induce apoptosis. Subsequent treatment with 10 µM of the proteasome inhibitor MG132 inhibited the proteasomal degradation of ubiquitylated proteins. Non-covalent protein interactions in whole cell lysates were inhibited by SDS in order to allow for the specific detection of HAX1 ubiquitylation. After the quenching of SDS, denatured lysates were incubated with an anti-FLAG resin. The analysis of immunoprecipitated HAX1 revealed a clear ubiquitylation of HAX1 in the presence of FBXO25, whereupon no HAX1 ubiquitylation could be detected under forced expression of FBXO9 (Figure 29).

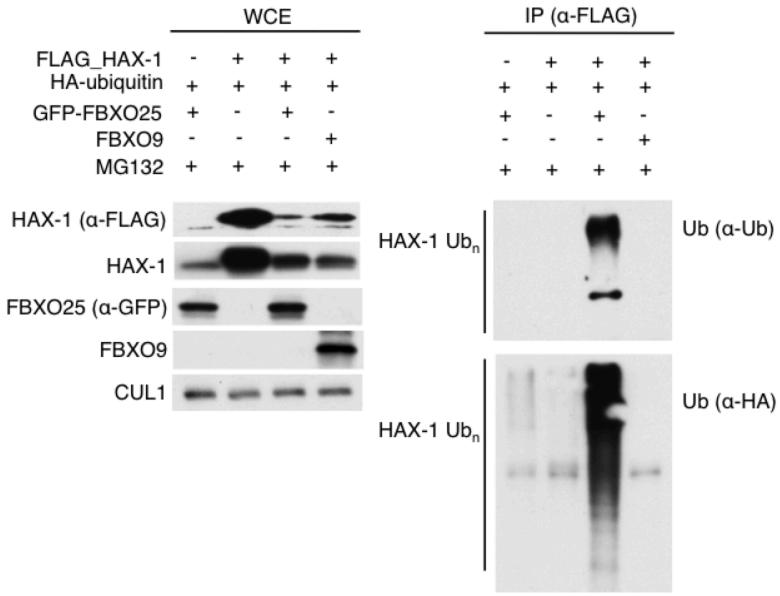

Figure 29: HAX1 is ubiquitylated *in vivo* via FBXO25. HEK293T cells were transfected with constructs encoding FLAG-HAX1, HA-ubiqutin, GFP-FBXO25 or GFP-FBXO9 and treated with paclitaxel and the proteasomal inhibitor MG132. Whole cell extract (WCE) were subjected to anti-FLAG immunoprecipitations (IP) using denaturing conditions. Whole cell extracts and IPs were separated by SDS-PAGE and analyses by immunoblotting using indicated antibodies. Ubiquitylation of immunoprecipitated HAX1 was probed by antibodies directed against ubiquitin (Ub) and HA.

To further proof the ubiquitylation of HAX1 via FBXO25, the HAX1 ubiquitylation reaction was additional reconstituted in an *in vitro* ubiquitylation assay (see 5.2.9.2). FLAG-tagged HAX1 wildtype was immunoprecipitated from HEK293T cells treated with 1 µg/ml etoposide for 20 hours (to enable for post-translational modification of the substrate) and subjected to an *in vitro* reaction conducted in the presence of SCF-complex components including either FBXO25 or FBXO9 purified from insect cells, E1/E2 enzymes, recombinant ubiquitin and ATP. The ubiquitin immunoblot of the reactions demonstrates a clear *in vitro* ubiquitylation of HAX1 in the presence of FBXO25, whereupon only a slight background signal could be detected in samples incubated with the control F-box protein FBXO9 (Figure 30).

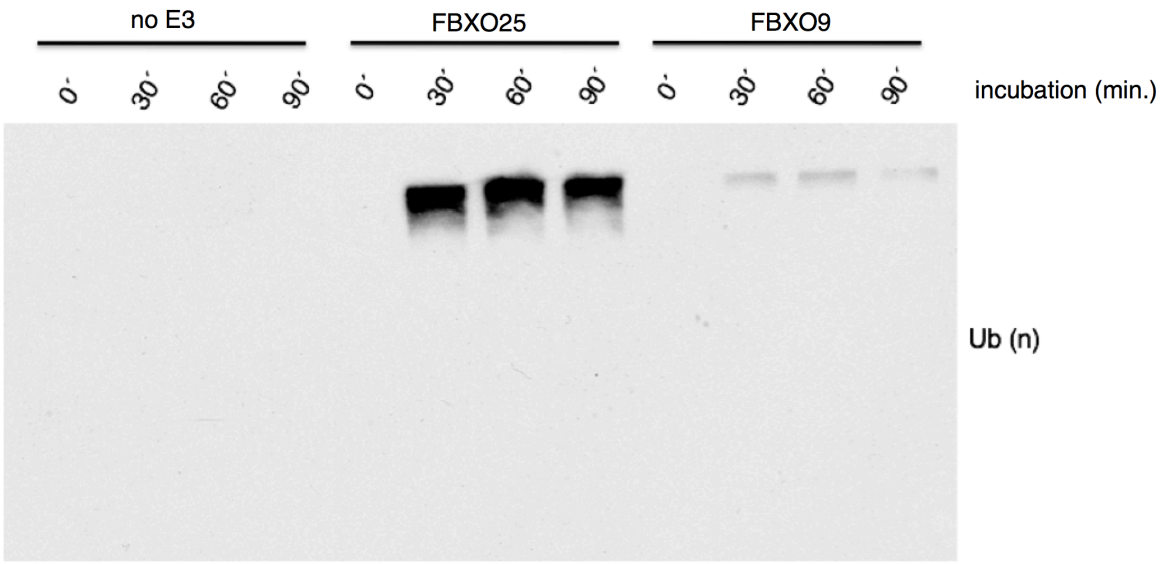

Figure 30: FBXO25 ubiquitylates HAX1 *in vitro*. FLAG-tagged HAX1 wildytype was immunoprecipitated from HEK293T cells treated with etoposide for 20 hours. Purified HAX1 was subjected to *in vitro* reactions containing E1/E2 enzymes, SCF-components (SCF^{FBXO25}, SCF^{FBXO9} or no E3 ligase), ubiquitin chains and ATP. Incubation time was started by addition of ATP to the reaction. Time points were collected at 0 (ATP addition), 30, 60 and 90 minutes (min.) of reaction time. Samples were separated by SDS-PAGE and ubiquitylation was analyzed by immunoblotting using an antibody directed against ubiquitin (Ub).

6.4.2 Ubiquitylation of HAX1 is dependent on PRKCD

Previous experiments indicated a HAX1 ubiquitylation directed by the SCF^{FBXO25} E3 ubiquitin ligase. To further evaluate the dependency of the ubiquitylation event on PRKCD, the ubiquitylation recation of HAX1 was reconstituted *in vitro* in the presence or absence of PRKCD. FLAG-tagged HAX1 wildtype or the FLAG-tagged $HAX1^{S210A}$ mutant were purified from HEK293T

cells and subjected to an ubiquitylation reaction containing purified E1/E2 enzymes, SCF^{FBXO25} or SCF^{FBXO9}, ubiquitin, ATP and two different concentrations of purified PRKCD. Immunoblotting for HAX1 demonstrated that the HAX1 wildtype was efficiently ubiquitylated in the presence of SCF^{FBXO25}, whereupon the addition of increasing concentrations of PRKCD led to a decrease of unmodified HAX1 levels and an increase in ubiquitylated HAX1. In contrast, the $HAX1^{S210A}$ phospho-degron mutant could not be ubiquitylated by SCF^{FBXO25} in the presence or absence of PRKCD. Moreover, pre-treatment of HAX1 with lambda-phosphatase prevented the ubiquitylation of HAX1 wildtype, indicating that phosphorylation of HEK293T cells derived HAX1 enabled the ubiquitylation by SCF^{FBXO25} (Figure 31). [*In vitro* ubiquitylation experiment chapter 6.4.3 performed by Vanesa Fernández-Sáiz, Technische Universität München, Germany]

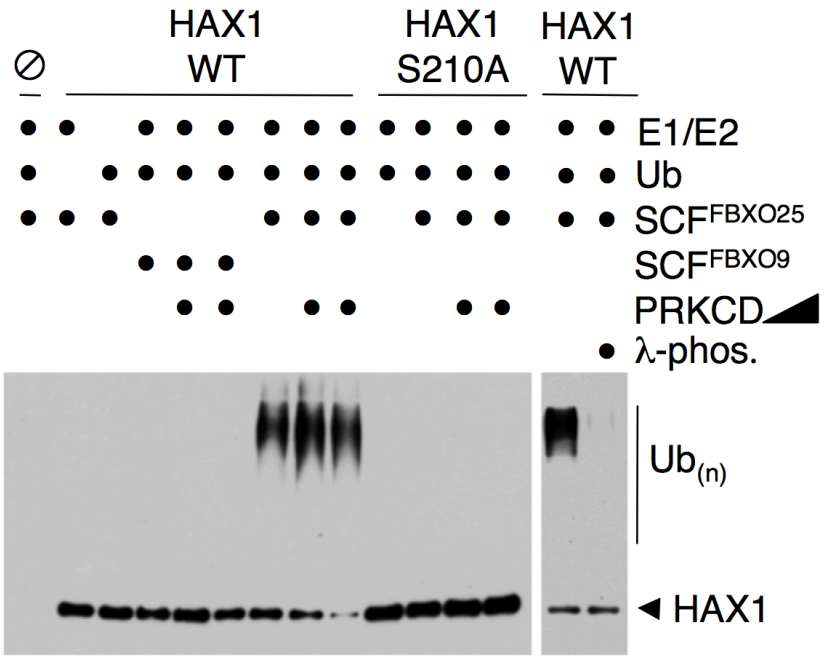

Figure 31: HAX1 is ubiquitylated in the presence of SCF^{FBXO25} and PRKCD. FLAG-tagged HAX1 wildtype or $HAX1^{S210A}$ were purified from HEK293T cells and subjected to *in vitro* reactions containing E1/E2 enzymes, ubiquitin (Ub), SCF^{FBXO25} or SCF^{FBXO9}, purified PRKCD and lambda-phosphase (λ-phos.) as indicated. Samples were separated by SDS-PAGE and ubiquitylation was visualized by immunoblotting using an antibody directed against HAX1, $Ub_{(n)}$ indicates polyubiquitylated forms of HAX1. [Data provided by Vanesa Fernández-Sáiz, Technische Universität München, Germany]

In summary, HAX1 is directly ubiquitylated by the SCF^{FBXO25} E3 ubiquitin ligase, a process that is mediated by phosphorylation of serine 210 of HAX1 by PRKCD.

6.5 FBXO25 suppresses lymphomagenesis and lymphoma growth *in vivo*

6.5.1 Fbxo25 expression levels influence the growth of pre-existing lymphoma cells

To further investigate the role of Fbxo25 in the growth of lymphoma cells and their resistance towards chemotherapeutic agents, the well-established spontaneous Eμ-myc mouse model (Adams, Harris et al. 1985) was chosen. Eμ-myc lymphoma-derived cells [provided by Susanne Kratzat, Technische Universität München, Germany] were retrovirally transduced with shRNA targeting Fbxo25 expression, or a non-targeting control. Immunoblotting indicated a reduction of Fbxo25 in cells treated with shRNA against Fbxo25 (Figure 32a, left panel). In line with previous observations, knock-down of Fbxo25 led to a clear stabilization of Hax1 as compared to sh_Control. Subsequent treatment of sh_Control and sh_Fbxo25 with 1 μg/ml of the apoptosis inducing agent paclitaxel for 0, 4 and 24 hours demonstrated a decrease in apoptosis rates when Fbxo25 expression was partially silenced (Figure 32a, right panel). In a complementary approach, forced expression of Fbxo25 in Eμ-myc lymphoma-derived cells slightly destabilized Hax1 levels (Figure 32b, left panel) and led to a massive increase of the apoptotic cell population even in the absence of an additional apoptotic stimulus (Figure 32b, right panel).

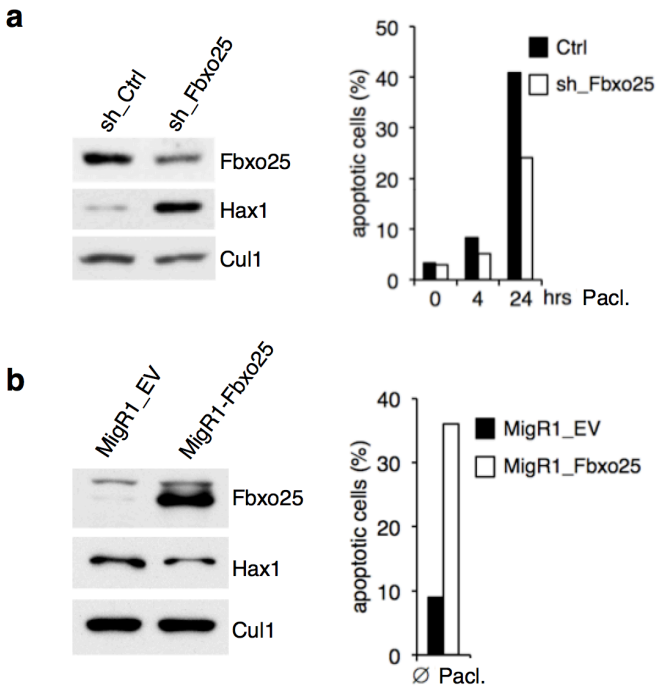

Figure 32: Fbxo25 levels modulate apoptosis rates of Eμ-myc lymphoma-derived cells. (**a**) Eμ-myc lymphoma cells were retrovirally transduced with shRNA targeting Fbxo25 expression (sh_Fbxo25) or non-targeting control (sh_Ctrl). Whole cell lysates were separated by SDS-PAGE and immunoblotted using antibodies directed against Fbxo25, Hax1 and Cul1. In a parallel approach, transduced control (Ctrl) and sh_Fbxo25 cells were treated with paclitaxel (Pacl.) for 0, 4 and 24 hours. FACS analysis for propidium iodide (PI) positivity was used to determine the rate of apoptotic cells ($n = 1$). (**b**) Eμ-myc lymphoma cells were retrovirally transduced with the overexpression vector MigR1_Fbxo25 or control (MigR1_EV). Whole cell lysates were separated by SDS-PAGE and immunoblotted using antibodies directed against Fbxo25, Hax1 and Cul1. Apoptotic cell populations were analyzed by FACS as described in a ($n = 1$).

Data collected from Eμ-myc lymphoma cells indicated a potential growth and survival advantage of cells with low protein levels of Fbxo25, whereupon forced expression of Fbxo25 seemed to inhibit the growth of pre-existing lymphoma cells (Figure 32). To further test the effect of variations in Fbxo25 protein levels on lymphoma growth and survival, Eμ-myc cells transduced with MLS_shFbxo25 (Fbxo25 knock-down), MigR1_Fbxo25 (Fbxo25 overexpression) or MigR1 vector control were transplanted into C57BL/6 wildtype mice (10 weeks of age, Harlan laboratories) [transplantation assisted by Viktoriya Tomiatti, Technische Universität München, Germany] (see 5.2.12.2.1). All transplanted female mice were housed, fed and bred equally. The distribution of mice in the three experimental groups (sh_Fbxo25, MigR1_Fbxo25 and control) was conducted randomly. Disease state of the transplanted mice was specified by the presence of palpable lymph nodes and the impairment of the general health status. Time point of sacrifice was determined by an independent member of the mouse care facility with no insight into the experimental design. All animal experiments were thereby performed in agreement with the local ethical guidelines and approved by the District Government of Upper Bavaria. Tail vain injected mice receiving Eμ-myc lymphoma-derived cells transduced to overexpress Fbxo25 showed significant prolonged survival compared to recipient mice transplanted with control vector cells (Figure 33). Moreover, knock-down of Fbxo25 even accelerated the lymphoma growth of Eμ-myc cells and induced a reduced survival of recipient mice.

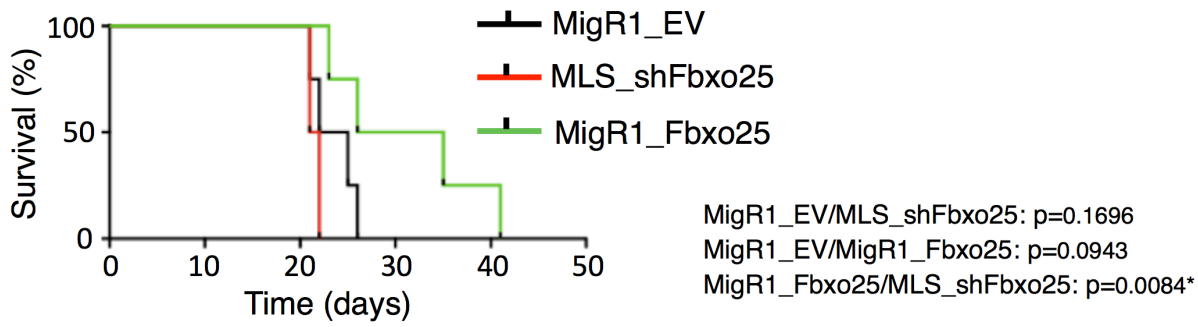

Figure 33: Expression levels of Fbxo25 mediate the growth of Eμ-myc lymphoma cells *in vivo*. Eμ-myc lymphoma cells, retrovirally transduced with the IRES-GFP constructs: MigR1_Fbxo25, MSL_shFbxo25 or MigR1_EV (empty vector control) were sorted for GFP-positivity. Each 5.5 x 10^3 GFP-positive cells were injected intraveniously into C57BL/6 inbred mice. Mice were followed for lymphoma onset, disease state of the transplanted mice was specified by the presence of palpable lymph nodes and the impairment of the general health status. Time point of sacrifice was determined by an independent member of the mouse care facility with no insight into experimental design. Graph represents the Kaplan-Meier survival curves for the neutral control (MigR1_EV, black, $n = 4$), Fbxo25 overexpression (MigR1_Fbxo25, green, $n = 4$) and Fbxo25 knock-down (MLS_shFbxo25, red, $n = 4$). * $P < 0.05$, Mantleel-Cox test.

The analyses of spleens of sacrificed mice revealed a reduced spleen weight of mice receiving Eμ-myc lymphoma cells transduced to overexpress Fbxo25 compared to MigR1_EV control (Figure 34a). Animals injected with Eμ-myc cells transduced with MLS_shFbxo25 demonstrated an increased overall spleen weight as compared to the MigR1_EV control group. The additional immunohistochemitry (see 5.2.12.2.2.1) based analysis of lymph nodes of the MigR1_EV versus MigR1_Fbxo25 experimental group indicated increased levels of spontaneous apoptosis visualized by cleaved caspase 3 under forced expression of Fbxo25 (Figure 34b). B220 staining confirms the B-cell origin of the analyzed tumor tissue [Histopathology was analyzed by Martina Rudelius, Julius-Maximilians-University, Würzburg, Germany].

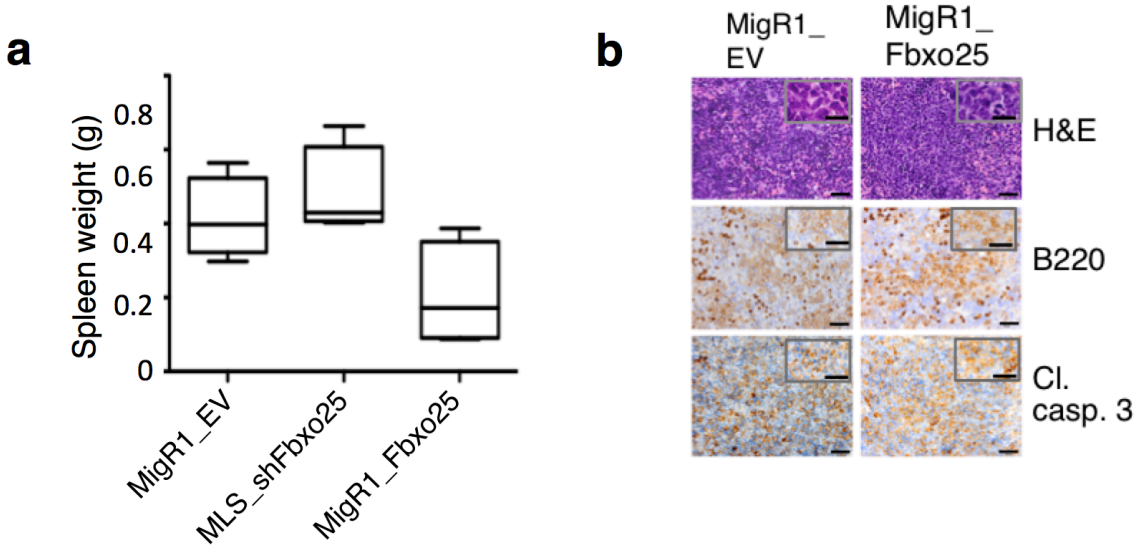

Figure 34: Fbxo25 expression levels influence spleen weight and spontaneous apoptosis of lymph node cells. (**a**) Spleen weight of animals from the MigR1_EV, MLS_shFbxo25 and MigR1_Fbxo25 presented in Figure 33. Box-and-whisker plots demonstrate the upper and lower quartiles (25 - 75%) with a line at the median. (**b**) Histopathology of lymph nodes derived from mice shown in Figure 33. Histomorphology was visualized by hematoxylin/eosin (H&E). B220 staining confirms the B-cell origin of depicted samples. Staining for cleaved caspase 3 (Cl. casp. 3) demonstrates *in situ* levels of spontaneous apoptosis. Scale bars denote 50 μm and 10 μm for inserts. [Histopathology data provided by Martina Rudelius, Julius-Maximilians-University, Würzburg, Germany]

6.5.2 Knock-down of Fbxo25 accelerates *de novo* lymphoma development

Fbxo25 levels were shown to influence apoptosis and growth rates of primary lymphoma cells. To further evaluate the role of Fbxo25 in *de novo* lymphomagenesis, Eμ-myc transgenic fetal liver cells as source of hematopoietic stem cells and progenitor cells (HSPCs) [provided by Susanne Kratzat, Technische Universität München, Germany] were retrovirally transduced with an internal ribosomal entry site IRES-GFP linked shRNA targeting *Fbxo25* or the corresponding vector

control. Transduced HSPCs were subsequently injected into sublethal irradiated C57BL/6 inbred mice [assisted by Viktoriya Tomiatti, Technische Universität München, Germany] (compare 5.2.12.3.1). 28 days after transplantation, the engraftment of HSPCs was determined by FACS analysis [assisted by Viktoriya Tomiatti, Technische Universität München, Germany]. The flow cytometric analysis indicates a clear B-cell population (CD45+; B220+) with GFP-positivity of approx. 15 - 35% (Figure 35). Of note, the GFP-positivity of B-cells was slightly increased in mice transplanted with shFbxo25 transduced cells, indicating a potential proliferative advantage of theses cells.

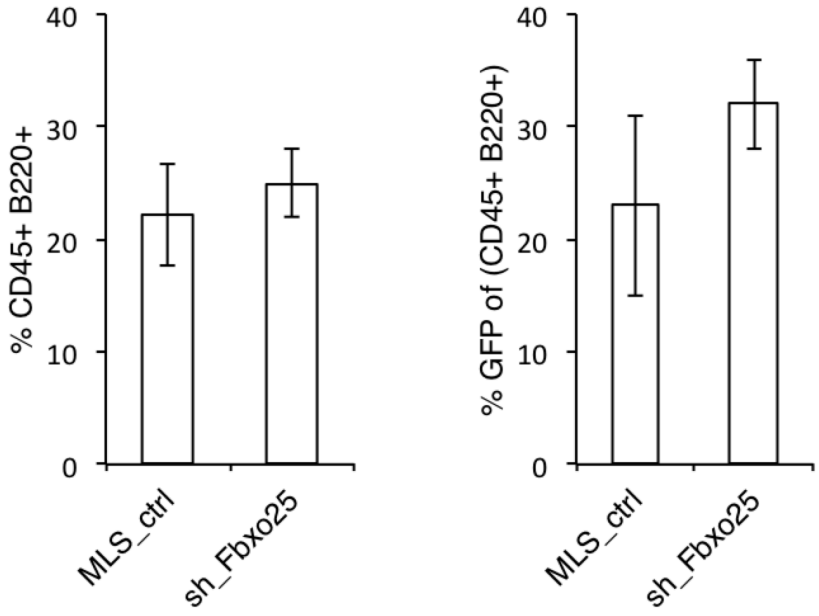

Figure 35: Engraftment analyses 28 days after transplantation with HSPCs. Blood derived from mice at day 28 post transplantation with the sh_Fbxo25 or control vector control (MLS_ctrl) transduced hematopoietic cell/progenitor cells (HSPCs) was analyzed by flow cytometry using CD45 and B220 markers to identify the CD45+; B220+ B-cell population (left panel). Percentage of GFP-positive B-cells was determined as GFP+ subpopulation of the CD45+; B220+ cells (rigth panel) (n = 5, ± standard deviation) [FACS analysis supported by Viktoriya Tomiatti, Technische Universität München, Germany].

The follow up of *de novo* lymphomagensis in the described transplantation model demonstrated accelerated lymphoma development and significantly reduced survival rates in animals reconstituted with Fbxo25 shRNA HSPCs as compared to animals reconstituted with the corresponding control HSPCs (Figure 36).

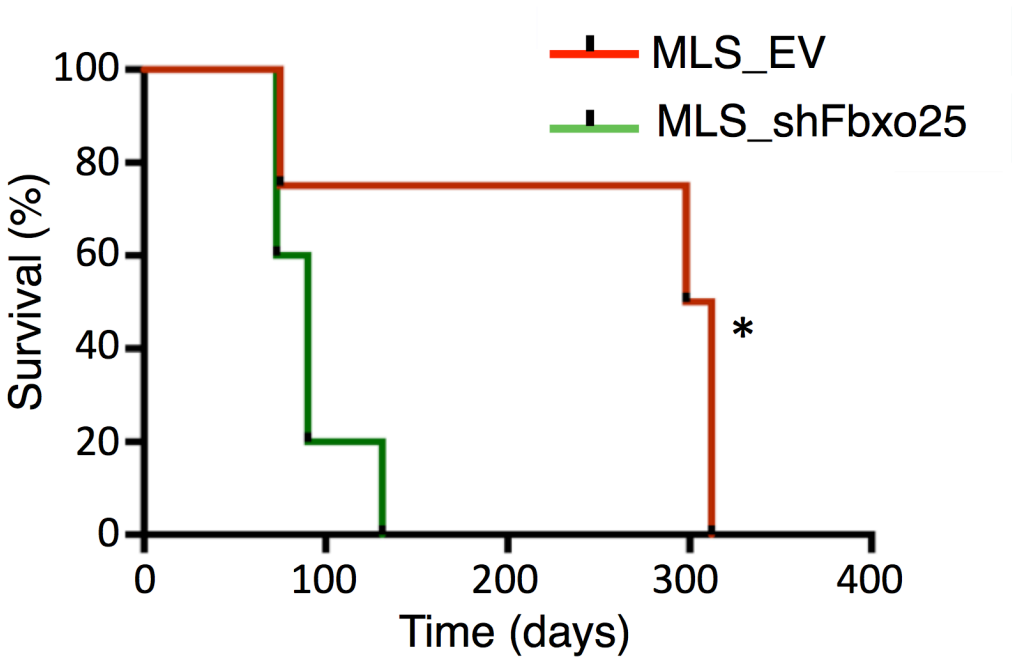

Figure 36: Fbxo25 suppresses lymphoma development *in vivo*. Kaplan-Meier survival curves for vector control (MLS_EV, red, $n = 4$) and Fbxo25 knock-down (MLS_shFbxo25, green, $n = 5$). Mice were irradiated and transplanted with hetrozygous Eμ-myc transgenic fetal liver cells retrovirally transduced with shFbxo25 or the corresponding control. *$P < 0.05$, Mantel-Cox test.

Immunoblotting analyses of lymphomas derived from transplanted animals revealed GFP-positivity of tumors, indicating the transplanted HSPCs as tumor-initiating cells (Figure 37a). Knock-down of Fbxo25 resulted in a massively increased level of Hax1 and a reduction of spontaneous apoptosis as indicated by lower levels of cleaved caspase 3 compared to the corresponding control tumors. An additional performed immunohistochemistry based analysis of lymphomas from both transplantation groups demonstrated the B-cell origin of lymphomas as visualized by B220 staining and indicated reduced levels of spontaneous apoptosis, visualized by cleaved caspase 3, in lymphomas from animals reconstituted with Fbxo25 shRNA HSPCs as compared to animals reconstituted with control HSPCs (Figure 37b) [Histopathology analyzed by Martina Rudelius, Julius-Maximilians-University, Würzburg, Germany] (for methodology see 5.2.12.3.3.1 and 5.2.12.3.3.2).

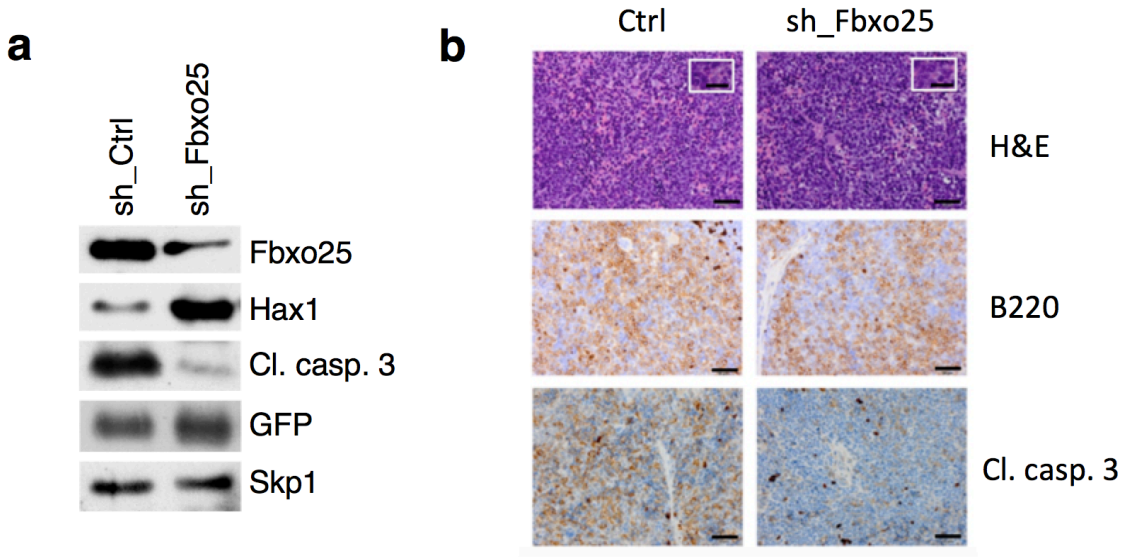

Figure 37: Knock-down of Fbxo25 increases levels of Hax1 and reduces spontaneous apoptosis of lymphoma cells. (**a**) Immunoblotting analyses of whole cell extracts derived from lymph nodes of mice reconstituted with Fbxo25 shRNA HSPCs or control HSPCs. Lysates were seperated by SDS-PAGE and probed with antibodies directed against Fbxo25, Hax1, cleaved caspase 3 (Cl. casp 3), GFP and Skp1 (loading control). (**b**) Immunohistochemistry of representative lymph nodes of mice reconstituted with Fbxo25 shRNA HSPCs or control HSPCs. Cells were stained to visualize histomorphology (H&E), B-cell origin (B220) and rates of spontaneous apoptosis as visualized by cleaved caspase 3 (Cl. casp 3). Scale bars denote 50 µm and 10 µm for inserts. [Histopathology data provided by Martina Rudelius, Julius-Maximilians-University, Würzburg, Germany]

6.5.3 Knock-down of FBXO25 increases lymphoma growth in a human xenotransplant model

The initial analyses of CGH array data sets indicated an enrichment of genomic *FBXO25* deletions in primary mantle cell lymphoma (MCL) samples. In order to further investigate the effect of a reduced FBXO25 dosage on the proliferation and apoptosis of human MCL, a xenotransplantation approach was selected. Granta-519 cells, a human MCL cell line with no alteration of the *FBXO25* gene locus (Rubio-Moscardo, Climent et al. 2005), were lentivirally transduced with control shRNA or specific shRNA targeting FBXO25 expression. 8 x 10^6 transduced Granta-519 cells were subcutaneously injected into the flanks of nonobese diabetic severe combined immunodeficient (NOD-SCID) mice [assisted by Anna-Maria Karmann, Technische Universität München, Germany] (see 5.2.12.4.1). To avoid an influence of mouse selection on the tumor growth, both conditions (shCtrl and shFBXO25) were applied into right and left flank of each mouse. Despite the overall aggressive nature of the selected xenotransplantation

model, shRNA mediated knock-down of FBXO25 significantly increased lymphoma growth as determined by [^{18}F]fluorodeoxyglucose positron emission tomography (PET) imaging 26 and 28 days post injection [PET analyses supported by Jolanta Slawska, Technische Universität München, Germany] (Figure 38a, upper panel) (see 5.2.12.4.2). Metabolic tumor volume measured at days 26 and 28 post injection underlines the significant higher volume of tumors derived from FBXO25 shRNA transduced Granta-519 cells compared to control [analysis performed by Zhoulei Li, Technische Universität München, Germany] (Figure 38a, lower panel). After sacrifice of mice on day 28 post injection, tumor weight and volume were determined after explantation. Tumors derived from Granta-519 cells with knock-down of FBXO25 showed significant lower tumor weight and tumor volume compared to the corresponding controls (Figure 38b).

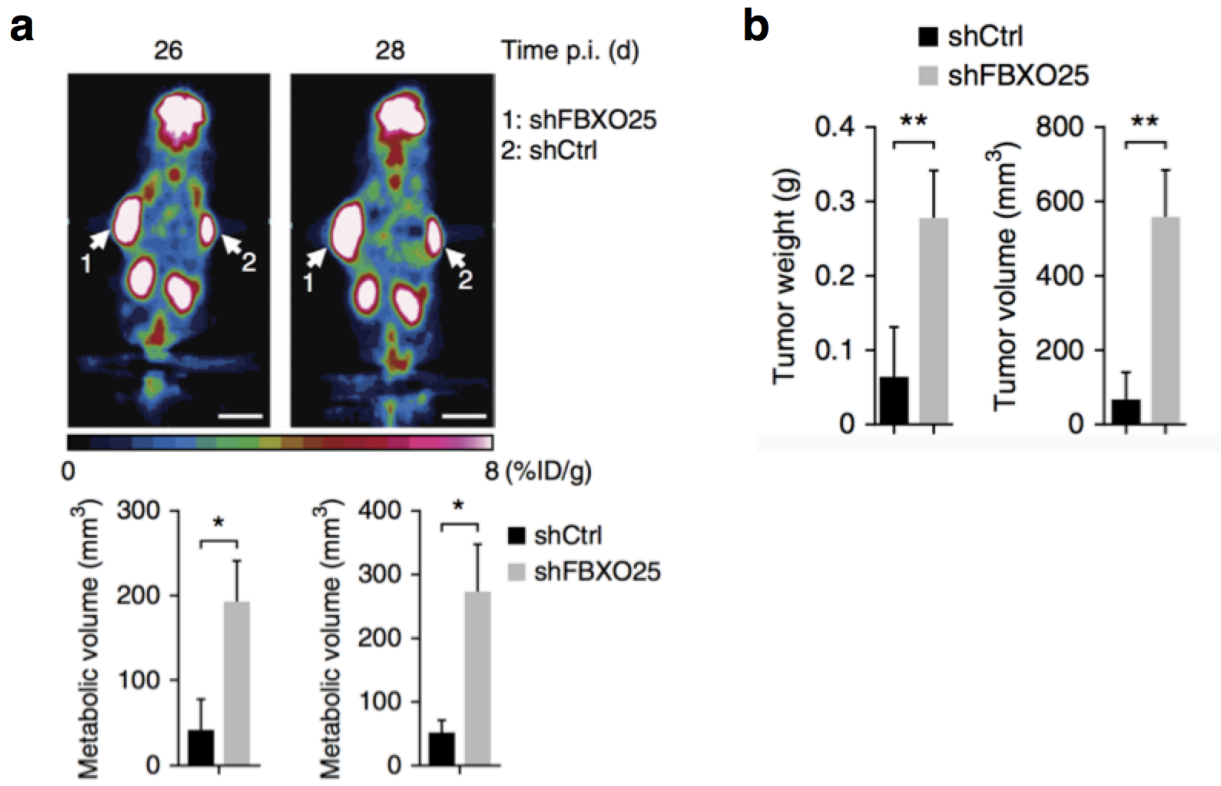

Figure 38: Knock-down of FBXO25 increases lymphoma growth in a human xenotransplantation model. (**a**) FDG-PET imaging of representative human MCL xenografts at days 26 and 28 post injection (p.i.) The colour scale indicates the percentage of injected dose per gram (%ID/g). Scale bars 10 mm (upper panel). Quantification of metabolic tumor volume by FDG uptake at the indicated time points (n = 7 tumors with shCtrl, n = 7 tumors with shFbxo25, mean ± s.e.m.). *P < 0.05, Student`s $t$ test. [Data of PET analysis provided by Zhoulie Li, Technische Universität München, Germany] (**b**) Metric tumor weight and volume of the tumors in **a** after sacrifice of injected mice ($n$ = 8 tumors with shCtrl, $n$ = 8 tumors with shFbxo25, mean ± s.e.m.). **$P$ < 0.01, Student`s t test.

After measurement of weight and size of explanted turmors, tumors were subjected to analyses by immunoblotting and immunohistochemistry. Whole cell lysates from tumors derived from xenografts of Fbxo25 shRNA transduced Granta-519 cells showed reduced levels of FBXO25 that correlated with a massive increase of HAX1 and a reduction of claeved caspase 3 as marker of spontaneous apoptosis as compared to tumors from control xenografts (Figure 39a). Immunohistochemistry based analyses revealed a clear B-cell origin of the observed tumors (depicted by CD20 staining). Moreover, tumors derived from the shFBXO25 knock-down group showed strongly decreased levels of spontaneous apoptosis in histopathology compared to control tumors (Figure 39b) [Histopathology of tumors was analyzed by Martina Rudelius, Julius-Maximilians-University, Würzburg, Germany] (methods see 5.2.12.4.3).

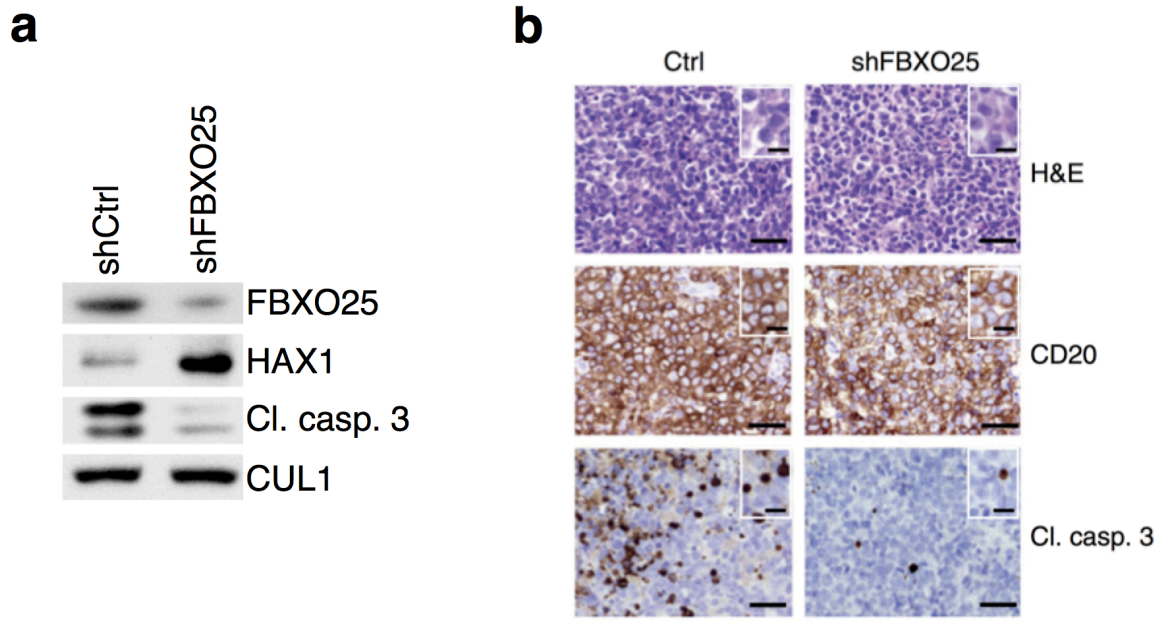

Figure 39: Tumors of Granta-519 xenografts with FBXO25 knock-down reveal elevated levels of HAX1 and reduced spontaneous apoptosis. (**a**) Immunoblotting analyses of whole cell extracts derived from xenografts of Granta-519 cells transduced with shFBXO25 or control (shCtrl). Lysates were separated by SDS-PAGE and probed with antibodies directed against FBXO25, HAX1, cleaved caspase 3 (Cl. casp 3) and CUL1 as loading control. (**b**) Immunohistochemistry of representative xenografts of Grants-519 cells with knock-down of FBXO25 or control (Ctrl). Cells were stained to visualize histomorphology (H&E), B-cell origin (CD20) and rates of spontaneous apoptosis as visualized by cleaved caspase 3 (Cl. casp 3). [Histopathology data provided by Martina Rudelius, Julius-Maximilians-University, Würzburg, Germany]

6.5.4 Overexpression of HAX1^{S210A} promotes lymphoma growth in a human xenotransplantation model

Previous studies in MEFs observed the phospho-degron mutant Hax1^{S210A} to protect cells from Fbxo25-mediated apoptosis. To further evaluate the effect of forced expression of the HAX1^{S210A} mutant on MCL lymphoma development, Granta-519 cells were retrovirally transduced to overexpress HAX1^{S210A} (pLPC_HAX1^{S210A}) or an empty vector control (pLPC_EV). 8 x 10^6 transduced Granta-519 cells were subcutaneously injected into the flanks of NOD-SCID mice [assisted by Anna-Maria Karmann, Technische Universität München, Germany]. To avoid an influence of mouse selection on the tumor growth, both conditions (pLPC_HAX1^{S210A} and pLPC_EV) were applied into right and left flank of each mouse. Despite the described aggressive nature of the selected xenograft model, forced expression of HAX1^{S210A} significantly increased lymphoma growth compared to control xenografts (Figure 40a). After euthanasie of injected mice, tumor weight and volume were measured metrically. Thereby, xenografts derived from Granta-519 cells transduced with pLPC-HAX1^{S210A} showed a significantly higher metric tumor weight and volume compared to the corresponding control xenografts (pLPC_EV) (Figure 40b).

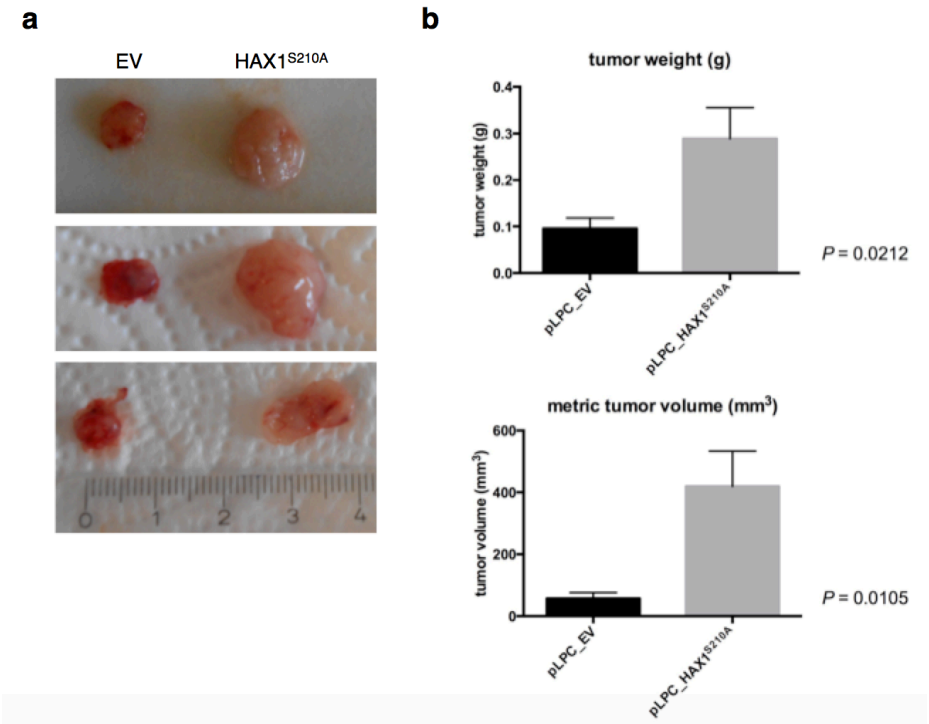

Figure 40: Overexpression of HAX1^{S210A} promotes lymphoma growth in a human xenotransplant model. (**a**) Images of representative xenograft tumors from Granta-519 cells transduced with pLPC_HAX1^{S210A} versus pLPC_EV control. (**b**) Metric tumor weight and volume of the tumors from Granta-519 xenograft groups after sacrifice of injected mice (n = 6 tumors with pLPC_EV control, n = 6 tumors with pLPC_HAX1^{S210A}).

6.6 Disruption of the PRKCD-FBXO25-HAX1 axis promotes survival of MCL cells

6.6.1 Genomic deletion of *FBXO25* protects MCL cells from apoptosis

The analysis of CGH array data sets previously suggested an enrichment of genomic *FBXO25* deletions in primary mantle cell lymphoma patient samples (Rubio-Moscardo, Climent et al. 2005), whereupon induced knock-down of FBXO25 significantly accelerated lymphoma growth of the human MCL cell line Granta-519 (see chapter 6.5.3). To further study the functional impact of *FBXO25* deletions on MCL cell proliferation and survival, different human MCL cell lines with deletion of the *FBXO25* locus or no alteration of the *FBXO25* locus were identifed. In regard to published aCGH analyses, the MCL cell lines Rec-1 and JVM-2 were selected as lines with a documented monoallelic deletion of the *FBXO25* gene locus, whereas the MCL cell lines Granta-519 and Jeko were identified as control lines with no published genomic deletion of the *FBXO25* locus (Rubio-Moscardo, Climent et al. 2005). To further evaluate the genomic deletion of *FBXO25* on the RNA expression level, RNA was extracted from all four MCL cell lines (Granta-519, Jeko, JVM-2 and Rec-1) and transscribed to cDNA. The results on quantitative PCR analyses of theses lines reveal a clear loss of approximately 50% of *FBXO25*-mRNA expression level within the monoallelic *FBXO25* deleted cell lines JVM-2 and Rec-1 (Figure 41a). In line with these data, analyses of FBXO25 protein expression levels indicate a clear decrease of FBXO25 protein within the MCL lines JVM-2 and Rec-1 as compared to the corresponding loading control (Figure 41b).

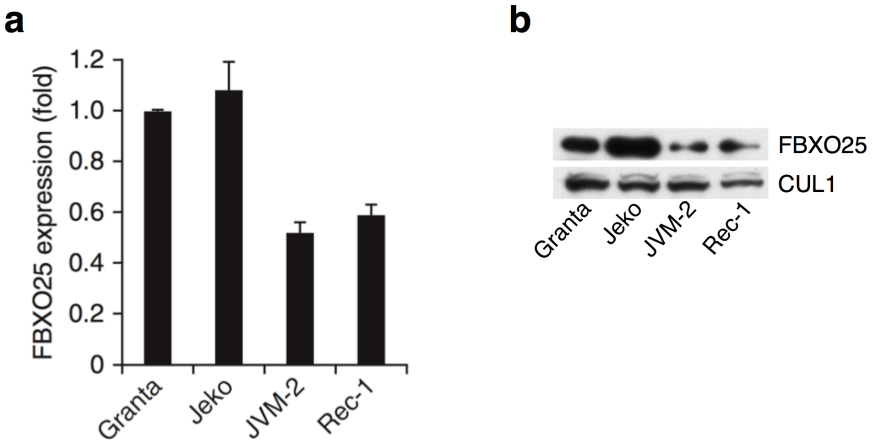

Figure 41: Identification of MCL cell lines with low RNA and protein levels of FBXO25. (**a**) Quantitative PCR for *FBXO25* mRNA expression levels in the human MCL cell lines Granta-519, Jeko, JVM-2 and Rec-1 (n = 3). (**b**) Immunoblotting analyses for protein expression levels in different human MCL cell lines. Whole cell lysates of indicated cell lines were separated by SDS-PAGE and analysed by immunoblotting using antibodies directed against FBXO25 and CUL1 (loading control).

In order to further confirm the monoallelic nature of the specific deletion of the *FBXO25* gene locus as observed by aCGH analyses (Rubio-Moscardo, Climent et al. 2005), selected MCL samples were subjected to fluorescence *in situ* hybridization (FISH). Data sets derived from this approach indicate a clear monoallelic deletion of the *FBXO25* gene locus in approximately 10% of screened samples (*n* = 31), whereas no biallelic deletion could be identifed using *FBXO25* specific FISH probes [FISH analyses performed by Sven Perner, University Hospital of Bonn, Germany]. As previously described by aCGH analyses, the monoallelic deletion of *FBXO25* within human MCL patient samples (Rubio-Moscardo, Climent et al. 2005) could be verified using gene specific FISH probes targeting *FBXO25* (Figure 42). Moreover, the monoallelic deletion of *FBXO25* within the MCL cell lines JVM-2 and Rec-1 could be verified via FISH [performed by Sven Perner, University Hospital of Bonn, Germany; data not shown].

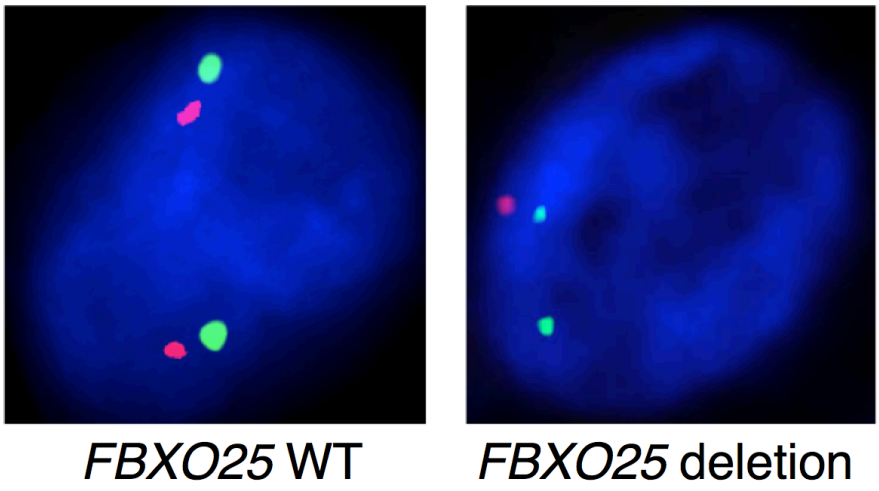

Figure 42: The specific *FBXO25* gene locus is monallelically deleted in human MCL. Fluorescence *in situ* hybridzation on formalin-fixed paraffin-embedded human MCL patient material. Green: centromere control probe for chromosome 8; red: *FBXO25* specific gene probe. [data provided by Sven Perner, University Hospital of Bonn, Germany]

The observed monallelic deletion of *FBXO25* in the Rec-1 MCL cell line hypothesizes a potential stabilization of HAX1 levels after induction of apoptosis compared to the non-deleted control MCL line Granta-519. To further test the stability of HAX1 in MCL lines with or without deletion of *FBXO25*, Rec-1 and Granta-519 cells were treated with 1 µg/ml etoposide for 0, 4, 24, 48 and 72 hours. Immunoblotting studies in Granta-519 cells, apoptotical stimulated by etoposide, showed a clear degradation of the anti-apoptotic molecule HAX1 after 48 hours, leading to a

massive increase of the apoptotic marker cleaved caspase 3 (Figure 43a, right part). In contrast, Rec-1 cells show overall reduced protein levels of FBXO25 leading to stabilization of HAX1 levels and avoidance of apoptosis as represented by the absence of cleaved caspase 3 (Figure 43a, left part). The additional performed quantification of HAX1 immunoblotting levels in these cell lines after 0, 24 and 48 hours of etoposide treatment underlined a significant stabilization of HAX1 protein levels in the monoallelic *FBXO25* deleted MCL cell line Rec-1 (data from two independent experimental approaches (Figure 43b).

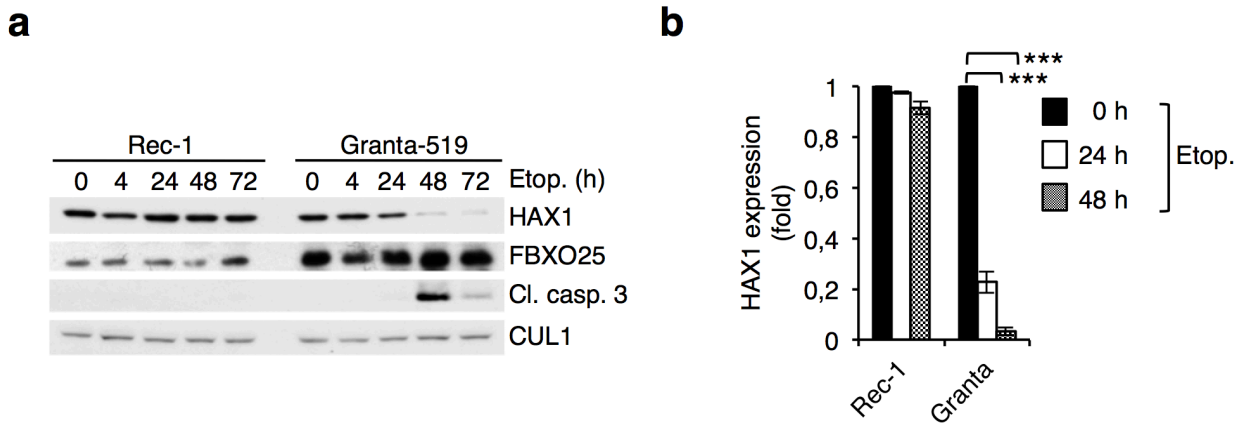

Figure 43: Deletion of *FBXO25* protects MCL cells from apoptosis. (**a**) Immunoblotting analysis of the MCL cell lines Rec-1 and Granta-519 after treatment with etoposide (Etop.) for 0, 4, 24, 48 and 72 hours (h). Whole cell lysates were separated by SDS-PAGE and immunoblotted with antibodies directed against HAX1, FBXO25, cleaved caspase 3 (Cl. casp. 3) and CUL1 (loading control). (**b**) Quantification of HAX1 protein expression levels as presented in **a**. The values given for the amount of HAX1 protein present in the samples at the 0 hour timepoint of etoposide (Etop.) treatment were set as 1 ($n = 2$, mean ± standard deviation). ***$P < 0.001$, one-way ANOVA.

6.6.2 Re-expression of FBXO25 in FBXO25 deleted MCL cell lines induces apoptosis

Low FBXO25 protein levels seemed to protect *FBXO25* deleted MCL cell lines from apoptosis (see previous chapter 6.6.1), an observation which corroborates the hypothesis that re-expression of FBXO25 in *FBXO25* deleted MCL cells might restore sensitivity towards apoptosis. In order to test this hypothesis, GFP-tagged FBXO25 or an empty vector control were transiently expressed in parallel in the *FBXO25*-deleted lymphoma lines Rec-1 and JVM-2 as well as in the non-deleted lines Granta-519 and Jeko. Nucleofection based reconstitution with FBXO25 wildtype

led to a reduction of HAX1 protein levels and substancially increased apoptosis, as visualized by cleaved caspase 3, in JVM-2 and Rec-1 cells (Figure 44a). In contrast, forced expression of GFP-tagged FBXO25 wildtype only induced minor or no visible effects on HAX1 and cleaved caspase 3 protein levels in the Granta-519 and Jeko MCL cell lines. An additional performed FACS analysis from three independent experimental replicates underlined a significant increase in apoptotic cell rates for JVM-2 and Rec-1 cells reconstituted with the FBXO25 wildtype compared to empty vector control (Figure 44b). FACS studies based on Granta-519 and Jeko cells overexpressing FBXO25 compared to empty vector control demonstrated only a slight but non-significant increase in the rates of propidium iodide (PI) positive, apoptotic MCL cells (Figure 44b).

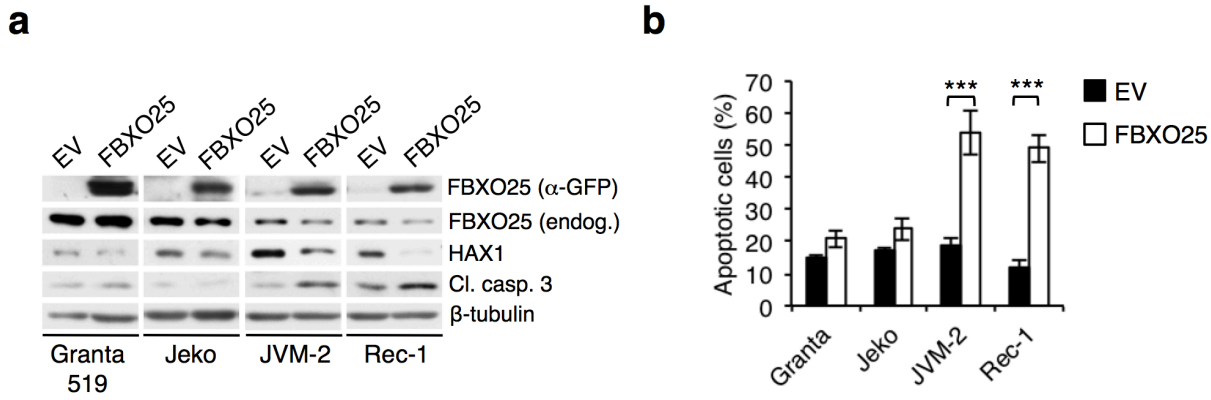

Figure 44: Re-expression of FBXO25 increases apoptosis rates of *FBXO25* deleted MCL cell lines. (**a**) Immunoblotting analyses of the *FBXO25* deleted MCL cell lines JVM-2 and Rec-1 and the *FBXO25* non-deleted lines Granta-519 and Jeko transiently transfected with GFP-tagged FBXO25 wildtype or an empty vector control. Whole cell lysates were separated by SDS-PAGE and protein levels were analyzed by immunoblotting using antibodies directed against GFP (overexpressed FBXO25), endogenous (endog.) FBXO25, HAX1, cleaved caspase 3 (Cl. casp. 3) and beta-tubulin (loading control). (**b**) FACS analysis of cells in **a** to determine apoptosis rates via propidium iodide (PI) staining. Values are averaged each with the data from two additional, independent experiments (n = 3, mean ± standard deviation). ***$P < 0.001$, Student`s t test.

6.6.3 Overexpression of PRKCD induces apoptosis more efficiently in *FBXO25* wildype cells

Studies from MEFs indicated that PRKCD failed to increase the rates of apoptosis when *Fbxo25* or *Hax1* were silenced genetically in MEFs [studies performed by Vanesa Fernández-Sáiz, Technische Universität München, Germany; data not shown]. This observation induced the

hypothesis that PRKCD might induce apoptosis more efficiently in MCL cell lines with no deletion of *FBXO25*. To subsequently test the effect of forced expression of PRKCD, the *FBXO25*-deleted cell lines JVM-2 and Rec-1 as well as the non-deleted lines Granta-519 and Jeko were transfected with FLAG-tagged PRKCD or the corresponding empty vector control. Transient overexpression of PRKCD in Granta-519 and Jeko cells induced a decrease of HAX1 protein levels in parallel with a clear increase of the apoptotic marker cleaved caspase 3 (Figure 45a). In contrast, PRKCD expression did not lead to a decrease of HAX1 nor efficiently induced apoptosis in JVM-2 and Rec-1 cells. Additional performed FACS analyses of three independent experiments underlined a significant induction of apoptosis by forced PRKCD expression in the FBXO25 wildtype lines Granta-519 and Jeko (Figure 45b). In comparison, FACS data from the *FBXO25* monoallelic deleted JVM-2 and Rec-1 cells overexpressing PRKCD compared to empty vector control demonstrated only a slight but not significant increase of apoptosis rates (Figure 45b).

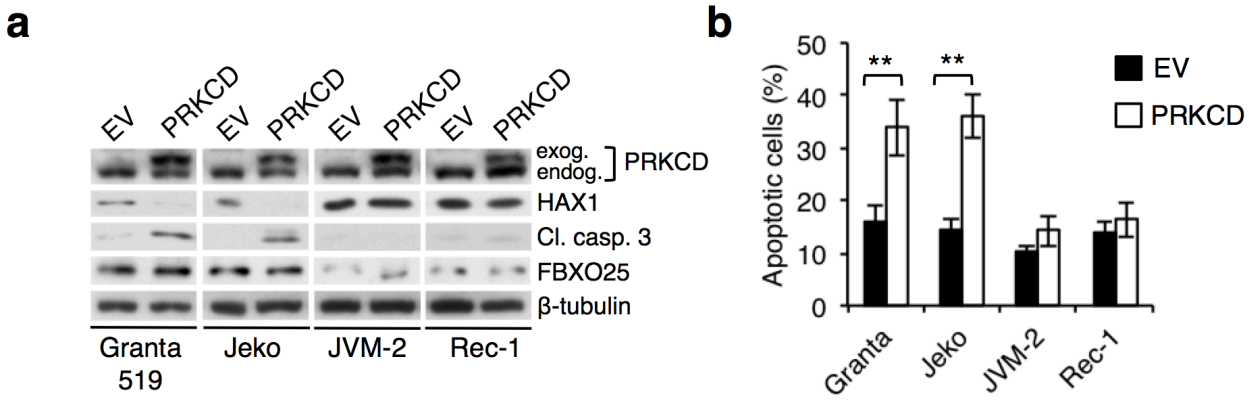

Figure 45: Re-expression of PRKCD efficiently induces apoptosis only in *FBXO25* non-deleted MCL cell lines. (**a**) Immunoblotting analyses of the *FBXO25* deleted MCL cell lines JVM-2 and Rec-1 and the *FBXO25* non-deleted lines Granta-519 and Jeko transiently transfected with FLAG-tagged PRKCD or empty vector control. Whole cell lysates were separated by SDS-PAGE and protein levels were analysed by immunoblotting using antibodies directed against exogenous (exog.) and endogenous (endog.) PRKCD, HAX1, cleaved caspase 3 (Cl. casp. 3), FBXO25 and beta-tubulin (loading control). (**b**) FACS analysis of cells in **a** to determine apoptosis rates via propidium iodide (PI) staining. Values are averaged each with the data from two additional, independent experiments (n = 3, mean ± standard deviation). **$P < 0.01$, Student`s t test.

6.6.4 Disruption of the PRKCD-FBXO25-HAX1 axis via deletion of *FBXO25* provides survival of MCL cells

To further underline that disruption of the PRKCD-FBXO25-HAX1 axis promotes the survival of MCL cells, an isogenic setting using the Granta-519 MCL cell line was chosen (as used for the xenograft transplantation model described within chapters 6.5.3 and 6.5.4). Granta-519 cells with RNAi-mediated knock-down of FBXO25 or corresponding sh_control cells were transiently transfected with FLAG-FBXO25, FLAG-PRKCD or an empty vector control and treated with 1 µg/ml etoposide for 0 and 48 hours. FACS analyses of vector control transfected cells indicate a slight decrease of the apoptotic cell population upon knock-down of FBXO25 (Figure 46). Forced expression of FBXO25 induced an increase of apoptosis rates in shFBXO25 and shCtrl treated Granta-519 cells, whereupon PRKCD induced apoptosis only in the presence of normal (shCtrl) FBXO25 levels. FACS analyses of the 48 hours of etoposide time point demonstrated that knock-down of FBXO25 protects cells significantly from apoptosis. Overexpression of FBXO25 promoted an elevation of apoptotic cell populations in both shCtrl and shFBXO25 cell lines. In contrast, forced expression of PRKCD significantly stimulated apoptosis after etoposide treatment in shCtrl MCL cells, whereupon no significant effect could be observed in FBXO25 knock-down MCL cells. Immunoblotting studies of equally treated cells underlined the effects observed by FACS [immunoblotting performed by Vanesa Fernández-Sáiz, Technische Universität München, Germany; data not shown].

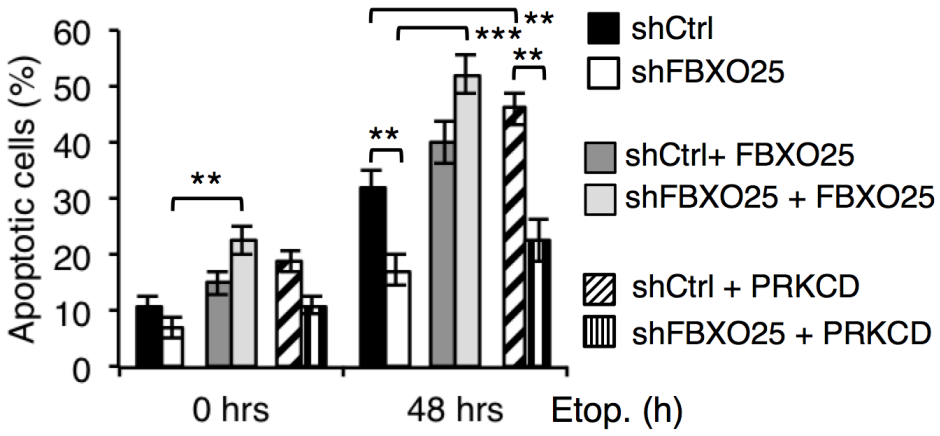

Figure 46: Disruption of the PRKCD-FBXO25-HAX1 axis promotes survival of MCL cells. FACS analyses of Granta-519 MCL cells. Granta-519 cells were virally transduced with shRNA constructs directed against FBXO25 mRNA or non-targeting control, selected with puromycin and transiently transfected with empty vector control, FLAG-FBXO25 or FLAG-PRKCD and subsequently treated with etoposide (Etop.) for 0 and 48 hours (h). Rates of apoptotic cells were determined by propidium iodide (PI) positivity in the analyses. Values are each averaged with the data from two additional, independent experiments (n = 3, mean ± standard deviation). $^{**}P < 0.01$, $^{***}P < 0.001$, one-way ANOVA.

In summary, disruption of the PRKCD-FBXO25-HAX1 axis by monoallelic deletion of the *FBXO25* gene allows for resistance towards apoptosis and promotes survival of MCL cell lines.

6.7 *FBXO25* is deleted and *HAX1* is mutated in primary human MCL patient samples

6.7.1 FBXO25 shows low expression in human MCL patient samples

Afore presented data indicate a clear pro-survival function of monoallelic *FBXO25* deletions in MCL cell lines *in vitro* and in an isogenic xenotransplantation *in vivo* model. To next investigate potential alterations of FBXO25 in primary MCL material, FBXO25 expression levels were analyzed by immunohistochemistry (IHC) in tissue microarrays (TMAs) from three cohorts of patients with MCL [performed by Martina Rudelius, Julius-Maximilians-University, Würzburg, Germany]. Thereby, cohort 1 comprised 45 primary MCL samples, cohort 2 encompassed 81 tissue samples and the analyzed cohort comprised 20 samples of the more aggressive blastoid variant (Dreyling, Kluin-Nelemans et al. 2011) of MCL. IHC analyses demonstrated a low expression level of FBXO25 in 33.3% (15/45) and 28.3% (23/81) of the MCL samples in cohorts 1 and 2 (Figure 47a). Subanalyses of the cohorts 1 and 2 in combination with the additional screened blastoid variant only MCL cohort 3 underlined a distinct enrichment of low expression levels of FBXO25 in the blastoid variant of MCL with a percentage of 46.7% (21/45) of screened samples. Moreover, low FBXO25 protein levels correlated significantly with high HAX1 protein levels in all screened cohorts (cohort 1: 13/15, $P < 0.0001$; cohort 2: 21/23, $P < 0.0001$ and cohort 3: 8/9; $P < 0.0001$) (Figure 47b).

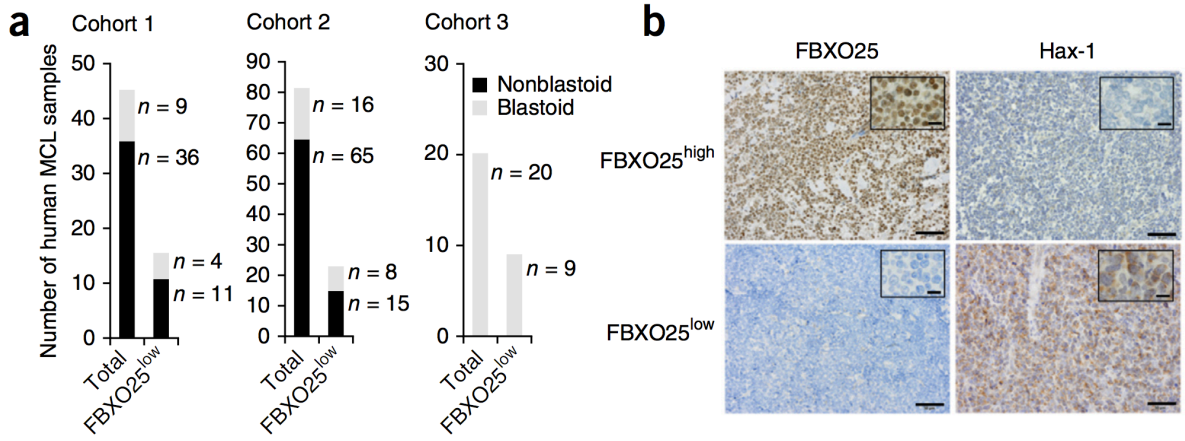

Figure 47: Identification of primary MCL patient samples with low expression of FBXO25. (**a**) FBXO25 expression levels as determined by immunohistochemistry in tissue microarrays derived from three patient cohorts of MCLs. Evaluated cohorts comprise 45 (cohort 1), 81 (cohort 2) and 20 (cohort 3) MCL patient samples. Expression of FBXO25 was quantified using the H score (see chapter 5.2.13.3). Cutoff values used were the following: FBXO25: 130 and HAX1: 170. [data provided by Martina Rudelius, Julius-Maximilians-University, Würzburg, Germany] (**b**) Representative sections of TMAs screened in **a** stained for FBXO25 and HAX1. Significant correlation of low FBXO25 protein levels and high HAX1 protein levels was observed in all cohorts; cohort 1: 13/15, $P < 0.0001$; cohort 2: 21/23, $P < 0.0001$ and cohort 3: 8/9; $P < 0.0001$; two-sided Fisher`s exact test. Scale bars denote 50 µm and 10 µm for inserts. [Histopathology data provided by Martina Rudelius, Julius-Maximilians-University, Würzburg, Germany]

IHC results for FBXO25 are in line with the observed monoallelic deletion of the 8p23.3 locus in MCL as determined by CGH array analyses (Schraders, Pfundt et al. 2005). Moreover, the higher frequencies of low FBXO25 levels in blastoid MCL are underscored by the findings of a study that demonstrated a frequent deletion of a 8p23 chromosomal segment in blastoid and leukemic MCL samples in 79% (15/19) of screened patient samples (Martinez-Climent, Vizcarra et al. 2001).

6.7.2 *FBXO25* DNA copy number correlates with *FBXO25* mRNA levels

Immunohistochemistry identified low expression levels of FBXO25 in human MCL samples (see chapter 6.7.1). In order to further validate theses data, *FBXO25* gene copy number and gene expression from cohorts 2 and 3 were validated by quantitative PCR when sufficient material for DNA/RNA extraction was available [extraction of DNA and RNA supported by Anna-Maria Karmann, Technische Universität München, Germany]. Samples with low FBXO25 expression in IHC analyses consequently revealed reduced *FBXO25* mRNA expression levels (cohort 2: 29.9%, 23/77 and cohort 3: 47.4%, 9/19) (Figure 48, left part). Moreover, FBXO25 expression levels in IHC also correlated with reduced amounts of *FBXO25* DNA (cohort 2: 29.9%, 20/67 and cohort 3: 47.4%, 9/19) (Figure 48, right part). The observed reduction in *FBXO25* DNA amount of approximately 50% was in line with the observed monoallelic deletion of the *FBXO25* locus.

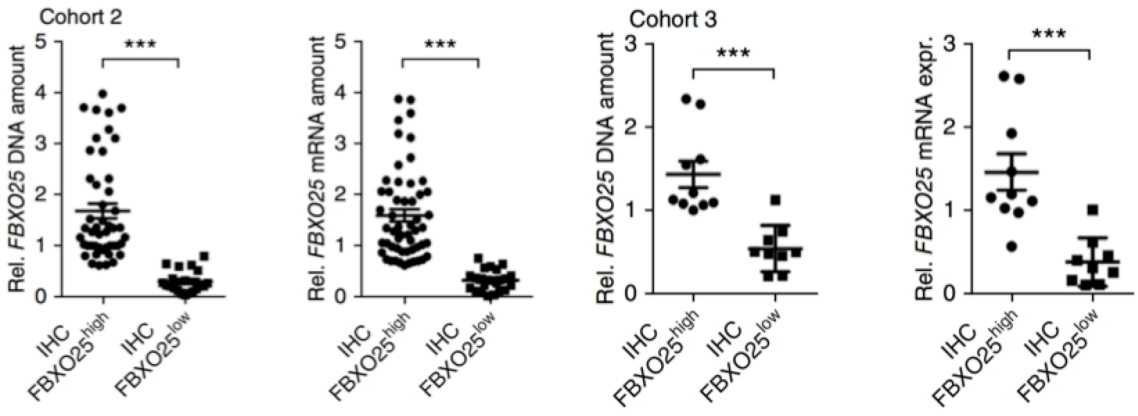

Figure 48: Analyses of *FBXO25* DNA and mRNA levels in human MCL patient samples. *FBXO25* DNA copy number and mRNA levels of *FBXO25* in MCL cohorts 2 and 3. Samples were grouped according to FBXO25 levels as determined by IHC. Rel., relative. Error bars denote ± s.e.m. *** $P < 0.001$, Student`s *t* test.

Data collected from IHC, DNA and RNA level analyses identified a nearly full concordance linking the heterozygous loss of the *FBXO25* locus to reduced mRNA and protein expression levels (IHC to *FBXO25* DNA: 94.6% and IHC to mRNA levels of *FBXO25*: 98%).

6.7.3 *HAX1* is mutated in primary MCL patient samples

To further investigate the potential presence of genomic *HAX1* mutations that might contribute to a stabilization of HAX1 after induction of apoptosis, *HAX1* was sequenced in 114 MCL patient samples of the cohorts 1 and 2. Analyses of the sequencing files identified four MCL cases with genomic mutations leading to an amino acid exchange of serine 210 of HAX1 to alanine (Figure 49, left panel). Of note, Ser210 of HAX1 has previously been described as the critical residue within the HAX1 phospho-degron leading to a FBXO25-mediated degradation of HAX1 by the UPS. The detected *HAX1* mutations were tumor specific and could not be detected in germline DNA derived from normal healthy tissue of the corresponding patient (Figure 49, right panel).

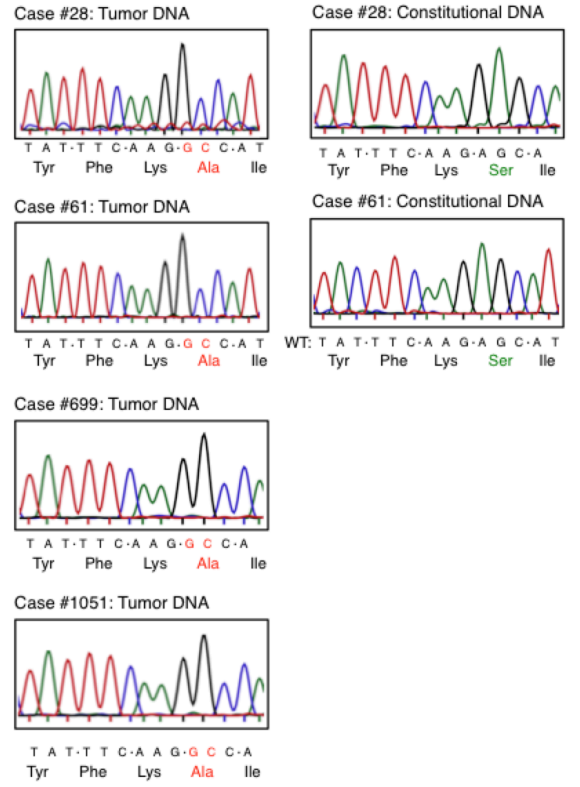

Figure 49: *HAX1* is mutated in primary MCL patient samples. *HAX1* was sequenced in 114 MCL cases from cohorts 1 and 2. Identified mutations were subclones and resequenced to ascertain the tandem mutations residing on the same allele (6 independent clones per case). Chromatograms demonstrate the genomic information for the region spanning the critical serine residue 210 of HAX1. Additional sequence analyses of germline DNA of cases #28 and #61 (8 clones per constitutional DNA) underline the somatic origin of the observed mutations in *HAX1*.

The additional sequencing of 37 primary MCL patient samples from cohort 1 identified no single mutation of FBXO25 within these samples, underlining the monoallelic deletion of *FBXO25* as central tumor mechanism to inactivate the F-box protein.

6.7.4 FBXO25 and HAX1 protein levels correlate in human MCL samples

Immunoblotting analyses on protein extracts derived from formalin-fixed paraffin-embedded MCL patient tissues of cohorts 1 and 2 confirmed the observations from IHC and sequencing studies (for methodology see 5.2.13.5). Within cohort 1, case #1 served as control and showed normal FBXO25 levels and moderate HAX1 levels, whereupon the *FBXO25* monoallelic deleted cases #12 and #24 show a massive reduction in FBXO25 levels correlating with an increase in HAX1 protein levels. In contrast, $HAX1^{S210A}$ mutated cases #28 and #61 showed highest HAX1 levels despite the presence of normal FBXO25 levels (Figure 50, left panel). The additional performed analyses of six cases from cohort 2 reveal high levels of FBXO25 and moderate HAX1 levels in the *FBXO25* wildtype cases #104 and #131. The heterozygous loss of *FBXO25* in cases #644 and #1192 induces an elevation of HAX1 levels, whereupon mutation of serine 210 of HAX1 stabilizes HAX1 in the presence of normal FBXO25 protein levels as represented by cases #699 and #1051 (Figure 50, right panel).

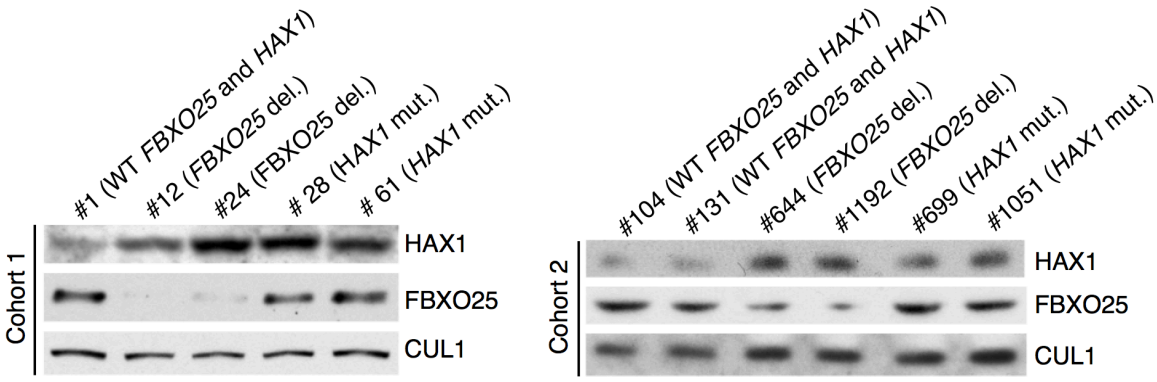

Figure 50: HAX1 and FBXO25 levels correlate on immunoblotting levels in human MCL samples. Immunoblot analyses of extracts from 11 formalin-fixed paraffin-embedded human MCL samples of cohorts 1 (left panel) and 2 (right panel). Proteins were extracted from tissue slices, separated by SDS-PAGE and probed with antibodies directed aginst HAX1, FBXO25 and CUL1 (loading control). Del., deleted; mut., mutated.

In order to further evalute the results from immunoblotting, cases with documented mutations of the *HAX1* gene were analyzed by immunohistochemistry [performed by Martina Rudelius, Julius-Maximilians-University, Würzburg, Germany] (compare 5.2.13.3). IHC analyses of the HAX1 mutated cases #28, #61, #699 and #1051 stained for HAX1 and FBXO25 indiced high levels of HAX1 despite normal FBXO25 expression (Figure 51). Moreover, analyses of

immunoblotting and IHC analyses indicate that *FBXO25* deletions and *HAX1* mutations are mutually exclusive events.

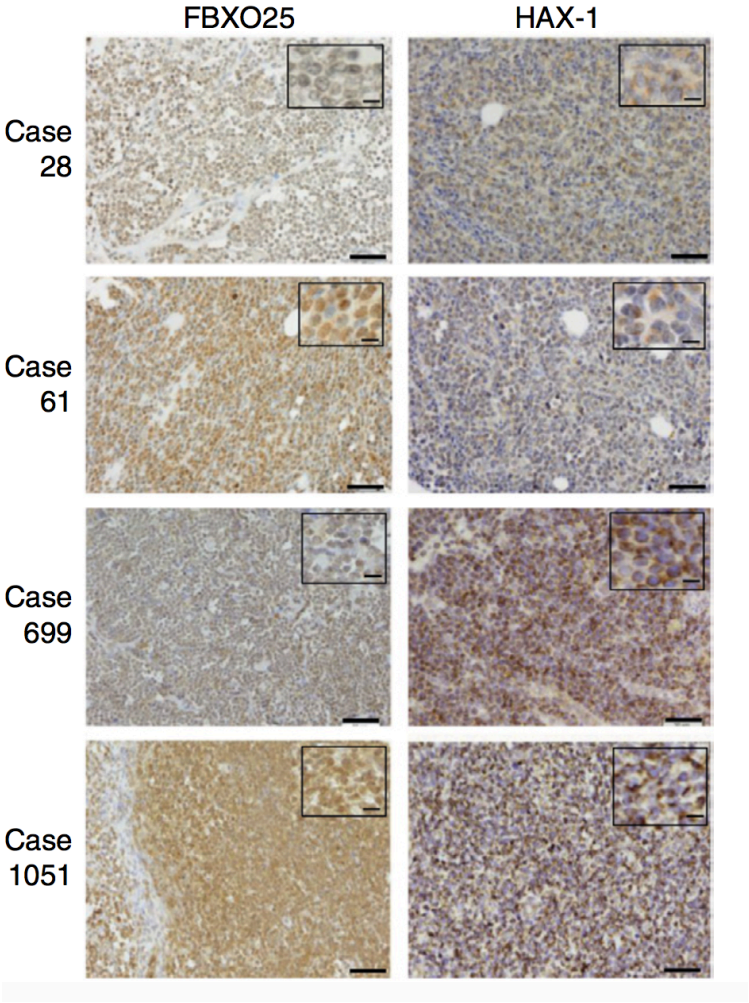

Figure 51: Mutation of *HAX1* stabilizes HAX1 in the presence of normal FBXO25 levels. Representative IHC performed on sections derived from MCL samples mutated at serine 210 of HAX1 in cohort 1 (cases 28 and 61) and cohort 2 (cases 699 and 1051). Samples were stained for FBXO25 and HAX1. Scale bars denote 50 µm and 10 µm for inserts. [Histopathology data provided by Martina Rudelius, Julius-Maximilians-University, Würzburg, Germany]

In summary, analyses of primary MCL patient samples indicate that *FBXO25* is monoallelical deleted and *HAX1* is mutated in MCL patients. Moreover, deletions of *FBXO25* and *HAX1* mutations are mutually exclusive.

6.8 The FBXO25-HAX1 axis regulates cell surface expression of CXCR4

Hax1$^{-/-}$ mice were described to survive not longer than 14 weeks due to massive apoptosis of neurons and reduced cellularity of lymphoid tissues (Chao, Parganas et al. 2008);(Peckl-Schmid, Wolkerstorfer et al. 2010), underlining the pro-survival function of Hax1. Moreover, *Hax1*$^{-/-}$ B-cells showed a significant decrease of the protein expression levels of the C-X-C chemokine receptor 4 (CXCR4) (Peckl-Schmid, Wolkerstorfer et al. 2010), a main regulator of hematopoietic stem cell homing and migration (Alsayed, Ngo et al. 2007). Immunoblotting data derived from the tumors of C57BL/6 mice reconstituted with Fbxo25 shRNA heterozygous Eμ-myc HSPCs (compare chapter 6.5.2) indicated an increase of Cxcr4 protein levels compared to tumors derived from animals transplanted with control HSPCs [data not shown].

6.8.1 HAX1 interacts with CXCR4 and regulates its overall protein levels

To evaluate the direct dependency of CXCR4 and HAX1 protein levels, Granta-519 cells transduced with pLPC_empty vector control or pLPC_HAX1^{S210A} (as used for the xenotransplantation model described in chapter 6.5.4) were analyzed towards their expression levels of HAX1 and CXCR4. Immunoblotting analyses revealed a massive increase of HAX1 levels, due to the forced expression of the non-degradable HAX1^{S210A} mutant, that went along with a clear increase of CXCR4 protein levels in whole cell lysates (Figure 52).

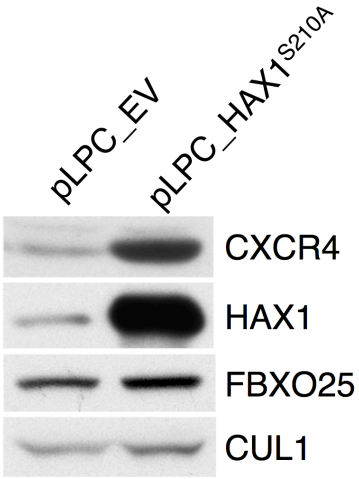

Figure 52: CXCR4 protein levels are dependent on HAX1 protein expression. Immunblotting study of Granta-519 cells retrovirally transduced with pLPC_empty vector control (pLPC_EV) or pLPC_HAX1^{S210A}. Whole cell lysates were separated by SDS-PAGE and immunoblotted with antibodies directed against CXCR4, HAX1, FBXO25 and CUL1 (loading control).

Waldenström macroglobulinemia (Morbus Waldenström) represents an immunoproliferative disorder that is characterized by germline mutations in the C-terminal part of CXCR4, which stabilize CXCR4 surface expression (Hunter, Xu et al. 2014), leading to constitutive CXCR4 activity and pro-proliferative CXCR4-dependent ERK-signaling (Cao, Hunter et al. 2015). In order to evaluate the effect of the WHIM-like (Warts, Hypogammaglobulinemia, Immunodefficiency and Myelokathexis) mutations of CXCR4 derived from Morbus Waldenström (Hernandez, Gorlin et al. 2003) on a potential interaction with HAX1, $CXCR4^{R334X}$, $CXCR4^{S339fs342X}$ and $CXCR4^{E343X}$ were cloned as FLAG-tagged expression constructs. HEK293T cells were transiently transfected with FLAG-tagged CXCR4 wildtype, $CXCR4^{R334X}$, $CXCR4^{S339fs342X}$, $CXCR4^{E343X}$ or an empty vector control and FLAG-tagged proteins were immunoprecipitated using an anti-FLAG resin. Immunoblotting studies indicate a clear co-immunoprecipitation of CXCR4 with endogenous HAX1 that is slightly increased for the WHIM-like mutants of CXCR4 (Figure 53, left panel). Moreover, treatment of cells with the CXCR4 antagonist AMD3100 (Cashen, Nervi et al. 2007) abrogated the binding of HAX1 to the CXCR4 wildtype, whereupon the interaction of HAX1 with the WHIM-like mutants of CXCR4 remained stable (Figure 53, right panel).

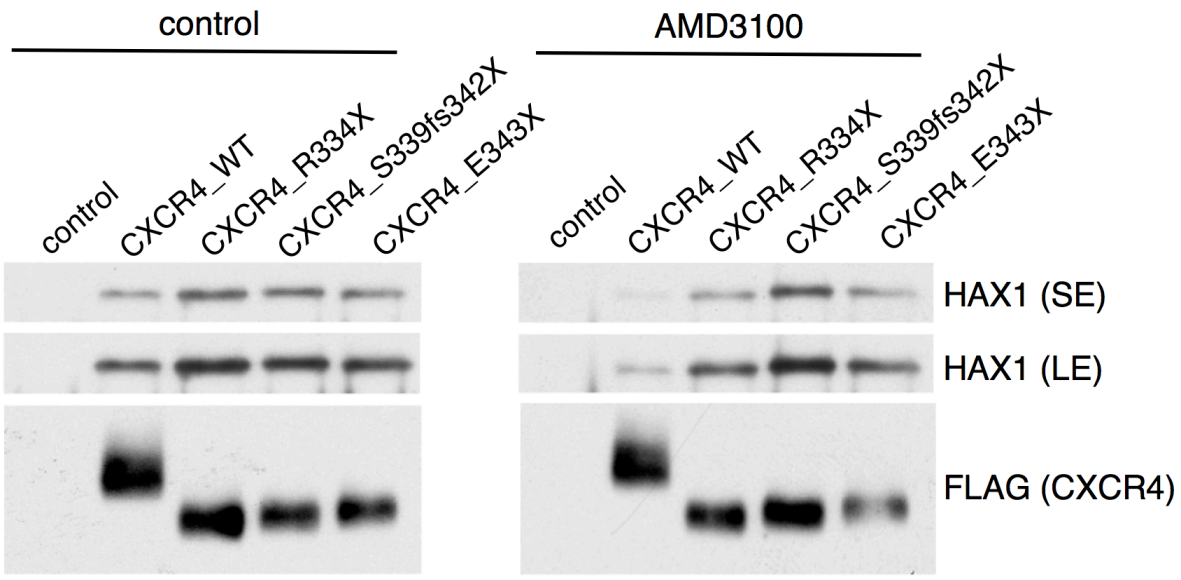

Figure 53: AMD3100 inhibits the interaction of HAX1 and CXCR4 wildtype but not with WHIM-like mutated CXCR4. HEK293T cells were transfected with FLAG-tagged CXCR4 wildtype, $CXCR4^{R334X}$, $CXCR4^{S339fs342X}$, $CXCR4^{E343X}$ or an empty vector control (control) and subsequently treated with AMD3100 or solvent for 6 hours. Whole cell lysates were subjected to an immunoprecipitation approach unsing an anti-FLAG resin. Immunoprecipitated proteins were separated by SDS-PAGE and analyzed by immunoblotting using antibodies directed against HAX1 and FLAG (CXCR4). SE, short exposure; LE, long exposure.

6.8.2 HAX1 influences CXCR4 levels and CXCR4-dependent downstream signaling

HAX1 has been shown to interact with CXCR4 and to influence the overall protein levels of CXCR4. In order to further evaluate the impact of Hax1 towards Cxcr4 downstream signaling, *Hax1*$^{-/-}$ MEFs and their wildtype counterparts were stimulated with the natural Cxcr4 ligand Sdf-1, and Cxcr4 downstream signaling was tested via immunoblotting. Hax1 wildtype MEFs stimulated with Sdf-1 revealed an increase of pErk1/2 as marker of Cxcr4 downstream signaling activity (Figure 54a). In contrast, *Hax1*$^{-/-}$ MEFs did not respond to Sdf-1 stimulation as visualized by the missing increase of pErk1/2, whereupon Cxcr4 levels showed in general a strong decrease in *Hax1*$^{-/-}$ MEFs compared to wildtype MEFs. To subsequently demonstrate the dependency of the observed effect on Hax1, *Hax1*$^{-/-}$ MEFs were retrovirally transduced to re-express Hax1 wildtype (MigR1_Hax1) or an empty vector control. Immunoblotting data indicate that re-expression of Hax1 induced an increase in overall Cxcr4 protein levels and also promoted activation of Cxcr4 dependent downstream signaling, as visualized by the increase of pErk1/2 levels, even in the absence of the receptor ligand Sdf-1 (Figure 54b).

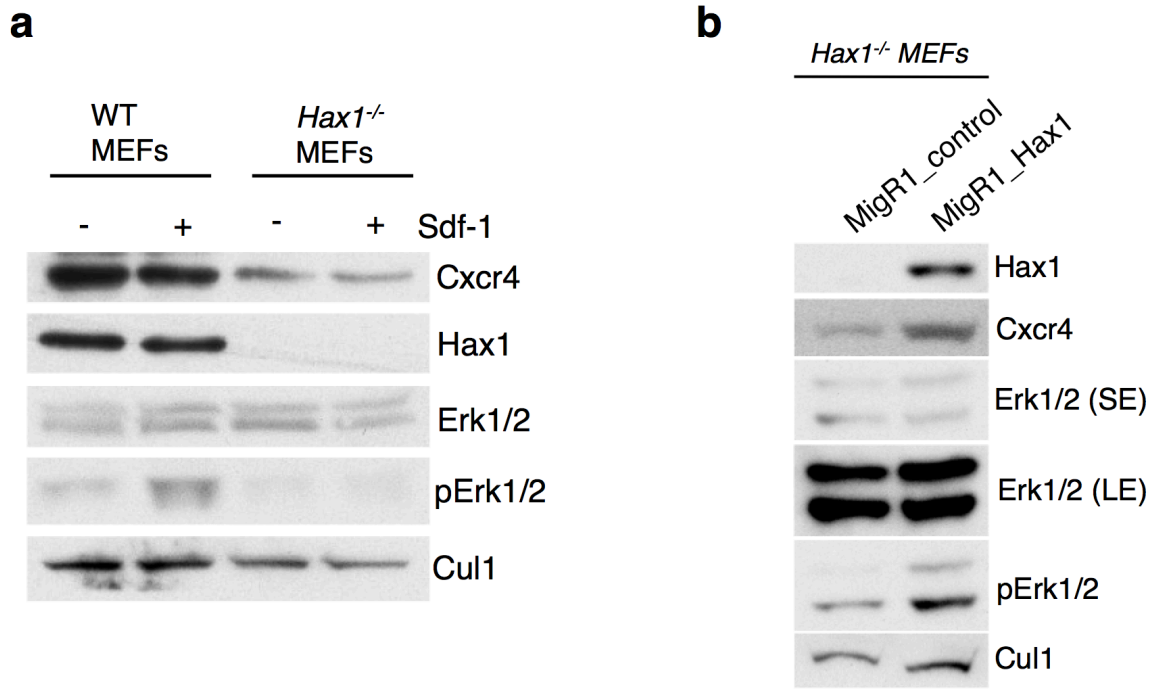

Figure 54: Hax1 regulates the downstream signaling of Cxcr4. (**a**) *Hax1* wildtype (WT MEFs) and *Hax1*$^{-/-}$ MEFs were treated with Sdf-1 or solvent for 6 hours. Whole cell lysates were separated by SDS-PAGE and protein levels were determined by immunoblotting using antibodies directed against Cxcr4, Hax1, Erk1/2, phospho-Erk1/2 (pErk1/2) and Cul1 (loading control). (**b**) *Hax1*$^{-/-}$ MEFs were retrovirally transduced with MigR1_Hax1 or an empty vector control (MigR1_control). Whole cell lysates were separated by SDS-PAGE and subjected to immunoblotting using antibodies directed against Hax1, Cxcr4, Erk1/2, phospho-Erk1/2 (pErk1/2) and Cul1 (loading control). SE, short exposure; LE, long exposure.

6.8.3 HAX1 regulation of CXCR4 levels occurs post-translational

To subsequently investigate whether Hax1 influences the Cxcr4 levels dependent on translation or post-translational, *Hax1*$^{-/-}$ MEFs and their wildtype counterparts were tested for their content of *Cxcr4* mRNA using two specific quantitative PCR primer pairs (for sequences see 5.1.4.3). The results equally obtained with both primer pairs indicate an increased amount of Cxcr4 mRNA in *Hax1*$^{-/-}$ MEFs as compared to control (Figure 55), suggesting a post-translational regulation of Cxcr4 protein levels by Hax1.

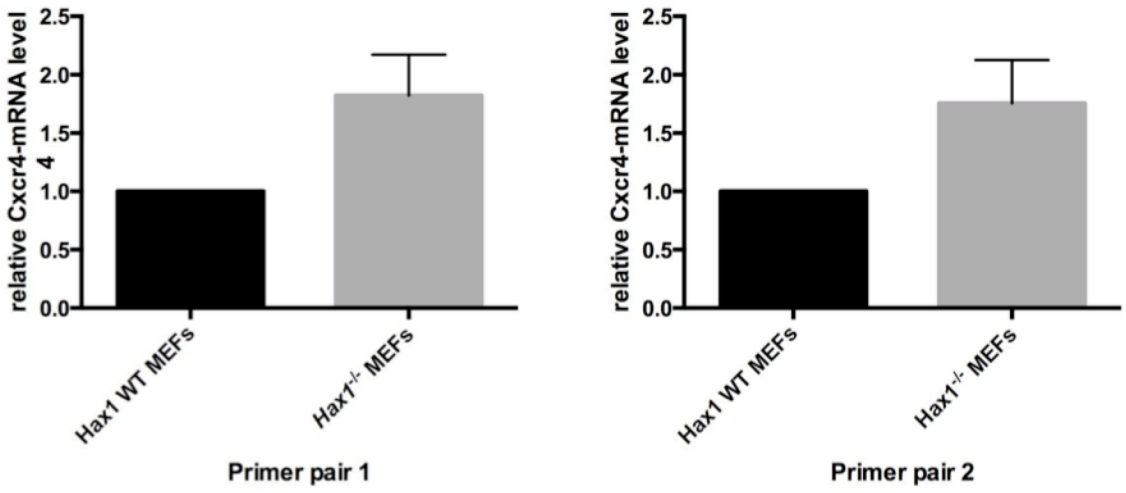

Figure 55: Hax1 regulation of Cxcr4 levels occurs post-translational. Whole cell RNA was extracted from *Hax1*$^{-/-}$ MEFs and their wildtype counterparts (*Hax1* WT MEFs) and transcribed to cDNA. cDNA of *Cxcr4* was amplified with two specific primer pairs and compared to the expression level of the *RPPA_P0* house keeping gene. Values are averaged each with the data from two additional, independent experiments (n = 3, mean ± standard deviation).

To further test the effect of a HAX1 knock-down onto overall and cell surface expression levels of CXCR4, SU-DHL-8 B-cell lymphoma cells were transduced with two shRNA constructs targeting HAX1 and a non-targeting vector control. CXCR4 whole cell levels were determined at days 3 and 8 post infection, whereupon cell surface expression of CXCR4 was measured by flow cytometry at day 3 post infection. Immunoblotting studies at day 3 post infection confirmed the knock-down of HAX1 but did not show a change in the overall protein levels of CXCR4, whereupon CXCR4 downstream signaling was reduced as visualized by a decrease of pERK1/2 levels (Figure 56b). In line with the reduced pERK1/2 signaling, flow cytometry data indicate a clear reduction of CXCR4 surface expression underlining HAX1 as potential cell surface expression stabilisator of

CXCR4 (Figure 56a). Immunoblotting studies performed 8 days post infection of SU-DHL-8 cells indicate a clear decrease in the overall protein levels and a reduction of pERK1/2 levels that was already observed on day 3 post infection. The observed effects of HAX1 knock-down on CXCR4 surface and overall expression levels support the previously observed post-translational effect of HAX1 on CXCR4 expression.

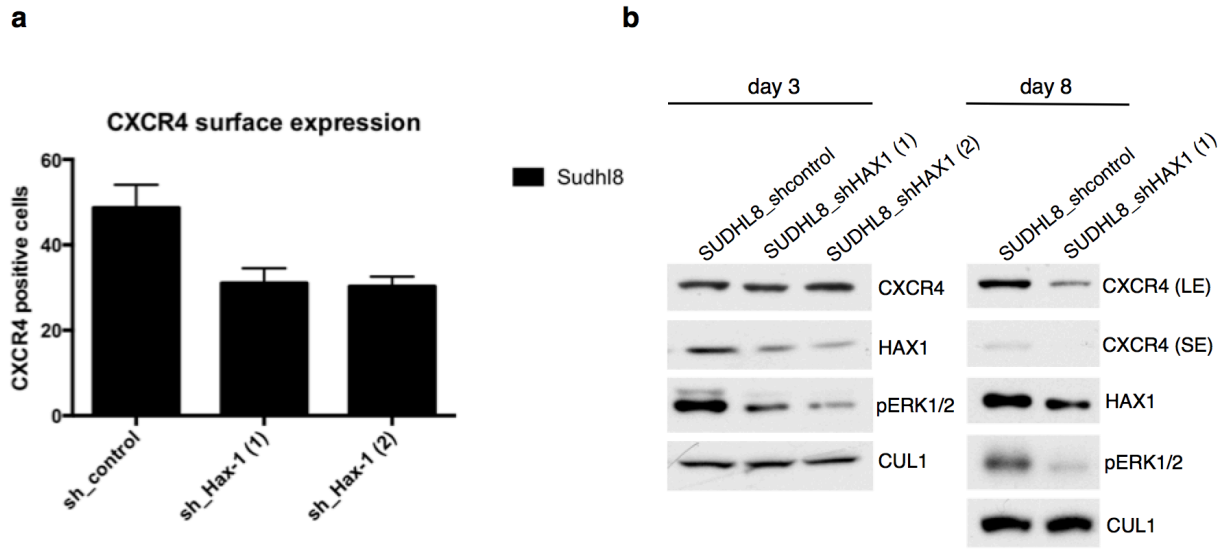

Figure 56: HAX1 influences cell surface expression and stability of CXCR4. (**a**) Flow cytometric analysis of CXCR4 surface expression of SU-DHL-8 cells transduced with two shRNA constructs targeting HAX1 (sh_HAX1 (1) and sh_HAX1 (2)) or a non-targeting control. Cells were fixed in formalin and surface expression was determined by antibodies directed against CXCR4. Values are averaged each with the data from two additional, independent experiments (n = 3, mean ± standard deviation). (**b**) Immunoblotting of SU-DHL-8 cells transduced with two shRNA constructs targeting HAX1 (sh_HAX1 (1) and sh_HAX1 (2)) or a non-targeting control at days 3 and 8 post infection. Whole cell lysates were separated by SDS-PAGE and subjected to immunoblotting using antibodies directed against CXCR4, HAX1, pERK1/2 and CUL1 (loading control). SE, short exposure; LE, long exposure.

6.8.4 HAX1 levels influence the resistance of MCL cell lines towards AMD3100 treatment

Previous results indicated an effect of HAX1 knock-down on the surface expression and the downstream signaling of CXCR4 in a B-cell lymphoma cell line (see 6.8.3). To subsequently elucidate the role of HAX1 protein levels in the resistance of MCL cell lines towards the CXCR4 inhibitor AMD3100, a cell line with high HAX1 levels, due to a monoallelic deletion of *FBXO25* (Rec-1) and the control MCL cell lines (Jeko and Granta-519) were tested according to CXCR4 surface expression levels after treatment with AMD3100 (compare cell lines in chapter 6.6.1). Flow

cytometric analyses using an antibody directed against CXCR4 indicated a clear decrease in the CXCR4 surface levels of Jeko and Granta-519 cells after treatment with AMD3100 for 6 hours (Figure 57). In contrast, AMD3100 treatment induced only a slight decrease in CXCR4 membrane expression of Rec-1 cells underlining high HAX1 protein expression levels as a protective factor against AMD3100-induced CXCR4 internalization in B-cell lymphoma.

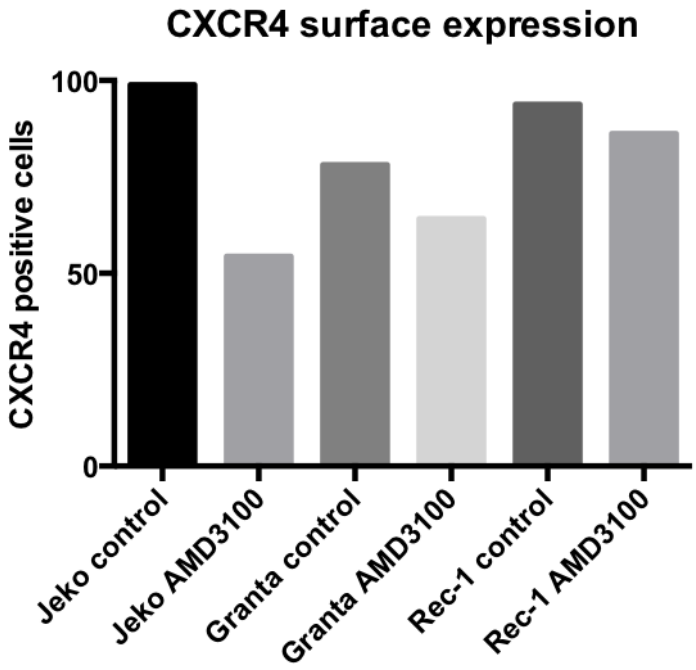

Figure 57: Monoallelic deletion of *FBXO25* protects cells from AMD3100 induced CXCR4 internalization. Flow cytometric analysis of CXCR4 surface expression of Jeko, Granta-519 and Rec-1 MCL cell lines treated with the CXCR4 inhibitor AMD3100 or solvent for 6 hours. Cells were fixed in formalin and surface expression was determined by antibodies directed against CXCR4. Immunoglobulin G (IgG) staing was used as negative control. $n = 1$.

In summary, HAX1 has been described as novel interactor of the chemokine receptor CXCR4 that regulates cell surface expression and whole cell levels of CXCR4 in a post-translational manner. Moreover, high levels of HAX1, e.g. caused by a monoallelic deletion of the HAX1-E3 ubiquitin ligase *FBXO25*, provide resistance towards AMD3100 induced CXCR4 inhibition and destabilization of CXCR4 cell surface expression.

7 Discussion

Data derived from the present study unravel a novel pro-apoptotic pathway comprising the ubiquitin-proteasomal degradation of the anti-apoptotic molecule HAX1 via the previously orphan E3-ubiquitin ligase SCF^{FBXO25}, a process that is spatially and timely controlled by PRKCD as regulatory kinase. In a physiological cellular setting, application of an apoptotic stimulus (e.g. chemotherapeutic agent) induces the sequential translocation of PRKCD to nucleus and mitochondria, thereby leading to specific phosphorylation of nuclear FBXO25 and mitochondrial HAX1. Phosphorylation of FBXO25 within its conserved nuclear export signal (NES) induces a translocation of FBXO25 from nucleus to mitochondria thereby co-localizing with HAX1. The PRKCD-mediated phosphorylation of HAX1 within its evolutionary conserved phospho-degron facilitates the recruitment of HAX1 to the SCF^{FBXO25} E3 ligase inducing the ubiquitylation and subsequent 26S-proteasomal degradation of HAX1 (Figure 58, left panel). In contrast, monoallelic deletion of *FBXO25* or mutation of the HAX1 phospho-degron disrupts the described apoptosis pathway and promotes survival of mantle cell lymphoma cells. The monoallelic loss of *FBXO25*, as observed in approximately 24% of screened MCL patient samples, leads to a lack of functional SCF^{FBXO25} ligase complexes and stabilizes HAX1 after induction of apoptosis (Figure 58, middle part), whereupon HAX1 phospho-degron mutations block the recognition of HAX1 by SCF^{FBXO25} and likewise induce a stabilization of HAX1 (Figure 58, right panel).

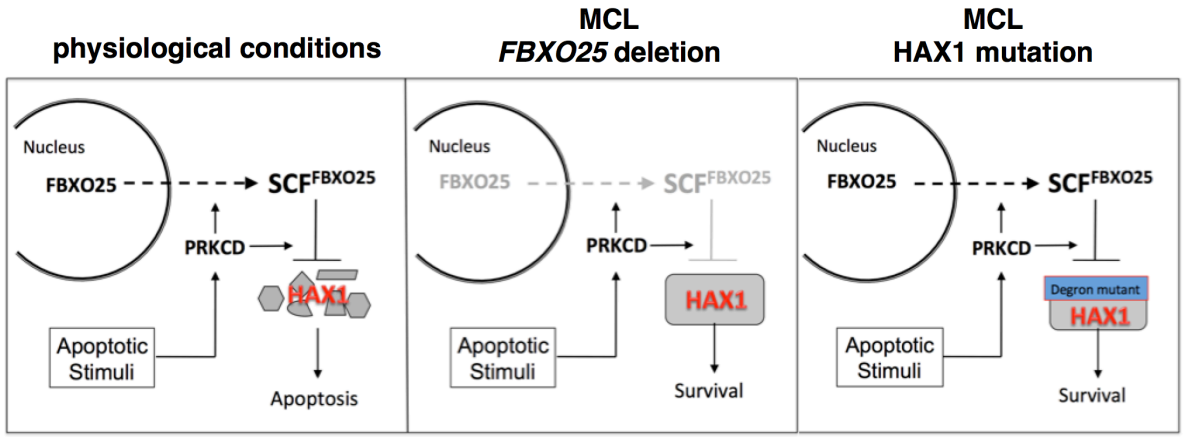

Figure 58: Graphic representation of the PRKCD-FBXO25-HAX1 axis under physiological conditions and its disruption in MCL. Under physiological conditions, apoptotic stimulation induces a sequential phosphorylation of nuclear FBXO25 and mitochondrial HAX1 by PRKCD. NES-phosphorylated FBXO25 translocates to mitochondria and recruits the degron-phosphorylated HAX1 to the SCF^{FBXO25} E3 ligase complex, thus mediating ubiquitylation and proteasomal degradation of HAX1 and induction of cell death (left panel). In contrast, MCL tumors harbor monoallelic deletions of *FBXO25* (middle panel) or phospho-degron mutations of HAX1 (right panel) that promote survival of MCL cells after induction of apoptosis via stabilization of HAX1. [Graphic modified from Florian Bassermann, Technische Universität München, Germany]

Moreover, the present study identifies HAX1 as an essential regulator of CXCR4 cell surface expression and downstream signaling, thus underlining an essential function of the PRKCD-FBXO25-HAX1 axis in the control of homing and migration of hematopoietic (stem) cells.

The following chapters will discuss the functional role of the PRKCD-FBXO25-HAX1 axis in apoptotic signaling (chapter 7.1), the importance of disrupting the PRKCD-FBXO25-HAX1 axis for survival of MCL cells (chapter 7.2) and the regulation of CXCR4 expression and signaling via HAX1 (chapter 7.3). Moreover, HAX1 will be discussed as potential novel therapeutic target structure in the treatment of MCL and other B-cell malignancies.

7.1 FBXO25 and PRKCD regulate the response towards apoptotic stimuli via ubiquitin-proteasomal degradation of HAX1

7.1.1 FBXO25 as potential novel tumor suppressor involved in the regulation of apoptosis

The UPS regulates the degradation of the vast majority of all cellular proteins (Rock, Gramm et al. 1994) and thereby contributes essentially to the regulation of cell cycle progression, differentiation and apoptosis (Schenkein 2002). Albeit proteasomal inhibition e.g. by bortezomib has significantly improved the treatment of B-cell malignancies (Dimopoulos, Delimpasi et al. 2014), further insights into the molecular regulation of specific degradation processes and their deregulation in cancer is required to identify novel biomarkers and therapeutic target structures allowing for a more target-oriented treatment of selected tumor types. A CGH array analysis based approach in search for novel deregulated UPS components in B-cell lymphoma identified the chromosomal region 8p23.3 as hotspot region for a tumor suppressor gene frequently deleted in MCL and to a lower extent in DLBCL (Baumann 2011). A more stringent analysis within the present study demonstrated *FBXO25*, encoding the F-box protein FBXO25, within the minimal common region of deletion of 8p23.3 (chapters 3.4 and 6.1.1). The exclusive monoallelic nature of the *FBXO25* deletions observed in approximately 24% of MCL samples underlines *FBXO25* as an interesting candidate for a novel haplo-insufficient tumor suppressor gene.

A mass spectrometry based approach for interactors of FBXO25 confirmed the presence of all SCF-components (SKP1/CUL1/ROC1) and identified the anti-apoptotic molecule HAX1 as potential substrate of the previously orphan SCF^{FBXO25} E3-ubiquitin ligase (Baumann 2011). Subsequent studies for the stability of HAX1 (chapter 6.1.1) demonstrate HAX1 as short-lived

protein that gets degraded immediately after induction of apoptosis, underlining a potential role of HAX1 as substrate of the UPS. Binding studies confirmed the mass spectrometry data sets by unraveling an interaction of HAX1 with FBXO25 and the SCF-core components CUL1 and SKP1, an interaction that was highly specific for FBXO25 and could not be detected with variable other F-box proteins (chapter 6.1.2). Moreover, interaction of FBXO25 and HAX1 increased after treatment with etoposide, an apoptosis inducing agent, underlining the targeted proteasomal degradation of an anti-apoptotic molecule after induction of apoptosis and anticipating FBXO25 as previously undescribed component of an apoptosis regulating pathway (chapter 6.1.3). In line with the anticipated proteasome mediated degradation of HAX1 via the SCF^{FBXO25} ligase, proteasomal inhibition by MG132 as well as knock-down of FBXO25 expression levels prevented the degradation of HAX1 (chapter 6.1.3). Regarding the function of FBXO25 as apoptosis regulating molecule, knock-down of FBXO25 stabilized HAX1 and prolongated the execution of apoptosis. In contrast, forced expression of FBXO25 destabilized HAX1 and led to induction of apoptosis even in the absence of an external apoptotic stimulus. Knock-down or forced expression of FBXO25 completely failed to influence apoptotic markers in a *Hax1* knock-out model, encouraging HAX1 as the relevant substrate of SCF^{FBXO25} in the investigated apoptosis pathway and excluding an indirect effect of FBXO25 levels on HAX1 (chapter 6.1.3).

The observed degradation of HAX1 via a SCF-complex determined by the F-box protein FBXO25 presupposes a co-localization of both molecules to allow for ubiquitylation of HAX1 via SCF^{FBXO25}. Immunofluorescence studies in the frame of the present work demonstrate FBXO25 within the nucleus of untreated cells and HAX1 at mitochondrial membranes, a staining pattern that is in line with previously published data on FBXO25 (Manfiolli, Maragno et al. 2008) and HAX1 (Suzuki, Demoliere et al. 1997). The observed separation of endogenous FBXO25 and HAX1 in different cellular compartments prevents the interaction of both molecules in untreated cells and did not support the initial prospect of a constant co-localization of FBXO25 and HAX1. Of note, application of an apoptotic stimulus induced the translocation of nuclear FBXO25 to site of mitochondria leading to co-localization with HAX1 and enabling a potential degradation process of HAX1 (see chapter 6.1.4). Additional performed immunofluorescence based studies confirmed the independence of the observed shuttling process from the presence of functional TP53 as FBXO25 translocation could be observed similarly in *Tp53* wildtype and knock-out MEFs (Olsson, Manzl et al. 2007) (see chapter 6.1.4), underlining the importance of the analyzed mechanism independent of the cellular TP53 status.

To further elucidate the mechanistic base of the observed FBXO25 translocation event, sequence analyses were performed on the FBXO25 protein sequence and confirmed a NLS, allowing for nuclear localization of FBXO25, and unraveled the additional presence of an evolutional highly conserved NES motif, potentially facilitating the nuclear export of FBXO25.

Indeed, mutation of a conserved serine residue within the NES (Ser178 of FBXO25) led to a significant nuclear retention of mutated FBXO25 upon apoptotic stimulation compared to the FBXO25 wildtype (see chapter 6.2.1). Forced expression of the FBXO25 wildtype increased the levels of FBXO25 phosphorylated at serine residue 178 and induced a decrease in HAX1 levels as well as an increase of apoptotic cells determined by flow cytometric analyses. In contrast, the FBXO25 NES-mutant (Ser178) completely failed to induce apoptosis signaling and even protected cells from etoposide induced apoptosis, suggesting a dominant negative function of FBXO25^{S178A} over endogenous wildtype FBX025 (see chapter 6.2.1). Moreover, data derived from experiments in the present study indicate the phosphorylation of the NES-associated serine residue S178 of FBXO25 as essential requirement for the pro-apoptotic signaling cascade dependent on FBXO25.

In contrast to other E3-ubiquitin ligases of the RING finger type, SCF-complexes recruit their substrates dependent on a post-translational modification, usually the phosphorylation of a substrate intrinsic phospho-degron motif (Petroski and Deshaies 2005);(Fernandez-Saiz, Targosz et al. 2013). In this regard, mapping studies and conserved domain searches demonstrated the amino acid region 201-230 of HAX1 as essential protein part for the recruitment by SCF^{FBXO25}. Mutation of the three conserved serine residues Ser206, Ser210 and Ser212 of HAX1 followed by interaction studies identified the presence of serine residue Ser210 of HAX1 as prerequisite for interaction with FBXO25 (see chapter 6.2.2). The HAX1^{S210A} mutant showed complete resistance towards etoposide induced degradation and protected cells significantly more from apoptosis as the degradable HAX1 wildtype (see chapter 6.2.2). Here presented data sets from the HAX1^{S210A} mutant as well as derived from a self-made phospho-specific antibody directed against phospho-Ser210 of HAX1 demonstrate that phosphorylation of serine 210 of HAX1 is the essential modification allowing for FBXO25-mediated degradation of HAX1 and subsequent execution of the pro-apoptotic caspase cascade.

7.1.2 SCF^{FBXO25}-mediated ubiquitylation and degradation of HAX1 requires the activity of PRKCD

Previously discussed data indicate an essential role of the phosphorylations of Ser178 of FBXO25 and Ser210 of HAX1 in the execution of pro-apoptotic signaling. The analysis of FBXO25 and HAX1 protein sequences for conserved kinase recognition and phosphorylation motifs identified both serines as potential sites of the pro-apoptotic kinase PRKCD.

PRKCD represents the only isozyme of the PKC family with pro-apoptotic activity, which has been described to be dependent on a sequential re-distribution of PRKCD to different cellular compartments, exceptionally nucleus and mitochondria (Yoshida 2007). The functional

understanding of these translocation events in the regulation of apoptosis remained still absent. The present study for the first time demonstrates that PRKCD translocates to nucleus and mitochondria to phosphorylate FBXO25 and HAX1, and that the FBXO25-HAX1 axis is the central pathway by which PRKCD exerts its pro-apoptotic activity. In line with the previously published data on the translocation of PRKCD (Yoshida 2007), immunofluorescence based studies indicate a sequential shuttling of PRKCD to nucleus and mitochondria, thereby co-localizing with nuclear FBXO25 and HAX1 at site of mitochondria (see 6.3.1). To further elucidate the role of PRKCD in the nuclear export of FBXO25 after induction of apoptosis, FBXO25 shuttling was microscopically imaged in *Prkcd* knock-out MEFs (Leitges, Mayr et al. 2001). Results obtained from etoposide treated cells indicate a clear nuclear retention of FBXO25 in the absence of Prkcd that could similarly be observed after mutation of the central serine residue of the FBXO25 NES-motif, suggesting the PRKCD-mediated phosphorylation of Ser178 of FBXO25 as requirement for the translocation of FBXO25 to mitochondria (see chapter 6.3.2).

Data derived from the *Prkcd* knock-out mouse model indicate that loss of Prkcd leads to an expansion of the B-lymphocyte compartment (Chao, Parganas et al. 2008), whereupon genetic loss of *Hax1* leads to the premature death of affected animals due to a nearly complete loss of B-cells in spleen, thymus and bone marrow (Peckl-Schmid, Wolkerstorfer et al. 2010). In order to further evaluate the role of these two functionally opposing proteins in the context of Fbxo25, wildtype and *Prkcd* knock-out MEFs were stimulated to undergo apoptosis. Loss of Prkcd resulted in a clear loss of phospho-Fbxo25 (Ser178) and phospho-Hax1 (Ser210), leading to stabilization of cellular Hax1 levels after induction of apoptosis and a significant decrease of apoptosis rates as determined by flow cytometric analyses (see chapter 6.3.3). These data indicate that FBXO25 links the functionally opposing proteins PRKCD and HAX1 by allowing for a PRKCD-mediated degradation of the anti-apoptotic molecule HAX1. In line with this hypothesis, application of the PRKCD inhibitor rottlerin decreases the interaction of FBXO25 and HAX1, indicating that PRKCD activity is required to further enhance downstream signaling of the newly described apoptosis regulating pathway (see 6.2.4). Of note, rottlerin has been described as inappropriate inhibitor of PRKCD, which might also inhibit other kinases at concentrations used within this study (Soltoff 2007). To further exclude side effects of rottlerin on the published data, the impact of PRKCD on the interaction and ubiquitylation of HAX1 by FBXO25 was additionally demonstrated in an *in vitro* ubiquitylation setting.

In vitro phosphorylation studies of FBXO25 and HAX1 demonstrate that PRKCD, but not another PKC isozyme, directly phosphorylates Ser178 of FBXO25 and Ser210 of HAX1, thus depicting a dual phosphorylation process on levels of ligase and substrate that is mediated by PRKCD as regulatory kinase (see chapter 6.3.5). *In vivo* and *in vitro* ubiquitylation assays unravel a robust ubiquitylation of HAX1 in the presence of SCF^{FBXO25} that could not be observed in the

presence of a different F-box protein as well as in the absence of a functional E3 ligase complex. Moreover, the *in vitro* study indicates that ubiquitylation of the HAX1 wildtype is enhanced in the presence of increasing concentrations of purified PRKCD, whereupon no ubiquitylation at all could be observed for the HAX1^{S210A} mutant (see chapter 6.4). The observed decrease of the lower non-ubiquitylated HAX1 band after incubation with all required ubiquitylation components can be explained by increased ubiquitylation of HAX1 upon increasing PRKCD concentrations leading to a shift of HAX1 to the upper ubiquitylated form (Figure 31).

The sequential phosphorylation of nuclear FBXO25 and mitochondrial HAX1 enabling the subsequent ubiquitylation and degradation of HAX1, identifies PRKCD as regulatory kinase that temporally and timely regulates the ubiquitylation of HAX1 as UPS substrate. This specific regulatory mechanism described within the present study provides a hitherto unappreciated way of restricting the ubiquitylation and 26S-proteasomal degradation of a specific substrate to a specific cellular context.

7.2 Disruptions of the PRKCD-FBXO25-HAX1 axis accelerate lymphomagenesis and protect MCL cells from apoptosis

7.2.1 FBXO25 suppresses lymphoma growth and development through HAX1 stabilization in *in vivo* mouse models

So far, the present study unraveled the mechanistic principle of SCF^{FBXO25}-mediated ubiquitylation of the anti-apoptotic molecule HAX1 in a PRKCD-dependent manner. To further evaluate the impact of the newly described PRKCD-FBXO25-HAX1 axis onto the growth of pre-existing lymphoma cells as well as onto the *de novo* development of B-cell lymphomas, the spontaneous Eμ-myc lymphoma mouse model (Eischen, Weber et al. 1999) and a xenotranplantation NOD-SCID model were chosen.

Knock-down of Fbxo25 in Eμ-myc lymphoma-derived cells resulted in a strong increase of Hax1 protein levels and promoted resistance towards paclitaxel induced apoptosis. In contrast, forced expression of Fbxo25 by retroviral transduction decreased cellular Hax1 levels and induced spontaneous apoptosis of infected cells as compared to similarly treated control cells, underlining that the apoptosis promoting function of Fbxo25 was similarly present in lymphoma cells derived from the Eμ-myc mouse model (see 6.5.1). Subsequent injection of described cells into C57BL/6 wildtype mice served to investigate the role of Fbxo25 levels in the growth and survival of pre-existing lymphoma cells. Mice injected with Eμ-myc lymphoma cells transduced to overexpress

Fbxo25 showed a significantly prolonged survival due to decreased proliferation of the injected tumor cells. In contrast, mice receiving tumor cells with knock-down of Fbxo25 survived even shorter than animals receiving the corresponding control cells. In regard to the highly aggressive nature of the used model, the decrease of survival in the shFbxo25 group, compared to control, underlines the pro-proliferative phenotype of a Fbxo25 knock-down that event accelerates lymphoma formation in an already highly aggressive tumor model, even if not in a significant manner. The additional performed analyses of spleen weights of sacrificed mice indices reduced spleen weight of mice reconstituted with Eμ-myc lymphoma cells overexpressing Fbxo25, whereupon knock-down of Fbxo25 in Eμ-myc cells increased the spleen weight of recipient mice as compared to the corresponding control. In line with previous observations, histopathology of mice injected with Eμ-myc lymphoma-cells transduced to overexpress Fbxo25 indicates higher levels of apoptosis as visualized by cleaved caspase 3 and also indicates the B-cell origen of observed lymph node tumors (see chapter 6.5.1). Results obtained from the presented Eμ-myc lymphoma-cell injection approach underline an anti-proliferative or pro-apoptotic role of Fbxo25 onto B-cell populations in spleen and lymph nodes that is in line with the B-cell defective phenotype of *Hax1* knock-out mice (Chao, Parganas et al. 2008).

To investigate the potential impact of Fbxo25 onto *de novo* B-cell lymphomagenesis, irradiated C57BL/6 wildtype mice were transplanted with HSPCs modified in the expression levels of Fbxo25. 28 days post transplantation, engraftment was analyzed by flow cytometric analyses of blood cells and demonstrated an increase of overall and GFP-positive B-cell populations of mice reconstituted with shFbxo25 hematopoietic stem cell progenitor cells as compared to control, underlining the pro-proliferative advantage of B-cells with lower expression levels of Fbxo25. In line with this initial observation made from blood samples derived from both experimental groups, animals reconstituted with shFbxo25 HSPSc showed a significant decrease in survival rates, compared to the shcontrol group, indicating the lymphomagenesis promoting effect of the Fbxo25 knock-down (see chapter 6.5.2). Moreover, immunoblotting analyses of tumors derived from this transplantation model indicated an increase of Hax1 levels and a decrease of spontaneous apoptosis rates in tumors derived from the shFbxo25 experimental group, an observation that was additionally confirmed by histopathological staining of murine tumor samples. Recapitulatory, data derived from injection and transplantation models confirm the apoptosis-promoting, lymphomagenesis-suppressing role of Fbxo25, at least within the murine system.

To further evaluate the effect of modifications of the FBXO25-HAX1 axis in a human lymphoma model, Granta-519 MCL cells were transduced with RNAi directed against FBXO25 or a non-targeting control and subcutaneously injected into NOD-SCID mice. Data derived from this isogenic xenotransplantation model reveal increased metabolic and metric tumor volume and weight of tumors originating from shFBXO25 Granta-519 cells, whereupon the derived tumors

reveal higher levels of the pro-survival molecule HAX1 and a massive decrease of spontaneous apoptosis as visualized by immunoblotting and immunohistochemistry (see chapter 6.5.3). The complementary approach using Granta-519 cells transduced to overexpress the proteasomal non-degradable $HAX1^{S2010A}$ mutant, or control, confirmed the previous mechanistic data on the survival-promoting function of this mutant. Xenotransplants arising from Granta-519 cells with forced expression of $HAX1^{S210A}$ showed a massive increased tumor volume and weight (see chapter 6.5.4), thus underlining the protective role of this mutant towards spontaneous apoptosis of MCL tumor cells.

In summary, the Eμ-myc lymphoma model based approaches as well as the xenotransplantation approach using the human MCL cell line Granta-519 underline the tumor suppressive function of FBXO25 as hypothesized by the previous mechanistic cell culture based experiments. The observed pro-proliferative, apoptosis preventing effects of both knock-down of Fbxo25 and forced expression of the non-degradable variant of HAX1 reinforce the anti-tumor protective role of the regulation of HAX1 levels via SCF^{FBXO25} and are in complete agreement with the published data sets on Hax1 as essential regulator of B-cell survival and proliferation (Chao, Parganas et al. 2008).

7.2.2 FBXO25 and HAX1 regulate the survival of MCL tumor cells

CGH array analyses on primary human MCL patient samples and cell lines indicated a monoallelic deletion of the *FBXO25* gene locus in 29% of MCL patient samples and 33% of screened MCL cell lines (Rubio-Moscardo, Climent et al. 2005). Quantitative PCR analyses and immunoblotting studies of the predicted *FBXO25* monoallelic deleted MCL cell lines JVM-2 and Rec-1 as well as of two non-deleted lines (Granta-519 and Jeko) demonstrated a reduction of approximately 50% of *FBXO25* mRNA correlating with a decrease in FBXO25 protein expression levels (see chapter 6.6.1), thus underlining a potential role of FBXO25 as haploinsufficient tumor suppressor. Additional performed FISH studies confirmed the exclusive monoallelic nature of *FBXO25* deletions as observed by aCGH analyses (Rubio-Moscardo, Climent et al. 2005) and excluded the impact of FBXO25 mRNA instability or transcriptional deregulation on the observed protein levels. When treated with an apoptosis inducing stimulus, the *FBXO25* wildtype cell line Granta-519 showed a clear destabilization of HAX1 and a timely increase of apoptotic markers (see chapter 6.6.1). In contrast, the *FBXO25* monoallelic deleted line Rec-1 showed resistance toward apoptotic stimulation caused by stabilization of the anti-apoptotic molecule HAX1. The observations in this MCL cell line based approaches are in full accord with data previously collected from MEFs with a knock-down of Fbxo25 (compare chapter 6.1.3). Forced expression of

FBXO25 within a *FBXO25* wildtype background (Granta-519 and Jeko MCL cell lines) did neither strongly affect HAX1 protein levels nor induced significant rates of spontaneous apoptosis in these cells, demonstrating that not a FBXO25-deficiency promotes the survival of these MCL cell lines (see chapter 6.6.2). In contrary, re-expression of FBXO25 in the *FBXO25* monoallelic deleted lines JVM-2 and Rec-1 induced a clear decrease in cellular HAX1 protein levels and led to an increase of apoptosis rates, even in the absence of an additional external stimulus. These data indicate that the disruption of the FBXO25-mediated degradation of HAX1 via genomic deletion of *FBXO25* represents the essential survival promoting mechanism within JVM-2 and Rec-1 cells and that reconstitution of a functional FBXO25 protein level completely abrogates the pro-survival advantage of these tumor cells.

PRKCD has previously been described to induce apoptosis (Yoshida 2007). Indeed, forced expression of PRKCD significantly promoted apoptosis in the *FBXO25* non-deleted lines Granta-519 and Jeko (see chapter 6.6.3), whereat HAX1 levels were clearly decreased even in the absence of an additional apoptotic stimulus. In contrast, PRKCD completely failed to induce apoptosis in the *FBXO25* deleted lines JVM-2 and Rec-1 underlining that the pro-apoptotic effect of PRKCD is fully dependent on the presence of a functional FBXO25-mediated degradation of HAX1. Observations from the four tested cell lines were validated in an isogenic approach using the Granta-519 MCL cell line. Knock-down of FBXO25 promoted survival of MCL cells similarly in this isogenic setting, whereupon PRKCD could exert its pro-apoptotic activity only in the presence of normal protein expression levels of FBXO25 (compare chapter 6.6.4). In summary, collected data indicate that disruption of the PRKCD-FBXO25-HAX1 axis, e.g. via the monoallelic deletion of the *FBXO25* gene locus, allows for resistance towards apoptosis and promotes essentially the survival of MCL cell lines. In order to validate the importance of disruptions of the PRKCD-FBXO25-HAX1 axis for human tumorigenesis, primary MCL patient samples were analyzed towards tumor-promoting modifications of *FBXO25* and *HAX1*. Histopathological analyses of three MCL patient cohorts unraveled low expression of FBXO25 in 33.3%, 28.3% and 46.7% (only blastoid variants) of the corresponding MCL patient derived samples. Of note, low FBXO25 expression correlated significantly with an increase of cellular HAX1 levels, as validated by an immunohistochemistry scoring approach. The accumulation of low FBXO25 levels especially in the more aggressive, blastoid variant of MCL underlines the importance of disruptions of the FBXO25-dependent axis for the proliferative phenotype of this entity and is in full agreement with an increase of 8p23.3 deletions in blastoid and leukemic MCL samples as previously published (Martinez-Climent, Vizcarra et al. 2001)(compare chapter 6.7.1). To further exclude a post-translational downregulation of FBXO25 protein expression levels within the screened MCL patient samples, RNA and DNA were extracted from these samples when sufficient material was available. Quantification of *FBXO25* DNA and mRNA using gene and transcript specific primer

pairs for *FBXO25,* revealed reduced *FBXO25* mRNA expression levels in 29.9% and 47.4% of MCL cohorts 2 and 3, an observation that was in full agreement with approximately 50% reduced DNA levels in these samples, thus underling the monoallelic nature of *FBXO25* deletions as observed in aCGH (Rubio-Moscardo, Climent et al. 2005) and FISH studies. Of note, the reduced number of samples represented within the mRNA and DNA quantification analyses (see chapter 6.7.2) is reasoned by a lack of corresponding patient material or the exclusion of samples with polyploide chromosome sets that did not allow an accurate and reproducible analysis of DNA content. Data collected by quantification of mRNA and DNA as well as by immunohistochemistry indicate that *FBXO25* is monoallelically deleted in primary MCL patient samples with deletion rates of approximately 30 percent. Despite the significant correlation of FBXO25 and HAX1 protein levels in immunohistochemistry, some samples showed strongly increased HAX1 expression levels in the presence of normal levels of FBXO25. To unravel the underlying pro-survival mechanism, the *HAX1* gene was sequenced in all available samples of cohorts 1 and 2. Sequence analyses revealed the presence of genomic *HAX1* mutations, leading to amino acid mutations of Ser210 of HAX1 to an alanine, that were not present in constitutional, non-tumor DNA of the corresponding patient (see chapter 6.7.3). Additional performed immunoblotting and immunohistochemistry based approaches supported the results previously collected by quantitative PCR and sequencing studies. *FBXO25* monoallelic deleted MCL samples showed increased protein levels of HAX1 that could secondary observed in samples with the HAX1^{S210A} mutation, leading to a non-degradable form of HAX1 (compare chapter 6.7.4). Of note, *HAX1* mutations and *FBXO25* deletions were mutually exclusive, underlining that one single disruption of the FBXO25-HAX1 degradation axis is sufficient to promote the survival of MCL cells.

In summary, data derived from primary human MCL patient samples confirm the presence of disruptions of the PRKCD-FBXO25-HAX1 axis in primary tumors and underline the hypothesized role of *FBXO25* as novel tumor suppressor gene and the role of *HAX1* as novel proto-oncogene in the context of human B-cell lymphoma.

7.3 HAX1 expression levels regulate the cell surface expression and downstream signaling of CXCR4

Beside its role as potent anti-apoptotic molecule, HAX1 has been described to play an essential role in regulating endocytosis and cell surface expression of receptor molecules involved in the migration of tumor cells (Radhika, Onesime et al. 2004);(Ramsay, Keppler et al. 2007).

Independent of these studies, Peckl-Schmid and colleagues observed a significant loss of the hematopoietic stem cell homing and migration receptor Cxcr4 in the knock-out background of *Hax1* (Peckl-Schmid, Wolkerstorfer et al. 2010). To further validate a potential direct effect of the PRKCD-FBXO25-HAX1 axis onto cell surface expression and downstream signaling of CXCR4, Granta-519 cells transduced to overexpress the non-degradable HAX1^{S210A} variant or an empty vector control, were probed in an immunoblotting assay. Indeed, strong expression of HAX1 resulted in a massive increase of cellular CXCR4 protein levels (see chapter 6.8.1) indicating that elevated HAX1 levels directly mediate an up-regulation of overall CXCR4 protein levels. To next proof a direct association of CXCR4 and HAX1, the interaction of both molecules was tested under untreated condition as well as under treatment with the CXCR4 inhibitor AMD3100/Plerixafor that is clinically used to mobilize hematopoietic stem cell progenitor cells for a later autologous stem cell transplantation based on the internalization of the homing receptor CXCR4 (Cashen, Nervi et al. 2007). In untreated conditions, HAX1 showed interaction with CXCR4, whereupon treatment with AMD3100 abrogated the binding of both molecules, indicating that internalization of CXCR4 might potentially depend on the disruption of the CXCR4 interaction with HAX1 (compare chapter 6.8.1, second part). In contrast to the CXCR4 wildtype, the WHIM-like mutants of CXCR4, known to show highly stable surface expression (Hunter, Xu et al. 2014), did not lose interaction with HAX1 even in the presence of the CXCR4 antagonist AMD3100. These data, together with the previously published finding that CXCR4 endosomal recycling and intracellular trafficking are dependent on its C-terminal tail (Busillo and Benovic 2007), indicate that dissociation of CXCR4 and HAX1 might lead to internalization of CXCR4, a mechanism disrupted through mutation and shortening of the C-terminal part of CXCR4 in the WHIM-like mutants. To further validate the effect of HAX1 levels onto the direct downstream signaling of CXCR4, *Hax1* wildtype and knock-out MEFs were compared according to their activation of Cxcr4 downstream signaling in the presence of the natural Cxcr4 ligand Sdf-1. *Hax1* wildtype MEFs showed a robust activation of phospho-Erk1/2 signaling towards Sdf-1 treatment, whereupon no phospho-Erk1/2 activation could be observed in the *Hax1* knock-out background (compare chapter 6.8.2). These data, in combination with the observation of nearly complete loss of Cxcr4 surface expression in the *Hax1* knock-out model (FACS data not included within the present study), underline Hax1 might be required for functional surface expression of Cxcr4 and might also be functional required for downstream signaling of Cxcr4 via the Erk1/2 pathway. To rescue the effect of the *Hax1* knock-out, Hax1 wildtype was re-expressed in the *Hax1*$^{-/-}$ fibroblasts. The elevation of cellular Hax1 levels induced an increase of Cxcr4 protein levels and led to the activation of phospho-Erk1/2 downstream signaling even in the absence of the Cxcr4-ligand Sdf-1 (see chapter 6.8.2). The results of this approach indicate that loss of Hax1 is sufficient to block the Cxcr4 downstream signaling via the Erk1/2 pathway and that this phenotype can be rescued via the reconstitution of physiological

protein expression levels of Hax1. To further exclude an effect of Hax1 on translation and mRNA stability of Cxcr4, the Cxcr4 mRNA content of *Hax1* wildtype and knock-out MEFs was compared using two different Cxcr4 specific primer pairs. Both primer pairs showed consistently that the mRNA levels of Cxcr4 were even elevated in the *Hax1*$^{-/-}$ system as compared to control, underlining the post-translational downregulation of Cxcr4 expression levels in cells deficient of Hax1 (see chapter 6.8.3).

In line with the data collected for the functionality of the PRKCD-FBXO25-HAX1 in human MCL cell lines and patient samples, the regulation of CXCR4 surface expression and signaling in dependency of HAX1 expression levels should also be validated within the context of human B-cell lymphoma cell lines. SU-DHL-8 cells were transduced with two different shRNA constructs targeting HAX1 or the corresponding control construct. The knock-down of HAX1 directly (day three post infection) led to a decrease of CXCR4 surface expression and correlatively induced a down-regulation of CXCR4 downstream signaling via the ERK1/2 pathways. Of note, only CXCR4 surface expression was affected at this early time point, no alterations of the overall CXCR4 protein expression levels could be observed at day three post infection (compare chapter 6.8.3). At day eight post infection, the down regulation of phospho-ERK1/2 signaling remained stable upon knock-down of HAX1, whereupon the overall CXCR4 levels showed a massive decrease, underlining an acute negative effect of HAX1 loss on the surface stabilization of CXCR4 and a slower, post-translational regulated effect on the overall cellular protein levels of CXCR4. In line with the previously published data on a continuous endocytosis process required for functionality of CXCR4 (Busillo and Benovic 2007), these data indicate that HAX1 might regulate the proper surface expression of CXCR4, whereupon knock-down of HAX1 interfers with the proper endocytosis cycle of CXCR4 and induces subsequently a decrease of overall CXCR4 protein levels. As AMD3100 has been shown to induce the internalization of CXCR4 (Cashen, Nervi et al. 2007) resulting in a comparable loss of surface downregulation of CXCR4 as obtained with a knock-down of HAX1 protein expression, the novel hypothesis raised that high protein levels of HAX1, caused by a monoallelic deletion of *FBXO25*, might lead to an increased resistance towards AMD3100 induced internalization of the chemokine receptor CXCR4. The results obtained from treatment of MCL cell lines without (Jeko and Granta-519) and with monoallelic deletion of *FBXO25* (Rec-1) underlined a clearly detectable loss of CXCR4 surface expression in Jeko and Granta-519 cells, whereupon only a minor effect could be observed in Rec-1 MCL cells (see chapter 6.8.4). Overall collected data within the present study for the first time indicate that HAX1 is an essential molecule in the post-translational regulation of CXCR4 surface expression. Moreover, elevated levels of HAX1, as caused by inhibition of its ubiquitin-proteasomal degradation via SCF^{FBXO25}, elevate CXCR4 surface expression, activate constitutive active downstream signaling of CXCR4 and promote resistance towards AMD3100 induced

internalization of CXCR4 that is required for a proper mobilization of hematopoietic stem cell as required for autologous stem cell transplantation approaches (Larochelle, Krouse et al. 2006).

7.4 Summary

The present study describes a novel pro-apoptotic pathway involving ubiquitin-proteasomal degradation of the anti-apoptotic molecule HAX1 via the previous orphan SCF^{FBXO25} E3-ubiquitin ligase. The degradation process is initiated and spatially and temporally controlled by PRKCD as the regulatory kinase of the ligase as well as its substrate. Moreover, the present study for the first time demonstrates that the previously observed re-distribution of PRKCD to nucleus and mitochondria (Yoshida 2007) serves to target nuclear FBXO25 to mitochondrial HAX1 to mediate its proteasomal degradation, underlining the FBXO25-HAX1 axis as the essential pathway by which PRKCD exerts its previously observed pro-apoptotic activity (DeVries-Seimon, Ohm et al. 2007). Notably, a mouse model with a genetic deletion of *Prkcd* resulted in reduced apoptosis of B-cells and an expansion of the B-lymphocyte compartment (Chao, Parganas et al. 2008), whereupon genomic deletion of *Hax1* resulted in an early death of mice due to an overall loss of lymphocytes (Chao, Parganas et al. 2008). The present work provides with FBXO25 a regulatory hub that integrates the functionally opposing roles of PRKCD and HAX1 and unravels a novel mechanism of how B-cell survival and proliferation are regulated in order to avoid lymphomagenesis. Insight into how deregulation of the PRKCD-FBXO25-HAX1 axis allows tumor cells to evade apoptosis is essential to understand lymphomagenesis and provides insight into potential novel therapeutic target structures. As such, the present study identifies monoallelic deletion of *FBXO25* and phospho-degron mutations of HAX1 in human MCL samples, describing genomic mutations that lead to a circumvention of PRKCD- and FBXO25-mediated degradation of HAX1 and promote lymphoma development *in vivo*.

Independent of its anti-apoptotic role, the present study unravels an essential role of HAX1 in the regulation of the surface expression and downstream signaling of the hematopoietic stem cell homing and migration receptor CXCR4. Loss of HAX1 abrogated CXCR4 activity, whereupon stabilization of HAX1 expression due to genomic deletion of FBXO25 promoted resistance towards the clinical used CXCR4 antagonist AMD3100/Plerixafor (Larochelle, Krouse et al. 2006).

The present study suggests roles of FBXO25 as novel haploinsufficient tumor suppressor and *HAX1* as a novel proto-oncogene. Although disruptions of the PRKCD-FBXO25-HAX1 axis were identified to promote lymphoma development, these alterations may indeed have more extensive implications in other cell and tumor types as underlined by the functionality of these mechanisms in non-hematopoietic cells, e.g. MEFs. Moreover, HAX1 has been shown to be

overexpressed in a variety of hematologic and non-hematologic malignancies (Yap, Koontz et al. 2011);(Kwiecinska, Ottosson-Wadlund et al. 2011);(Li, Tang et al. 2013);(Wei, Li et al. 2014) suggesting alterations of the PRKCD-FBXO25-HAX1 axis as widely spread in variable tumor types. The inhibition of the anti-apoptotic molecules BCL2 and BCL6 has emerged as novel potent therapy approach in the treatment of lymphoma (Souers, Leverson et al. 2013);(Cerchietti, Ghetu et al. 2010). In line with this, data derived from the present study suggest HAX1 as promising therapeutic target structure in the treatment of MCL and other malignancies with *FBXO25* deletions, HAX1 mutations or hyperactivated CXCR4 surface expression and downstream signaling.

8 Outlook

The present study identified the knock-down of Fbxo25/FBXO25 as lymphoma growth promoting and lymphomagenesis supporting factor within the Eμ-myc transgenic mouse model as well as within an isogenic xenograft transplantation model using the Granta-519 MCL cell line. The ongoing construction of a conditional *Fbxo25* knock-out mouse strain should further provide information on whether the loss of *Fbxo25* itself is sufficient to induce lymphomagenesis, even without constitutive active c-Myc as used in the Eμ-myc transgenic mouse model. Moreover, the *Fbxo25*$^{-/-}$ setting could be further used to study the effect of a conditional loss of Fbxo25 gene expression on the constitutive activation of Cxcr4 downstream signaling via stabilization of Hax1 and its potential role in lymphomagenesis.

The stabilization of the pro-survival molecule HAX1 via disruption of the PRKCD-FBXO25 axis has been presented as novel tumor promoting mechanism in MCL, whereupon the functionality of the PRKCD-FBXO25-HAX1 axis has also been shown for divers human and murine cell lines. In line with the observed overexpression of HAX1 in variable hematopoietic and non-hematopoietic tumor entities (Yap, Koontz et al. 2011);(Li, Jiang et al. 2015);(Wei, Li et al. 2014);(Kwiecinska, Ottosson-Wadlund et al. 2011), further studies should provide insight into potential disruptions of the PRKCD-FBXO25-HAX1 axis as central survival providing factor of tumor cells of e.g. colorectal cancer, thus investigating the role of HAX1 as potential novel therapeutic target structure within these entities. Moreover, further studies are needed to characterize HAX1 as regulator of CXCR4 cell surface expression and migration. The present study indeed demonstrates the chemokine receptor CXCR4 as novel interactor of HAX1, an observation that is in line with the previously described interaction of HAX1 with migration-associated integrin receptors (Ramsay, Keppler et al. 2007), whereat the mechanistic background of the CXCR4-HAX1 interaction remains to be demonstrated. Independent from previous data, CXCR4 surface levels have recently been shown to be negative influenced by targeted inhibition of Bruton tyrosine kinase (BTK) by ibrutinib (Chen, Chang et al. 2016), a kinase inhibitor approved for the clinical treatment of MCL and CLL (Wang , Rule et al. 2013);(Byrd , Furman et al. 2013). In this regard, further studies should provide insight into how far HAX1 might be involved in ibrutinib-mediated downregulation of CXCR4 and resistance of WHIM-like CXCR4 mutants towards ibrutinib (Cao, Hunter et al. 2015), providing HAX1 as potential novel target structure to overcome resistance towards BTK inhibition.

9 Literature

Aboumrad, E., A. M. Madec and C. Thivolet (2007). "The CXCR4/CXCL12 (SDF-1) signalling pathway protects non-obese diabetic mouse from autoimmune diabetes." Clin Exp Immunol **148**(3): 432-439.

Adams, J. M., A. W. Harris, C. A. Pinkert, L. M. Corcoran, W. S. Alexander, S. Cory, R. D. Palmiter and R. L. Brinster (1985). "The c-myc oncogene driven by immunoglobulin enhancers induces lymphoid malignancy in transgenic mice." Nature **318**(6046): 533-538.

Al-Maghrebi, M., H. Brule, M. Padkina, C. Allen, W. M. Holmes and Z. E. Zehner (2002). "The 3' untranslated region of human vimentin mRNA interacts with protein complexes containing eEF-1gamma and HAX-1." Nucleic Acids Res **30**(23): 5017-5028.

Alsayed, Y., H. Ngo, J. Runnels, X. Leleu, U. K. Singha, C. M. Pitsillides, J. A. Spencer, T. Kimlinger, J. M. Ghobrial, X. Jia, G. Lu, M. Timm, A. Kumar, D. Cote, I. Veilleux, K. E. Hedin, G. D. Roodman, T. E. Witzig, A. L. Kung, T. Hideshima, K. C. Anderson, C. P. Lin and I. M. Ghobrial (2007). "Mechanisms of regulation of CXCR4/SDF-1 (CXCL12)-dependent migration and homing in multiple myeloma." Blood **109**(7): 2708-2717.

Amerik, A. Y. and M. Hochstrasser (2004). "Mechanism and function of deubiquitinating enzymes." Biochim Biophys Acta **1695**(1-3): 189-207.

Argatoff, L. H., J. M. Connors, R. J. Klasa, D. E. Horsman and R. D. Gascoyne (1997). "Mantle cell lymphoma: a clinicopathologic study of 80 cases." Blood **89**(6): 2067-2078.

Avet-Loiseau, H., R. Garand, F. Gaillard, A. Daviet, M. P. Mellerin, N. Robillard, I. Bouyge, S. Arcot, M. Batzer, P. Talmant, J. L. Harousseau, N. Milpied and R. Bataille (1998). "Detection of t(11;14) using interphase molecular cytogenetics in mantle cell lymphoma and atypical chronic lymphocytic leukemia." Genes Chromosomes Cancer **23**(2): 175-182.

Barekman, C. L., N. S. Aguilera and S. L. Abbondanzo (2001). "Low-grade B-cell lymphoma with coexpression of both CD5 and CD10. A report of 3 cases." Arch Pathol Lab Med **125**(7): 951-953.

Bassermann, F., C. von Klitzing, A. L. Illert, S. Munch, S. W. Morris, M. Pagano, C. Peschel and J. Duyster (2007). "Multisite phosphorylation of nuclear interaction partner of ALK (NIPA) at G2/M involves cyclin B1/Cdk1." J Biol Chem **282**(22): 15965-15972.

Basu, A. and D. Pal (2010). "Two faces of protein kinase Cdelta: the contrasting roles of PKCdelta in cell survival and cell death." ScientificWorldJournal **10**: 2272-2284.

Baumann, U. (2011). Characterization of the SCF-Fbxo25-E3-ubiquitin ligase (Master-Thesis).

Becker, M., B. Tschechne, M. Reeb, U. Schwinger, H. R. Bruch, M. Frank and L. Strassl (2015). "Bendamustine as first-line treatment in patients with advanced indolent non-Hodgkin lymphoma and mantle cell lymphoma in German routine clinical practice." Ann Hematol **94**(9): 1553-1558.

Bejjani, B. A. and L. G. Shaffer (2006). "Application of array-based comparative genomic hybridization to clinical diagnostics." J Mol Diagn **8**(5): 528-533.

Bernard, M., R. Gressin, F. Lefrere, B. Drenou, B. Branger, S. Caulet-Maugendre, P. Tass, N. Brousse, F. Valensi, N. Milpied, L. Voilat, A. Sadoun, C. Ghandour, M. Hunault, R. Leloup, L. Mannone, O. Hermine and T. Lamy (2001). "Blastic variant of mantle cell lymphoma: a rare but highly aggressive subtype." Leukemia **15**(11): 1785-1791.

Bharti, A., S. K. Kraeft, M. Gounder, P. Pandey, S. Jin, Z. M. Yuan, S. P. Lees-Miller, R. Weichselbaum, D. Weaver, L. B. Chen, D. Kufe and S. Kharbanda (1998). "Inactivation of DNA-dependent protein kinase by protein kinase Cdelta: implications for apoptosis." Mol Cell Biol **18**(11): 6719-6728.

Blass, M., I. Kronfeld, G. Kazimirsky, P. M. Blumberg and C. Brodie (2002). "Tyrosine phosphorylation of protein kinase Cdelta is essential for its apoptotic effect in response to etoposide." Mol Cell Biol **22**(1): 182-195.

Blombery, P. A., M. Wall and J. F. Seymour (2015). "The molecular pathogenesis of B-cell non-Hodgkin lymphoma." Eur J Haematol **95**(4): 280-293.

Bodrug, S. E., B. J. Warner, M. L. Bath, G. J. Lindeman, A. W. Harris and J. M. Adams (1994). "Cyclin D1 transgene impedes lymphocyte maturation and collaborates in lymphomagenesis with the myc gene." EMBO J **13**(9): 2124-2130.

Boehm, J. S., J. J. Zhao, J. Yao, S. Y. Kim, R. Firestein, I. F. Dunn, S. K. Sjostrom, L. A. Garraway, S. Weremowicz, A. L. Richardson, H. Greulich, C. J. Stewart, L. A. Mulvey, R. R. Shen, L. Ambrogio, T. Hirozane-Kishikawa, D. E. Hill, M. Vidal, M. Meyerson, J. K. Grenier, G. Hinkle, D. E. Root, T. M. Roberts, E. S. Lander, K. Polyak and W. C. Hahn (2007). "Integrative Genomic Approaches Identify IKBKE as a Breast Cancer Oncogene." Cell **129**(6): 1065-1079.

Boztug, K. and C. Klein (2009). "Novel genetic etiologies of severe congenital neutropenia." Curr Opin Immunol **21**(5): 472-480.

Buckley, S. M., B. Aranda-Orgilles, A. Strikoudis, E. Apostolou, E. Loizou, K. Moran-Crusio, C. L. Farnsworth, A. A. Koller, R. Dasgupta, J. C. Silva, M. Stadtfeld, K. Hochedlinger, E. I. Chen and I. Aifantis (2012). "Regulation of pluripotency and cellular reprogramming by the ubiquitin-proteasome system." Cell Stem Cell **11**(6): 783-798.

Budczies, J., F. Klauschen, B. V. Sinn, B. Győrffy, W. D. Schmitt, S. Darb-Esfahani and C. Denkert (2012). "Cutoff Finder: A Comprehensive and Straightforward Web Application Enabling Rapid Biomarker Cutoff Optimization." PLoS ONE **7**(12): e51862.

Burnette, W. N. (1981). ""“Western Blotting”: Electrophoretic transfer of proteins from sodium dodecyl sulfate-polyacrylamide gels to unmodified nitrocellulose and radiographic detection with antibody and radioiodinated protein A." Analytical Biochemistry **112**(2): 195-203.

Busillo, J. M. and J. L. Benovic (2007). "Regulation of CXCR4 signaling." Biochim Biophys Acta **1768**(4): 952-963.

Byrd , J. C., R. R. Furman , S. E. Coutre , I. W. Flinn , J. A. Burger , K. A. Blum , B. Grant , J. P. Sharman , M. Coleman , W. G. Wierda , J. A. Jones , W. Zhao , N. A. Heerema , A. J. Johnson , J. Sukbuntherng , B. Y. Chang , F. Clow , E. Hedrick , J. J. Buggy , D. F. James and S. O'Brien (2013). "Targeting BTK with Ibrutinib in Relapsed Chronic Lymphocytic Leukemia." New England Journal of Medicine **369**(1): 32-42.

Camacho, E., L. Hernandez, S. Hernandez, F. Tort, B. Bellosillo, S. Bea, F. Bosch, E. Montserrat, A. Cardesa, P. L. Fernandez and E. Campo (2002). "ATM gene inactivation in mantle cell lymphoma mainly occurs by truncating mutations and missense mutations involving the phosphatidylinositol-3 kinase domain and is associated with increasing numbers of chromosomal imbalances." Blood **99**(1): 238-244.

Cao, Y., Z. R. Hunter, X. Liu, L. Xu, G. Yang, J. Chen, C. J. Patterson, N. Tsakmaklis, S. Kanan, S. Rodig, J. J. Castillo and S. P. Treon (2015). "The WHIM-like CXCR4(S338X) somatic mutation activates AKT and ERK, and promotes resistance to ibrutinib and other agents used in the treatment of Waldenstrom's Macroglobulinemia." Leukemia **29**(1): 169-176.

Cardozo, T. and M. Pagano (2004). "The SCF ubiquitin ligase: insights into a molecular machine." Nat Rev Mol Cell Biol **5**(9): 739-751.

Carlsson, G., A. A. Aprikyan, R. Tehranchi, D. C. Dale, A. Porwit, E. Hellstrom-Lindberg, J. Palmblad, J. I. Henter and B. Fadeel (2004). "Kostmann syndrome: severe congenital neutropenia associated with defective expression of Bcl-2, constitutive mitochondrial release of cytochrome c, and excessive apoptosis of myeloid progenitor cells." Blood **103**(9): 3355-3361.

Carlsson, G., I. van't Hooft, M. Melin, M. Entesarian, E. Laurencikas, I. Nennesmo, A. Trebinska, E. Grzybowska, J. Palmblad, N. Dahl, M. Nordenskjold, B. Fadeel and J. I. Henter (2008). "Central nervous system involvement in severe congenital neutropenia: neurological and neuropsychological abnormalities associated with specific HAX1 mutations." J Intern Med **264**(4): 388-400.

Casciola-Rosen, L., M. Garcia-Calvo, H. G. Bull, J. W. Becker, T. Hines, N. A. Thornberry and A. Rosen (2007). "Mouse and human granzyme B have distinct tetrapeptide specificities and abilities to recruit the bid pathway." J Biol Chem **282**(7): 4545-4552.

Cashen, A. F., B. Nervi and J. DiPersio (2007). "AMD3100: CXCR4 antagonist and rapid stem cell-mobilizing agent." Future Oncol **3**(1): 19-27.

Cenciarelli, C., D. S. Chiaur, D. Guardavaccaro, W. Parks, M. Vidal and M. Pagano (1999). "Identification of a family of human F-box proteins." Curr Biol **9**(20): 1177-1179.

Cepko, C. and W. Pear (2001). Overview of the Retrovirus Transduction System. Current Protocols in Molecular Biology, John Wiley & Sons, Inc.

Cerchietti, L. C., A. F. Ghetu, X. Zhu, G. F. Da Silva, Z. Shijun, M. Matthews, K. L. Bunting, J. M. Polo, C. Farès, C. H. Arrowsmith, S. N. Yang, M. Garcia, A. Coop, A. D. MacKerell, G. G. Privé and A. Melnick (2010). "A small molecule inhibitor of BCL6 kills DLBCL cells in vitro and in vivo." Cancer cell **17**(4): 400-411.

Chao, J. R., E. Parganas, K. Boyd, C. Y. Hong, J. T. Opferman and J. N. Ihle (2008). "Hax1-mediated processing of HtrA2 by Parl allows survival of lymphocytes and neurons." Nature **452**(7183): 98-102.

Cheah, C. Y., J. F. Seymour and M. L. Wang (2016). "Mantle Cell Lymphoma." J Clin Oncol **34**(11): 1256-1269.

Chen, S. S., B. Y. Chang, S. Chang, T. Tong, S. Ham, B. Sherry, J. A. Burger, K. R. Rai and N. Chiorazzi (2016). "BTK inhibition results in impaired CXCR4 chemokine receptor surface expression, signaling and function in chronic lymphocytic leukemia." Leukemia **30**(4): 833-843.

Cheung, K. J., S. P. Shah, C. Steidl, N. Johnson, T. Relander, A. Telenius, B. Lai, K. P. Murphy, W. Lam, A. J. Al-Tourah, J. M. Connors, R. T. Ng, R. D. Gascoyne and D. E. Horsman (2009). "Genome-wide profiling of follicular lymphoma by array comparative genomic hybridization reveals prognostically significant DNA copy number imbalances." Blood **113**(1): 137-148.

Ciechanover, A. (2005). "N-terminal ubiquitination." Methods Mol Biol **301**: 255-270.

Ciechanover, A. (2006). "The ubiquitin proteolytic system: from a vague idea, through basic mechanisms, and onto human diseases and drug targeting." Neurology **66**(2 Suppl 1): S7-19.

Ciechanover, A., A. Orian and A. L. Schwartz (2000). "Ubiquitin-mediated proteolysis: biological regulation via destruction." Bioessays **22**(5): 442-451.

Cilenti, L., M. M. Soundarapandian, G. A. Kyriazis, V. Stratico, S. Singh, S. Gupta, J. V. Bonventre, E. S. Alnemri and A. S. Zervos (2004). "Regulation of HAX-1 anti-apoptotic protein by Omi/HtrA2 protease during cell death." J Biol Chem **279**(48): 50295-50301.

Cinar, M., F. Hamedani, Z. Mo, B. Cinar, H. M. Amin and S. Alkan (2013). "Bruton tyrosine kinase is commonly overexpressed in mantle cell lymphoma and its attenuation by Ibrutinib induces apoptosis." Leuk Res **37**(10): 1271-1277.

Clague, M. J. and S. Urbe (2010). "Ubiquitin: same molecule, different degradation pathways." Cell **143**(5): 682-685.

Cleary, M. L., S. D. Smith and J. Sklar (1986). "Cloning and structural analysis of cDNAs for bcl-2 and a hybrid bcl-2/immunoglobulin transcript resulting from the t(14;18) translocation." Cell **47**(1): 19-28.

Cross, T., G. Griffiths, E. Deacon, R. Sallis, M. Gough, D. Watters and J. M. Lord (2000). "PKC-delta is an apoptotic lamin kinase." Oncogene **19**(19): 2331-2337.

Dal Col, J., P. Zancai, L. Terrin, M. Guidoboni, M. Ponzoni, A. Pavan, M. Spina, S. Bergamin, S. Rizzo, U. Tirelli, A. De Rossi, C. Doglioni and R. Dolcetti (2008). "Distinct functional significance of Akt and mTOR constitutive activation in mantle cell lymphoma." Blood **111**(10): 5142-5151.

Dang, Chi V. (2012). "MYC on the Path to Cancer." Cell **149**(1): 22-35.

Darken, M. A. (1964). "PUROMYCIN INHIBITION OF PROTEIN SYNTHESIS." Pharmacol Rev **16**: 223-243.

Davis, H. E., M. Rosinski, J. R. Morgan and M. L. Yarmush (2004). "Charged Polymers Modulate Retrovirus Transduction via Membrane Charge Neutralization and Virus Aggregation." Biophysical Journal **86**(2): 1234-1242.

Desai, M., K. Newberry, Z. Ou, M. Wang and L. Zhang (2014). "Lenalidomide in relapsed or refractory mantle cell lymphoma: overview and perspective." Therapeutic Advances in Hematology **5**(3): 91-101.

DeVries-Seimon, T. A., A. M. Ohm, M. J. Humphries and M. E. Reyland (2007). "Induction of apoptosis is driven by nuclear retention of protein kinase C delta." J Biol Chem **282**(31): 22307-22314.

Di Noia, J. and M. S. Neuberger (2002). "Altering the pathway of immunoglobulin hypermutation by inhibiting uracil-DNA glycosylase." Nature **419**(6902): 43-48.

Dickins, R. A., M. T. Hemann, J. T. Zilfou, D. R. Simpson, I. Ibarra, G. J. Hannon and S. W. Lowe (2005). "Probing tumor phenotypes using stable and regulated synthetic microRNA precursors." Nat Genet **37**(11): 1289-1295.

Dimitrova, N., Y.-C. M. Chen, D. L. Spector and T. de Lange (2008). "53BP1 promotes NHEJ of telomeres by increasing chromatin mobility." Nature **456**(7221): 524-528.

Dimopoulos, M. A., S. Delimpasi, E. Katodritou, A. Vassou, M. C. Kyrtsonis, P. Repousis, Z. Kartasis, A. Parcharidou, M. Michael, E. Michalis, D. Gika, A. Symeonidis, A. Pouli, K. Konstantopoulos, E. Terpos and E. Kastritis (2014). "Significant improvement in the survival of patients with multiple myeloma presenting with severe renal impairment after the introduction of novel agents." Ann Oncol **25**(1): 195-200.

Dominguez, D., B. Montserrat-Sentis, A. Virgos-Soler, S. Guaita, J. Grueso, M. Porta, I. Puig, J. Baulida, C. Franci and A. Garcia de Herreros (2003). "Phosphorylation regulates the subcellular location and activity of the snail transcriptional repressor." Mol Cell Biol **23**(14): 5078-5089.

Dreyling, M. (2011). "Therapy of mantle cell lymphoma: new treatment options in an old disease or vice versa?" Semin Hematol **48**(3): 145-147.

Dreyling, M. and S. Ferrero (2016). "The role of targeted treatment in mantle cell lymphoma: is transplant dead or alive?" Haematologica **101**(2): 104-114.

Dreyling, M., H. C. Kluin-Nelemans, S. Bea, E. Hartmann, I. Salaverria, G. Hutter, P. Perez-Galan, G. Roue, C. Pott, S. Le Gouill, S. Cortelazzo, S. Rule, G. Hess, F. Zaja, U. Vitolo, M. Szymczyk, J. Walewski, V. Ribrag, M. Unterhalt, O. Hermine and E. Hoster (2011). "Update on the molecular pathogenesis and clinical treatment of mantle cell lymphoma: report of the 10th annual conference of the European Mantle Cell Lymphoma Network." Leuk Lymphoma **52**(12): 2226-2236.

Duan, H., H. Xiang, L. Ma and L. M. Boxer (2008). "Functional long-range interactions of the IgH 3' enhancers with the bcl-2 promoter region in t(14;18) lymphoma cells." Oncogene **27**(53): 6720-6728.

Duan, S., L. Cermak, J. K. Pagan, M. Rossi, C. Martinengo, P. F. di Celle, B. Chapuy, M. Shipp, R. Chiarle and M. Pagano (2012). "FBXO11 targets BCL6 for degradation and is inactivated in diffuse large B-cell lymphomas." Nature **481**(7379): 90-93.

Eastman, Q. M., T. M. Leu and D. G. Schatz (1996). "Initiation of V(D)J recombination in vitro obeying the 12/23 rule." Nature **380**(6569): 85-88.

Eichner, R., M. Heider, V. Fernandez-Saiz, F. van Bebber, A. K. Garz, S. Lemeer, M. Rudelius, B. S. Targosz, L. Jacobs, A. M. Knorn, J. Slawska, U. Platzbecker, U. Germing, C. Langer, S. Knop, H. Einsele, C. Peschel, C. Haass, U. Keller, B. Schmid, K. S. Gotze, B. Kuster and F. Bassermann (2016). "Immunomodulatory drugs disrupt the cereblon-CD147-MCT1 axis to exert antitumor activity and teratogenicity." Nat Med.

Eischen, C. M., J. D. Weber, M. F. Roussel, C. J. Sherr and J. L. Cleveland (1999). "Disruption of the ARF-Mdm2-p53 tumor suppressor pathway in Myc-induced lymphomagenesis." Genes Dev **13**(20): 2658-2669.

Fadeel, B. and E. Grzybowska (2009). "HAX-1: a multifunctional protein with emerging roles in human disease." Biochim Biophys Acta **1790**(10): 1139-1148.

Fadeel, B. and S. Orrenius (2005). "Apoptosis: a basic biological phenomenon with wide-ranging implications in human disease." Journal of Internal Medicine **258**(6): 479-517.

Fadeel, B., A. Ottosson and S. Pervaiz (2008). "Big wheel keeps on turning: apoptosome regulation and its role in chemoresistance." Cell Death Differ **15**(3): 443-452.

Felgner, P. L., T. R. Gadek, M. Holm, R. Roman, H. W. Chan, M. Wenz, J. P. Northrop, G. M. Ringold and M. Danielsen (1987). "Lipofection: a highly efficient, lipid-mediated DNA-transfection procedure." Proc Natl Acad Sci U S A **84**(21): 7413-7417.

Fernandez-Saiz, V., B. S. Targosz, S. Lemeer, R. Eichner, C. Langer, L. Bullinger, C. Reiter, J. Slotta-Huspenina, S. Schroeder, A. M. Knorn, J. Kurutz, C. Peschel, M. Pagano, B. Kuster and F. Bassermann (2013). "SCFFbxo9 and CK2 direct the cellular response to growth factor withdrawal via Tel2/Tti1 degradation and promote survival in multiple myeloma." Nat Cell Biol **15**(1): 72-81.

Ferrando, A. A. (2013). "SOX11 is a mantle cell lymphoma oncogene." Blood **121**(12): 2169-2170.

Fisher, R. I. (1996). "Mantle-cell lymphoma: classification and therapeutic implications." Ann Oncol **7 Suppl 6**: S35-39.

Flordal Thelander, E., K. Ichimura, V. P. Collins, S. H. Walsh, G. Barbany, A. Hagberg, A. Laurell, R. Rosenquist, C. Larsson and S. Lagercrantz (2007). "Detailed assessment of copy number alterations revealing homozygous deletions in 1p and 13q in mantle cell lymphoma." Leuk Res **31**(9): 1219-1230.

Franke, T. F., C. P. Hornik, L. Segev, G. A. Shostak and C. Sugimoto (2003). "PI3K/Akt and apoptosis: size matters." Oncogene **22**(56): 8983-8998.

Freedman, D. A., L. Wu and A. J. Levine (1999). "Functions of the MDM2 oncoprotein." Cell Mol Life Sci **55**(1): 96-107.

Frescas, D. and M. Pagano (2008). "Deregulated proteolysis by the F-box proteins SKP2 and beta-TrCP: tipping the scales of cancer." Nat Rev Cancer **8**(6): 438-449.

Fridman, J. S. and S. W. Lowe (2003). "Control of apoptosis by p53." Oncogene **22**(56): 9030-9040.

Galimberti, S. and M. Petrini (2010). "Temsirolimus in the treatment of relapsed and/or refractory mantle cell lymphoma." Cancer Manag Res **2**: 181-189.

Gallagher, A. R., A. Cedzich, N. Gretz, S. Somlo and R. Witzgall (2000). "The polycystic kidney disease protein PKD2 interacts with Hax-1, a protein associated with the actin cytoskeleton." Proc Natl Acad Sci U S A **97**(8): 4017-4022.

Germeshausen, M., M. Grudzien, C. Zeidler, H. Abdollahpour, S. Yetgin, N. Rezaei, M. Ballmaier, B. Grimbacher, K. Welte and C. Klein (2008). "Novel HAX1 mutations in patients with severe congenital neutropenia reveal isoform-dependent genotype-phenotype associations." Blood **111**(10): 4954-4957.

Gloeckner, C. J., K. Boldt, A. Schumacher, R. Roepman and M. Ueffing (2007). "A novel tandem affinity purification strategy for the efficient isolation and characterisation of native protein complexes." PROTEOMICS **7**(23): 4228-4234.

Gomathinayagam, R., J. Muralidharan, J. H. Ha, L. Varadarajalu and D. N. Dhanasekaran (2014). "Hax-1 is required for Rac1-Cortactin interaction and ovarian carcinoma cell migration." Genes Cancer **5**(3-4): 84-99.

Gopal, A. K., J. G. Rajendran, S. H. Petersdorf, D. G. Maloney, J. F. Eary, B. L. Wood, T. A. Gooley, S. A. Bush, L. D. Durack, P. J. Martin, D. C. Matthews, F. R. Appelbaum, I. D. Bernstein and O. W. Press (2002). "High-dose chemo-radioimmunotherapy with autologous stem cell support for relapsed mantle cell lymphoma." Blood **99**(9): 3158-3162.

Görlich, D., S. Kostka, R. Kraft, C. Dingwall, R. A. Laskey, E. Hartmann and S. Prehn (1995). "Two different subunits of importin cooperate to recognize nuclear localization signals and bind them to the nuclear envelope." Current Biology **5**(4): 383-392.

Greiner, T. C., M. J. Moynihan, W. C. Chan, D. M. Lytle, A. Pedersen, J. R. Anderson and D. D. Weisenburger (1996). "p53 mutations in mantle cell lymphoma are associated with variant cytology and predict a poor prognosis." Blood **87**(10): 4302-4310.

Griner, E. M. and M. G. Kazanietz (2007). "Protein kinase C and other diacylglycerol effectors in cancer." Nat Rev Cancer **7**(4): 281-294.

Grzybowska, E. A., V. Zayat, R. Konopinski, A. Trebinska, M. Szwarc, E. Sarnowska, E. Macech, J. Korczynski, A. Knapp and J. A. Siedlecki (2013). "HAX-1 is a nucleocytoplasmic shuttling protein with a possible role in mRNA processing." FEBS J **280**(1): 256-272.

Hagens, O., E. Minina, S. Schweiger, H.-H. Ropers and V. Kalscheuer (2006). "Characterization of FBX25, encoding a novel brain-expressed F-box protein." Biochimica et Biophysica Acta (BBA) - General Subjects **1760**(1): 110-118.

Halldorsdottir, A. M., A. Lundin, F. Murray, L. Mansouri, S. Knuutila, C. Sundstrom, A. Laurell, H. Ehrencrona, B. Sander and R. Rosenquist (2011). "Impact of TP53 mutation and 17p deletion in mantle cell lymphoma." Leukemia **25**(12): 1904-1908.

Han, J., L. A. Goldstein, W. Hou, C. J. Froelich, S. C. Watkins and H. Rabinowich (2010). "Deregulation of mitochondrial membrane potential by mitochondrial insertion of granzyme B and direct Hax-1 cleavage." J Biol Chem **285**(29): 22461-22472.

Han, Y., Y. S. Chen, Z. Liu, N. Bodyak, D. Rigor, E. Bisping, W. T. Pu and P. M. Kang (2006). "Overexpression of HAX-1 protects cardiac myocytes from apoptosis through caspase-9 inhibition." Circ Res **99**(4): 415-423.

Hansen, L. H., S. Knudsen and S. J. Sorensen (1998). "The effect of the lacY gene on the induction of IPTG inducible promoters, studied in Escherichia coli and Pseudomonas fluorescens." Curr Microbiol **36**(6): 341-347.
Harper, S. and D. W. Speicher (2011). "Purification of proteins fused to glutathione S-tranferase." Methods in molecular biology (Clifton, N.J.) **681**: 259-280.

Harris, A. W. (1988). "The E mu-myc transgenic mouse. A model for high-incidence spontaneous lymphoma and leukemia of early B cells." The Journal of Experimental Medicine **167**(2): 353-371.

Harris, N. L., E. S. Jaffe, H. Stein, P. M. Banks, J. K. Chan, M. L. Cleary, G. Delsol, C. De Wolf-Peeters, B. Falini, K. C. Gatter and et al. (1994). "A revised European-American classification of lymphoid neoplasms: a proposal from the International Lymphoma Study Group." Blood **84**(5): 1361-1392.

Heo, J., R. Eki and T. Abbas (2016). "Deregulation of F-box proteins and its consequence on cancer development, progression and metastasis." Semin Cancer Biol **36**: 33-51.

Hernandez, L., S. Bea, M. Pinyol, G. Ott, T. Katzenberger, A. Rosenwald, F. Bosch, A. Lopez-Guillermo, J. Delabie, D. Colomer, E. Montserrat and E. Campo (2005). "CDK4 and MDM2 gene alterations mainly occur in highly proliferative and aggressive mantle cell lymphomas with wild-type INK4a/ARF locus." Cancer Res **65**(6): 2199-2206.

Hernandez, P. A., R. J. Gorlin, J. N. Lukens, S. Taniuchi, J. Bohinjec, F. Francois, M. E. Klotman and G. A. Diaz (2003). "Mutations in the chemokine receptor gene CXCR4 are associated with WHIM syndrome, a combined immunodeficiency disease." Nat Genet **34**(1): 70-74.

Hershko, A. and A. Ciechanover (1998). "The ubiquitin system." Annu Rev Biochem **67**: 425-479.

Hopp, T. P., K. S. Prickett, V. L. Price, R. T. Libby, C. J. March, D. Pat Cerretti, D. L. Urdal and P. J. Conlon (1988). "A Short Polypeptide Marker Sequence Useful for Recombinant Protein Identification and Purification." Nat Biotech **6**(10): 1204-1210.

Hoster, E., M. Dreyling, W. Klapper, C. Gisselbrecht, A. van Hoof, H. C. Kluin-Nelemans, M. Pfreundschuh, M. Reiser, B. Metzner, H. Einsele, N. Peter, W. Jung, B. Wormann, W. D. Ludwig, U. Duhrsen, H. Eimermacher, H. Wandt, J. Hasford, W. Hiddemann and M. Unterhalt (2008). "A new prognostic index (MIPI) for patients with advanced-stage mantle cell lymphoma." Blood **111**(2): 558-565.

Humphries, M. J., K. H. Limesand, J. C. Schneider, K. I. Nakayama, S. M. Anderson and M. E. Reyland (2006). "Suppression of apoptosis in the protein kinase Cdelta null mouse in vivo." J Biol Chem **281**(14): 9728-9737.
Humphries, M. J., A. M. Ohm, J. Schaack, T. S. Adwan and M. E. Reyland (2008). "Tyrosine phosphorylation regulates nuclear translocation of PKCdelta." Oncogene **27**(21): 3045-3053.

Hunter, Z. R., L. Xu, G. Yang, Y. Zhou, X. Liu, Y. Cao, R. J. Manning, C. Tripsas, C. J. Patterson, P. Sheehy and S. P. Treon (2014). "The genomic landscape of Waldenstrom macroglobulinemia is characterized by highly recurring MYD88 and WHIM-like CXCR4 mutations, and small somatic deletions associated with B-cell lymphomagenesis." Blood **123**(11): 1637-1646.

Iqbal, J., W. G. Sanger, D. E. Horsman, A. Rosenwald, D. L. Pickering, B. Dave, S. Dave, L. Xiao, K. Cao, Q. Zhu, S. Sherman, C. P. Hans, D. D. Weisenburger, T. C. Greiner, R. D. Gascoyne, G. Ott, H. K. Muller-Hermelink, J. Delabie, R. M. Braziel, E. S. Jaffe, E. Campo, J. C. Lynch, J. M. Connors, J. M. Vose, J. O. Armitage, T. M. Grogan, L. M. Staudt and W. C. Chan (2004). "BCL2 translocation defines a unique tumor subset within the germinal center B-cell-like diffuse large B-cell lymphoma." Am J Pathol **165**(1): 159-166.

Jackson, D. N. and D. A. Foster (2004). "The enigmatic protein kinase Cdelta: complex roles in cell proliferation and survival." FASEB J **18**(6): 627-636.

Jang, J. W., W. Y. Lee, J. H. Lee, S. H. Moon, C. H. Kim and H. M. Chung (2011). "A novel Fbxo25 acts as an E3 ligase for destructing cardiac specific transcription factors." Biochem Biophys Res Commun **410**(2): 183-188.

Jares, P. and E. Campo (2008). "Advances in the understanding of mantle cell lymphoma." Br J Haematol **142**(2): 149-165.

Jares, P., D. Colomer and E. Campo (2007). "Genetic and molecular pathogenesis of mantle cell lymphoma: perspectives for new targeted therapeutics." Nat Rev Cancer **7**(10): 750-762.

Jares, P., D. Colomer and E. Campo (2012). "Molecular pathogenesis of mantle cell lymphoma." J Clin Invest **122**(10): 3416-3423.

Jeong, H. S., E. S. Jung, Y. J. Sim, S. J. Kim, J. W. Jang, K. S. Hong, W. Y. Lee, H. M. Chung, K. T. Park, Y. S. Jung, C. H. Kim and K. S. Kim (2015). "Fbxo25 controls Tbx5 and Nkx2-5 transcriptional activity to regulate cardiomyocyte development." Biochim Biophys Acta **1849**(6): 709-721.

Jin, J., T. Cardozo, R. C. Lovering, S. J. Elledge, M. Pagano and J. W. Harper (2004). "Systematic analysis and nomenclature of mammalian F-box proteins." Genes Dev **18**(21): 2573-2580.

Jordan, M. A., K. Wendell, S. Gardiner, W. B. Derry, H. Copp and L. Wilson (1996). "Mitotic block induced in HeLa cells by low concentrations of paclitaxel (Taxol) results in abnormal mitotic exit and apoptotic cell death." Cancer Res **56**(4): 816-825.

Juvekar, A., S. Manna, S. Ramaswami, T. P. Chang, H. Y. Vu, C. C. Ghosh, M. Y. Celiker and I. Vancurova (2011). "Bortezomib induces nuclear translocation of IkappaBalpha resulting in gene-specific suppression of NF-kappaB--dependent transcription and induction of apoptosis in CTCL." Mol Cancer Res **9**(2): 183-194.

Kaboord, B. and M. Perr (2008). "Isolation of proteins and protein complexes by immunoprecipitation." Methods Mol Biol **424**: 349-364.

Kamitani, T., K. Kito, H. P. Nguyen and E. T. H. Yeh (1997). "Characterization of NEDD8, a Developmentally Down-regulated Ubiquitin-like Protein." Journal of Biological Chemistry **272**(45): 28557-28562.

Kang, Y. J., M. Jang, Y. K. Park, S. Kang, K. H. Bae, S. Cho, C. K. Lee, B. C. Park, S. W. Chi and S. G. Park (2010). "Molecular interaction between HAX-1 and XIAP inhibits apoptosis." Biochem Biophys Res Commun **393**(4): 794-799.

Kaplan, E. L. and P. Meier (1958). "Nonparametric estimation from incomplete observation." J. Amer. Statist. Assn **53**: 457-481.

Kim, E. S. and S. Dhillon (2015). "Ibrutinib: a review of its use in patients with mantle cell lymphoma or chronic lymphocytic leukaemia." Drugs **75**(7): 769-776.

King, D., J. Ramachandra and D. Yeomanson (2014). "Lymphadenopathy in children: refer or reassure?" Arch Dis Child Educ Pract Ed **99**(3): 101-110.

Kingston, R. E., C. A. Chen and H. Okayama (2003). "Calcium phosphate transfection." Curr Protoc Cell Biol **Chapter 20**: Unit 20 23.

Kipreos, E. T. and M. Pagano (2000). "The F-box protein family." Genome Biol **1**(5): REVIEWS3002.

Kitagawa, K. and M. Kitagawa (2016). "The SCF-type E3 Ubiquitin Ligases as Cancer Targets." Curr Cancer Drug Targets **16**(2): 119-129.

Klein, C. (2011). "Genetic defects in severe congenital neutropenia: emerging insights into life and death of human neutrophil granulocytes." Annu Rev Immunol **29**: 399-413.

Klein, C., M. Grudzien, G. Appaswamy, M. Germeshausen, I. Sandrock, A. A. Schaffer, C. Rathinam, K. Boztug, B. Schwinzer, N. Rezaei, G. Bohn, M. Melin, G. Carlsson, B. Fadeel, N. Dahl, J. Palmblad, J. I. Henter,

C. Zeidler, B. Grimbacher and K. Welte (2007). "HAX1 deficiency causes autosomal recessive severe congenital neutropenia (Kostmann disease)." Nat Genet **39**(1): 86-92.

Komander, D. and M. Rape (2012). "The ubiquitin code." Annu Rev Biochem **81**: 203-229.

Kraus, J. A., D. J. Dabbs, S. Beriwal and R. Bhargava (2012). "Semi-quantitative immunohistochemical assay versus oncotype DX[reg] qRT-PCR assay for estrogen and progesterone receptors: an independent quality assurance study." Mod Pathol **25**(6): 869-876.

Kurtova, A. V., A. T. Tamayo, R. J. Ford and J. A. Burger (2009). "Mantle cell lymphoma cells express high levels of CXCR4, CXCR5, and VLA-4 (CD49d): importance for interactions with the stromal microenvironment and specific targeting." Blood **113**(19): 4604-4613.

Kwiecinska, A., A. Ottosson-Wadlund, R. Ceder, R. C. Grafstrom, E. Bjorck, M. Nordenskjold, A. Porwit and B. Fadeel (2011). "HAX-1 expression in human B lymphoma." Leukemia **25**(5): 868-872.

la Cour, T., L. Kiemer, A. Molgaard, R. Gupta, K. Skriver and S. Brunak (2004). "Analysis and prediction of leucine-rich nuclear export signals." Protein Eng Des Sel **17**(6): 527-536.

Laemmli, U. K. (1970). "Cleavage of Structural Proteins during the Assembly of the Head of Bacteriophage T4." Nature **227**(5259): 680-685.

Lam, A. K., A. Galione, F. A. Lai and S. Zissimopoulos (2013). "Hax-1 identified as a two-pore channel (TPC)-binding protein." FEBS Lett **587**(23): 3782-3786.

Langdon, W. Y., A. W. Harris, S. Cory and J. M. Adams (1986). "The c-myc oncogene perturbs B lymphocyte development in Eμ-myc transgenic mice." Cell **47**(1): 11-18.

Lange, A., R. E. Mills, C. J. Lange, M. Stewart, S. E. Devine and A. H. Corbett (2007). "Classical Nuclear Localization Signals: Definition, Function, and Interaction with Importin α." Journal of Biological Chemistry **282**(8): 5101-5105.

Larochelle, A., A. Krouse, M. Metzger, D. Orlic, R. E. Donahue, S. Fricker, G. Bridger, C. E. Dunbar and P. Hematti (2006). "AMD3100 mobilizes hematopoietic stem cells with long-term repopulating capacity in nonhuman primates." Blood **107**(9): 3772-3778.

Latres, E., R. Chiarle, B. A. Schulman, N. P. Pavletich, A. Pellicer, G. Inghirami and M. Pagano (2001). "Role of the F-box protein Skp2 in lymphomagenesis." Proc Natl Acad Sci U S A **98**(5): 2515-2520.

Lee, A. Y., Y. Lee, Y. K. Park, K. H. Bae, S. Cho, H. Lee do, B. C. Park, S. Kang and S. G. Park (2008). "HS 1-associated protein X-1 is cleaved by caspase-3 during apoptosis." Mol Cells **25**(1): 86-90.

Lee, J. H. and T. T. Paull (2007). "Activation and regulation of ATM kinase activity in response to DNA double-strand breaks." Oncogene **26**(56): 7741-7748.

Leibersperger, H., M. Gschwendt, M. Gernold and F. Marks (1991). "Immunological demonstration of a calcium-unresponsive protein kinase C of the delta-type in different species and murine tissues. Predominance in epidermis." J Biol Chem **266**(22): 14778-14784.

Leitges, M., M. Mayr, U. Braun, U. Mayr, C. Li, G. Pfister, N. Ghaffari-Tabrizi, G. Baier, Y. Hu and Q. Xu (2001). "Exacerbated vein graft arteriosclerosis in protein kinase Cδ–null mice." The Journal of Clinical Investigation **108**(10): 1505-1512.

Li, B., Q. Hu, H. Wang, N. Man, H. Ren, L. Wen, N. Nukina, E. Fei and G. Wang (2010). "Omi/HtrA2 is a positive regulator of autophagy that facilitates the degradation of mutant proteins involved in neurodegenerative diseases." Cell Death Differ **17**(11): 1773-1784.

Li, B., Q. Hu, R. Xu, H. Ren, E. Fei, D. Chen and G. Wang (2012). "Hax-1 is rapidly degraded by the proteasome dependent on its PEST sequence." BMC Cell Biol **13**: 20.

Li, H., W. L. Thorstad, K. J. Biehl, R. Laforest, Y. Su, K. I. Shoghi, E. D. Donnelly, D. A. Low and W. Lu (2008). "A novel PET tumor delineation method based on adaptive region-growing and dual-front active contours." Medical Physics **35**(8): 3711-3721.

Li, M., Y. Tang, W. Zang, X. Xuan, N. Wang, Y. Ma, Y. Wang, Z. Dong and G. Zhao (2013). "Analysis of HAX-1 gene expression in esophageal squamous cell carcinoma." Diagn Pathol **8**: 47.

Li, W., M. H. Bengtson, A. Ulbrich, A. Matsuda, V. A. Reddy, A. Orth, S. K. Chanda, S. Batalov and C. A. Joazeiro (2008). "Genome-wide and functional annotation of human E3 ubiquitin ligases identifies MULAN, a mitochondrial E3 that regulates the organelle's dynamics and signaling." PLoS One **3**(1): e1487.

Li, X., J. Jiang, R. Yang, X. Xu, F. Hu, A. Liu, D. Tao, Y. Leng, J. Hu, J. Gong and X. Luo (2015). "Expression of HAX-1 in colorectal cancer and its role in cancer cell growth." Mol Med Rep **12**(3): 4071-4078.

Liu, Y. and R. K. Mallampalli (2016). "Small molecule therapeutics targeting F-box proteins in cancer." Semin Cancer Biol **36**: 105-119.

Livak, K. J. and T. D. Schmittgen (2001). "Analysis of Relative Gene Expression Data Using Real-Time Quantitative PCR and the 2−ΔΔCT Method." Methods **25**(4): 402-408.

Livneh, E. and D. D. Fishman (1997). "Linking protein kinase C to cell-cycle control." Eur J Biochem **248**(1): 1-9.

Lopez-Girona, A., D. Mendy, T. Ito, K. Miller, A. K. Gandhi, J. Kang, S. Karasawa, G. Carmel, P. Jackson, M. Abbasian, A. Mahmoudi, B. Cathers, E. Rychak, S. Gaidarova, R. Chen, P. H. Schafer, H. Handa, T. O. Daniel, J. F. Evans and R. Chopra (2012). "Cereblon is a direct protein target for immunomodulatory and antiproliferative activities of lenalidomide and pomalidomide." Leukemia **26**(11): 2326-2335.

Lovec, H., A. Grzeschiczek, M. B. Kowalski and T. Moroy (1994). "Cyclin D1/bcl-1 cooperates with myc genes in the generation of B-cell lymphoma in transgenic mice." EMBO J **13**(15): 3487-3495.

Lowry, O. H., N. J. Rosebrough, A. L. Farr and R. J. Randall (1951). "PROTEIN MEASUREMENT WITH THE FOLIN PHENOL REAGENT." Journal of Biological Chemistry **193**(1): 265-275.

Lu, W., H. K. Lee, C. Xiang, S. Finniss and C. Brodie (2007). "The phosphorylation of tyrosine 332 is necessary for the caspase 3-dependent cleavage of PKCdelta and the regulation of cell apoptosis." Cell Signal **19**(10): 2165-2173.

Lydeard, J. R., B. A. Schulman and J. W. Harper (2013). "Building and remodelling Cullin-RING E3 ubiquitin ligases." EMBO Rep **14**(12): 1050-1061.

Ma, Y., U. Pannicke, K. Schwarz and M. R. Lieber (2002). "Hairpin opening and overhang processing by an Artemis/DNA-dependent protein kinase complex in nonhomologous end joining and V(D)J recombination." Cell **108**(6): 781-794.

Maasho, K., A. Marusina, N. M. Reynolds, J. E. Coligan and F. Borrego (2004). "Efficient gene transfer into the human natural killer cell line, NKL, using the Amaxa nucleofection system." J Immunol Methods **284**(1-2): 133-140.

Majumder, P. K., N. C. Mishra, X. Sun, A. Bharti, S. Kharbanda, S. Saxena and D. Kufe (2001). "Targeting of protein kinase C delta to mitochondria in the oxidative stress response." Cell Growth Differ **12**(9): 465-470.

Manfiolli, A. O., A. L. Maragno, M. M. Baqui, S. Yokoo, F. R. Teixeira, E. B. Oliveira and M. D. Gomes (2008). "FBXO25-associated nuclear domains: a novel subnuclear structure." Mol Biol Cell **19**(5): 1848-1861.

Maragno, A. L., M. M. Baqui and M. D. Gomes (2006). "FBXO25, an F-box protein homologue of atrogin-1, is not induced in atrophying muscle." Biochim Biophys Acta **1760**(6): 966-972.

Martinez-Climent, J. A., E. Vizcarra, D. Sanchez, D. Blesa, I. Marugan, I. Benet, F. Sole, F. Rubio-Moscardo, M. J. Terol, J. Climent, E. Sarsotti, M. Tormo, E. Andreu, M. Salido, M. A. Ruiz, F. Prosper, R. Siebert, M. J. S. Dyer and J. García-Conde (2001). "Loss of a novel tumor suppressor gene locus at chromosome 8p is associated with leukemic mantle cell lymphoma." Blood **98**(12): 3479-3482.

Matassa, A. A., L. Carpenter, T. J. Biden, M. J. Humphries and M. E. Reyland (2001). "PKCdelta is required for mitochondrial-dependent apoptosis in salivary epithelial cells." J Biol Chem **276**(32): 29719-29728.

McCurrach, M. E. (2001). "Methods for studying pro- and antiapoptotic genes in nonimmortal cells." Methods Cell Biol. **66**: 197-227.

Mellor, H. and P. J. Parker (1998). "The extended protein kinase C superfamily." Biochem J **332 (Pt 2)**: 281-292.

Metzger, M. B., V. A. Hristova and A. M. Weissman (2012). "HECT and RING finger families of E3 ubiquitin ligases at a glance." J Cell Sci **125**(Pt 3): 531-537.

Miething, C., S. Feihl, C. Mugler, R. Grundler, N. von Bubnoff, F. Lordick, C. Peschel and J. Duyster (2006). "The Bcr-Abl mutations T315I and Y253H do not confer a growth advantage in the absence of imatinib." Leukemia **20**(4): 650-657.

Miyamoto, A., K. Nakayama, H. Imaki, S. Hirose, Y. Jiang, M. Abe, T. Tsukiyama, H. Nagahama, S. Ohno, S. Hatakeyama and K. I. Nakayama (2002). "Increased proliferation of B cells and auto-immunity in mice lacking protein kinase Cdelta." Nature **416**(6883): 865-869.

Modem, S. and T. R. Reddy (2008). "An anti-apoptotic protein, Hax-1, inhibits the HIV-1 rev function by altering its sub-cellular localization." J Cell Physiol **214**(1): 14-19.

Moffat, J., D. A. Grueneberg, X. Yang, S. Y. Kim, A. M. Kloepfer, G. Hinkle, B. Piqani, T. M. Eisenhaure, B. Luo, J. K. Grenier, A. E. Carpenter, S. Y. Foo, S. A. Stewart, B. R. Stockwell, N. Hacohen, W. C. Hahn, E. S. Lander,

D. M. Sabatini and D. E. Root (2006). "A lentiviral RNAi library for human and mouse genes applied to an arrayed viral high-content screen." Cell **124**(6): 1283-1298.

Montagnoli, A., F. Fiore, E. Eytan, A. C. Carrano, G. F. Draetta, A. Hershko and M. Pagano (1999). "Ubiquitination of p27 is regulated by Cdk-dependent phosphorylation and trimeric complex formation." Genes Dev **13**(9): 1181-1189.

Morris, E. J., K. Evason, C. Wiand, T. J. L'Ecuyer and A. B. Fulton (2000). "Misdirected vimentin messenger RNA alters cell morphology and motility." J Cell Sci **113 (Pt 13)**: 2433-2443.

Mujtaba, T. and Q. P. Dou (2011). "Advances in the understanding of mechanisms and therapeutic use of bortezomib." Discov Med **12**(67): 471-480.

Murata, S., H. Yashiroda and K. Tanaka (2009). "Molecular mechanisms of proteasome assembly." Nat Rev Mol Cell Biol **10**(2): 104-115.

Muratani, M. and W. P. Tansey (2003). "How the ubiquitin-proteasome system controls transcription." Nat Rev Mol Cell Biol **4**(3): 192-201.

Myung, J., K. B. Kim and C. M. Crews (2001). "The Ubiquitin-Proteasome Pathway and Proteasome Inhibitors." Medicinal research reviews **21**(4): 245-273.

Nethe, M. and P. L. Hordijk (2010). "The role of ubiquitylation and degradation in RhoGTPase signalling." J Cell Sci **123**(Pt 23): 4011-4018.

Neutzner, A., S. Li, S. Xu and M. Karbowski (2012). "The ubiquitin/proteasome system-dependent control of mitochondrial steps in apoptosis." Semin Cell Dev Biol **23**(5): 499-508.

Neutzner, M. and A. Neutzner (2012). "Enzymes of ubiquitination and deubiquitination." Essays Biochem **52**: 37-50.

Nijman, S. M., M. P. Luna-Vargas, A. Velds, T. R. Brummelkamp, A. M. Dirac, T. K. Sixma and R. Bernards (2005). "A genomic and functional inventory of deubiquitinating enzymes." Cell **123**(5): 773-786.

Nirmalan, N. J., P. Harnden, P. J. Selby and R. E. Banks (2009). "Development and validation of a novel protein extraction methodology for quantitation of protein expression in formalin-fixed paraffin-embedded tissues using western blotting." The Journal of Pathology **217**(4): 497-506.

Nishizuka, Y. (1992). "Intracellular signaling by hydrolysis of phospholipids and activation of protein kinase C." Science **258**(5082): 607-614.

Nogai, H., B. Dorken and G. Lenz (2011). "Pathogenesis of non-Hodgkin's lymphoma." J Clin Oncol **29**(14): 1803-1811.

Oda, E., R. Ohki, H. Murasawa, J. Nemoto, T. Shibue, T. Yamashita, T. Tokino, T. Taniguchi and N. Tanaka (2000). "Noxa, a BH3-only member of the Bcl-2 family and candidate mediator of p53-induced apoptosis." Science **288**(5468): 1053-1058.

Olsson, A., C. Manzl, A. Strasser and A. Villunger (2007). "How important are post-translational modifications in p53 for selectivity in target-gene transcription and tumour suppression?" Cell Death Differ **14**(9): 1561-1575.

Ortiz, D. F., J. Moseley, G. Calderon, A. L. Swift, S. Li and I. M. Arias (2004). "Identification of HAX-1 as a protein that binds bile salt export protein and regulates its abundance in the apical membrane of Madin-Darby canine kidney cells." J Biol Chem **279**(31): 32761-32770.

Ott, G., J. Kalla, M. M. Ott, B. Schryen, T. Katzenberger, J. G. Muller and H. K. Muller-Hermelink (1997). "Blastoid variants of mantle cell lymphoma: frequent bcl-1 rearrangements at the major translocation cluster region and tetraploid chromosome clones." Blood **89**(4): 1421-1429.

Ott, G., A. Rosenwald and E. Campo (2013). "Understanding MYC-driven aggressive B-cell lymphomas: pathogenesis and classification." Blood **122**(24): 3884-3891.

Paddison, P. J., A. A. Caudy, R. Sachidanandam and G. J. Hannon (2004). "Short hairpin activated gene silencing in mammalian cells." Methods Mol Biol **265**: 85-100.

Palmieri, C., C. Falcone, E. Iaccino, F. M. Tuccillo, M. Gaspari, F. Trimboli, A. De Laurentiis, L. Luberto, M. Pontoriero, A. Pisano, E. Vecchio, O. Fierro, M. R. Panico, M. Larobina, S. Gargiulo, N. Costa, F. Dal Piaz, M. Schiavone, C. Arra, A. Giudice, G. Palma, A. Barbieri, I. Quinto and G. Scala (2010). "In vivo targeting and growth inhibition of the A20 murine B-cell lymphoma by an idiotype-specific peptide binder." Blood **116**(2): 226-238.

Palombella, V. J., O. J. Rando, A. L. Goldberg and T. Maniatis (1994). "The ubiquitin-proteasome pathway is required for processing the NF-kappa B1 precursor protein and the activation of NF-kappa B." Cell **78**(5): 773-785.

Paoluzzi, L. and O. A. O'Connor (2006). "Mechanistic rationale and clinical evidence for the efficacy of proteasome inhibitors against indolent and mantle cell lymphomas." BioDrugs **20**(1): 13-23.

Pasqualucci, L., V. Trifonov, G. Fabbri, J. Ma, D. Rossi, A. Chiarenza, V. A. Wells, A. Grunn, M. Messina, O. Elliot, J. Chan, G. Bhagat, A. Chadburn, G. Gaidano, C. G. Mullighan, R. Rabadan and R. Dalla-Favera (2011). "Analysis of the coding genome of diffuse large B-cell lymphoma." Nat Genet **43**(9): 830-837.

Pear, W. S., J. P. Miller, L. Xu, J. C. Pui, B. Soffer, R. C. Quackenbush, A. M. Pendergast, R. Bronson, J. C. Aster, M. L. Scott and D. Baltimore (1998). Efficient and Rapid Induction of a Chronic Myelogenous Leukemia-Like Myeloproliferative Disease in Mice Receiving P210 bcr/abl-Transduced Bone Marrow.

Peckl-Schmid, D., S. Wolkerstorfer, S. Konigsberger, G. Achatz-Straussberger, S. Feichtner, E. Schwaiger, N. Zaborsky, M. Huemer, I. K. Gratz, R. Schibli, M. Lamers, R. Crameri, K. Moser, E. O. Luger and G. Achatz (2010). "HAX1 deficiency: impact on lymphopoiesis and B-cell development." Eur J Immunol **40**(11): 3161-3172.

Perez-Galan, P., H. Mora-Jensen, M. A. Weniger, A. L. Shaffer, 3rd, E. G. Rizzatti, C. M. Chapman, C. C. Mo, L. S. Stennett, C. Rader, P. Liu, N. Raghavachari, M. Stetler-Stevenson, C. Yuan, S. Pittaluga, I. Maric, K. M. Dunleavy, W. H. Wilson, L. M. Staudt and A. Wiestner (2011). "Bortezomib resistance in mantle cell lymphoma is associated with plasmacytic differentiation." Blood **117**(2): 542-552.

Petroski, M. D. and R. J. Deshaies (2005). "Function and regulation of cullin-RING ubiquitin ligases." Nat Rev Mol Cell Biol **6**(1): 9-20.

Pickart, C. M. and M. J. Eddins (2004). "Ubiquitin: structures, functions, mechanisms." Biochim Biophys Acta **1695**(1-3): 55-72.

Pickart, C. M. and D. Fushman (2004). "Polyubiquitin chains: polymeric protein signals." Curr Opin Chem Biol **8**(6): 610-616.

Pinyol, M., S. Bea, L. Pla, V. Ribrag, J. Bosq, A. Rosenwald, E. Campo and P. Jares (2007). "Inactivation of RB1 in mantle-cell lymphoma detected by nonsense-mediated mRNA decay pathway inhibition and microarray analysis." Blood **109**(12): 5422-5429.

Pinyol, M., L. Hernandez, M. Cazorla, M. Balbin, P. Jares, P. L. Fernandez, E. Montserrat, A. Cardesa, C. Lopez-Otin and E. Campo (1997). "Deletions and loss of expression of p16INK4a and p21Waf1 genes are associated with aggressive variants of mantle cell lymphomas." Blood **89**(1): 272-280.

Pommier, Y., E. Leo, H. Zhang and C. Marchand (2010). "DNA Topoisomerases and Their Poisoning by Anticancer and Antibacterial Drugs." Chemistry & Biology **17**(5): 421-433.

Ponader, S., S. S. Chen, J. J. Buggy, K. Balakrishnan, V. Gandhi, W. G. Wierda, M. J. Keating, S. O'Brien, N. Chiorazzi and J. A. Burger (2012). "The Bruton tyrosine kinase inhibitor PCI-32765 thwarts chronic lymphocytic leukemia cell survival and tissue homing in vitro and in vivo." Blood **119**(5): 1182-1189.

Puig, O., F. Caspary, G. Rigaut, B. Rutz, E. Bouveret, E. Bragado-Nilsson, M. Wilm and B. Seraphin (2001). "The tandem affinity purification (TAP) method: a general procedure of protein complex purification." Methods **24**(3): 218-229.

Qian, Z., L. Zhang, Z. Cai, L. Sun, H. Wang, Q. Yi and M. Wang (2011). "Lenalidomide synergizes with dexamethasone to induce growth arrest and apoptosis of mantle cell lymphoma cells in vitro and in vivo." Leuk Res **35**(3): 380-386.

Radhika, V., D. Onesime, J. H. Ha and N. Dhanasekaran (2004). "Galpha13 stimulates cell migration through cortactin-interacting protein Hax-1." J Biol Chem **279**(47): 49406-49413.

Ramsay, A. G., M. D. Keppler, M. Jazayeri, G. J. Thomas, M. Parsons, S. Violette, P. Weinreb, I. R. Hart and J. F. Marshall (2007). "HS1-associated protein X-1 regulates carcinoma cell migration and invasion via clathrin-mediated endocytosis of integrin alphavbeta6." Cancer Res **67**(11): 5275-5284.

Randle, S. J. and H. Laman (2016). "F-box protein interactions with the hallmark pathways in cancer." Semin Cancer Biol **36**: 3-17.

Rao, E., C. Jiang, M. Ji, X. Huang, J. Iqbal, G. Lenz, G. Wright, L. M. Staudt, Y. Zhao, T. W. McKeithan, W. C. Chan and K. Fu (2012). "The miRNA-17 approximately 92 cluster mediates chemoresistance and enhances tumor growth in mantle cell lymphoma via PI3K/AKT pathway activation." Leukemia **26**(5): 1064-1072.

Ray, A., M. K. James, S. Larochelle, R. P. Fisher and S. W. Blain (2009). "p27Kip1 inhibits cyclin D-cyclin-dependent kinase 4 by two independent modes." Mol Cell Biol **29**(4): 986-999.

Reya, T., A. W. Duncan, L. Ailles, J. Domen, D. C. Scherer, K. Willert, L. Hintz, R. Nusse and I. L. Weissman (2003). "A role for Wnt signalling in self-renewal of haematopoietic stem cells." Nature **423**(6938): 409-414.

Riccardi, C. and I. Nicoletti (2006). "Analysis of apoptosis by propidium iodide staining and flow cytometry." Nat Protoc **1**(3): 1458-1461.

Rieger, A. M., K. L. Nelson, J. D. Konowalchuk and D. R. Barreda (2011). "Modified Annexin V/Propidium Iodide Apoptosis Assay For Accurate Assessment of Cell Death." Journal of Visualized Experiments : JoVE(50): 2597.

Rock, K. L., C. Gramm, L. Rothstein, K. Clark, R. Stein, L. Dick, D. Hwang and A. L. Goldberg (1994). "Inhibitors of the proteasome block the degradation of most cell proteins and the generation of peptides presented on MHC class I molecules." Cell **78**(5): 761-771.

Rubio-Moscardo, F., J. Climent, R. Siebert, M. A. Piris, J. I. Martin-Subero, I. Nielander, J. Garcia-Conde, M. J. Dyer, M. J. Terol, D. Pinkel and J. A. Martinez-Climent (2005). "Mantle-cell lymphoma genotypes identified with CGH to BAC microarrays define a leukemic subgroup of disease and predict patient outcome." Blood **105**(11): 4445-4454.

Rummel, M. J., S. de Vos, D. Hoelzer, H. P. Koeffler and W. K. Hofmann (2004). "Altered apoptosis pathways in mantle cell lymphoma." Leuk Lymphoma **45**(1): 49-54.

Saiki, R. K., D. H. Gelfand, S. Stoffel, S. J. Scharf, R. Higuchi, G. T. Horn, K. B. Mullis and H. A. Erlich (1988). "Primer-directed enzymatic amplification of DNA with a thermostable DNA polymerase." Science **239**(4839): 487-491.

Sander, S., Dinis P. Calado, L. Srinivasan, K. Köchert, B. Zhang, M. Rosolowski, Scott J. Rodig, K. Holzmann, S. Stilgenbauer, R. Siebert, L. Bullinger and K. Rajewsky (2012). "Synergy between PI3K Signaling and MYC in Burkitt Lymphomagenesis." Cancer Cell **22**(2): 167-179.

Sarnowska, E., E. A. Grzybowska, K. Sobczak, R. Konopinski, A. Wilczynska, M. Szwarc, T. J. Sarnowski, W. J. Krzyzosiak and J. A. Siedlecki (2007). "Hairpin structure within the 3'UTR of DNA polymerase beta mRNA acts as a post-transcriptional regulatory element and interacts with Hax-1." Nucleic Acids Res **35**(16): 5499-5510.

Schenkein, D. (2002). "Proteasome inhibitors in the treatment of B-cell malignancies." Clin Lymphoma **3**(1): 49-55.

Schiff, P. B., J. Fant and S. B. Horwitz (1979). "Promotion of microtubule assembly in vitro by taxol." Nature **277**(5698): 665-667.

Schmidt, M., J. Hanna, S. Elsasser and D. Finley (2005). "Proteasome-associated proteins: regulation of a proteolytic machine." Biol Chem **386**(8): 725-737.

Schneider-Poetsch, T., J. Ju, D. E. Eyler, Y. Dang, S. Bhat, W. C. Merrick, R. Green, B. Shen and J. O. Liu (2010). "Inhibition of eukaryotic translation elongation by cycloheximide and lactimidomycin." Nat Chem Biol **6**(3): 209-217.

Schraders, M., R. Pfundt, H. M. Straatman, I. M. Janssen, A. G. van Kessel, E. F. Schoenmakers, J. H. van Krieken and P. J. Groenen (2005). "Novel chromosomal imbalances in mantle cell lymphoma detected by genome-wide array-based comparative genomic hybridization." Blood **105**(4): 1686-1693.

Schulz, H., J. F. Bohlius, S. Trelle, N. Skoetz, M. Reiser, T. Kober, G. Schwarzer, M. Herold, M. Dreyling, M. Hallek and A. Engert (2007). "Immunochemotherapy with rituximab and overall survival in patients with indolent or mantle cell lymphoma: a systematic review and meta-analysis." J Natl Cancer Inst **99**(9): 706-714.

Scuoppo, C., C. Miething, L. Lindqvist, J. Reyes, C. Ruse, I. Appelmann, S. Yoon, A. Krasnitz, J. Teruya-Feldstein, D. Pappin, J. Pelletier and S. W. Lowe (2012). "A tumour suppressor network relying on the polyamine-hypusine axis." Nature **487**(7406): 244-248.

Shapiro, A. L., E. Viñuela and J. V. Maizel Jr (1967). "Molecular weight estimation of polypeptide chains by electrophoresis in SDS-polyacrylamide gels." Biochemical and Biophysical Research Communications **28**(5): 815-820.

Sherr, C. J. and J. D. Weber (2000). "The ARF/p53 pathway." Curr Opin Genet Dev **10**(1): 94-99.

Shi, H., A. Djikeng, T. Mark, E. Wirtz, C. Tschudi and E. Ullu (2000). "Genetic interference in Trypanosoma brucei by heritable and inducible double-stranded RNA." RNA **6**(7): 1069-1076.

Silverman, J. S., J. R. Skaar and M. Pagano (2012). "SCF ubiquitin ligases in the maintenance of genome stability." Trends Biochem Sci **37**(2): 66-73.

Simmen, T. (2011). "Hax-1: a regulator of calcium signaling and apoptosis progression with multiple roles in human disease." Expert Opin Ther Targets **15**(6): 741-751.

Skaar, J. R., J. K. Pagan and M. Pagano (2013). "Mechanisms and function of substrate recruitment by F-box proteins." Nat Rev Mol Cell Biol **14**(6): 369-381.

Skaar, J. R., J. K. Pagan and M. Pagano (2014). "SCF ubiquitin ligase-targeted therapies." Nat Rev Drug Discov **13**(12): 889-903.

Skaar, J. R. and M. Pagano (2009). "Control of cell growth by the SCF and APC/C ubiquitin ligases." Curr Opin Cell Biol **21**(6): 816-824.

Skarbnik, A. P. and A. H. Goy (2015). "Mantle cell lymphoma: state of the art." Clin Adv Hematol Oncol **13**(1): 44-55.

Skerra, A. and T. G. Schmidt (2000). "Use of the Strep-Tag and streptavidin for detection and purification of recombinant proteins." Methods Enzymol **326**: 271-304.

Smith, M. R. (2011). "Should there be a standard therapy for mantle cell lymphoma?" Future Oncol **7**(2): 227-237.

Smith, S. M. (2012). "Targeting mTOR in mantle cell lymphoma: current and future directions." Best Pract Res Clin Haematol **25**(2): 175-183.

Soh, J.-W. and I. B. Weinstein (2003). "Roles of Specific Isoforms of Protein Kinase C in the Transcriptional Control of Cyclin D1 and Related Genes." Journal of Biological Chemistry **278**(36): 34709-34716.

Sohail, A., J. Klapacz, M. Samaranayake, A. Ullah and A. S. Bhagwat (2003). "Human activation-induced cytidine deaminase causes transcription-dependent, strand-biased C to U deaminations." Nucleic Acids Res **31**(12): 2990-2994.

Solenthaler, M., E. Matutes, V. Brito-Babapulle, R. Morilla and D. Catovsky (2002). "p53 and mdm2 in mantle cell lymphoma in leukemic phase." Haematologica **87**(11): 1141-1150.

Solimando, A. G., D. Ribatti, A. Vacca and H. Einsele (2016). "Targeting B-cell non Hodgkin lymphoma: New and old tricks." Leuk Res **42**: 93-104.

Soltoff, S. P. (2007) "Rottlerin: an inappropriate and ineffective inhibitor of PKC&#x3b4." Trends in Pharmacological Sciences **28**(9): 453-458.

Souers, A. J., J. D. Leverson, E. R. Boghaert, S. L. Ackler, N. D. Catron, J. Chen, B. D. Dayton, H. Ding, S. H. Enschede, W. J. Fairbrother, D. C. Huang, S. G. Hymowitz, S. Jin, S. L. Khaw, P. J. Kovar, L. T. Lam, J. Lee, H. L. Maecker, K. C. Marsh, K. D. Mason, M. J. Mitten, P. M. Nimmer, A. Oleksijew, C. H. Park, C. M. Park, D. C. Phillips, A. W. Roberts, D. Sampath, J. F. Seymour, M. L. Smith, G. M. Sullivan, S. K. Tahir, C. Tse, M. D. Wendt, Y. Xiao, J. C. Xue, H. Zhang, R. A. Humerickhouse, S. H. Rosenberg and S. W. Elmore (2013). "ABT-199, a potent and selective BCL-2 inhibitor, achieves antitumor activity while sparing platelets." Nat Med **19**(2): 202-208.

Stadtmauer, E. A., A. O'Neill, L. J. Goldstein, P. A. Crilley, K. F. Mangan, J. N. Ingle, I. Brodsky, S. Martino, H. M. Lazarus, J. K. Erban, C. Sickles and J. H. Glick (2000). "Conventional-dose chemotherapy compared with high-dose chemotherapy plus autologous hematopoietic stem-cell transplantation for metastatic breast cancer. Philadelphia Bone Marrow Transplant Group." N Engl J Med **342**(15): 1069-1076.

Steinberg, S. F. (2004). "Distinctive activation mechanisms and functions for protein kinase Cdelta." Biochem J **384**(Pt 3): 449-459.

Stewart, S. A., D. M. Dykxhoorn, D. Palliser, H. Mizuno, E. Y. Yu, D. S. An, D. M. Sabatini, I. S. Chen, W. C. Hahn, P. A. Sharp, R. A. Weinberg and C. D. Novina (2003). "Lentivirus-delivered stable gene silencing by RNAi in primary cells." RNA **9**(4): 493-501.

Stolz, A., N. Ertych and H. Bastians (2011). "Tumor suppressor CHK2: regulator of DNA damage response and mediator of chromosomal stability." Clin Cancer Res **17**(3): 401-405.

Suh, K. S., T. Tanaka, S. Sarojini, G. Nightingale, R. Gharbaran, A. Pecora and A. Goy (2013). "The role of the ubiquitin proteasome system in lymphoma." Crit Rev Oncol Hematol **87**(3): 306-322.

Sun, S. J., L. Feng, G. Q. Zhao and Z. M. Dong (2012). "HAX-1 promotes the chemoresistance, invasion, and tumorigenicity of esophageal squamous carcinoma cells." Dig Dis Sci **57**(7): 1838-1846.

Suzuki, Y., C. Demoliere, D. Kitamura, H. Takeshita, U. Deuschle and T. Watanabe (1997). "HAX-1, a novel intracellular protein, localized on mitochondria, directly associates with HS1, a substrate of Src family tyrosine kinases." J Immunol **158**(6): 2736-2744.

Swaffield, J. C. and S. A. Johnston (2001). "Affinity purification of proteins binding to GST fusion proteins." Curr Protoc Mol Biol **Chapter 20**: Unit 20 22.

Tagawa, H., S. Karnan, R. Suzuki, K. Matsuo, X. Zhang, A. Ota, Y. Morishima, S. Nakamura and M. Seto (2005). "Genome-wide array-based CGH for mantle cell lymphoma: identification of homozygous deletions of the proapoptotic gene BIM." Oncogene **24**(8): 1348-1358.

Teixeira, F. R., A. O. Manfiolli, C. S. Soares, M. M. Baqui, T. Koide and M. D. Gomes (2013). "The F-box protein FBXO25 promotes the proteasome-dependent degradation of ELK-1 protein." J Biol Chem **288**(39): 28152-28162.

Teixeira, F. R., S. Yokoo, C. A. Gartner, A. O. Manfiolli, M. M. Baqui, E. M. Assmann, A. L. Maragno, H. Yu, P. de Lanerolle, J. Kobarg, S. P. Gygi and M. D. Gomes (2010). "Identification of FBXO25-interacting proteins using an integrated proteomics approach." Proteomics **10**(15): 2746-2757.

Terpe, K. (2003). "Overview of tag protein fusions: from molecular and biochemical fundamentals to commercial systems." Appl Microbiol Biotechnol **60**(5): 523-533.

Tomayko, M. M. (1989). "Determination of subcutaneous tumor size in athymic (nude) mice." Cancer Chemother Pharmacol.(24): 148-154.

Tonegawa, S. (1983). "Somatic generation of antibody diversity." Nature **302**(5909): 575-581.
Torres, K. and S. B. Horwitz (1998). "Mechanisms of Taxol-induced cell death are concentration dependent." Cancer Res **58**(16): 3620-3626.

Toujani, S., P. Dessen, N. Ithzar, G. Danglot, C. Richon, Y. Vassetzky, T. Robert, V. Lazar, J. Bosq, L. Da Costa, C. Perot, V. Ribrag, C. Patte, J. Wiels and A. Bernheim (2009). "High resolution genome-wide analysis of chromosomal alterations in Burkitt's lymphoma." PLoS One **4**(9): e7089.

Trebinska, A., K. Hogstrand, A. Grandien, E. A. Grzybowska and B. Fadeel (2014). "Exploring the anti-apoptotic role of HAX-1 versus BCL-XL in cytokine-dependent bone marrow-derived cells from mice." FEBS Lett **588**(17): 2921-2927.

Trebinska, A., A. Rembiszewska, K. Ciosek, K. Ptaszynski, S. Rowinski, J. Kupryjanczyk, J. A. Siedlecki and E. A. Grzybowska (2010). "HAX-1 overexpression, splicing and cellular localization in tumors." BMC Cancer **10**: 76.

Tsujimoto, Y., E. Jaffe, J. Cossman, J. Gorham, P. C. Nowell and C. M. Croce (1985). "Clustering of breakpoints on chromosome 11 in human B-cell neoplasms with the t(11;14) chromosome translocation." Nature **315**(6017): 340-343.

Uruno, T., P. Zhang, J. Liu, J. J. Hao and X. Zhan (2003). "Haematopoietic lineage cell-specific protein 1 (HS1) promotes actin-related protein (Arp) 2/3 complex-mediated actin polymerization." Biochem J **371**(Pt 2): 485-493.

Vafiadaki, E., D. A. Arvanitis, S. N. Pagakis, V. Papalouka, D. Sanoudou, A. Kontrogianni-Konstantopoulos and E. G. Kranias (2009). "The Anti-apoptotic Protein HAX-1 Interacts with SERCA2 and Regulates Its Protein Levels to Promote Cell Survival." Molecular Biology of the Cell **20**(1): 306-318.

Vallumsetla, N., J. Paludo and P. Kapoor (2015). "Bortezomib in mantle cell lymphoma: comparative therapeutic outcomes." Ther Clin Risk Manag **11**: 1663-1674.

Veitch, N. C. (2004). "Horseradish peroxidase: a modern view of a classic enzyme." Phytochemistry **65**(3): 249-259.

Volkmann, J., U. Reuning, M. Rudelius, N. Häfner, T. Schuster, A. B. v. Rose, J. Weimer, F. Hilpert, M. Kiechle, M. Dürst, N. Arnold, B. Schmalfeldt, A. Meindl and J. Ramser (2013). "High expression of crystallin αB represents an independent molecular marker for unfavourable ovarian cancer patient outcome and impairs TRAIL- and cisplatin-induced apoptosis in human ovarian cancer cells." International Journal of Cancer **132**(12): 2820-2832.

Vose, J. M. (2015). "Mantle cell lymphoma: 2015 update on diagnosis, risk-stratification, and clinical management." Am J Hematol **90**(8): 739-745.

Wajant, H. (2002). "The Fas signaling pathway: more than a paradigm." Science **296**(5573): 1635-1636.

Wang , M. L., S. Rule , P. Martin , A. Goy , R. Auer , B. S. Kahl , W. Jurczak , R. H. Advani , J. E. Romaguera , M. E. Williams , J. C. Barrientos , E. Chmielowska , J. Radford , S. Stilgenbauer , M. Dreyling , W. W. Jedrzejczak , P. Johnson , S. E. Spurgeon , L. Li , L. Zhang , K. Newberry , Z. Ou , N. Cheng , B. Fang , J. McGreivy , F. Clow , J. J. Buggy , B. Y. Chang , D. M. Beaupre , L. A. Kunkel and K. A. Blum (2013). "Targeting BTK with Ibrutinib in Relapsed or Refractory Mantle-Cell Lymphoma." New England Journal of Medicine **369**(6): 507-516.

Wei, X. J., S. Y. Li, B. Yu, G. Chen, J. F. Du and H. Y. Cai (2014). "Expression of HAX-1 in human colorectal cancer and its clinical significance." Tumour Biol **35**(2): 1411-1415.

Weiner, G. J. (2010). "Rituximab: mechanism of action." Semin Hematol **47**(2): 115-123.

Welcker, M. and B. E. Clurman (2008). "FBW7 ubiquitin ligase: a tumour suppressor at the crossroads of cell division, growth and differentiation." Nat Rev Cancer **8**(2): 83-93.

Winston, J. T., D. M. Koepp, C. Zhu, S. J. Elledge and J. W. Harper (1999). "A family of mammalian F-box proteins." Curr Biol **9**(20): 1180-1182.

Xiang, H., E. J. Noonan, J. Wang, H. Duan, L. Ma, S. Michie and L. M. Boxer (2011). "The immunoglobulin heavy chain gene 3' enhancers induce Bcl2 deregulation and lymphomagenesis in murine B cells." Leukemia **25**(9): 1484-1493.

Yang, J., X. Liu, K. Bhalla, C. N. Kim, A. M. Ibrado, J. Cai, T. I. Peng, D. P. Jones and X. Wang (1997). "Prevention of apoptosis by Bcl-2: release of cytochrome c from mitochondria blocked." Science **275**(5303): 1129-1132.

Yap, S. V., J. M. Koontz and A. Kontrogianni-Konstantopoulos (2011). "HAX-1: a family of apoptotic regulators in health and disease." J Cell Physiol **226**(11): 2752-2761.

Yedavalli, V. S., H. M. Shih, Y. P. Chiang, C. Y. Lu, L. Y. Chang, M. Y. Chen, C. Y. Chuang, A. I. Dayton, K. T. Jeang and L. M. Huang (2005). "Human immunodeficiency virus type 1 Vpr interacts with antiapoptotic mitochondrial protein HAX-1." J Virol **79**(21): 13735-13746.

Yoshida, K. (2007). "PKCdelta signaling: mechanisms of DNA damage response and apoptosis." Cell Signal **19**(5): 892-901.

Yoshida, K., H. G. Wang, Y. Miki and D. Kufe (2003). "Protein kinase Cdelta is responsible for constitutive and DNA damage-induced phosphorylation of Rad9." EMBO J **22**(6): 1431-1441.

Zayat, V., A. Balcerak, J. Korczynski, A. Trebinska, J. Wysocki, E. Sarnowska, M. Chmielarczyk, E. Macech, R. Konopinski, M. Dziembowska and E. A. Grzybowska (2015). "HAX-1: a novel p-body protein." DNA Cell Biol **34**(1): 43-54.

Zhang, Y. and Y. Xiong (2001). "A p53 amino-terminal nuclear export signal inhibited by DNA damage-induced phosphorylation." Science **292**(5523): 1910-1915.

Zhao, M., L. Xia and G. Q. Chen (2012). "Protein kinase cdelta in apoptosis: a brief overview." Arch Immunol Ther Exp (Warsz) **60**(5): 361-372.

Zhao, W., J. R. Waggoner, Z. G. Zhang, C. K. Lam, P. Han, J. Qian, P. M. Schroder, B. Mitton, A. Kontrogianni-Konstantopoulos, S. L. Robia and E. G. Kranias (2009). "The anti-apoptotic protein HAX-1 is a regulator of cardiac function." Proc Natl Acad Sci U S A **106**(49): 20776-20781.

Zilfou, J. T. and S. W. Lowe (2009). "Tumor suppressive functions of p53." Cold Spring Harb Perspect Biol **1**(5): a001883.

Zimm, B. H. and S. D. Levene (1992). "Problems and prospects in the theory of gel electrophoresis of DNA." Quarterly Reviews of Biophysics **25**(02): 171-204.

10 List of figures

12 Publication

Data sets of the present dissertation were previously published in:

Baumann, U., Fernandez-Saiz, V., Rudelius, M., Lemeer, S., Rad, R., Knorn, A.M., Slawska, J., Engel, K., Jeremias, I., Li, Z., Tomiatti, V., Illert, A.L., Targosz, B.S., Braun, M., Perner, S., Leitges, M., Klapper, W., Dreyling, M., Miething, C., Lenz, G., Rosenwald, A., Peschel, C., Keller, U., Kuster, B., Bassermann, F. "Disruption of the PRKCD-FBXO25-HAX-1 axis attenuates the apoptotic response and drives lymphomagenesis". **Nature Medicine** (2014) 20, 1401-1409.

11 Danksagung

Da auch jedes noch so aussichtsreiche Projekt nicht ohne die Hilfe Anderer ein Erfolg werden kann, möchte ich mich an dieser Stelle herzlich bei all jenen bedanken, die zum Gelingen der vorliegenden Arbeit maßgeblich beigetragen haben. Zunächst möchte ich mich bei Prof. Dr. Florian Bassermann bedanken, der es mir ermöglicht hat, diese Dissertation in seiner hoch motivierten Forschungsgruppe durchzuführen, und der mir von Beginn an das Vertrauen geschenkt hat, dieses Projekt zum Erfolg führen zu können. Danke für die wissenschaftliche und menschliche Unterstützung, aber auch für die freie Hand, von Bewährtem abzuweichen und neue auch einmal verrückte Techniken ausprobieren zu dürfen. Nachfolgend möchte ich Prof. Dr. Christian Peschel danken, der es mir ermöglicht hat, das vorliegende Projekt an der III. Medizinischen Klinik des Klinikums rechts der Isar der Technischen Universität München durchzuführen. Ein besonderer Dank steht auch allen Kooperationspartnern zu, ohne die an einen erfolgreichen Abschluss des Projektes nicht zu denken gewesen wäre. Besonders zu erwähnen sind hierbei Prof. Dr. Bernhard Küster und Dr. Simone Lemeer für die ausschlaggebende massenspektrometrische Analyse, die den Grundstein gelegt hat, Dr. Martina Rudelius für die histopathologischen Analysen sämtlicher humanen und murinen Proben, die das Projekt erst zu einem "großen" gemacht haben und Prof. Dr. Ulrich Keller für die Hilfe beim Einstieg in das Gebiet der Tierversuche.

Special thanks goes to my mentor Dr. Vanesa Fernández-Saíz for showing me a great variety of different molecular biological techniques and the relevant tricks how to survive in this business. Thank you for solutions how to solve every single problem and experimental approach inculding: how to conserve a squirrel +/- 3 x 10^4 flees, how to paint with Coomassie and how to make fire with a Kindle batterie.

Danke an Dr. Bianca-Sabrina Targosz, die "beste Master-Studenten-Ausbilderin der Welt", die fachliche Grundlage meines wissenschaftlichen Erfolgs gelegt zu haben. Mein herzlichster Dank gilt Anna-Maria Karmann für die organisierte Unterstützung in allen Projektlagen, mir die Angst vor Mausarbeit genommen zu haben, aber auch für die Rolle Toilettenpapier (wenn alle Papiertaschentücher aufgebraucht waren) als das Projekt einmal nicht laufen wollte, und vor allem für die ehrliche Freundschaft die hoffentlich ein Leben lang halten wird. Nachfolgend möchte ich mich bei den Mädels der AG Bassermann, und Michael, für das perfekte Arbeitsumfeld, die Unterstützung in allen Lagen und die motivierte Umgebung bedanken. Mein abschließender Dank gilt Familie und Freunden die mich zu allen Zeitpunkten treu unterstützt haben, auch wenn ich allzu oft fasziniert von diesen "Proteinen mit den komischen Namen" gesprochen habe.

DANKE!